NF-κB activation in skeletal muscle during ageing: role in development of sarcopenia.

Thesis submitted in accordance with the requirements of the University of Liverpool for the degree of Doctor in Philosophy

By

Euan David Owen

March 2021

Abstract

Sarcopenia is the loss of muscle mass and function in older age. An increase in pro-inflammatory cytokines is associated with many age-related conditions including sarcopenia. A chronic activation of nuclear factor kappa-light-chain enhancer of activated B cells (NF-κB) has been shown in muscles from old wild type (WT) and this has also been shown in a model of accelerated loss of muscle mass and function, mice lacking CuZn superoxide dismutase (SOD1KO mice). The consequence of such a chronic activation of NF-κB is unclear, but muscle is known to be an endocrine organ, with changes in the release of cytokines and chemokines, particularly following contractions where pro inflammatory cytokines can be released. In advancing age there is a notable decrease in muscle mass, with substantial loss of protein, suggesting that the balance between protein synthesis and degradation is net negative. Activation of NF-κB is also associated with activation of protein degradation processes.

The aims of is thesis were to: 1) Quantify the changes in mass, structure and function of muscles of old WT and adult SOD1KO mice compared with adult WT mice; 2) Determine the localisation of nuclei with increase activation of the canonical pathway of NF-κB in muscles of old WT and adult SOD1KO compared with adult WT mice; 3) Identify whether any changes in cytokine and chemokine levels in the plasma of old WT and adult SOD1KO mice are associated with increased cytokine production by muscle and 4) to determine whether activation or inhibition of protein turnover pathways are associated with changes in NF-κB activity in muscles of old WT mice when compared with adult WT mice.

Morphological and functional characteristics of muscle were examined using the tissue cell geometry plugin on ImageJ and MyoVision. Components of the NF-κB pathway were measured through qPCR and western blotting of lysates from gastrocnemius muscles and by immunohistochemistry analysis of EDL muscles. The levels of cytokines and chemokines were determined in muscle lysates and plasma and in media derived from isolated muscle fibres from adult WT, old WT and adult SOD1KO mice. The association of nuclear localisation of p65 with the regenerative stage of the muscle fibre was also examined in a model of regenerating *extensor digitorum longus* (EDL) muscles from adult WT, old WT and SOD1KO mice following injury induced via $BaCl_2$ injection into the EDL muscle. Finally, fractional synthesis rates of individual proteins were determined in muscles of adult WT and old WT mice using heavy water SILAM where mice and unlabelled proteomics was also performed on these mice. The datasets from these experiments were compared with an RNA sequencing dataset to determine whether transcription was the driving factor in differences observed in fractional synthesis rates.

There was an increase in inflammatory cytokines/chemokines in the plasma of old WT mice and an increase in specific chemokines in muscle homogenates or released from isolated muscle fibres from old WT muscles, suggesting that muscle of old WT mice may be a source of specific cytokines/chemokines, some of which add to the plasma pool and others acting more locally. The levels and patterns of cytokines/chemokines in plasma and muscle of adult SOD1KO mice were very different, suggesting that these mice are a poor model of inflammaging. Higher levels of p65 (the major transcription factor involved with canonical NF-κB activation) were observed in muscle fibres containing a centrally positioned nucleus, seen particularly in muscles of SOD1KO mice and during regeneration following chemically induced muscle damage but it is unlikely that this activation results in a substantial increase in release of cytokines/chemokines by these muscle fibres. Bioinformatic analysis of the unlabelled proteomics dataset revealed there was a clear upregulation of protein degradation pathways and protein misfolding pathways in the muscles of old WT mice. There was little evidence for changes in overall protein synthesis rates suggesting that increased protein degradation is the main driver of muscle protein loss with age. Increased activation of NF-κB may play a role in increased activation of degenerative pathways in muscles of old WT mice, but further analyses including inhibitor studies are required to confirm the role of NF-κB.

Dedicated to my mum and dad

Thank you for everything.

Acknowledgements

I would like to thank The University of Liverpool for the opportunities given to me. I would also like to thank the National Institute of Ageing for the generous funding for the project.

A huge thank you to my primary supervisor, Professor Anne McArdle for giving me endless amounts of opportunity and supervision throughout my PhD. Thank you Dr Aphrodite Vasilaki for always having an open door and encouraging me every step of the process. Thank you, Dr Natalie Pollock for all your guidance through the early years of my scientific career. And thank you again to all three for making my PhD experience absolutely invaluable.

A big thank you to the other members of the rest of the Musculoskeletal Biology group, most notably to Professor Malcolm Jackson. And of course a massive thank you Shah and Mattia for sharing the stress of the journey. Thank you, Kay for always being on hand to help.

Thank you to Professor Rob Beynon and the lab at The Centre for Proteome Research for helping with the proteomics experiments. Thank you also to Dr Dean Hammond for the help in processing the proteomics data. Thank you as well to Dr Caroline Staunton for providing the RNAseq data. A big thank you for also helping me get to San Diego. Thank you to our US collaborators in Michigan and Oklahoma for helping me feel part of the group and always engaging with me in exciting discussions.

I would not have been able to do any of this without help from friends I have met along the way. Thank you to Conor, Lina, James, and of course my flatmate, Adam. Thank you for always taking the bins out.

Thank you to Francesca. I could never thank you enough for the love and support you have given to me through some of the best and some of the most challenging times. Thank you for pushing me to succeed at every opportunity and making me into a better scientist. You have made me feel like I can achieve anything.

Finally, the biggest thank you to my second major funders - my mum and dad. I am incredibly lucky as a son and will be forever grateful for the happy life you have ensured I have. You have helped me to achieve the unachievable. I love you both and appreciate everything you have done for me.

List of figures

List of tables

Abbreviations

^2H_2O	Deuterium oxide
ACh	Acetyl choline
ACKR	Atypical chemokine receptor
ADP	Adenosine diphosphate
ANOVA	Analysis of variance
AP-1	Activator Protein 1
APC	Antigen presenting cell
APS	Ammonium persulphate
ATP	Adenosine triphosphate
B1	Type 1 B cell
B2	Type 2 B cell
$BaCl_2$	Barium chloride
βc	Common β-chain
BCA-1	B cell attracting chemokine 1
Bcl3	B cell lymphoma
Bnip-3	BCL2 interacting protein 3
bp	Base pairs
Breg	Regulatory B cell
BSA	Bovine serum albumin
cCKR	Conventional chemokine receptor
cDC	Conventional DC
ChIP	Chromatin immunoprecipitation
CLP	Common lymphoid progenitor
CMP	Common myloid progenitor
CRP	C-reactive protein
CSA	Cross sectional area
CTX	Cardiotoxin
DAMP	Damage associated molecule pattern
DAPI	4',6-diamidino-2-phenlindole
DC	Dendritic cell
DMD	Duchenne Muscular Dystrophy
DMSO	Dimethyl sulfoxide
DPX	Dibutylphthalate polystyrene xylene
DTT	1,4 Dithiothreitol
E1	Ubiquitin-activating enzyme
E2	Ubiquitin-conjugating enzyme
E3	Ubiquitin-ligating enzyme
EDL	Extensor digitorum longus
EDTA	Ethylenediaminetetraacetic acid
ELR	Glutamic acid-leucine-argenine motif
EMSA	Electromotility shift assay
EPP	End plate potential

ER	Endoplasmic reticulum
ERAD	Endoplasmic reticulum associated degradation
EtOH	Ethanol
F-actin	Filamentous actin
FBS	Foetal bovine serum
FDB	Flexor digitorum brevis
FSG	Fish scale gelatine
Gabarap1	γ-aminobutyric acid receptor-associated protein 1
G-actin	Globular actin
γc	common γ-chain
G-CSF	Granulocyte colony stimulating factor
GM-CSF	Granulocyte/monocyte colony stimulating factor
GPCR	G-protein coupled receptor
GTN	Gastrocnemius
H_2O_2	Hydrogen peroxide
HEPES	4-(2-hydroxyethyl)-1-piperazineethanesulfonic acid
Hsp	Heat shock protein
Ig	Immunoglobulin
IHM	Interacting head motif
IκB	Inhibitor of NF-κB
IKK	Inhibitor of NF-κB kinase
IL	Interleukin
IL-1 R	IL-1 receptor
IL-10R	IL-10 receptor
IL-1RAcP	IL-1R accessory protein
IL-2Rα	IL-1R α chain
IL-2Rβ	IL-1R β chain
IP-10	Inteferon gamma-induced protein 10
k	Protein turnover rate constant
KCl	Potassium chloride
LAMP-2	Lysosome-associated membrane protein 2
LC3	Microtubule-associated proteins 1A/1B light chain 3B
LC-MSMS	Liquid chromatography-tandem mass spec
LPS	Lipopolysaccheride
LUBAC	Linear ubiquitin assembly complex
m0	Monoisotopic mass spectral peak
MAPK	Mitogen associated kinase
MEM	Minumium essential media
MEPP	Minature end plate potential
$MgCl_2$	Magnesium chloride
MHC	Major histocompatibility complex
MIP	Monocyte inflammatory protein
MPB	Muscle protein breakdown
MPS	Muscle protein synthesis

mRNA	Messenger RNA
mTNF-α	Monomeric TNF-α
MuRF-1	Muscle specific RING finger protein-1
MyHC	Myosin heavy chain
MyLC	Myosin light chain
MZ	Marginal zone
nAChR	Nicotinic acetyl choline receptor
NaOH	Sodium hydroxide
NBF	Neutral Buffered Formalin
NELF	Negative elongation factor
NEMO	NF-κB essential modulator
NFAT	Nuclear factor of activated T cells
NF-κB	Nuclear factor kappa-light-chain enhancer of activated B cells
NIK	NF-κB inducing kinase
NK	Natural killer
NMJ	Neuromuscular junction
NTX	Notoxin
PAMP	Pattern associated molecular pattern
PBS	Phosphate buffered solution
PCA	Principle component analysis
pDC	Plasmacytoid DC
Pi	Inorganic phosphate
PMSF	Phenylmethylsulfonyl fluoride
Pol	Polymerase
P-TEFb	Positive transcription elongation factor b
qPCR	quantitative polymerase chain reaction
rel	Relish
RER	Rough ER
RIA	Relative isotope abundance
RIPA	Radioimmunoprecipitation assay
Rnp	Regulatory particle of non-ATPase
ROS	Reactive oxygen species
Rpl	Ribosomal protein of the large subunit
Rps	Ribosomal protein of the small subunit
RPS27A	Ubiquitin-40S ribosomal protein S27a
Rtp	Regulatory particle of triple ATPase
SCF1	Stem cell factor 1
SCF^{βTrCP}	skp, cullin, f-box containing complex
SDS	Sodium dodecyl sulphate
SDS-PAGE	SDS-Polyacrylamide gel electrophoresis
SEM	Standard error of the mean
SNARE	soluble N-ethylmaleimide-sensitive fusion protein attachment protein receptors
snRNP	Small nuclear ribonucleoproteins
SOD	Superoxide dismutase

SOD1	CuZn SOD
SOD2	Mn SOD
Sodium chloride	NaCl
STAT5	Signal transducer and activator of transcription factor 5
sTNF-α	Soluble TNF-α
TACE	TNF converting enzyme
TAK1	Mitogen associated kinase kinase kinase 7
TBK1	TANK binding kinase 1
TBS	Tris-buffered saline
TBS-T	TBS-tween
TCM	Central memory T cell
TCR	T cell receptor
TECK	Thymus expressed chemokine
TEM	effector memory T cell
TEMED	Tetramethylethylenediamine
TF	Transcription factor (general)
TFA	Trifluoroacetic acid
TGF	Transforming growth factor
Th0	Naïve T cell
TIR	Toll/IL-R
TLR	Toll-like receptor
TnC	Troponin C
TNF	Tumour necrosis factor
TNFR	TNF receptor
TnI	Troponin I
TnT	Troponin T
TRAF	TNFR associated factor
Tris-HCL	Tris-hydrochloride
Trm	tissue resident T cell
t-tubules	Transverse tubules
TVM	Virtual memory T cell
UBA52	Ubiquitin-60S ribosomal protein L40
WGA	Wheat germ agglutinin
WT	Wild type
XBP1	X-box binding protein
XPB	Xeroderma pigmentosum type B
elF4EBP1	eukaryotic translation factor 4E binding protein 1
FOXO1	foxhead box protein O1
IGF-1	Insulin-like growth factor 1
MPB	Muscle protein breakdown
MPS	Muscle protein synthesis
p70s6K	p70 ribosomal s6 kinase
4EBP1	and initiation factor 4E binding protein 1
LMP	Mow molecular mass peptide

MECL	Multicatalytic endopeptidase complex subunit
DUBs	Deubiquitinating enzymes
SILAM	Stable isotope labelling in mammals
m/z	Mass to charge ratio
LC-MS	Liquid chromatography-mass spec
FDR	False discovery rate
GO	Gene ontology
KEGG	Kyoto encyclopedia of genes and genomes
PC	Principle component
BIP	Binding immunoglobular protein
VINC	Vinculin
PDI	Protein disulfide isomerase
UPR	Unfolded protein response
ENPL	Endoplasmin
ACT	Actin
IPA	Ingenuity pathway analysis
NDUF	NADH:ubiquinone oxidoreductase supernumeracy
PGAM	Phosphogylcerate mutase family protein
PKM	Pyruvase kinase

Contents

Chapter 1: General Background

There are three types of muscle in vertebrates: smooth, cardiac, and skeletal. Cardiac and smooth muscles are largely involved in involuntary processes. Cardiac muscle facilitates contraction of heart tissue and the smooth muscle is found in the respiratory, circulatory, digestive, and reproductive tracts (Martini et al. 2017). Skeletal muscle is the only muscle type under conscious control and its main purpose is to generate force between two bones to enable movement. The body contains approximately 660 individual muscles which operate under nervous stimulation, and together, they enable the full range of movements of the human body as well as of postural and temperature control (Miller et al. 2017). The mass of skeletal muscle comprises over a third of total body weight of a human (Janssen et al. 2000).

As we age, a reduction in skeletal muscle mass and function occurs (Larsson et al. 2019) which impacts significantly on the quality of life of older people. Inflammation is described as the main driver of skeletal muscle atrophy although the mechanisms responsible are poorly understood (Curtis et al. 2015). Skeletal muscle is proposed to be a source of cytokines and it is hypothesised that they play a role in the hyperinflammatory state presented in old age. The overall aim of the work carried out in this thesis was to investigate the role of skeletal muscle as an endocrine organ during systemic inflammation of ageing (inflammaging) and the potential mechanisms involved.

1.1 Muscle Structure and Function

The primary cell type of muscle tissue is a multinucleated, post mitotic muscle fibre. These muscle fibres (or myofibres) are the functional cell unit of muscle and contain the cellular machinery to allow contraction of muscle. Muscle also contains vasculature, nerve axons, fat and connective tissues. Bundles of muscle fibres are arranged in a layer of connective tissue called the perimysium. The muscle is surrounded by another layer of connective tissue known as the epimysium (**Figure 1.1**) (Frontera & Ochala 2015).

Muscle fibres contain highly specialised organelles called myofibrils. These account for up to 80% of total volume of the muscle (Huff-Lonergan 2009). The function of muscle relies on the contractile machinery, which is internal to each myofibril. The two major protein constituents of muscle are actin and myosin, with myosin accounting for around 25% of the total protein content of muscle (Balagopal et al. 1997). These proteins exist in a highly organised structure with repeating units referred to as sarcomeres between fixed structures termed Z-disc (Draper & Hodge 1949). This repeating structure gives muscle its striated appearance when observed longitudinally (**Figure 1.1**).

Muscle fibres contain another muscle specific organelle called the sarcoplasmic reticulum which holds a large store of calcium ions (Ca^{2+}) (Kawai & Konishi 1994). Invaginations in the muscles sarcolemma called transverse tubules (t-tubules) which are large internalised networks of plasma membrane (Jayasinghe & Launikonis 2013). These are coupled with the sarcoplasmic reticulum via dihydropyridine and ryanodine receptors allowing for voltage activated Ca^{2+} release. This is needed for the rapid and coordinated release of Ca^{2+} into the cytoplasm (Santulli et al. 2017). The sarcoplasmic reticulum and t-tubules form triads in close proximity to myofibrils (Ogata & Yamasaki 1997).

Due to their high energy requirements, muscle fibres also contain a large number of mitochondria in order to supply energy in the form of adenosine triphosphate (ATP). The mitochondria in muscle have been shown to be part of networks with the sarcolemma and t-tubule triads (Ogata & Yamasaki 1997).
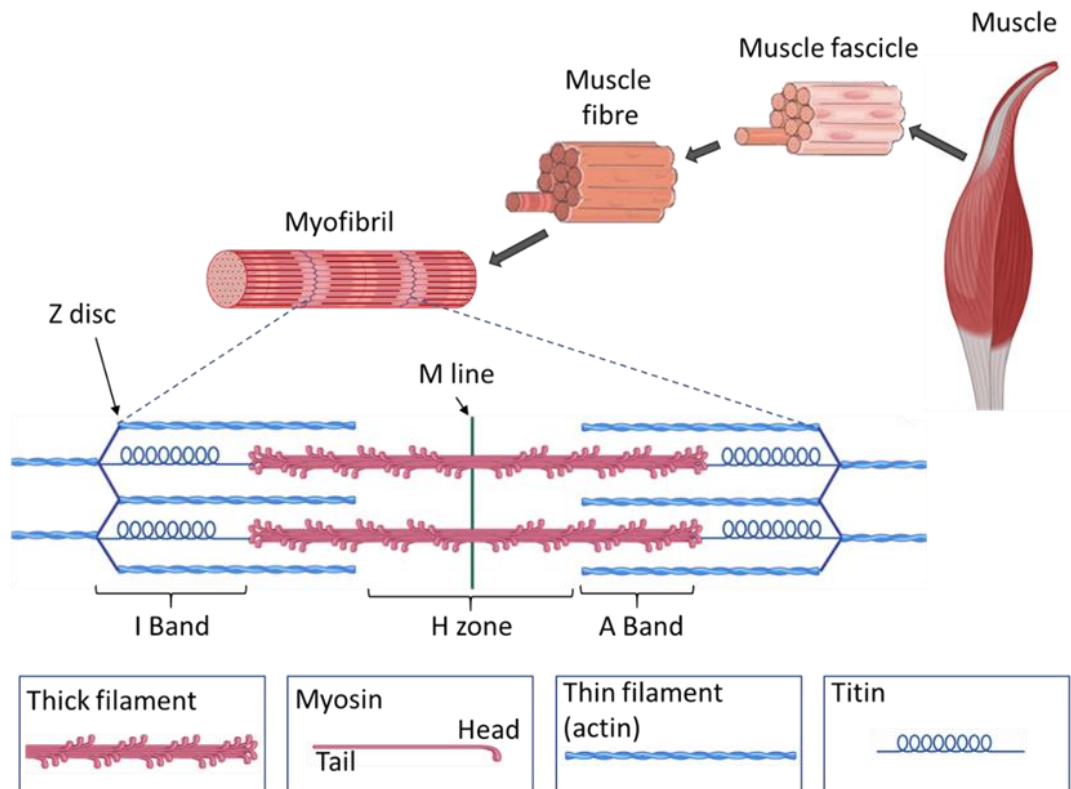
Figure 1.1: The composition and structure of muscle tissue. Muscle tissue can be divided into muscle fascicles containing single muscle fibres. *Single muscle fibres contain the contractile organelles, "myofibrils" which are formed of sarcomeres. The major components of these sarcomeres are myosin (present in the thick filament), and actin (present in the thin filaments). Drawn using BioRender (BioRender, Toronto, Canada)*

1.1.1 The sarcomere

The two major functional protein components of the sarcomere are myosin and actin. These proteins exist in all mammalian cells to facilitate cell motility and intracellular transport and localisation of organelles and macromolecules (Barlan & Gelfand 2017). The actin forms helical filaments which can act as rails for the myosin motor proteins to translocate across. The class of myosin present in the sarcomere is myosin II of which there are 15 subtypes.

All type II myosins are hexamers composed of two parallel myosin heavy chains (MyHCs). These form alpha helices 1500 Å in length called the rod section, connected by a lever arm region, converter domain and motor domain to two globular myosin heads. An essential

myosin light chains (MyLCs) and a regulatory MyLC associate close to the head domain of each MyHC (Rayment & Holden 1994). The motor domain is the enzymatic region which contains the ATP binding site and actin binding face (Rayment et al. 1993).

Each thick filament of sarcomeres is formed of around 200-400 molecules of aggregated myosin proteins, staggered by interspaced helices forming a helix of myosin heads (Au 2004; Hu et al. 2016) The filaments are joined by proteins found in the M-line; the section of the sarcomere in the centre of the bare region of myosin thick filaments mainly containing myomesin (which anchors myosin rods), creatine kinase and M-protein forming a hexagonal lattice. This section gives stability to the sarcomere au (Au 2004). Titin (also known as connectin) anchors the myosin to the Z-disc, introducing an elastic force to oppose the stretching of sarcomeres. This ensures the M line is always centrally positioned in the sarcomere. The z-disc is a lattice structure at adjoining each sarcomere which is bound to titin and actin filaments (Clark et al. 2002) (**Figure 1.1**).

Actin filaments are formed primarily of the monomer: globular actin (G-actin). These monomer proteins polymerise to form filamentous actin (F-actin) along which runs the regulatory proteins tropomyosin and troponin (Hanson & Lowy 1963; Von Der Ecken et al. 2015). Tropomyosin is formed of a rod of 2 alpha helical around 40 nm in length. In relaxed muscle, tropomyosin interacts with the 1 and 2 subdomains of 7 monomers of G-actin. Another part of this complex is 1 troponin complex formed of 3 components: Troponin C (TnC), Troponin I (TnI) and Troponin T (TnT). TnC can detect the presence of Ca^{2+} ions, TnI is an inhibitory unit and TnT is the unit which interacts with tropomyosin (Greaser & Gergely 1973; Bowman & Lindert 2019). In muscles in the resting state, the helical structure of tropomyosin is wrapped around the F-actin, preventing interaction with the myosin heads (Risi et al. 2017; Pirani et al. 2005).

1.1.2 Sliding filament theory and excitation contraction coupling

The sliding filament theory was first composed by Huxley and Niedergerke in the 1950s (Huxley & Niedergerke 1954; Huxley & Hanson 1954). In this model, the thick and thin filaments are interspaced in a regular pattern throughout the sarcomere. The actin filament contains myosin binding clefts for the cross linking of the myosin head. In muscles relaxed state, tropomyosin is bound to the binding clefts, interrupting the interaction of actin and myosin (Pirani et al. 2005; Gordon et al. 2001). The most relaxed state of muscle is where the myosin heads are doubled back on to the tail in a configuration termed the interacting head motif (IHM); the purpose of which is to reduce the ATP requirement (Hyun et al. 2008).

Upon nerve stimulation, the increase in Ca^{2+} concentration causes a conformational change in tropomyosin allowing the myosin head to move across the actin and through the repeat of this motion, muscle contraction occurs (Risi et al. 2017). Each cycle requires the hydrolytic conversion of ATP into adenosine diphosphate (ADP) and inorganic phosphate (Pi) via an ATPase enzyme. Here ATP starts bound to the myosin head (M-ATP) and is hydrolysed to form M-ADP-Pi. This head can bind to actin resulting in the formation of A-M-ADP-Pi. Actin binding to the complex results in the release of Pi and ADP allowing the level arm to rotate, moving the actin and myosin relative to each other. AM then binds ATP allowing the actin to detach giving the start product of M.ATP (**Figure 1.2**). This is known as the contraction cycle (Wittinghofer & Geeves 2016; Squire 2019).
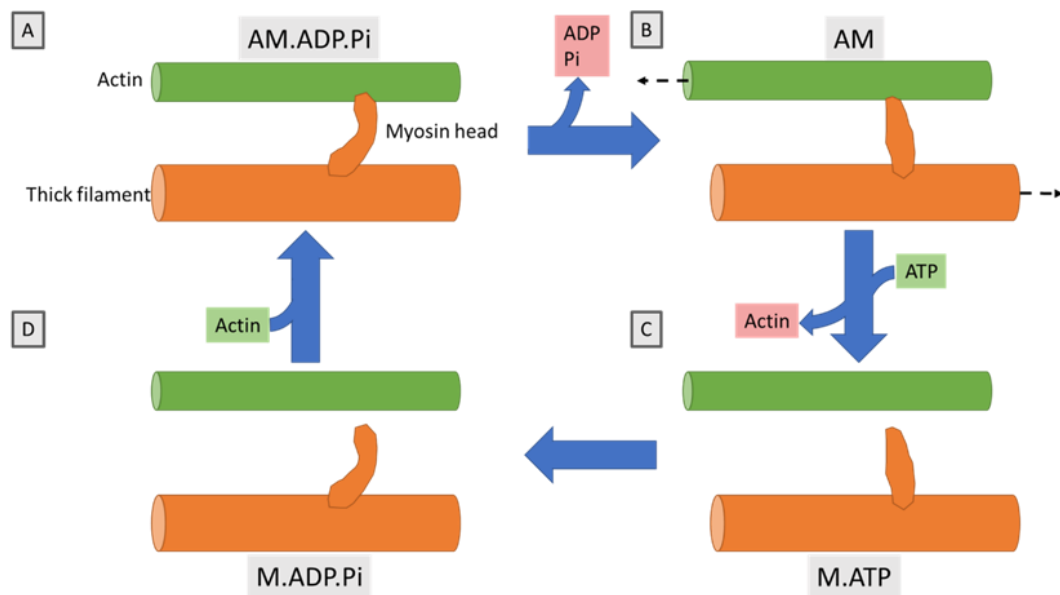
Figure 1.2: Simplified scheme of the ATP dependent contractile cycle. *The attached state (A), end-state following the release of ADP (B), detached state initiated by the binding of ATP (C) and hydrolysis of ATP resulting in the myosin head conformational change (D). Adapted from Squire, (2019)*

Contraction begins with an incoming action potential down the t-tubule sarcolemma. This is detected in the triad by the dihydropyridine receptor in the sarcolemma and the signal is transduced via a conformational change to the ryanodine receptor releasing large quantities of Ca^{2+} ions from the sarcoplasmic reticulum (Schneider 1994; Ikemoto & Yamamoto 2000). The high concentration of Ca^{2+} results in ions of Ca^{2+} binding to the troponin complex component, TnC, which allows the disassociation of tropomyosin from the actin filaments (Gordon et al. 2001; Risi et al. 2017). This in turn allows interaction between the thick and thin filaments resulting in the initiation of the contraction cycle described in **Section 1.1.3**.

1.1.3 The neuromuscular junction

The neuromuscular junction (NMJ) is the centre point of the motor unit where the motor unit is a distal motor neuron and the fibres it innervates. NMJs include the nerve terminal (pre-synapse), the synaptic cleft and the motor endplate on the muscle fibre (post-synapse)

and is how the nerve and muscle communicate a signal to contract using acetyl choline (ACh).

An overview of the synapse is shown in **Figure 1.3**.
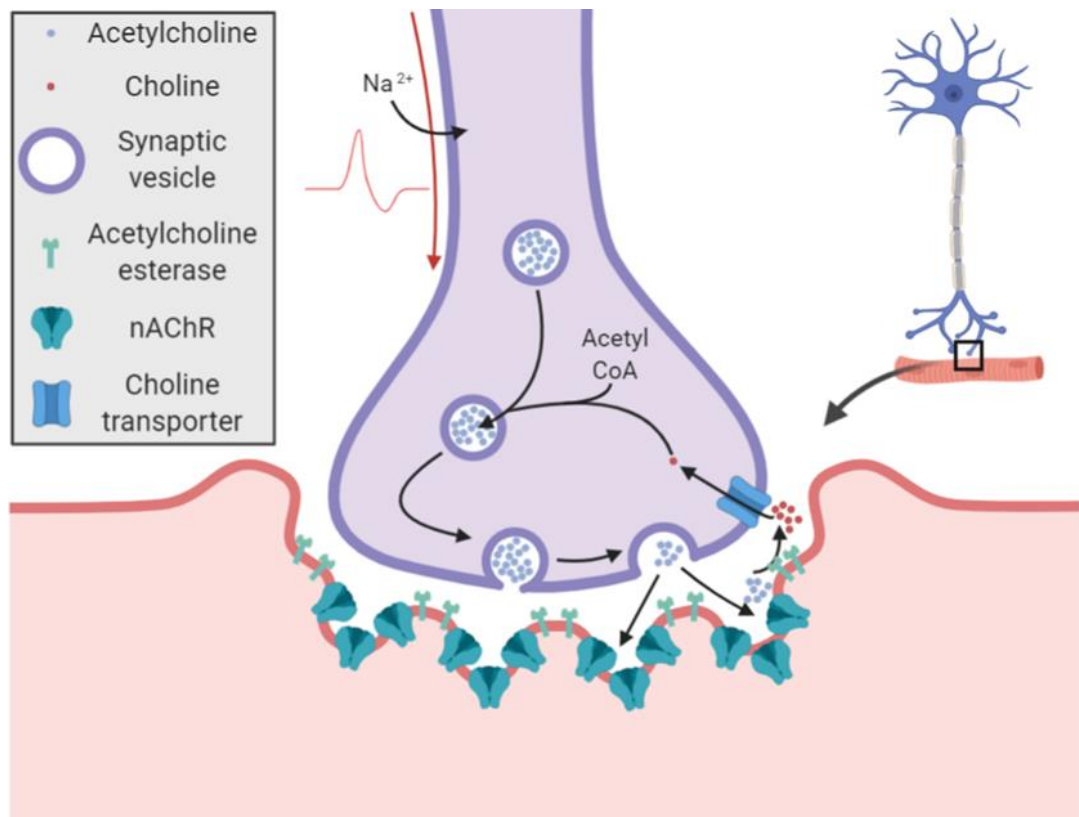
Figure 1.3: Schematic of the neuromuscular junction showing the presynaptic distal motor nerve, synaptic cleft and post synaptic motor endplate. The incoming action potential through the motor nerve allows the release of acetyl choline from vesicles into the synaptic cleft to act upon nicotinic acetyl choline receptors on the endplate. The acetyl choline is then broken down into acetate and choline by acetyl choline esterase in the synaptic cleft to be transported back into the nerve axon for recycling. Drawn using BioRender (BioRender, Toronto, Canada).

1.1.3.1 Pre-synapse

ACh is synthesised from acetyl-Coenzyme A CoA in the distal motor neuron where it is then packed, in an energy dependent process, into vesicles. These vesicles are mostly kept in close proximity to the nerve membrane opposing the nicotinic ACh receptors (nAChRs) of the muscle fibre across the synaptic cleft (Rizzoli & Betz 2004). NMJs are highly reliable due to

both the ACh vesicles and the receptors being well in excess of what is needed to propagate a signal for contraction (Hunter et al. 2016).

Vesicle attachment and fusion to the plasma membrane is in response to an incoming action potential (AP). The AP leads to an influx of Ca^{2+} ions through voltage gated calcium channels. The increase in Ca^{2+} activate the soluble N-ethylmaleimide-sensitive fusion protein attachment protein receptors (SNARE) proteins to attach and fuse the vesicles to the plasma membrane, releasing ACh into the synaptic cleft (Chanaday et al. 2019).

1.1.3.2 Post-synapse

The muscle motor endplate at the post-synapse is host to a large amount of nAChRs belonging to the cys-loop superfamily of ligand gated ion channels. nAChRs are made of 5 subunits with a central pore which can facilitate the movement of cations such as Na^+ and Ca^{2+} (Cheng et al. 2015). In muscle, 6 subunits exist: α_1, β_1, δ (foetal), γ and ε (adult). In muscle, the nAChRs always contain 2 alpha subunits, 1 beta unit, 1 gamma unit and either a delta or an epsilon subunits. In foetal muscle, the subunits co-assemble to form $\alpha_1\beta_1\gamma\delta$ receptors (Zouridakis et al. 2009). Soon after birth, the synthesis of the foetal delta subunit is outcompeted by the more stable adult epsilon unit in synchronicity throughout all fast muscle in response to receptor use with slow muscle showing some delay (Missias et al. 1996).

The nAChRs require 2 molecules of ACh to be activated acting at the (high affinity) $\alpha{:}\delta$ and (low affinity) $\alpha{:}\gamma/\varepsilon$ interfaces (Unwin & Fujiyoshi 2012). This results in a conformation change to the channel allowing the central core to open and increases the permeability of the motor endplate to Na^+ and K^+ ions (Dani 2016). There is an influx of Na^+ efflux of K^+ to the muscle fibre depolarising the end plate. This depolarisation is known as an end plate potential (EPP) and once this reaches a threshold, an action potential propagates across the sarcolemma (Dani 2016). This action potential causes an influx of Ca^{2+} ions into the muscle fibre leading

to the depolarisation of the t-tubule sarcolemma resulting in muscle contraction via excitation-contraction coupling. In resting conditions, miniature endplate potentials (MEPPs) can be recorded on the muscle. These are likely the result of the contents of single ACh vesicles being released and detected on the endplate. MEPPs do not depolarise the membrane of the muscle motor endplate to reach the endplate threshold potential and allow contraction (Sellin et al. 1996).

1.1.3.3 Synaptic cleft

The synaptic cleft is the 60-70 nm (in vertebrates) space between the distal nerve terminal membrane and the muscle endplate (Koper et al. 2012). This synaptic space has a meshwork of extracellular matrix ECM containing α and β laminins, agrin and collagens in order to a stabilise the synapse, ensure the topology of the synapse, and allow transmission across the synapse (Singhal & Martin 2011). The synaptic cleft also contains the enzyme, acetyl choline esterase, produced by muscle fibres, which hydrolyses the ACh to acetate and choline (Chan et al. 1999). Around 50 % of the choline is then transported back into the motor neuron to be recycled into more ACh (Črešnar et al. 1994).

1.1.4 Fibre types

The phenotype of individual muscle fibres are under the control of dynamic changes such as hormonal influence, response to injury, and age (Schiaffino & Reggiani 2011). The factors included in the phenotype include but are not limited to excitability, contraction mechanism, and metabolic preference (Schiaffino & Reggiani 2011).

Up until the late 1960s, muscle fibres have been divided into two categories: slow twitch (type 1; red) and fast twitch (type 2; white) fibres depending on how myoglobin rich the muscle is. Myoglobin, a haemoprotein not dissimilar to haemoglobin, provides muscle with an O_2 source to use in oxidative energy generation (Ordway & Garry 2004). Type 2 fibres can

be further subdivided into types 2A, 2X and 2B. Each fibre type and subtype has a defined myosin ATPase (Bárány 1967).

Type 1 fibres, also referred to as 'slow-oxidative' are innervated by relatively small axons with a smaller planar area, lower number of branches, and smaller branch length (Prakash et al. 1996). These fibres are highly resistant to fatigue from repeated and lengthy contraction (Lin et al. 2002). The major isoform of myosin heavy chain found in these fibres is MYHC1 coded by the *MYH7* gene (Haddad et al. 2008). Myosin light chain 2 (MyL2) is the regulatory MyLC isoform found in slow type 1 muscle fibres (Bicer & Reiser 2004). These fibres tend to be smaller, more vascularised, have higher mitochondrial content and use oxidative phosphorylation of triglycerides as their major fuel source (Schiaffino & Reggiani 2011). Type 1 muscle fibres are more prevalent in postural muscles such as the soleus giving the muscle its red appearance (Soukup et al. 2002). In the soleus, NMJs are larger in area, have a larger vesicle pool and the ACh is removed from the synaptic cleft slower than in muscles with predominantly type 2 fibres (Wood & Slater 1997; Reid et al. 1999; Sketelj et al. 1997).

The 3 subgroups of type 2 "fast" fibres, 2A, 2X and 2B are innervated by progressively larger axons respectively (Prakash et al. 1996). These fibres are less resistant to fatigue but are faster, more powerful and have a smaller cross-sectional areal (CSA) than the slow twitch fibres (Larsson et al. 1991). The major heavy chain isotype for type 2A (fast-oxidative) is MyHC2A transcribed from the *MYH2* gene and are fatigue resistant (Pandorf et al. 2006). Type 2A fibres use a mix of oxidative phosphorylation and glycolysis to produce energy and have lower mitochondrial content than type 2 fibres (Peter et al. 1972; Schiaffino et al. 1970). Type 2X fibres are less resistant to fatigue than type 2A and contain MHC2X coded by the *MYH1* gene (Haddad et al. 2008). These fibres use glycolysis to produce energy and as such have a higher glycogen content than type 1 and type 2A fibres (Greenhaff et al. 1993).

The final muscle fibre type, type 2B (or fast-glycolytic), is coded by the *MYH4* gene. These fibres staining for the type 2B ATPase, detect for MyHC-2X myosin (Smerdu et al. 1994). This fibre type is fast fatigable and is found in muscles used for fast, powerful movements such as the gastrocnemius (GTN) muscle (Burke et al. 1971). Fibres can also have feature of a mix of different fibre types. These are called hybrid fibre types and it has been shown that these fibre types exist on a spectrum and fibres type can be switched over time and is under hormonal control amongst other factors such as loading (Caiozzo et al. 2003).

1.2 Sarcopenia

1.2.1 Structural and functional changes in sarcopenia

Sarcopenia is described as the age-related loss of muscle mass and function (Larsson et al. 2019). Progressive age-related muscle atrophy is most likely the most dramatic and significant age-related decline in elderly humans. This atrophy incurs significant loss of muscle function, leading to slowing movement and weakness. With advancing age this can result in an increase in falls and so fall-related injuries and frailty eventuating in a loss of independence (Hemenway et al. 1994; Young and Skelton, 1994). Gaining an understanding of the process of age-related muscle loss is of the utmost importance due to an increasingly ageing demographic, likely as a result of improved health and living conditions. This understanding involves an observation of impairments in the central and peripheral nervous systems and the skeletal muscle system (Larsson et al. 2019).

The age-related loss of muscle mass is a muscle atrophy experienced by all mammals in the later stages of life. Intrinsic and extrinsic changes regulating muscle ageing in humans also occur in rodents, indicating that mice and rats are relevant models of human sarcopenia. A reduction in lean muscle mass, fibre number, fibre CSA and loss of motor unit number in a spectrum of muscles from humans and rodents has been shown with advancing age in the past 50 years (Lexell & Henriksson-Larsen 1983; Porter et al. 1995; Sayed et al. 2016;

Sakellariou et al. 2016; Tang et al. 2019; Brooks & Faulkner 1988; Sheth et al. 2018; McArdle et al. 2004; Walsh et al. 2015; Messa et al. 2019; Zhu et al. 2019).

This loss of function manifests as slow, inhibited or reduced movement of muscles resulting in the weaknesses leading to increases in fall related injuries amongst the elderly. A grip strength test in elderly patients is a good predictor of impaired mobility and physiological age (Souza Saraiva et al. 2019). Strength in a mixed human cohort was significantly reduced in forearm, hip and knee muscles with isometric, concentric and eccentric knee extensions being reduced to by 30-40% (Kasukawa et al. 2017; Frontera et al. 2000; Porter et al. 1995). In mice, fore limb strength has been observed to be reduced with grip strength testing and hind limb measurements of a spectrum of muscles have shown a reduction in force generation *in-* and *ex-vivo* (Ge et al. 2016; Brooks & Faulkner 1988; Sheth et al. 2018; McArdle et al. 2004).

Loss of neuromuscular integrity has long been considered a major feature of muscle ageing. Ageing is associated with loss of whole motor units and motor neurons. The loss of muscle that occurs with ageing occurs with loss of motor units in both humans and rodents (Campbell et al. 1973; Sheth et al. 2018). In young and adult humans and animals, damage to terminal axons and motor unit turnover occurs during everyday activities and is repaired by sprouting and regrowth of axons from the damaged nerve leading to rapid re-innervation of NMJs (Delbono 2003). With increasing age, re-innervation does not occur appropriately and re-innervation by sprouting from adjacent axons or NMJ occurs (Larsson & Ansved 1995). The effect of this is an increased grouping of fibres of a single type (Larsson & Ansved 1995) with the formation of "giant" motor units which are eventually lost (Matthews et al. 2011). A 25–50% reduction in the number of motor neurons occurs in man and rodents with ageing (Rowan et al. 2012; Tomlinson & Irving 1977) with selective loss of large fast α-motor neurons (Narici & Maffulli 2010; Sonjak et al. 2019). Studies have reported loss of innervation

of individual fibres in muscles of older individuals. During ageing in humans and rodents, NMJs become fragmented from their usual "pretzel-like" structure to a broken and fragmented (Arizono et al. 1984; Valdez et al. 2010). Our research group have reported that ~15 % of individual muscle fibres from (26-28 month) old mice were completely denervated and ~80 % of NMJs showed disruption (Vasilaki et al. 2016). Maintenance of the NMJ is increasingly seen to be key to interventions that may maintain muscle mass and function in older age (Ham et al. 2020).

This NMJ disruption is likely the product of neuronal degradation leading to a loss of muscle-nerve communication leading to disassembly of the nAChR clusters on the motor endplate. The effects of this disruption and denervation are likely to be multiple. Evidence suggests that there is considerable reserve in the overlap of pre- and post- synaptic structures such that overlap is well in excess of what is needed to propagate a signal for contraction (Hunter et al. 2016). In contrast, there is evidence that reduction or loss of neuronal input can lead to muscle fibre atrophy potentially due to an increase in oxidative stress (Staunton et al. 2019; Pollock et al. 2017; Scalabrin et al. 2019).

1.2.2 Mechanisms Responsible for the Development of Sarcopenia: Role of Reactive Oxygen Species (ROS) and Inflammation

1.2.2.1 Altered Reactive oxygen species (ROS) Generation and Muscle Ageing.

Reactive oxygen species (ROS) are extremely reactive molecules derived from molecular oxygen. ROS are thought to be predominantly produced by the mitochondria as a product of the electron transport chain (Chen et al., 2003). The main source of ROS is thought to be the mitochondria; however recent studies have identified other sources of ROS (Sakellariou et al., 2013). ROS have vital roles in cell signalling; however, in excess they can also cause damage to macromolecules (Powers et al., 2010). ROS production is relatively high in skeletal muscle, as skeletal muscle has high oxygen consumption and it is well known that ROS, in

particular superoxide, are produced during skeletal muscle contraction (Reid et al., 1992; Sakellariou et al., 2013).

To counteract the production of ROS, cells have an antioxidant defence system which converts ROS into none or less damaging products to prevent any deleterious effects. The antioxidant defence system includes antioxidant defence enzymes such as the superoxide dismutases (SODs) and catalase. ROS are implicated in the ageing across all organs in all species due to the increase in oxidative damage to lipids, proteins, and nucleic acids such as DNA (Harman 1956). Muscle fibres have a high capacity for energy metabolism, and as such generate a large amount of ROS and reactive nitrogen species by NAD(P)H oxidase enzymes in the plasma membrane and by mitochondria and t-tubules (Sakellariou et al. 2014b). Fundamental changes in redox signalling and homeostasis occur during ageing (Jackson & Mcardle 2011).

Denervation of muscle, such as that seen in muscle of old mice and humans, leads to mitochondrial dysfunction and increased muscle generation of ROS, and it is proposed that this is the mechanism by which atrophy occurs (Scalabrin et al. 2019; Pollock et al. 2017).

1.2.2.2 *Models of Modified ROS: Focus on the SOD1KO mouse as a model of accelerated sarcopenia.*

In non-mammalian models, some interventions designed to reduce the activities of ROS, such as overexpression of CuZn, superoxide dismutase (SOD1), catalase or both in Drosophila (Orr & Sohal, 1993; 1994; Orr et al, 2003) or treatment with a MnSOD (SOD2) and catalase mimetic in C. Elegans (Melov et al, 2000) extended lifespan, but these effects are not universally observed and are controversial (Gems & Doonan, 2009). In mammals, only few genetic manipulations designed to reduce ROS activities have resulted in increased lifespan (Schriner et al, 2005; Yoshida et al, 2005). Many studies have reported that mitochondrial ROS generation is increased in skeletal muscle during ageing (see Van Remmen & Jones, 2009

for a review) and that this occurs in association with impaired mitochondrial function and oxidative damage to mitochondrial components (Jang & Van Remmen, 2009). There are some studies that indicate manipulation of ROS activities can preserve muscle function during ageing (Schriner et al, 2005; Broome et al, 2006).

Superoxide dismutase (SOD) was first discovered by McCord and Fridovich (McCord et al., 1969) and is responsible for the dismutation of superoxide radical into hydrogen peroxide (H_2O_2) and oxygen. Mammalian skeletal muscle contains two prominent types of SOD; copper and zinc superoxide dismutase (CuZnSOD) and manganese superoxide dismutase (MnSOD). MnSOD is also known as SOD2 and is located in the mitochondria (Weisiger et al., 1973) with a manganese ion attached to its active site whereas CuZn is also known as SOD1 and contains copper and zinc. CuZnSOD is localised to mitochondrial intermembrane space and in the cytoplasm (Crapo et al., 1992). Mammalian skeletal muscle also expresses a third superoxide; extracellular SOD, which scavenges extracellular superoxide (Folz et al. 1999).

Mice lacking CuZn superoxide dismutase (SOD1KO mice) are born with a similar muscle mass to WT mice, but show a premature muscle ageing phenotype with an accelerated loss of muscle mass and function (Muller et al. 2007) that is also characterised by significant disruption of the motor neurons and NMJs (Deepa et al. 2019) (**Figure 1.4**). Disruption of nerve-muscle linkage in this model appears to result from loss of redox homeostasis in the motor neurons resulting in NMJ breakdown and loss of muscle mass and function (Sakellariou et al. 2014b).
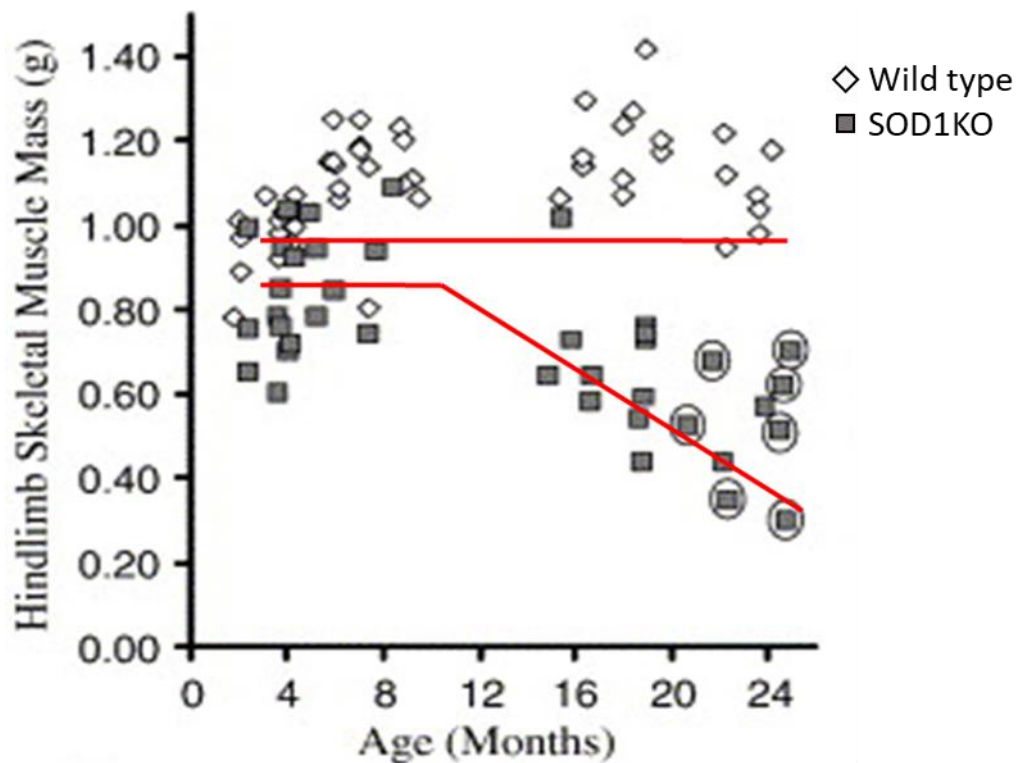
Muller et al, FRBM 2006

Figure 1.4: Increased ROS generation in the muscle of CuZn superoxide dismutase null mice results in accelerated loss of muscle mass and function (Muller et al. 2006)

The SOD1KO mouse has been shown to exhibit increased sensitivity to ROS (Huang et al. 1997). SOD1KO mice display many of the functional losses associated with frailty in humans (Deepa et al. 2017). SOD1KO mice have an accelerated decrease in body mass, adult mice demonstrate a decrease in wheel running capacity and performance on a Rota-rod test, and increase in oxidative damage to macromolecules (Muller et al. 2006). A significant decrease in mass of all muscle types is also observed, with the exception of the postural *soleus* muscle (Muller et al. 2006; Jang et al. 2010; Larkin et al. 2011). Alongside the loss of muscle mass, is a loss of muscle force generation, even when normalised to the cross sectional area of the muscle (Muller et al. 2006; Jang et al. 2010), suggesting a weakening of the remaining muscle in a similar manner to muscles of old mice and humans. The SOD1KO mice demonstrate a deterioration in the NMJs which is reflected in a parallel loss of synaptic function (Jang et al. 2010; Deepa et al. 2019; Larkin et al. 2011).

41

Several additional genetic manipulations have attempted to identify the importance of removal of Sod1 in individual tissues and the impact on the muscle loss and weakness. Thus, in SOD1KO mice where SOD1 has been rescued in the nerves, a significant level of muscle weakness was still observed but there was no overall muscle atrophy and therefore this cannot be considered to be a model of sarcopenia (Zhang et al. 2013; Sataranatarajan et al. 2015) but provided a mechanism by which knockout of SOD1 results in accelerated loss of muscle mass and function. In contrast, muscle specific knockout of SOD1 resulted in a minor decrease in overall force generation of gastrocnemius muscles, but surprisingly, an increase in muscle mass with no evidence of NMJ degeneration (Zhang et al. 2013; Sakellariou et al. 2014a), suggesting that altered ROS generation by muscles alone does not play a primary role in the muscle loss seen in SOD1KO mice. A neuron specific knockout of SOD1 resulted in a minor decrease in the mass of some muscles, most notably the quadriceps (Sataranatarajan et al. 2020). There was also a small but significant decrease in force generation from the GTN muscles (Sataranatarajan et al. 2020).

Based on findings from the above SOD1 knockout mouse models, there is a proposed, "two-hit" hypothesis – the first hit being a compromise to redox homeostasis in the neuron, and the second being an increase in mitochondrial ROS in muscle potentially affecting the ability of the muscle to respond to stress in support of the neuron, inducing further damage to the NMJs (Deepa et al. 2019).

The mechanisms by which imbalance in ROS homeostasis leads to muscle atrophy is unclear, but it is proposed that this may ultimately initiate the upregulation of proinflammatory signals in muscle, resulting in activation of nuclear factor kappa-light-chain enhancer of activated B cells (NF-κB) and chronic inflammation in the muscles and surrounding tissues (Meng & Yu 2010; McArdle et al. 2019).

1.2.2.3 Inflammation

Originally coined in 2000, 'inflammaging' is the term used to describe the association of increase inflammatory mediation with advancing age (Franceschi et al. 2000). Chronic inflammation is associated with numerous diseases associated with ageing such as cardiovascular disease, chronic kidney disease, type 2 diabetes and sarcopenia (Ferrucci & Fabbri 2018). These diseases are linked by both the prevalence in ageing and the occurrence of inflammatory mediators such as cytokines (Ferrucci & Fabbri 2018).

An increase in levels of inflammatory markers such as plasma Interleukin-6 (IL-6), Tumour necrosis factor alpha (TNF-α), and C-reactive protein (CRP) have been associated with a higher patient mortality and the onset of sarcopenia in a number of studies (Ferrucci et al. 2002; Bautmans et al. 2011). Elevated CRP is associated with low chair stand performance in men and women and loss of handgrip strength in men and women over 55 (Hamer & Molloy 2009). Studies have reported increases in Interleukin (IL)-1α, IL-1β, IL-6, IL-8, IL-10, IL-12, IL-13, granulocyte-colony stimulating factor (G-CSF), granulocyte/monocyte-CSF (GM-CSF), macrophage inflammatory protein (MIP)-1/CCL2, transforming growth factor (TGF)-α, interferon gamma-induced protein 10 (IP-10)/CXCL10, eotaxin/CCL11, tumour necrosis factor (TNF)-α, CCL2, CCL5 and CXCL10 within the plasma of humans with ageing (Kim et al. 2011; Wang et al. 2017; Hoefer et al. 2017; Valdez et al. 2010; Rea et al. 2018; Tung et al. 2015; Gerli et al. 2001; Bonfante et al. 2017). Administration of the common non-steroidal anti-inflammatory drug ibuprofen significantly decreased age related muscle mass in rats (Rieu et al. 2009) providing further evidence of a role for inflammation in the development of sarcopenia. The source of the systemic cytokines seen in old age is not known, however there are numerous proposed cells. We know that cells of the innate and adaptive immune systems producer relatively large amounts of cytokines and chemokines. Macrophages secrete various chemokines such as CXCL9, CXCL10 , and CXCL11 which can, in turn, recruit T-cells (Oneissi Martinez et al. 2008). Muscle accounts for around 40% of body mass, so an

increase in cytokine production and release by muscle fibres would potentially result in a considerable contribution to systemic inflammation (da Silva et al. 2019).

One proposed source of inflammaging is the increased presence of senescent cells. Cellular senescence was initially described by Hayflick in 1965 to describe the limit to the number of cellular division cycles a cell can perform (Hayflick 1965). Cells which have reached this limit are described as "senescent" and are characterised by replicative arrest, resistance to apoptosis, active tumour suppression pathways, chromatin rearrangement, and the development of the senescence associated secretory phenotype (SASP) (Khosla et al. 2020). The SASP varies between cells and tissues but generally includes the secretion of factors such as pro-inflammatory cytokines, chemokines, ROS, proteases, nucleotides and growth factors (Khosla et al. 2020; Kirkland 2013). Genetic ablation of senescent cells or administration of anti-senescence (senolytic) agents and removal of factors known to be involved in the SASP have alleviated age-related diseases in animal models and restored grip strength and activity in old mice (Xu et al. 2015). Implantation of senescent cells also reduced physical performance of mice (Xu et al. 2018). Knockout of senescent P16^{Ink4a} cells in mice successfully extended healthy lifespan and significantly reduced the age dependent deterioration of several organs including the kidneys, adipocytes and skeletal muscle (Baker et al. 2016; Baker et al. 2011).

The mechanisms by which an increase in systemic pro-inflammatory cytokines result in sarcopenia, at least in part, are unclear. A number of studies have shown that treatment of muscles and myoblasts with pro-inflammatory cytokines results in muscle weakness and atrophy and data from our laboratory suggest that this results in the activation of the NF-κB pathway via the increased production of mitochondrial ROS (Li & Reid 2000; Lightfoot et al. 2015). A chronic upregulation of NF-κB signalling and content have been observed in muscles of old mice (Vasilaki et al. 2006b; Vasilaki et al. 2010; Cuthbertson et al. 2005) and a chronic

increase in NF-κB DNA binding activity has also been reported in SOD1KO mice, alongside an increase in circulatory cytokines and some increased β-galactosidase stained cells (Vasilaki et al. 2010; Deepa et al. 2017). The NF-κB pathway is the major cellular pro-inflammatory pathway, known to upregulate catabolic processes through action on E3-ligases such as Murf-1 and atrogin-1 (Li et al. 2005; Gomes et al. 2001) and evidence of chronic activation suggests that this may be important in activation of degradation pathways in muscle of old mice.

The NF-κB activation process in muscle is complicated. In response to an acute period of exercise, particularly damaging exercise of healthy human muscle, a significant increase in NF-κB signalling is seen, followed by increased muscle expression of mRNA of cytokines (Hollander et al. 2001; Vella et al. 2012). This cytokine signalling results in an infiltration and activation of immune cells which take an active role in the tissue repair but may also contribute to further damage. NF-κB activation can also result in the activation of cytoprotective genes such as the antioxidant defence proteins (McArdle et al. 2002; Toumi et al. 2006) NF-κB activation in skeletal muscle derived myoblast cells can been achieved with exposure to increasing concentration of H_2O_2 (Sen et al. 1997; Zhou et al. 2001). In the muscle of old mice and SOD1KO mice, muscle shows an inability to activate NF-κB signalling post exercise, in a similar manner to muscles of old mice (Vasilaki et al. 2010; Vasilaki et al. 2006b).

1.3 NF-κB signalling

1.3.1 Overview

The NF-κB pathway is the major intracellular inflammatory system which exists in most multicellular organisms (Ryzhakov et al. 2013; Silverman & Maniatis 2001). In animals, this transcription factor is central to coordinating inflammation, adaptive and innate immune responses, cell differentiation, proliferation, and survival (Silverman & Maniatis 2001).

The NF-κB family of proteins consists of 5 monomers and their active dimers which form the NF-κB transcription factor, acting on the κB sequence of DNA. NF-κB is under the control of specific inhibitors of NF-κB (IκB) which are coordinated by IκB kinases (IKK) through post translational modification (Hoffmann et al. 2003). This signalling pathway is split into two major branches, the canonical pathway and the non-canonical pathway and though these have commonalities, they are distinct pathways with different stimuli and downstream resolutions (Pires et al. 2018).

1.3.2 NF-κB monomers and dimers

1.3.2.1 Monomers

Transcription via the NF-κB pathway is controlled primarily by five protomers: p65 (RelA), RelB, c-Rel, p50 and p52 (Hoffmann et al. 2003). These can be broken into type I (p65, RelB, and c-Rel) and type II (p100/p52, and p105/p50) NF-κB proteins. The active monomers of the type II proteins cleaved from the larger precursor proteins p105 and p100 to form p50 and p52 respectively (Qing et al. 2007; Li & Ghosh 1996).

The NF-κB monomers all contain the rel homology domain proximal to the N terminal. The rel homology domain is a 300 amino acid domain which is critical to allowing the association of these monomers to form functional dimers, the process of nuclear location and DNA binding, and IκB interactions (Baldwin 1996). The rel homology domain facilitates these processes through containing the proteins N-terminal domain, dimerisation domain and nuclear location signal. The dimerization domain and N-terminal domain enable dimerization of the NF-κB monomers and the nuclear location signal is a flexible domain which adopts specific conformations depending on binding to other proteins such as IκB and importin proteins in the nuclear envelope (Friedrich et al. 2006).

The rel homology domain proteins also contain a c-terminal transactivation domain which is not structurally conserved between subunits but exists functionally. The two monomer

products of precursor proteins, p50 and p52, do not contain transactivation domains and therefore, are not transcriptionally active (Smale 2012). They contain a glycine rich region which is an artefact from the proteolytic processing. The three transcriptionally active relish (rel) homology domain proteins are p65, c-Rel and RelB in order from most to least potent (Mitchell et al. 2016).

1.3.2.2 Dimerisation of NF-κB

The ~100 amino acid dimerization domain of NF-κB was discovered via the first crystal structure of the rel homology domain bound to DNA (Ghosh et al. 1995). Around 12 – 15 residues participate in the dimerization of NF-κB monomers and very few of these residues contribute to the bonding energetically. The RelB dimerization domain has an atypical topology consisting of two intertwined monomers which could influence its effects on DNA binding affinities (Huang et al. 2005).

The five NF-κB transcription factor monomers can form 15 possible combinations of dimers. Of these, 12 are considered to bind to the DNA κB sequence of which 9 contain at least 1 protein containing a transactivation domain (p65, RelB or c-Rel). Three can bind DNA but do not contain a transactivation domain so would only function as activators with additional coactivators (Smale 2012). The remaining three possible dimers form low affinity dimers which cannot bind DNA but may coactivate with the B cell lymphoma (Bcl3) or IκB proteins, or could act as repressors of NF-κB signalling (Fujita et al. 1993; Yamamoto & Takeda 2008) (**Figure 1.5**).

	p65	RelB	cRel	p50	p52
p65	p65 p65 *				
RelB	p65 RelB Δ	RelB RelB Δ			
cRel	p65 cRel *	RelB cRel Δ	cRel cRel *		
p100	p65 p50 *	RelB p50 *	cRel p50 *	p50 p50 X	
p105	p65 p52 *	RelB p52 *	cRel p52 *	p50 p52 X	p52 p52 X
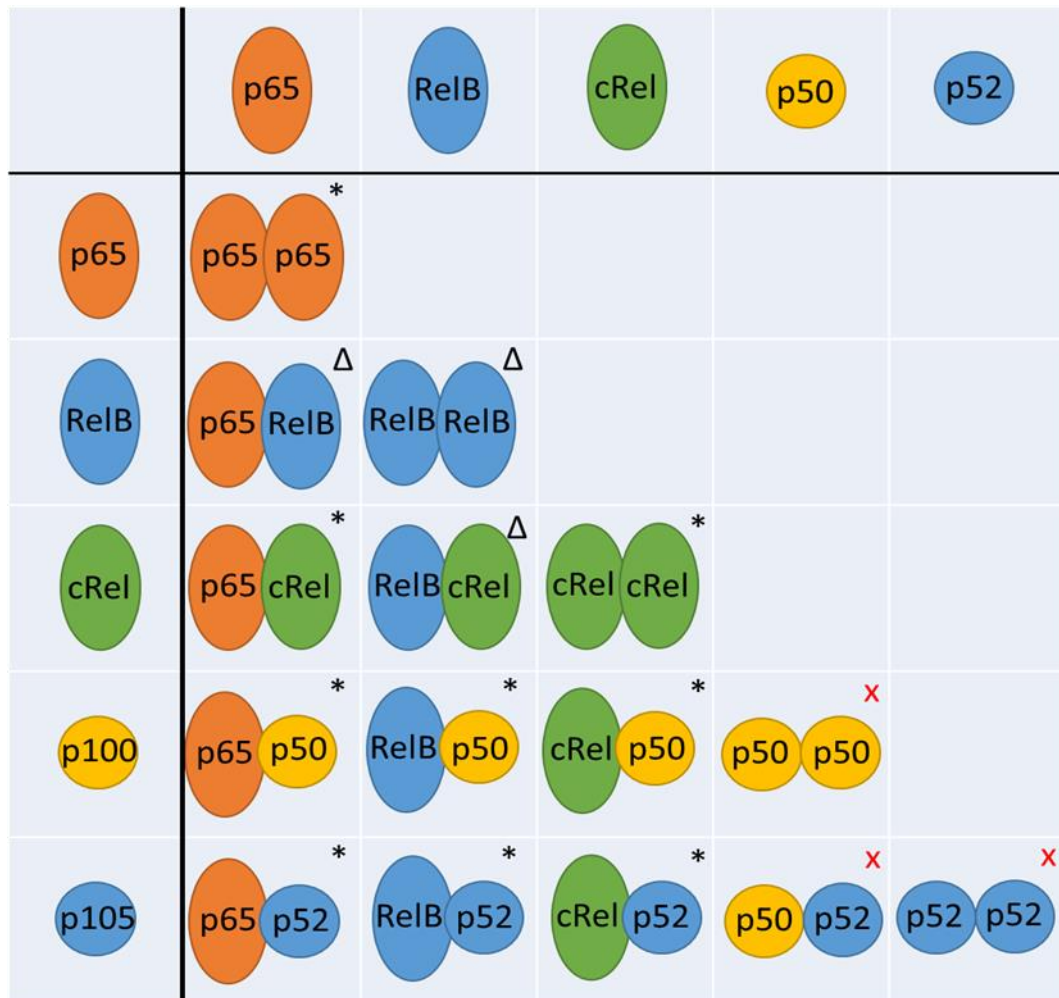
Figure 1.5: Transcriptional activity of each of the 15 NF-κB dimers. *denotes dimers which contain at least 1 transactivation domain and therefore bind DNA and actively allow transcription of downstream products. Δ denotes dimers which function as activators only with functional co-activators and X denotes dimers which form low affinity dimers which do not have transactivation activity by themselves.*

The NF-κB dimers exist at different levels in different cells (Phelps et al. 2000). The dimers exist in various relative amounts which can largely be attributed to the binding affinities of the monomers to one another, the expression of monomer genes, activation of precursor proteins (via partial proteasomal degradation), and dimer degradation (Ghosh et al. 2012). In terms of expression of the monomer genes, p65 and RelB are highly expressed across most cell types whereas c-Rel expression is confined to lymphoid and dendritic cells (Liou & Hsia 2003). It is understood that all of the NF-κB monomers are transcriptional targets of p65

mediated transcription including p65 itself (Bren et al. 2001; Sung et al. 2014; Almaden et al. 2014).

Although there is a lack of quantitative evidence, when observing p65 and p50 monomers, the p65:p50 heterodimer is the most prevalent dimer in most cell types, followed by the p50 homodimer. The p65:p50 heterodimer has been shown to have the highest binding affinity with the two homodimers of its constituent monomers being lower in binding affinity (Tsui et al. 2015). It is therefore postulated that the general rule is dimers formed of a type I (p65, RelB, and c-Rel) and a type II (p100/p52, and p105/p50) subunit have the highest stability, dimers of two type I subunits have the lowest with dimers formed of type II subunits being in between these two (Mitchell et al. 2016).

1.3.2.3 NF-κB DNA binding

Early in the discovery of the NF-κB pathway, the DNA binding consensus region was determined to be 5'-GGGRNWYYCC-3' where R is a purine, N is any base, W is either adenine or thymine and Y is a pyrimidine (**Figure 1.6**). The sequence has been shown to be variable with these variations having preferences for different dimers (Kunsch et al. 1992). The sequence can be variable in length (9-11 bps) and variable in its sequence and still have affinity for certain NF-κB transcription factors. The human genome is known to contain just under 14,000 NF-κB binding regions (Zhao et al. 2014). The entire rel homology domain is needed to allow NF-κB to bind and its DNA binding region is much larger than the DNA binding regions of other conventional transcription factors (Kuriyan & Thanos 1995).

More recently, the pseudo-palindromic NF-κB consensus sequence has been recognised as two half-site sequences: each half site being responsible for the binding of one monomer of the dimer pair. The type I subunits interact with a 5 bp half-site whereas type II interact with a 4 bp half site. For this reason, the active site can be preferred by two 4 bp half-sites, two 5 bp subunits or a 4 bp plus a 5 bp subunit (Siggers et al. 2012). Between these half sites is a

central base pair which is not contacted by either subunit; this is usually A:T and can be used as a central point of reference for studying the κB site sequence. The central base pair plus the two 4-5 bp extensions result in the κB site being between 9 and 11 bps (**Figure 1.6**) (Siggers et al. 2012).
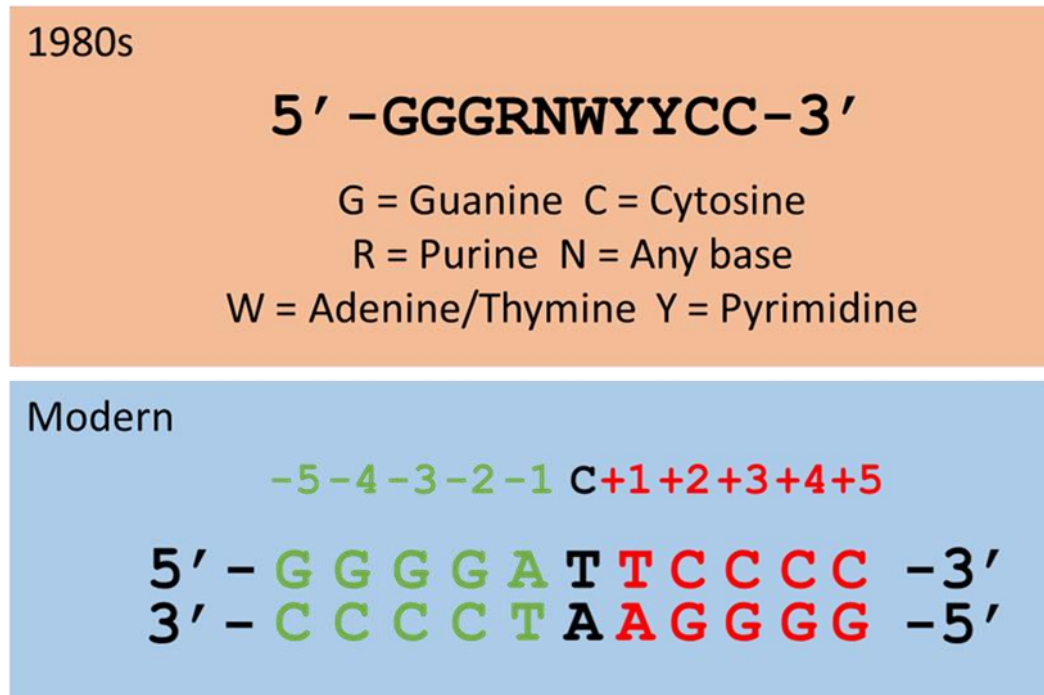
Figure 1.6: The originally derived classic consensus region of the κB DNA element (upper panel) and the nucleotide sequence of the major histocompatibility complex (MHC) κB region with one half site highlighted in red and the other in green and the central position in black (upper panel).

Single nucleotide variations in the κB signal can dramatically affect the contact through the contact of NF-κB subunits or the dynamics of NF-κB binding making these sites complex to study (Leung et al. 2005). In addition to this, non-classical sites exist which can use different coactivators for the induction of NF-κB transcription (Wang et al. 2012). Most studies that have examined κB binding sites have used the cytokines, TNFα and IL-1β, or lipopolysaccharide (LPS) to induce NF-κB activation which would preferentially activate the canonical pathway and thus will bias the discovery of canonical κB sites.

1.3.3 IκB family

The function of IκB proteins is to stablise NF-κB in the cytoplasm rather than the nucleus. In doing so, NF-κB cannot bind to DNA and is therefore, transcriptionally inactive. There are eight known IκB proteins which contain ankyrin repeat domains; a 33 amino acid helical motif which complexes with at least one dimer of NF-κB (Huxford et al. 1998). Three of these mediate the classical NF-κB binding and are susceptible to proteasomal degradation. These are IκBα, IκBβ and IκBε and contain 6 ankyrin repeats flanked by two flexible unstructured sequences. The flexible region contains a high proportion of proline (P), glutamic acid (E), serine (S), threonine (T) residues and is consequently termed a PEST domain (Rogers et al. 1986). This feature is common to high turnover proteins (Ghosh et al. 2012).

IκBα, IκBβ and IκBε preferentially bind to dimers containing a p65 or c-Rel monomer (Malek et al. 2003). The prototypic member of this family is the IκBα protein. This readily complexes with p65:p50 dimers through a number of binding interactions. IκBα interacts with the homodimer mainly through the ankyrin repeat domain of the IκBα and dimerization domain of the NF-κB dimer (Huxford et al. 1998). In addition to this binding, IκBα also contacts the rel homology domain of p65 (Huxford et al. 1998). IκBα directly blocks the DNA binding cleft of p65:p50 dimer (Jacobs & Harrison 1998). The IκBα:p65:p65 complex is very similar to that of IκBα:p65:p50 (Malek et al. 2003).

When free of dimers, only the first four ankyrin repeats in IκBα adopt their fully folded and most stable structure (Croy et al. 2004). The remaining two and the PEST region, however, are not folded which is rare as ankyrin repeat domain proteins are usually a highly stable structure. The two other ankyrin repeats adopt a folded structure with the binding of an NF-κB dimer. This energetically pushes the binding of IκBα to NF-κB (Bergqvist et al. 2006). This is a reason IκBα needs to be fully degraded in order for NF-κB dimers to freely enter the

nuclei. Mutant, pre-folded IκBα does not bind with as great affinity to NK-κB (Truhlar et al. 2008).

The c-terminal of p105/IκBγ and p100/IκBδ are similar in structure to IκBs and can associate with dimers of NF-κB forming large complexes (Savinova et al. 2009). Dimers containing p105, c-Rel and processed p50 can be bound by p105 and dimers containing RelB, p52 and similarly p65 can be bound by p100 (Savinova et al. 2009). Through complete proteasomal degradation of these atypical inhibitors releases the dimer allowing nuclear translocation and DNA binding.

1.3.4 IKK complex

The IKK complex is the term for the complex of proteins responsible for phosphorylating the IκB proteins resulting in their ubiquitination and degradation. There are 4 kinases in the IKK family. These are IKKα, IKKβ, IKKε and TANK-binding kinase 1 (TBK1) (Ghosh et al. 2012). The two latter kinases are involved in the NF-κB pathway but are not involved in tagging the IκB proteins for degradation. Each of the kinases contains a kinase core domain, a leucine zipper motif which facilitates dimerisation, a helix-loop-helix domain and a c-terminal domain to interact with NF-κB essential modulator (NEMO) (Zandi et al. 1997). IKKα and IKKβ can form homo- and heterodimers but there is also a more common trimeric form. The trimeric IKK complex is composed of 3 subunits: IKKα, IKKβ and NEMO. NEMO contains two conical coiled domains, a leucine zipper motif, a zinc finger, and dimerization domain (Barczewski et al. 2019).

IKKβ is the subunit responsible for the phosphorylation of IκBα and can be activated by several upstream kinases. For example, transforming growth factor-β-activated kinase 1 activates IKKβ through phosphorylation of two residues (Ser177 and Ser181), activating its function (Wang et al. 2001) and so activating NF-κB.

1.3.5 The canonical pathway for NF-κB activation

The canonical NF-κB pathway is characteristically the action of the IKK complex on IκBα to release the p65:p50 dimer. While this is paradigmatic of the canonical pathway, it can also include other dimers and inhibitors. This pathway can be activated by several cytokines, pathogen associated molecular pattern molecules (PAMPS), damage associated molecule pattern molecules (DAMPS; one of which is ROS) and proteins in the antigen immune recognition pathway (Zhang et al. 2017).

The most well characterised canonical response to a stimulus is the cascade following TNFα binding to a TNF receptor (TNFR). Upon the binding of this ligand to its receptor allows the recruitment of adaptor proteins such as receptor-interacting serine/threonine-protein kinase 1, TNFR type 1-associated DEATH domain protein, TNFR associated factor (TRAF)2, cellular inhibitor of apoptosis protein-1 (cIAP), TAK1-binding protein and mitogen associated kinase kinase kinase 7 (TAK1 into a complex known as the linear ubiquitin assembly complex (LUBAC) (Hsu et al. 1995). The IKK complex is then phosphorylated by kinase components of the LUBAC assembly allowing activation and NEMO is polyubiquitylated (Zhou et al. 2004). IKKβ phosphorylates both Ser32 and Ser36 on IκBα or Ser19 and 23 on IκBβ (DiDonato et al. 1996). The E3 ubiquitin ligase, Skp, cullin, f-box containing complex (SCF)β^{TrCP} then polyubiquitinates IκBα for proteasomal degradation via the 26s proteasome (Winston et al. 1999).

The canonical pathway includes some built in controls such as the IκBα negative feedback loop. This is due to IκBα being a gene target of NF-κB. IκBα is synthesised following activation of NF-κB, increasing the inhibition of NF-κB and allowing the IκBα to scavenge NF-κB from the nucleus. This process is in place to prevent chronic NF-κB activation through repeated stimulus however, due to slow re-synthesis, this can take more than an hour to facilitate negative feedback. Cycling of this mechanism results in an oscillatory nature of NF-κB

activation with dimers being shuttled in and out of nuclei (Hoffmann et al. 2002). This oscillatory feature may also affect the transcription of target genes (Nelson et al. 2004) (**Figure 1.7**).
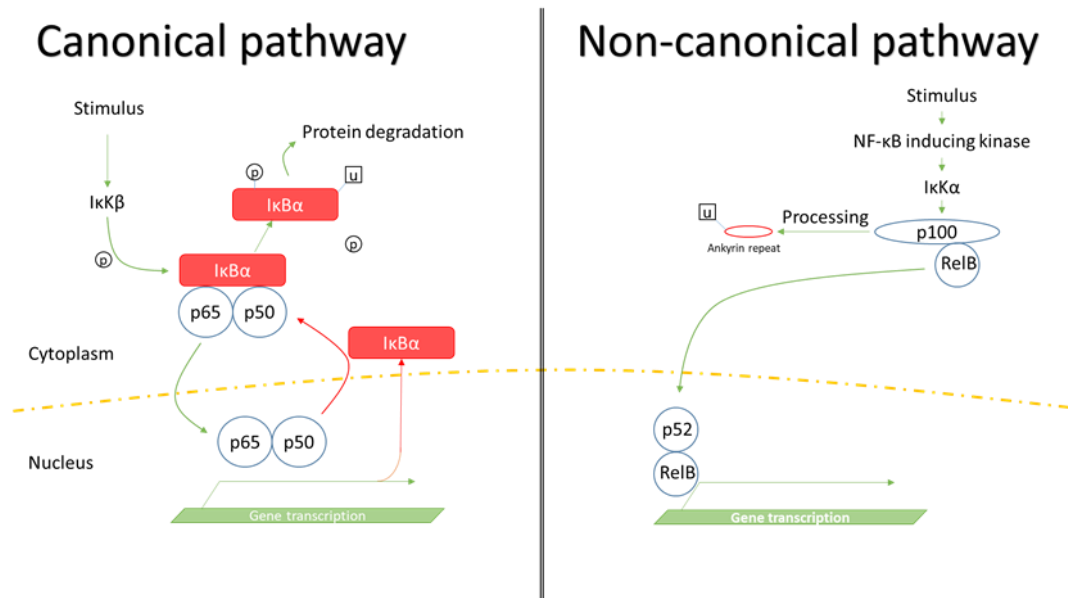
Figure 1.7: An overview of the major components of the NF-κB canonical and non-canonical pathways. The canonical pathway shows the IKKβ control of IκBα leading to its degradation, allowing the p65:p50 dimer to enter the nucleus and transcribe NF-κB targets – one of which is IκBα leading to the induction of NF-κB's major negative feedback loop. The canonical pathway shows NF-κB inducing kinase activating IKKα to facilitate the partial degradation of p100 to p52 via the proteasome. This allows the translocation of the p52:RelB dimer to the nucleus.

1.3.6 The non-canonical pathway for activation of NF-κB

The non-canonical pathway is NEMO-independent and is involved in B-cell survival, bone metabolism, and dendritic cell activation among other developmental processes. In the absence of signalling, NF-κB inducing kinase (NIK) is quickly turned over and degraded by the TNFR-associated factor (TRAF) - cIAP destruction complex. Upon stimulation of the TNFR, the TRAF-cIAP complex is disrupted, reducing the degradation of NIK, allowing it to accumulate (Qing et al. 2005). NIK then phosphorylates IKKα allowing activation of its kinase domain.

IKKα phosphorylates Ser176 and Ser180 on p100 (Ling et al. 1998). In most cells, p100 is normally complexed with RelB with the ankyrin repeat domain acting as an IκB (Solan et al. 2002). The phosphorylation leads to recognition by the SCFβ^{TrCP} ubiquitin ligase, and polyubiquitination allowing partial degradation by the 26s proteasome resulting in an active p50:RelB dimer (He et al. 2006). NIK can also release p100 where it is bound to a dimer as a standalone IκB (Savinova et al. 2009). Some specific chemokines are induced specifically by the non-canonical pathway. These include MIP-3a/CCL20, thymus expressed chemokine (TECK)/CCL25, B-cell attracting chemokine (BCA)-1/CXCL13, and stem cell factor (SCF)-1 (Dejardin et al. 2002).

1.3.7 NF-κB in muscle

In muscle, there is evidence for the expression of p65, p105/p50, p100/p52, RelB, and cRel although at a lower level than the others (Vella et al. 2014; Hunter et al. 2002; Judge et al. 2007; Durham et al. 2004). p65 (and phosphorylated p65) , p50, p52, RelB, are expressed in higher levels in muscle tissues of mice with Myotonic dystrophy type 1 compared with muscles of WT mice (Yadava et al. 2014). Basal NF-κB binding activity in the GTN and *extensor digitorum longus* (EDL) muscles is lower than in other tissues such as the liver, heart and the diaphragm (Durham et al. 2004) and there is evidence of alterations in NF-κB binding with changes in muscle use. Thus, the level of DNA binding in human muscle biopsies is reduced in those which have undertaken resistance exercise (Durham et al. 2004).

1.3.7.1 Acute activation of NF-κB

Phosphorylation of p65 occurs in muscle at 3-5 days following both freeze induced injury and injury with BaCl$_2$ (Nakazawa et al. 2017; Straughn et al. 2018). Nuclear translocation of p50 has been shown to increase in muscle during unloading along with increases in DNA binding of complexes containing p50 and cRel (Hunter et al. 2002).

H_2O_2 generated during contractions in muscles of adult WT mice activates a number of redox-regulated transcription factors, including NF-κB with a subsequent adaptation of the muscle through increased expression of regulatory enzymes and cytoprotective proteins necessary for remodelling of muscle tissue (McArdle et al. 2019).

Treatment of myofibres with TNF-α , IL-1α, IL-1β, and TNF-related weak inducer of apoptosis have been shown to increase NF-κB binding to DNA, NF-κB translocation without inducing apoptosis showing that the NF-κB pathway is sensitive to stimulation in muscle fibres (Li & Reid 2000; Yamaki et al. 2012). Canonical NF-κB inhibition results in increased differentiation of satellite cells ex and in-vivo (Straughn et al. 2018).

1.3.7.2 Chronic activation of NF-κB

Transgenic increase in constitutively active IKKβ in muscle results in a loss of muscle mass and fibre atrophy in muscles of mice via an upregulation of MuRF1, an E3 Ligase which mediates muscle atrophy via proteolysis (Cai et al. 2004). There is an upregulation in IKKβ, and IκBα alongside an increase in phosphorylation of IκBα in these muscles (Straughn et al. 2018). Muscle specific knockout of IKKβ in mice protected a number of muscles from a loss in muscle weight, tetanic force, reduction in fibre size, and promoted regeneration in denervated mouse muscles in response to denervation (Mourkioti et al. 2006). IKKα and IKKβ are both proposed to be integral to the development of atrophy in response to mechanical unloading (Gammeren et al. 2009).

Overexpression of NIK leads to atrophy of muscle fibres in mouse TA muscles and an increase in the E3 ligases atrogin-1 and MURF, the translation initiation faction elF4EBP1, and the transcription factor FOXO1 in myotubes (Fry et al. 2016). This shows that the non-canonical NF-κB pathway is potentially involved in muscle protein turnover within muscles (Wu et al. 2014). Reduction of p65 using small interfering RNA protects against cytokine induced muscle atrophy (Yamaki et al. 2012).

Prolonged hind-limb unloading increases DNA binding of NF-κB transcription factors in mice (Durham et al. 2004). The level of NF-κB activity has a direct effect on muscle mass as NF-κB DNA binding is majorly responsible for MuRF1 promotor activation in the atrophy of muscle (Wu et al. 2014).

Muscles of old mice demonstrate chronic constitutive activation of NF-κB (Vasilaki et al. 2006b) and an inability to further activate NF-κB following a non-damaging physiological contraction protocol (Vasilaki et al. 2006a). This inability to respond to contractions with NF-κB activation is associated with a severe attenuation of changes in gene expression that provide cryoprotection (Demirel et al. 2003; Hall 2002; Heydari et al. 2000; Locke & Tanguay 1996; Muramatsu et al. 1996; Rao et al. 1999; Vasilaki et al. 2006b). Our research group has demonstrated that the increased antioxidant enzyme activities evident following isometric contractions in muscles of adult rodents were abolished in old rodents and this inability to adapt was associated with the lack of complete activation of the appropriate transcription factors including NF-κB (Vasilaki et al. 2002; Vasilaki et al. 2006b).

It is proposed that systemic inflammation induces the chronic activation of the canonical NF-κB pathway in muscle whereas the non-canonical pathway is activated by muscle disuse similar to that observed in unloading (Jackman et al. 2013).

1.4 Cytokines, chemokines, and leukocytes

1.4.1 Cytokines

Cytokines are systemically released proteins which can influence inflammatory responses either to sustain or inhibit inflammation (Turner et al. 2014). These proteins form a complex network of interactions which act on both leukocyte and non-immune cells. Cytokines have been shown to be important mediators in many chronic diseases and they can facilitate the development of these diseases from more minor inflammatory insults (Turner et al. 2014).

TNF-α, named for its haemorrhagic, necrotic effect on tumours was initially discovered as an endotoxin in the serum of mice (Carswell et al. 1975). This cytokine is a mediator of differentiation, innate immunity, adhesion molecule expression, and growth among other biological processes (Turner et al. 2014). It is also cytostatic and cytolytic to tumour cells and proliferative in non-tumour cells (Gupta 2002).

TNF-α is the prototypic ligand of the TNF superfamily of type 2 transmembrane proteins which hosts 30 receptors with 19 ligands acting upon them to facilitate biological responses such as cellular differentiation, inflammation, and apoptosis (Vanamee & Faustman 2018). The two trimer glycoprotein receptors TNF-α can bind to are the TNFR1 and TNFR2 (Loetscher et al. 1990; Armitage 1994). While TNFR1 is widely expressed ubiquitously, TNFR2 is confined mainly to leukocytes and endothelial cells (Sedger & McDermott 2014). Muscle fibres express both TNFR subtypes on their surface (Hardin et al. 2008). Both receptors contain four cytosine rich domains (CRDs) which each contain a pre-ligand binding assembly needed for trimerisation (Li et al. 2013). Although these receptors are similar, they facilitate different cellular responses.

TNFR1 is the main mediator of the pro-inflammatory response and has a higher affinity for TNF-α (Peschon et al. 1998). Upon activation, TNFR1 can illicit one of two responses through adaptor proteins (Turner et al. 2014). In the first response, TNFR1 associated death domain is recruited allowing a complex formation with TRAF2 and receptor interacting protein (RIP). This complex formation leads to NF-κB signalling through kinase cascades (Park et al. 2000). A scheme of this pathway is shown in **Figure 1.8**. The second response which can occur via TNFR1 is through the internalisation of the receptor. The internalised receptor recruits fas-associated death domain and pro-caspase 8 leading to apoptosis of the cell (Scaffidi et al.

1999). Unlike TNFR1, TNFR2 contains no death domain but can cause an immune response directly via its TRAF binding motif (Xie 2013).
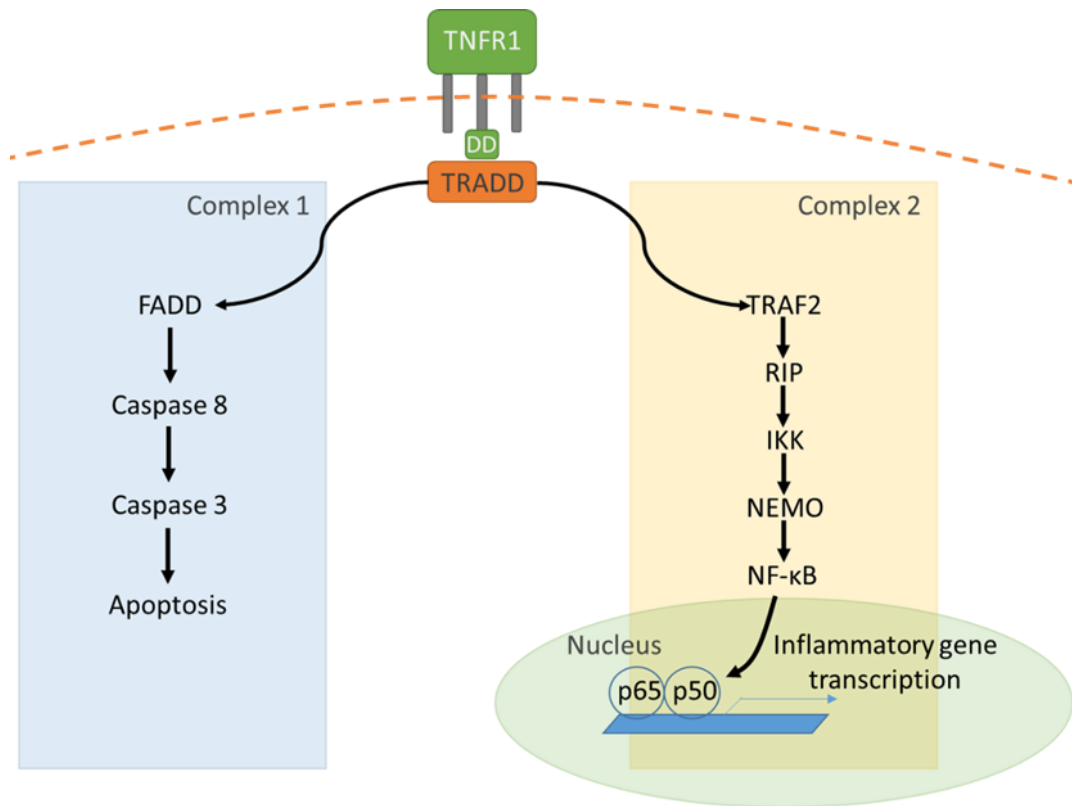
Figure 1.8: Schematic of activation of the NF-κB pathway and apoptotic pathways through varying pathways downstream of TNF-α binding to the TNFR1. *TNFR1 (Tumour necrosis factor receptor 1); DD (death domain); TRADD (TNFR1-associated death domain protein); FADD (Fas-associated death domain); TRAF2 (TNFR-associated protein 2); RIP (receptor interacting protein); IKK (Inhibitor of κB); NEMO (NF-κB essential modulator).*

Following ligand binding, the TNF-α receptors are cleaved from the membrane to release a soluble form of the receptor. This reduces the amount of free TNF-α and the surface TNF-α receptors (Porteu & Nathan 1990).

TNF-α is produced primarily by macrophages and other cell types including C2C12 muscle cells (**Table 1.1)** (Parameswaran & Patial 2010; Passey et al. 2016). TNF-α is produced as a transmembrane-bound monomeric precursor-protein, 17 kDa in mass (mTNF-α) t as trimers (Gearing et al. 1995). mTNF-α can be cleaved by TNF converting enzyme (TACE), a

metalloprotease (Moss et al. 1997). This releases a soluble form of TNF-α (sTNF-α. Both mTNF-α and s-TNFα are agonists upon their receptor, TNFR1 (Turner et al. 2014).

The remaining 10 kDa membrane bound peptide remnant of TNF-α is processed by signal peptide peptidase like 2a and 2b after which the intracellular domain of the membrane bound peptide can translocate to the nucleus and directly facilitate the production of interleukin IL-1β and IL-12 (Poggi et al. 2013).

1.4.1.2 Interleukins (ILs)

Interleukins are a group of inflammatory mediating cytokines named for their communicative role between leukocytes. This growing list of cytokines is grouped via their functional properties, receptors, and homology among other factors and includes proinflammatory mediators and anti-inflammatory mediators. The group is further broken into families (Akdis et al. 2016).

1.4.1.3 The IL-1 family

The IL-1 family has 11 proteins: 7 proinflammatory and 4 anti-inflammatory members (Boraschi et al. 2011). These cytokines are expressed mainly by macrophages and monocytes. IL-1α and IL-1β are synthesised by a multitude of cells including hepatocytes, neutrophils, and macrophages (Akdis et al. 2016). IL-1α is constitutively expressed in endothelial cells and in muscle under certain circumstances such as during regeneration (Chaweewannakorn et al. 2018). IL-1α is secreted as an active precursor (pro-IL-1α) which can be cleaved by calpain (Carruth et al. 1991). Like IL-1α, IL-1β is synthesised as pro-IL-1β, however, in this form the cytokine is inactive. IL-1 cleaving enzyme (ICE/caspase-1) contained in the inflammasome is responsible for the cleaving of pro-IL-1β into active IL-1β (Thornberry et al. 1992).

IL-1β which is proinflammatory and pyrogenic, is mainly synthesised in response to the action of DAMPs and PAMPs such as LPS acting upon a toll-like receptor (TLR). This allows the transcription of pro-IL-1β via the NF-κB pathway (Hiscott et al. 1993). This priming step does not result in the processing of pro-IL-1β, however, nod-like receptor protein 3 is activated via the NF-κB pathway allowing the activation of the inflammasome (Bauernfeind et al. 2009).

Though IL-1β and IL-1α have minimal sequence homology, both these ILs have similar binding and signalling properties at the IL receptors, IL-1R1 and IL-1R2 (Akdis et al. 2016). The functional IL-1 receptor (IL-1R) is formed from one IL-1R1 protein and one IL-1R accessory protein (IL-1RAcP) (Greenfeder et al. 1995). IL-1R is a TLR as it contains a Toll/IL-R (TIR) domain (Yamamoto et al. 2004). When IL-1β binds, IL-1R1 recruits IL-1RAcP, and through the TIR domain, myeloid differentiation primary response 88 interacts, thus facilitating transduction via the mitogen activated protein kinase (MAPK) and NF-κB pathways (Acuner Ozbabacan et al. 2014).

In a similar manner to TNFRs discussed in **Section 1.4.1.1**, IL-1Rs can undergo proteolytic processing resulting in shedding. This can have an inhibitory effect on IL-1β activation (Svenson et al. 1993). Further anti-inflammatory mechanisms are involved in the IL-1 family. For instance, IL-1R2 has a truncated intracellular domain thus making it inactive (McMahan et al. 1991). Therefore, IL-1R2 functions as a decoy receptor, sequestering IL-1 family activators such as IL-1β. The family also has antagonistic members such as IL-1 receptor antagonist of which there is 4 isoforms: one secreted form (sIL-1Ra) and three cytoplasmic (Arend 2002). This inhibits activation through preventing the recruitment of IL-1RAcP (Greenfeder et al. 1995).

IL-1β is shown to be increased in production in both isolated myoblasts and myotubes following exposure to LPS and TNF-α (**Table 1.1**) (Podbregar et al. 2013). Studies have also

shown that there is an increase in IL-6 following increasing mechanical stress, exposure to TNF-α and LPS (**Table 1.1**) (Passey et al. 2016; Peterson & Pizza 2009; Lightfoot et al. 2015).

1.4.1.4 The common γ chain family

The common γ-chain (γc) is a family of cytokines which all interact with the γc receptor subunit. The γc family is made up of the cytokines: IL-2, IL-4, IL-7, IL-9, IL-15 and IL-21 (Ross & Cantrell 2018). IL-2 binds to a high affinity IL-2R which has three subunits: IL-2R α-chain (IL-2Rα), IL-2R β-chain (IL-2Rβ), and γc (Sugamura et al. 1992). IL-2 plays a crucial role in t-cell proliferation and differentiation. Through the use of KO models of IL-2, it has also been recognised that IL-2 is important for the development of regulatory T cells (Furtado et al. 2002).

IL-2 regulation is tightly controlled by transcription factors such as NF-κB, and nuclear factor of activated T cells (Spolski et al. 2018). It can be expressed in CD4+ T cells following T-cell receptor (TCR) activation (Aronica et al. 1999). IL-2 is active against IL-2 receptors formed of combinations of the IL-2Rα, β and γ subunits with the highest affinity receptor being containing all 3 subunits (Waldmann 1989).

IL-4 is produced by TH2 cells, mast cells, and eosinophils among other cell types (Paul 2015). It is a major enhancer of TH2 cell development, increases the expression of CD23, upregulates B cell receptors, and mediates tissue adhesion and inflammation (Junttila 2018). IL-4 also suppresses TH1 development through epigenetic alterations (Dom Inguez et al. 2013). IL-4 is important in protection against extracellular parasites and regulation of allergic conditions (Gazzinelli-Guimarães et al. 2016).

1.4.1.5 Common β chain family

The common β chain (βc) family has 3 members: IL-3, IL-5, and GM-CFS. These cytokines all share a common β chain receptor subunit and all take part in haematopoiesis (Dougan et al. 2019). GM-CFS is named due to its ability to facilitate the differentiation of granulocytes from

common myeloid progenitor cells (CMPs). The GM-CFS receptor is a multimeric, type 1 cytokine receptor formed from the βc and α subunits (Hamilton 2008). GM-CSF is produced by cultured human muscle cells following mechanical strain (**Table 1.1**) (Peterson & Pizza 2009).

1.4.1.6 IL-10

The IL-10 family includes its prototypic member: IL-10, an anti-inflammatory cytokine produced by dendritic cells, Treg cells, macrophages, and mast cells (Couper et al. 2008; Grimbaldeston et al. 2007). In Treg cells, the production of IL-10 is dependent upon IL-2 (Barthlott et al. 2005). Antigen presenting cells downregulate the expression of major histocompatibility complex (MHC) class II on macrophages and monocytes (Spittler et al. 1995). Il-10 also reduces T-cell activation through the CD28 and CD2 receptors (Taylor et al. 2009; Joss et al. 2000). IL-10 functions through binding to the IL-10 receptor (IL-10R) with two subunits (IL-10R1 and IL-10R2) (Kotenko et al. 1997).

1.4.1.7 IL-16

IL-16 is an interleukin with chemokine activity and thus acts as a chemoattractant towards immune cells, specifically, T-cells (Krug et al. 2000). In this role, IL-16 promotes a TH1 response while suppressing TH2 responses (Lynch et al. 2003). It is synthesised as precursor protein of 80 kDa and cleaved by caspase 3 to be activated (Zhang et al. 1998). The cleavage results in a 17 kDa c-terminal which forms tetramers to facilitate cytokine and chemokine activity (Center et al. 1998). The 56 kDa N-terminal has cell cycle regulatory functions (Curiel-Lewandrowski et al. 2011). In T-cells, eosinophils and monocytes, IL-16 is constitutively expressed however in other cells, IL-16 is only produced following activation of specific pathways.

A list of cytokine sources, targets, receptors, and production in muscle is shown in **Table 1.1**.

Table 1.1: Cytokine cellular sources and targets adapted from Turner et al. (2014) and literature where cytokine has been sourced from isolated muscle fibres or muscle cells in culture. Receptors from Kanehisa & Goto (2000). Colon (:) signifies where receptors are formed of subunits. Granulocyte-macrophage colony stimulating factor (GM-CSF); Interleukin (IL); Tumour necrosis factor (TNF); Interferon (IFN); Dendritic cell (DC); Natural killer (NK); Colony stimulating factor 2 receptor (CSF2R); Cluster of differentiation 4 (CD4).

Cytokine	Main source	Muscle production references	Target cell	Receptors
GM-CSF	T cells, macrophages, fibroblasts	(Peterson & Pizza 2009)	Granulocyte, monocyte, eosinophil stem cell	CSF2RA:CSF2RB
IL-1β	Macrophage, B-cell, DC	(Podbregar et al. 2013)	B cell, NK cell, T-cell	IL1R1:IL1RAP, IL1R2
IL-2	T cell		T cell, B cell, NK cell	IL2RA:IL2RB:IL2RG, IL2RB:IL2RG
IL-4	Th cell		B cell, T cell, macrophage	IL4R:IL2RG
IL-6	Th cell, macrophage, fibroblast	(Peterson & Pizza 2009; Podbregar et al. 2013; Lightfoot et al. 2015)	Activated B-cell, plasma cell	IL6R:IL6ST
IL-10	T cell		B cell, macrophage	IL10R1:IL10R2
IL-16	T cell, eosinophil, mast cell, eosinophil, monocyte, DC, fibroblast, epithelial cell		T cell, monocytes, macrophage, eosinophil	CD4
TNF-α	Macrophage	(Passey et al. 2016)	Macrophage	TNFR1, TNFR2
IFN-γ	T-cells		Macrophage, neutrophil, monocyte	IFNGR1:IFNGR2

1.4.2 Chemokines

Chemokines are 8 – 12 kDa extracellular messengers defined by the presence of cysteine residues proximal to the N-terminal. They are named by these cysteine residues. In CC chemokines, the two cysteines closest to the N-terminal are directly next to one another. CXC chemokines have a variable residue separating the cysteines and CX3C chemokines cysteines are separated by three variable amino acid residues. In XC chemokines, the first and third cysteines are lacking. The nomenclature of chemokines starts with which of these groups the chemokine is contained, followed by L for "ligand" and an individual number (Turner et al. 2014). For example, CXCL2 belongs to the CXC group of ligands and is number 2 of the group. The cysteine residues maintain the structure of the proteins through cross bridges (**Figure 1.9**). These proteins form three β-sheets with an overlying α helix with a short

unstructured N-terminal (Clore & Gronenborn 1995). Most chemokines are named across similar functional orthologues between species – e.g. CCL11 in humans is a functional orthologue of CCL11 in mice.
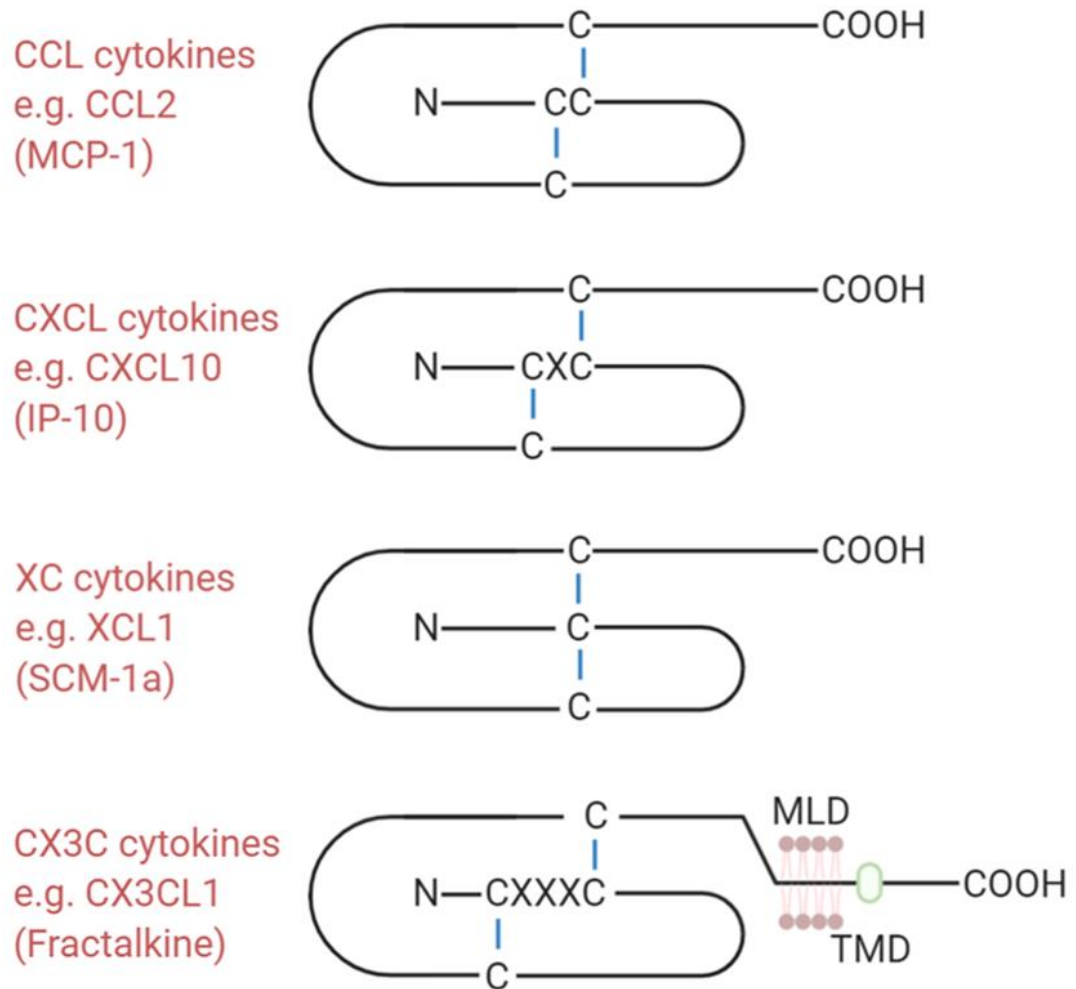
Figure 1.9: Figure showing a schematic for the structure of chemokines and their nomenclature. *Monocyte chemoattractant protein 1 (MCP1), Interferon gamma-induced protein 10 (IP-10), single cysteine motif 1a (SCM-1a), mucin like domain (MLD), transmembrane domain (TMD).*

1.4.2.1 Chemokine function

The major function of chemokines is to act as a guide for immune cells for the cells to move towards a site of infection or injury. Chemokines are mostly produced and secreted by immune cells (Sokol & Luster 2015). They do so by inducing integrin expression in epithelial

cells to allow leukocytes to cross the epithelium (Turner et al. 2014). Homeostatic chemokines are produced in tissues to control local immune cell migration (Zlotnik et al. 2006). Inflammatory chemokines are released by a wide number of cells in response to injury to take part in the response to inflammation (Zlotnik & Yoshie 2012). Some cytokines from the CXC class contain a motif of glutamic acid-leucine-arginine (ELR). These chemokines, termed ELR-positive chemokines are have angiogenic function (Giuliano et al. 2014).

1.4.2.2 Chemokine receptors

Chemokine receptors belong to a large superfamily of receptors known as G-protein coupled receptors (GPCRs). GPCRs are receptors get their name from their intracellular signalling relying on interactions with proteins named G-proteins. These have 7 transmembrane domains with an extracellular domain consisting of 3 loops and an N-terminus. The intracellular portion forms 4 loops and a c-terminal from which the G-proteins interact (Arimont et al. 2019).

Chemokines bind to conventional chemokine receptors (cCKRs) through interactions with the extracellular loops and the N-terminal. Like their ligand counterparts, cCKRs are named after the cytokine they are most associated with, however they contain an 'R' for receptor rather than 'L' for ligand (Hughes & Nibbs 2018). Like many other GPCRs, cCKRs form both homodimers and higher order aggregates with other cCKRs, atypical chemokine receptors (ACKRs) and non-chemokine GPCRs (Wang et al. 2011). A list of chemokines and their receptors is shown in **Table 1.2**.

Cytokine binding to the receptor is initiated with the N-terminal of the cCKR (site 1) interacting with the chemokine globular core. The N terminal of the chemokine interacts with residues ion the TM region of the cCKR (site 2). This is referred to as the two-step/two-site model where site 1 provides the wide range of specificity and site 2 facilitates signalling (Kleist et al. 2016).

Chemokine receptors are promiscuous with their binding with many of the receptors having the ability to interact with many chemokines. At the same time, many chemokines can interact with one or more cCKRs (Kunkel 1999). Homeostatic cCKRs usually only have one or two ligands (Zlotnik & Yoshie 2012). cCKRs can also interact with non-chemokine ligands such as HMGB1 (binds to CXCR4) and MIF (interacts with CXCR2 and CXCR4) (Schiraldi et al. 2012; Bernhagen et al. 2007).

Table 1.2: A list of chemokines and their receptors. *Adapted from Zlotnik & Yoshie (2012) and Araki-Sasaki et al. (2006). Monocyte chemoattractant protein (MCP); Macrophage inflammatory protein (MIP); Regulated on activation normal T cell expressed and secreted (RANTES); Thymus and activation regulated chemokine (TARC); Macrophage derived chemokine (MDC); Thymus expressed chemokine (TECK); cutaneous T cell-attracting chemokine (CTACK); keratinocytes-derived chemokine (KC); epithelial cell-derived neutrophil activating peptide 78(ENA-78); Interferon gamma-induced protein 10 (IP-10); B cell-attracting chemokine (BCA); small-inducible cytokine B16 (SCYB16).*

Family	Chemokine	Other name	Agonistic receptors	Antagonistic receptors
	CCL1	I-309	CCR8	
	CCL2	MCP-1	CCR2	
	CCL3	MIP-1a	CCR1, CCR5	
	CCL4	MIP-1b	CCR5	
	CCL5	RANTES	CCR1, CCR3, CCR5	
	CCL7	MCP-3	CCR1, CCR2, CCR3, CCR5, CCR8	
CCL	CCL11	Eotaxin	CCR3, CCR5	CXCR3, CCR2
	CCL12	MCP-5	CCR2	
	CCL17	TARC	CCR4	
	CCL19	MIP-3b	CCR7	
	CCL20	MIP-3a	CCR6	
	CCL22	MDC	CCR4	
	CCL24	Eotaxin-2	CCR3	
	CXCL1	TECK	CXCR2	
	CXCL2	CTACK	CXCR2	
	CXCL5	KC	CXCR2	
CXCL	CXCL10	MIP-2	CXCR3	
	CXCL11	ENA-78	CXCR3, CXCR7	CCR3
	CXCL12	IP-10	CXCR4, CXCR7	CCR3, CCR5
	CXCL13	BCA	CXCR5, CXCR3	
	CXC16	SCYB16	CXCR6	
CX3CL	CX3CL1	Fractalkine	CX3CR1	

There are also 4 atypical chemokine receptors - ACKR1, -2, -3, and -4 (Bonecchi & Graham 2016). Only one of these has been shown to facilitate a biological response: ACKR3 which

binds CXCL12 and CXCL11 (Burns et al. 2006). The other three do not have a modification of intracellular binding motifs including the aspartic acid-arginine-tyrosine (DRY) motif on the TM2 intracellular loop (Hughes & Nibbs 2018).

1.4.3 Immune cell types

Immune cells are a vast family of cells which facilitate immune regulation and host defence against invading pathogens and parasites orang. These cells can largely be sorted into two groups belonging to the innate / fast response immunity, or the adaptive / slow response immunity. All cells of the immune system are derived from multipotent haematopoietic stem cells (HSCs) (Torang et al. 2019). HSCs can differentiate into any blood cell. A scheme of the lineage for the immune cell types is shown in **Figure 1.10**.
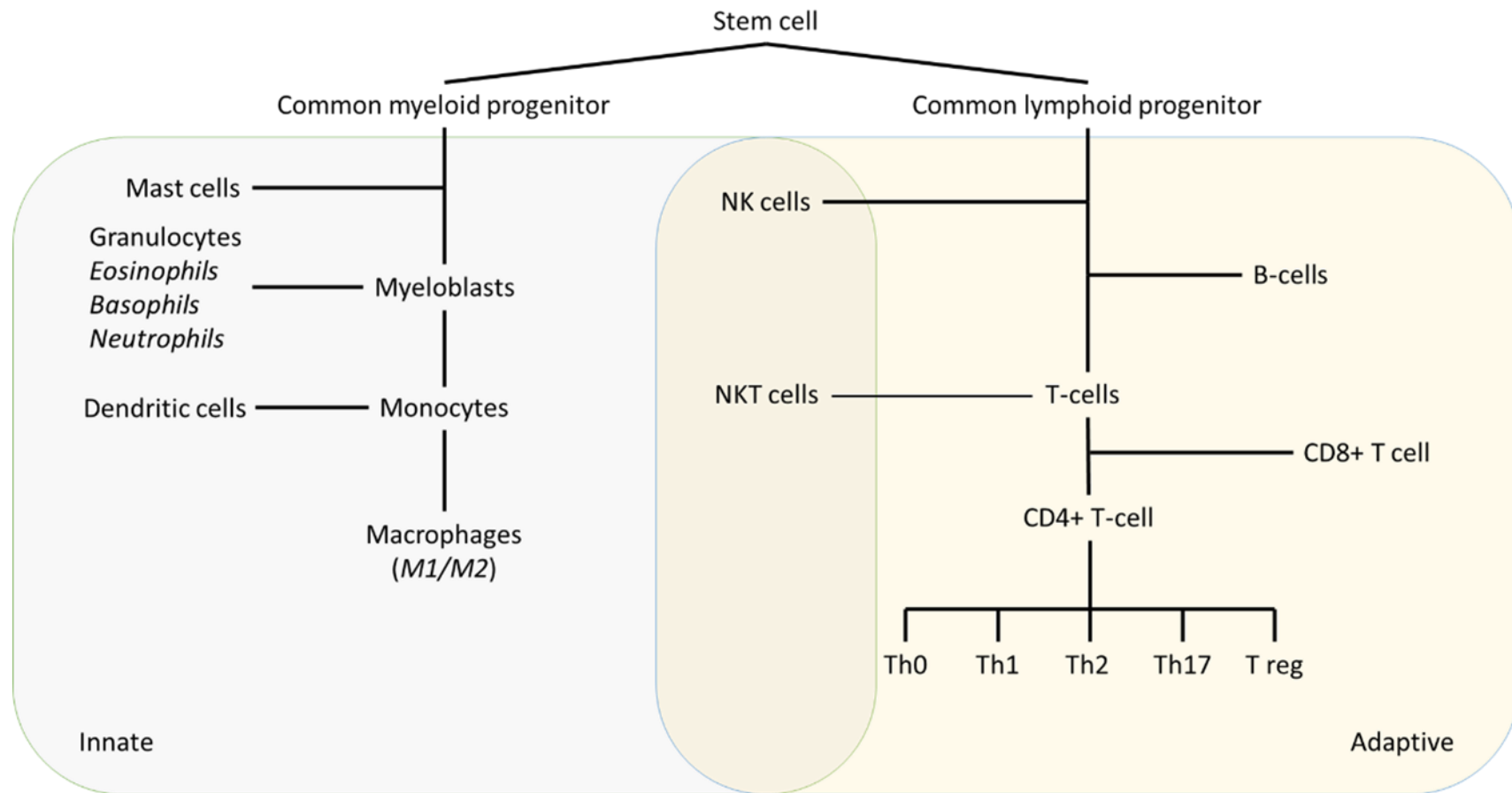
Figure 1.10: The tree of lineage of leukocytes originating from common stem cells grouped by their role in either the adaptive or innate immune system.
Adapted from Torang et al. 2019

In its most simplistic form, the innate immune system is a defence against all pathogens and is naïve to any potential previous encounter with the pathogen. The innate immune defence includes both physical barriers such as the skin and other epithelial cellular layers. The system is primed to respond to PAMPs and DAMPS through their respective receptors (Schroder & Tschopp 2010). During a pathogenic invasion, the innate immune response takes place rapidly on the initial recognition of the pathogen. The innate immune response is a complex and highly regulated cascade of events including the coordination of leukocytes, identification of the challenge, removal of foreign substances and activation of the adaptive arm of the immune response (Sokol & Luster 2015).

The cells of the innate immune system are derived from CMP cells which, in turn are derived from HSC cells. CMPs differentiate into a wide array of cell types alongside leukocytes, CMPs also differentiate to form erythrocytes and platelets through the megakaryocyte route of differentiation.

Mast cells are tissue-resident leukocytes meaning they reside and adapt to a tissues environment and lay dormant. Without stimuli, for example, within healthy tissue, mast cells maintain a constant number through both apoptosis and autophagy (Berent-Maoz et al. 2006; Ushio et al. 2011). Upon the introduction of a challenge, the number if mast cells dramatically increases in response (Crimi et al. 1991). Likewise, following muscle damage, there is an increase in recruitment of mast cells to the site of damage (Gorospe et al. 1996). While IL-3 plays a role in the development of mast cell progenitors in mice, IL-3 is not sufficient to facilitate the development in humans (Shimizu et al. 2008). Mast cell granules contain lysosomal enzymes and a low pH allowing the remodelling of extracellular matrix proteins and connective tissues (Garcia-Faroldi et al. 2013).

Eosinophils are leukocytes which belong to the granulocyte subgroup of cells alongside basophils, neutrophils and mast cells. They reside in the bone marrow which mature from CMP cells in response to IL-3, GM-CFS and IL-5 through their common β_c chain (Kalinauskaite-Zukauske et al. 2019). IL-5 facilitates eosinophil differentiation and aid their migration into blood vessels. Two potent chemokine attractants of eosinophils are eotaxin-1 (CCL11) and eotaxin-2 (CCL24) (Rankin et al. 2000). Eosinophils can help facilitate tissue repair at the sight of injury (Ramirez et al. 2018). Human eosinophils can facilitate a Th2 response when released (Persson et al. 2019).

Basophils derive from a common precursor of mast cells called the basophil/mast cell committed progenitor (Arinobu et al. 2005). The biggest driver of its differentiation from BMCPs is with activation of the signal transducer and activator of transcription factor 5 (STAT5) pathway, mainly by exposure to IL-3, GM-CFS and IL-5 (Li et al. 2015; Haak-Frendscho et al. 1988). Basophils are similar in structure and function to mast cells though do not take up residence in tissue (Voehringer 2013). Alongside mast cells, the function of basophils is to protect the host against parasites through the initiation of type 2 immunity via the release of cytokines and proteases (Voehringer 2017).

Neutrophils are the most abundant of the granulocytes and the most abundant of all the leukocytes, accounting for 60-70% the total number of leukocytes. Differentiation of neutrophils is controlled mainly by G-CSF allowing the cells to start expressing receptors including CXCR4, SDF-1 and TLR4. Human bone marrow produces 10^{11} neutrophils each day (Dancey et al. 1976). They are usually one of the first leukocytes to respond to an infected site and at the end of their lifecycles, neutrophils are phagocytosed by macrophages (Bratton & Henson 2011). Post-injury in vascular tissues such as liver, brain, and lungs, neutrophils migrate towards chemotactic factors released by those tissues into the bloodstream where

they tether via glycoproteins to endothelial cells, adhere, and then transmigrate across the endothelial surface towards their target (Kolaczkowska & Kubes 2013).

Dendritic cells (DCs) are antigen presenting cells (APCs), expressing high levels of MHC II on their surface (Abb et al. 1983). They contain pattern recognition receptors such as TLRs to aid antigen uptake (Segura & Villadangos 2009). In doing this they help facilitate cross signalling between the innate and adaptive immune systems. There are several subsets of dendritic cells. Conventional DCs (cDCs) have the function of antigen processing and the presenting of antigens to naïve T cells and are subdivided into two subsets: cDC1 and cDC2. The subset, cDC1 have a high proficiency in the activation of Th1 and natural killer cells through IL-12 release (Jongbloed et al. 2010). Plasmacytoid DCs (pDCs) produce a large amount of type 1 interferons (IFNs) in response to viral infection (Bao & Liu 2013).

Macrophages are phagocytic components of the innate immune system (Tauber 2003). While macrophages can develop from monocytes, macrophages are resident in tissues where they have been seeded before birth (Hashimoto et al. 2013). In the muscle tissue of mice, tissue resident macrophages are derived from both progenitors in the yolk sac and cells within the bone marrow of adult mice (Wang et al. 2020). It is thought that macrophages of different tissues have differences in some gene enhancer landscapes (Lavin et al. 2014). There are two subsets of macrophages: the first is the classical macrophage (M1; IFNγ-mediated) subtype and the second is the alternatively activated (M2; IL-4-mediated) subtype (Biswas & Mantovani 2010). Though these subtypes are polar opposites, macrophages are largely plastic in that phenotype switching can occur as influenced by the environment and other leukocytes present (Mosser & Edwards 2008). M1 macrophages are induced by IFN-γ and TNFα and promote a Th1 response by recruiting NK cells and T cells through the secretion of CXCL9, CXCL10, and CXCL11 to act on CXCR3 receptors (Oneissi Martinez et al. 2008).

M2 macrophages are anti-inflammatory in phenotype and activated largely by IL-4 and IL-13 (Anderson & Mosser 2002; Orecchioni et al. 2019). These macrophages scavenge cellular debris and cells undergoing apoptosis promoting tissue repair and healing (Shapouri-Moghaddam et al. 2018). Both M1 and M2 macrophages can express MHC-II and thus can act as antigen presenting cells (Ryszer 2015).

Unlike most other innate immune cells which are derived from CMP cells, most NK cells are derived from common lymphoid progenitor (CLP) cells (Kondo et al. 1997). NK cells develop in response to IL-2, IL-7 and IL-15 and other γc receptor ILs (Vosshenrich et al. 2005). NK cells are named natural killers due to them not having to be exposed to antigen in order to be activated unlike T cells, however, NK cells respond more rapidly upon re-exposure (Marcus & Raulet 2013). In parallel with their cytotoxic response, NK cells can produce pro-inflammatory cytokines such as TNFα or IFNγ to recruit more NK-cells (Reefman et al. 2010).

1.4.3.2 Adaptive immunity

The adaptive immune system is a defence against pathogens for which the body has been previously exposed to. This arm of the immune system is pathogen specific and is governed by cells derived from CLP multipotent cells.

B cells named for their discovery in the *bursa of fabricius* of birds, are both professional APCs and antibody producing cells. Through genetic rearrangement events, it is estimated B cells can synthesise 10^{16}-10^{18} unique antibody variants (Briney et al. 2019). Pathogen specific antibodies are able to neutralise invading pathogens and tag the pathogen in order to aid the homing of other leukocytes via opsonisation (tagging of pathogens with antibodies) or through the complement system (Forthal 2014).

There are 4 major subtypes of B-cells; these are type 1 (B1), and type 2 (B2), regulatory (Breg) and Marginal zone (MZ) B cells. B1 cells are derived mainly from progenitor cells within the foetal liver and to a lesser extent, adult bone marrow (Hardy et al. 2007). B1 produce natural,

mainly IgM type antibodies which exist at birth which protects against microbial pathogens and help to eliminate apoptotic and necrotic cell debris (Silverman 2015; Varambally et al. 2004).

B2 B-cells initially migration is guided by the CXCL13 ligand upon the CXCR5 receptors (Ansel et al. 2000). B cells can be activated through stimulation of their B cell receptor which can be modulated through binding of complement receptors and TLRs (Das et al. 2017). MZ B-cells are found in the marginal portion of the spleen and are not activated through BCRs but through TLRs (Hendricks et al. 2018). Breg cells dampen the immune response through the expression of anti-inflammatory cytokines such as IL-10 (Fillatreau et al. 2002).

CD4+ cells possess the CD4 TCR co-receptor for the TCR. CD4+ cells, also known as T helper cells, regulate the behaviour of other immune cells through the release of cytokines and chemokines (Luckheeram et al. 2012). CD4+ is the co-receptor of the TCR and can bind to the β2 domain of MHC class II which primarily presents extracellular pathogen derived antigens (Neefjes et al. 2011). There are several subtypes of CD4+ T cells, all of which have slightly different functions. All of these subtypes stem from the naïve T cell (Th0).

Th1 helper cells are activated by IL-12 and IFN-γ in response to intracellular pathogens such as protozoa or bacterial infiltration (Miller et al. 2009). Both IFN-γ and IL-12 are mainly produced in immune cells such as NK cells but are also produced in C2C12 muscle cells (Cheng et al. 2008; Romanazzo et al. 2015). NF-κB is key to the differentiation of Th1 cells with mice expressing NF-κB defects having a deficient Th1 response (Aronica et al. 1999). In response to activation, the Th1 cells release IFN-γ and IL-2, which both activates macrophages and activates antibody production in B-cells (Romagnani 1999).

Th2 helper cells are activated by the cytokines IL-4 and IL-2 and, through activation of Nuclear factor of activated T-cells (NFAT), Activator protein 1 (AP-1) and NF-κB, GATA binding protein 3 is expressed leading to Th2 differentiation (Oh & Ghosh 2013). While immune cells such as

basophils and NKT cells are major producers of IL-4, it is also produced by muscle fibres and is a factor in the fusion of satellite cells (Yoshimoto 2018; Horsley et al. 2003). IL-2 is largely only produced in CD4+ cells, though other immune cells also produce IL-2 at a low level (Wang et al. 2018). Th2 cells release IL-4, IL-5, IL-9, IL-10, IL-13 and IL-25 in order to attract eosinophils, basophils, mast cells and B cells. The mast cells release histamine amongst other chemical signals to encourage the removal of the parasites (Walker & McKenzie 2018).

Treg cells develop only with an intermediate amount of TCR signalling (Li & Rudensky 2016). Like their B cell counterparts, Treg cells are largely anti-inflammatory and as such dampen the immune response (Vignali et al. 2008). They are known to express high levels of the cytokine IL-1Ra which is an antagonist to IL-1 signalling (Mercer et al. 2010). They also secrete anti-inflammatory cytokines IL-10 TGFβ and IL-35 and actively uptake IL-2 (Asseman et al. 1999; Nakamura et al. 2001; de la Rosa et al. 2004).

T-cells expressing the CD8 protein on their cell surface are known to be cytotoxic T cells which can eradicate cells which are infected with viruses or tumorigenic cells (Cupovic et al. 2016) (Martínez-Lostao et al. 2015). This is mediated through the binding of MHC class I, the protein responsible for displaying peptides to cytotoxic T-cells, of an APC to the TCR. MHC I preferentially presents intracellular pathogen peptides (Neefjes et al. 2011). Once activated, the cytotoxic T cells produce cytotoxic components such as perforin and granzyme (Martínez-Lostao et al. 2015). They can also activate apoptosis in target cells through interaction with Fas ligands (Hassin et al. 2011).

A key member of the adaptive immune system is the memory T cell which gives the body the ability to have a memory of invading pathogens. Memory T cells can be derived either from CD4+ or CD8+ t-cells and as such are either MHC I or II reactive (Raeber et al. 2018). CD4+ memory T cells are regulated by IL-7 and IL-15 whereas CD8+ memory T cells rely more on IL-15 (Raeber et al. 2018; Judge et al. 2002). There are 4 defined subtypes of memory T cells:

central memory T (T$_{CM}$) cells, effector memory T (T$_{EM}$) cells, tissue resident T (T$_{rm}$) cells and virtual memory T (T$_{VM}$) cells. T$_{CM}$ cells are normally present in the lymphatic system and circulatory system. T$_{EM}$ cells are located in resident tissue or circulating and can be activated rapidly (Jameson & Masopust 2018).

There is established crosstalk between immune cells and muscle which has implications in skeletal muscle metabolism and turnover (Pillon et al. 2013). An example of this is resident immune cells in skeletal muscle can cause chronic inflammation to the tissue resulting in local high levels of cytokines. While there is no evidence that there is an increase in immune cells infiltrating into muscle with advanced age, there is observed dysfunction relating to leukocytes with age; most notable of these are macrophages of which there is a resident subpopulation within muscle (Wang et al. 2020). Macrophages have been shown to decrease in wound healing, phagocytosis and cytokine production with old age (Linehan & Fitzgerald 2015).

In summary, there is evidence of systemic inflammation in old rodents and humans. Although the source of such inflammation is unclear, muscle production of some pro-inflammatory cytokines has been shown to be increased with increasing age and this is associated with increased evidence of NF-κB DNA binding activity in muscle tissue. The chronic activation of NF-κB is proposed to result in modification of protein turnover either by decreased synthesis, increased degradation or both (Lang et al. 2000).

1.5 Protein turnover

Loss of protein balance or 'proteostasis' is believed to be one of the hallmarks of ageing described by *Lopez-Otin et al* (López-Otín et al. 2013).

$$Net\ protein\ balance = \ k_{synth} - \ k_{deg}$$

A negative protein balance is caused by muscle protein breakdown (MPB) being in excess of muscle protein synthesis (MPS) either by reducing synthesis or increasing degradation, or both, leading to a net loss in protein. The opposite is true for a positive protein balance. This balance is responsive to alterations in diet, exercise and inflammation.

1.5.1 Protein Synthesis

1.5.1.1 Transcription

The rate at which RNA is transcribed can directly affect the protein synthesis rate of particular proteins. There are 3 RNA polymerase (Pol) enzymes in eukaryotes of which PolII synthesises messenger RNA (mRNA) and microRNA. PolII binding happens at accessible promotor sites in euchromatic regions of DNA, some of which will contain CpG islands (sites where the GC content is higher than 50%) and some of which contain TATA elements (Deaton & Bird 2011). Transcription factors can bind to sequence specific sites near to promoters or enhancers to guide PolII towards the region for the initiation of transcription (Cramer 2019).

Transcription factors are required for the recognition of promoter regions which are part of the pre-initiation complex along with PolII and promoters (Schramm & Hernandez 2002). This requires one of six general transcription factors, named TFIIA, -B, -C, -D, -E, -F and -H (Orphanides et al. 1996). This complex opens the DNA double helix, separating the strands however, PolII requires the enzyme DNA translocase xeroderma pigmentosum type B (XPB) which utilises ATP hydrolysis to unwind the DNA (Grünberg et al. 2012).

Elongation, the building of the strand of RNA alongside the DNA template in the direction of 5' to 3' is facilitated by the transcription elongation complex which is minimally composed of RNA polymerase, double stranded DNA and RNA (Yamaguchi 2013). The unwound non-template strand of DNA forms what is known as the DNA bubble: a single strand of DNA guided by RNA polymerase around 14 bases in length (Pal & Ponticelli 2005). The rate of elongation is under the control of transcription elongation factors such as positive

transcription elongation factor b (P-TEFb) and negative elongation factor (NELF) (Krueger et al. 2010; Gilchrist et al. 2008).Promoter proximal pausing is a regulatory step which Animalia cells undergo. Between 20 and 120 bp from the SS, elongation via PolII pauses (Krumm et al. 1995). This pause can be caused by NELF protein or released by the action of P-TEFb (Wu et al. 2003; Li et al. 2018).

Considerable alteration in the transcriptome is seen in muscle during ageing, with alterations in inflammatory signalling and repair signalling amongst other systems (Lin et al. 2018). The transcription elongation speed in various tissues across an array of species is increased with ageing while the content of PolII is generally reduced with age in muscles of rats (Debès et al. 2019; Mobley et al. 2017).

1.5.1.2 Translation

Transcription produces pre-mRNA which includes intron sequences interrupting the coding exons of mRNA and this is matured via the splicing out of the intron to produce mature mRNA sequences. This process is facilitated by spliceosomes and their catalytic unit, small nuclear ribonucleoproteins (snRNPS), which are under the control of a highly regulated pathway (Will & Lührmann 2001). During splicing, pre-RNA is cleaved at the intron 5' end by the snRNP: U1. The 5' end then attaches to the branch site which is complementary to the 5' cut site forming a looped structure. The exons are then guided into proximity to each other, the 3' splice site is cut and a covalent bond is formed between the two (Konarska et al. 1985).

The main 4.3 mDa apparatus involved in protein translation is the 80s ribosome formed by a large 60S subunit and a smaller 40S subunit. The 40S subunit consists of 33 ribosomal proteins of the small subunit (Rps) proteins and 18S rRNA. The large subunit has 47 ribosomal proteins of the large subunit (Rpl) with 5.8S, 28S and 5S rRNA (Melnikov et al. 2012).

Through the action of various elongation factors, the mature mRNA is then attached, the 60S subunit is recruited resulting in the elongation and eventual termination of protein synthesis

(Rodnina 2016). During elongation, amino acids are added one at a time until the process is terminated by the stop codon (UAG, UAA or UGA). The ribosomes are then recycled to undergo the same cycle (Jackson et al. 2010).

Deletion of various initiation factors and elongation factors in *c. elegans* has yielded extensions to lifespan of more than 30% (Anisimova et al. 2018). It is also thought that with ageing there is a decrease in elongation factor activity, ribosome abundance, ribosomal RNA gene copy number and initiation rate; all of which would contribute to a decrease in protein synthesis with age (Anisimova et al. 2018).

1.5.1.3 Protein folding

For proteins to function correctly, they must adopt the correct structure. Small proteins generally fold dependent upon their amino acid sequence and do not require secondary components (Anfinsen, 1973). Larger proteins can be misfolded which can result in protein aggregation (Moreno-Gonzalez & Soto 2011). Accumulation of damage via oxidative stress can also result in the misfolding of proteins (Gregersen & Bross 2010).

As well as driving protein synthesis, ribosomes allow proteins to adoption the correct structure. During translation, the protein exits the ribosome through a narrow tunnel in which allows the folding of small proteins and allows some tertiary folding (Nilsson et al. 2015). On exiting the ribosome, the protein can take several routes to adopt the same structure for them to be functionally active (O'Brien et al. 2011).

After synthesis, proteins can be denatured, losing function. Denatured proteins can either be refolded or broken down for amino acid recycling (Saibil, 2013).Chaperone proteins are involved in the quality controls of protein synthesis. Within the cytosol, a folding system exists known as the chaperones. There are 5 main chaperone families in animals known as the heat shock protein (Hsp) 60, Hsp70, Hsp 90, small Hsp (sHsp), and Hsp100 families (Ciechanover & Kwon 2017). While all of these families have similar roles in protein folding

and degradation, they also have defined and multiple functions depending on the state of the cell. For example, Hsp70 facilitates misfolded proteins to be refolded but under other conditions facilitates the degradation of misfolded proteins (Mayer & Bukau 2005).

A constitutive increase in the levels of Hsps is seen in muscles of old mice and humans and a decrease in the response of Hsps to exercise (McArdle & Jackson 2017). The change in constitutive levels in muscles at rest may reflect an increase in the presence of misfolded proteins rather than an enhanced level of Hsps available to maintain protein function (McArdle & Jackson 2017). As muscles of adult mice demonstrate a robust and strong response to exercise, this blunted response in old mice and humans may be responsible for modifications in protein turnover in old age (Noble et al. 2008). Data from our laboratory has also shown that transgenic overexpression of particular Hsps provided some protection against the age-related loss of muscle mass and function (McArdle et al. 2004; Kayani et al. 2010), although whether this was due to improved protein turnover is unknown.

1.5.2 Protein Degradation

The other side of the protein balance equation is the rate of protein degradation also referred to as proteolysis. There are two major pathways which dictate the breakdown of protein for amino acid recycling. These two pathways are known as the lysosomal degradation pathway and the ubiquitin-proteasome pathway.

1.5.2.1 Lysosomal degradation pathway

Autophagy is the breakdown of self-proteins in response to a stimulus including stress, nutrient deprivation, or hypoxia (Hansen & Johansen 2011). Autophagy is controlled by autophagy related (ATG) proteins (Mizushima et al. 2011). Autophagy begins with the assembly of a phagophore - a structure composed of a double membrane which encapsulates cytoplasmic material (Axe et al. 2008). Once the phagophore fuses with itself into a bubble containing its target components, it is classified as an autophagosome. The

autophagosome can then fuse with the lysosome – another membrane bound organelle used to break down molecules. This fusion forms an organelle referred to as an autolysosome (Glick et al. 2010).

In muscles, the major myofibrillar proteins are not routinely degraded by lysosomal proteases (Attaix & Taillandier 1998). During ageing, there is a decrease in microtubule-associated proteins 1A/1B light chain 3B (LC3), lysosome-associated membrane protein 2 (LAMP-2), BCL2 interacting protein 3 (Bnip-3) and γ-aminobutyric acid receptor-associated protein 1 (Gabarap1) in muscle (Burks & Cohn 2011). These proteins are integral to facilitating autophagy with LC3 considered the central protein to autophagy (Hansen & Johansen 2011). These is an additional increase in Beclin-1 in muscles with age – a protein involved in the nucleation of phagophores (Burks & Cohn 2011; Kang et al. 2011). Autophagy inhibition through knocking out the autophagy related gene 7 gene in the muscles of adult mice results in a decrease in myofibre size and cross sectional area, an increase in number of centrally located nuclei, and an increase in the expression of atrogin-1 and muscle-specific RING finger protein 1 (MuRF-1) (Masiero et al. 2009).

1.5.2.2 Ubiquitin-proteasome pathway

1.5.2.2.1 Ubiquitin

Ubiquitin is a small protein which can covalently bond to proteins as a post translational modification for various signalling processes. There are 4 genes for ubiquitin in mammals; two of these: ubiquitin-60S ribosomal protein L40 (UBA52) and ubiquitin-40S ribosomal protein S27a (RPS27A) constitutively express single ubiquitin units whereas UBB and UBC express 3 – 4 or 9 – 10 units of Ub in tandem as an unanchored chain (Bianchi et al. 2015). RPS27A and UBA are fused proteins with ribosomal subunits.

Ubiquitin enzymes are responsible for the addition of ubiquitin to proteins targeted for degradation. Of these enzymes, there are 3 subtypes: ubiquitin-activating (E1) enzymes,

ubiquitin conjugating (E2) enzyme, and ubiquitin-ligating (E3) enzyme. These enzymes form a cascading system whereby ubiquitination is first initialised through adenylation on its C terminal -COOH group by the E1 enzyme in an ATP dependent reaction (Haas et al. 1982). The ubiquitin then binds to a cysteinyl residue on the E1 enzyme (Pelzer et al. 2007). Once active, the ubiquitin is transferred to a different cysteinyl on the E2 enzyme (Keszei & Sicheri 2017). In some instances, the E2 enzyme can directly ubiquitinate the target however in most cases, the E3 enzyme must be involved (Kao et al. 2012). Ubiquitin usually binds to its substrate at the epsilon amine group of a lysine residue however it can bind to other groups. The binding domains of ubiquitin are frequently discovered in close proximity to alpha helices (Randles & Walters 2012). The human genome contains genes for two E1 enzymes, near to 40 E2 enzymes and over 100 E3 enzymes (Fenteany et al. 2020). In mice, there is a single E1 activating enzyme, ~40 ubiquitin conjugating enzymes, and over 620 E3 ubiquitin ligase enzymes (Bradshaw et al. 2020).

 Ubiquitin PTMs come in many variations. The first and most simple is the monoubiquitination where a substrate has the addition of one ubiquitin molecule. Multi-monoubiquitination is where a substrate is bound by 2 or more unchained amino acids (Petroski & Deshaies 2003). Polyubiquitin chains can be achieved through the multimerisation of ubiquitin monomers acting on multiple binding sites on other ubiquitin monomers. A compact homogeneous chain results of a chain of ubiquitin monomers binding via interaction between their lys48 residue and the isoleucine 44 patch on the ubiquitin monomer. Mixed ubiquitin chains have variably bound ubiquitin monomer units (Kirkin et al. 2009). Ubiquitin chains can also be branched by one ubiquitin chain nucleating a further two chains. These branched ubiquitin chains have been shown to have increased favourability of proteins towards breakdown via the proteasomal pathway (Meyer & Rape 2014). It is these structures which are identified by the ubiquitin binding proteins on effector proteins.

Ubiquitin can be removed from a substrate through the action of a deubiquitinase enzyme of which the human genome contains around 86 genes (Eletr & Wilkinson 2014).

1.5.2.2.2 Proteasomal degradation

The proteasome is a large, multimeric structure which facilitates the enzymatic breakdown of proteins and allows recycling of amino acids. Over 80% of protein degradation can be attributed to the proteasome (Lilienbaum 2013). The structure of the 26S/30S proteasome is formed of two subcomplexes, the catalytic core particle (20S) and either one or two regulatory particles (RPs; 19S). Whether the proteasome contains one or two regulatory domains dictates whether the proteasome is a 26S or 30S proteasome (Da Fonseca & Morris 2008).

The 20S is made of 28 individual proteins arranged in a barrel shape. The barrel can be broken down into four rings (two α and two β) of monomers in a sequence of α-β-β-α. Each of these rings contains 7 individual proteins which are names either α_1 - α_7 or $\beta_1 - \beta_7$ depending on the ring (Tanaka 2009; Unno et al. 2002). In the β ring, the catalytic proteins which facilitate protein hydrolysis are β_1, β_2, and β_5 (**Figure 1.11**).
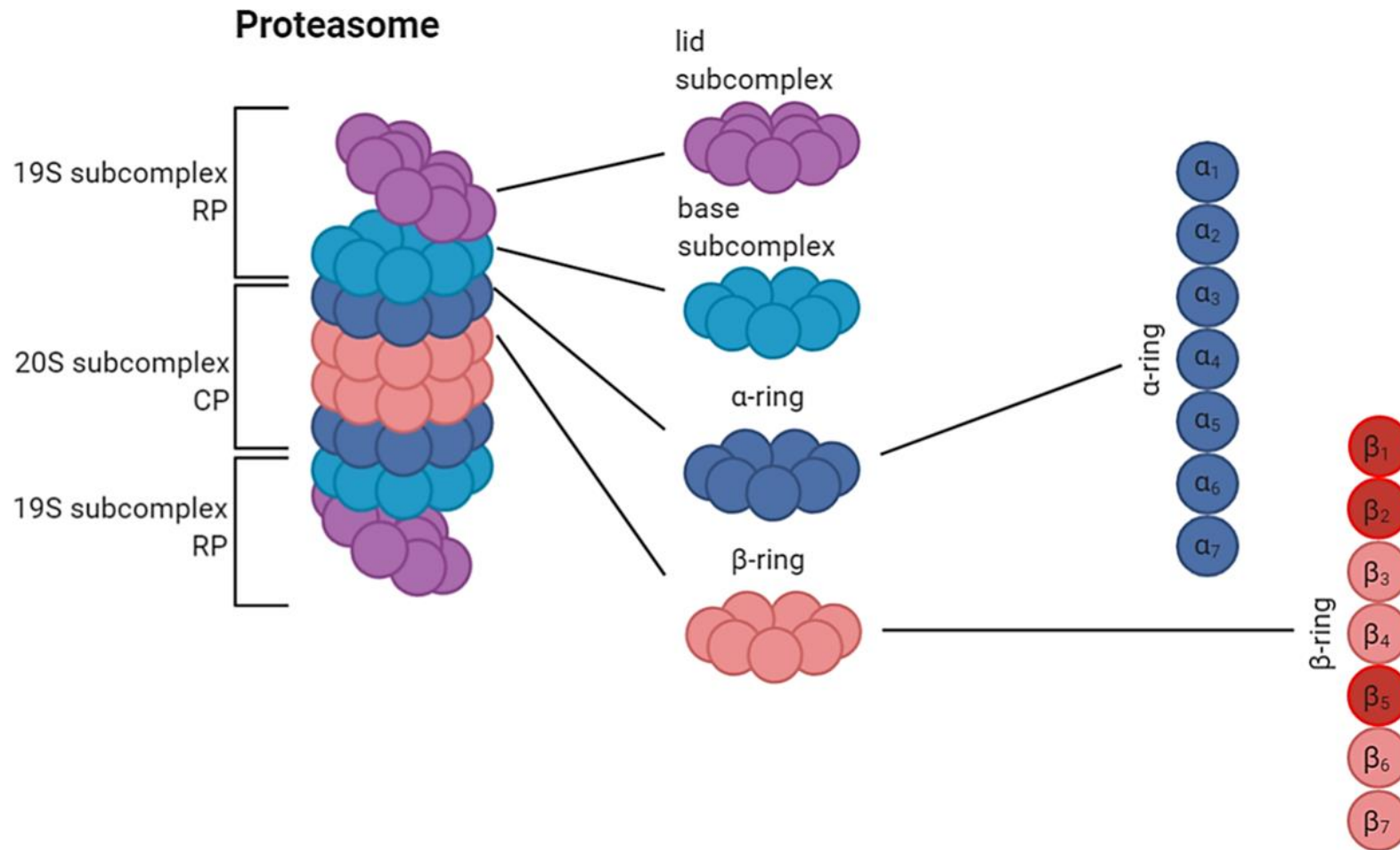
Figure 1.11: An outline for the structure of the proteasome. *The 19S regulatory particle (RP) can be broken down into the lid and base subcomplexes and the 20S catalytic particle can be divided into the α-ring gate and the catalytic β-ring chamber.*

The RP consists of two groups of protein units called regulatory particle of triple ATPase (Rtp) and regulatory particle of non-ATPase (Rtn). Together these form the base subcomplex and the lid subcomplex. The lid subcomplex is involved in deubiquitylation of substrate proteins. The protein subunit which facilitates the deubiquitination is the Rpn11 protein which cleaves polyubiquitin chains from the substrate (Worden et al. 2014).

The base complex is composed of 6 Rtp proteins and 4 Rtn proteins. Rpn10 contains a ubiquitin interacting motif (UIM) and Rpn13 contains a pleckstin-like receptor for ubiquitin (Pru) (Deveraux et al. 1995; Schreiner et al. 2008). Together these proteins recognise and capture polyubiquitinated and diubiquitinated substrates, respectively. Rpn1 and Rpn2 stack above the 20S proteasome structure allowing the interaction with the base subcomplex and allow the movement of protein substrates towards to β-ring (Rosenzweig et al. 2008). The base complex also forms a ring of Rtps which help to unfold the substrate before reaching the α-ring (Elsasser & Finley 2005).

The two catalytic β rings at the centre of the 20S are flanked by two α protein rings. These act as a gateway to the proteasome. The alpha proteins have an extended protrusion into the chamber space of the 20S subcomplex. The majority of the space is occupied by the α3 subunit (Da Fonseca & Morris 2008). This chamber obstruction is reduced upon the association of the 19S subcomplex to the 20S structure. This gating allows control of the breakdown of protein substrates by the proteasome.

In the β ring, the catalytic proteins which facilitate protein hydrolysis are $β_1$, $β_2$, and $β_5$. The $β_1$ subunit, or PSMB6, has peptidyl-glutamyl hydrolysing/caspase like activity which facilitates hydrolysis on the carboxyl side of hydrophobic residues (Orlowski 1990; Kisselev et al. 1999). The $β_2$ subunit has trypsin like activity meaning they cleave peptides on the carboxyl side of basic residues and $β_5$ cleave on the carboxyl side of glutamate residues meaning they are chymotrypsin like (Kisselev et al. 1999). The use of all three subunits results

in the proteasome having a broad specificity to peptides. The immunoproteasome is assembled when β_1, β_2, and β_5 are swapped preferentially for β_{1i}, β_{2i}, and β_{5i} respectively. These subunits allow for more antigen processing and presentation via MHC class I molecules (Guillaume et al. 2010; Murata et al. 2018).

In the muscles from old rats, there is an observed increase in the ubiquitination of total proteins when compared with that of adults (Altun et al. 2010). Alongside this is an increase in deubiquitinating enzymes and an increased rate of ubiquitination (Altun et al. 2010; Attaix et al. 2005). In addition to alterations in ubiquitination, there is an increase in muscle content of proteasomal subunits in the muscles of old rats when compared with that of muscles from adult mice (Altun et al. 2010). This is evidence that there are alterations to the pathways which degrade proteins in muscles of old animals.

1.5.2.3 Protein quality control

The response to protein misfolding and aggregation is a major consideration for the rate of protein turnover. Protein misfolds can be attributed to errors such as a dominant negative mutation (Liu et al. 2010). Thermodynamically, proteins can reach a multitude of stable conformations, the most stable being having the lowest free energy. For this reason, conditions such as temperature, pH, oxidative stress or toxic agents can lead to the generation of misfolded proteins (Hipp et al. 2019; Salahuddin et al. 2016). It is through that as many as 30% of newly synthesised proteins are misfolded (Schubert et al. 2000). A high accumulation of protein misfolding can lead to accumulation of the misfolded proteins into aggregates or fibrils which have a low free energy and are therefore, very stable. This is a common occurrence in neurodegenerative diseases such as Parkinson's disease, Alzheimer's disease and Creutzfeldt-Jakob disease (Dill & MacCallum 2012). As the accumulation of misfolded proteins can result in the disease states, the body has several mechanisms to remove or correct misfolding events one of which is chaperone mediated refolding and so

problems occur when the chaperone mediated system fails, such as during ageing. (**Section 1.4.1.4**).

1.5.2.4 Unfolded protein response

The endoplasmic reticulum (ER), specifically the rough ER (RER), is a membrane bound organelle involved in protein synthesis and folding, also known as the sarcoplasmic reticulum in skeletal muscle. RER is occupied by ribosomes and has a high content of specialised chaperones to facilitate function (Jan et al. 2014). The unfolded protein response (UPR) is a highly conserved system that upholds protein quality control within the cell. The UPR is activated upon the initiation of ER stress through overloading the capacity of ER to fold proteins (Lin et al. 2008). In response, the ER reduces protein synthesis to reduce misfolding events to a capacity whereby chaperones can aid in folding (Harding et al. 2000). The ER then increases in volume and upregulates the expression of chaperones and increases protein degradation via the endoplasmic reticulum associated degradation (ERAD) pathway, all through the X-box binding protein 1 (XBP1) transcription factor (Sriburi et al. 2004; Lee et al. 2003).

1.5.2.4.1 Endoplasmic reticulum associated (protein) degradation (ERAD)

The ERAD pathway follows a set of key steps leading to protein degradation. The protein substrate is first recognised and ubiquitinated via E3 enzymes, the substrate is expelled from the ER and then degraded by the proteasome. Thus, misfolded proteins are recognised in numerous ways such as by chaperones (Nishikawa et al. 2001). Ubiquitin E3 ligases tag the protein for degradation (Groisman et al. 2006). The substrate is then translocated to the cytosol where the proteasome is active. The ubiquitinated protein can then be degraded by the proteasome (**section 1.5.2.2.2**).

This thesis examines the role of inflammation has in the loss of muscle mass and function with particular focus on activation of NF-κB, cytokine expression, and the effects of this on protein turnover.

1.6 Hypothesis.

The overall hypothesis of this thesis was that the increased activation of NF-kB reported in muscles of old WT and adult SOD1KO mice will be associated with degenerated, denervated or regenerating muscle fibres and this results in an increased production of cytokines/chemokines by muscle which contribute to the chronic inflammation seen in old age (inflammaging). Further, such chronic activation of NF-kB activation will lead to modified protein turnover in muscles of old WT mice causing a net loss of muscle protein.

1.7 Overall aims of this thesis

The aims of the work reported in this thesis were:

1. To determine the localisation of nuclei with increased activation of the canonical pathway of NF-kB in quiescent muscles of old WT and adult SOD1KO compared with adult WT mice.

2. To identify whether any changes in the cytokine and chemokine levels in the plasma of old WT and adult SOD1KO mice are associated with altered cytokine/chemokine production by muscles and whether this is associated with the presence of degenerating/regenerating muscle fibres.

3. To examine and model differentially expressed proteins using unlabelled and deuterated water-based proteomics to determine whether activation or inhibition of protein turnover pathways are likely to be driven by changes in NF-kB activity in old compared with adult WT mice.

Chapter 2: Materials and methods

2.1 Mice

All animals were housed in a temperature-controlled room (22-25°C) with food and water provided *ad libitum* on a 12-h light/dark cycle in the University of Liverpool Biomedical services unit. All experimental procedures were performed under a UK Home Office licence (Home Office licence number P391895CA, approved 15/06/17) and complied with the UK Animals (Scientific Procedures) Act 1986 and were ethically approved by the University of Liverpool Animal Welfare Review Body.

Male C57BL/6J mice were used in these studies. The adult wild type (WT) mice ranged from 8-12 months old and the old mice were 24-28 months old. All WT mice were sourced from Charles River Laboratories (North Carolina, US).

SOD1KO mice are generated through homologous recombination of the SOD1 gene (Huang et al. 1997). Although SOD1KO and WT mice are indistinguishable early in life, homozygous SOD1KO mice have a shorter life span and chronically elevated oxidative stress is associated with progressive muscle atrophy and weakness, NMJ degeneration, muscle fibre loss, declines in nerve conduction, increased mitochondrial ROS generation, and impaired adaptive responses that in total, result in a phenotype by 8 months onward which resemble deficits observed late in life in 24 month and older WT mice (Elchuri et al. 2005; Busuttil et al. 2005; Jang et al. 2010; Muller et al. 2006; Larkin et al. 2011; Sims-Robinson et al. 2013; Vasilaki et al. 2010).

SOD1KO mice used throughout this thesis were sacrificed at 8-12 months old, when increased loss of muscle mass and function was evident (Muller et al. 2006; Jang et al. 2010). SOD1KO mice provide an excellent model to test hypotheses linking oxidative stress to sarcopenia as well as a unique system in which to gain insight into the mechanisms of age-associated atrophy and weakness.

2.2 Mouse experimental protocols.

2.2.1 Induction of muscle degeneration and regeneration by injection of Barium chloride ($BaCl_2$) into the EDL muscle.

Materials

$BaCl_2$ dihydrate (Sigma Aldrich, Missouri, US)

Steripod 0.9% w/v Sodium Chloride (NaCl) 20ml (Mölnlycke Health Care, Gothenburg, Sweden)

Veo insulin syringe (100 μL) with Ultra-Fine 6mm x 31G needle (Becton Dickinson, New Jersey, US)

1.2 % $BaCl_2$ in sterile phosphate buffered saline (PBS):

- 240 mg $BaCl_2$ dihydrate salt
- 20 mL sterile PBS (steripod) (Molnlycke Healthcare, Sweden)

Protocol

Adult WT, old WT, and adult SOD1KO mice were administered isoflurane until unresponsive as demonstrated by a toe pinch. Once sufficiently anaesthetised, mice were given an intramuscular (IM) injection of 1.2 % $BaCl_2$ into the right *EDL* muscle and allowed to recover for 3, 14, 28 and, 60 days post-injection. Immediately after injection, the mice were allowed to recover on heat mats and given wetted food. During the week following injection, mice were given wet food as a precaution for any reduction in mobility following treatment although no gross changes were seen. At the required time point, mice were anaesthetised as above, confirmation of death was confirmed through cessation of circulation, blood was taken from aorta and the EDL muscles dissected and frozen for cryosectioning in a transverse orientation (Section 2.3.1).

2.2.2 Determination of protein synthesis rates using Deuterium Oxide (^2H_2O)

Materials

Deuterium Oxide (^2H_2O) (Cambridge Isotope Laboratories, Essex, UK)

Phosphate buffered solution (PBS) Tablets (Sigma Aldrich, Missouri, US)

1 mL syringe (Becton Dickinson, New Jersey, US)

25 mm x 25G needle (Becton Dickinson, New Jersey, US)

99% ^2H_2O PBS:

- 1 PBS tablet
- 200 mL ^2H_2O

Protocol

Mice were restrained and an initial loading dose of ^2H_2O was administered via two 500 μL intraperitoneal injections of 99% ^2H_2O PBS; injected 4 hours apart. After the first injection, mice were given 8% ^2H_2O in normal drinking water to achieve plasma enrichment of ^2H_2O at ~4.5% as described by Kim *et al*. (2012). Mice were culled at 1, 2, 3, 4, 6, 9, 12, 15, 20, 30, 40, 50 and 60 days following initiation of the study (**Figure 2.1**) via overdose of pentobarbital and death was confirmed by cessation of circulation. Mice were injected at various time points and all culled over 3 days to avoid any issues related to long term storage of some samples. Plasma was collected via aortic bleed to measure the enrichment of ^2H_2O in the body. Muscles (including GTN muscles for protein synthesis analysis) were removed and snap frozen in liquid nitrogen and stored at -80 °C for future analysis.

Four adult and five old untreated WT mice were also culled and plasma and GTN muscles removed for unlabelled proteomics as described above.
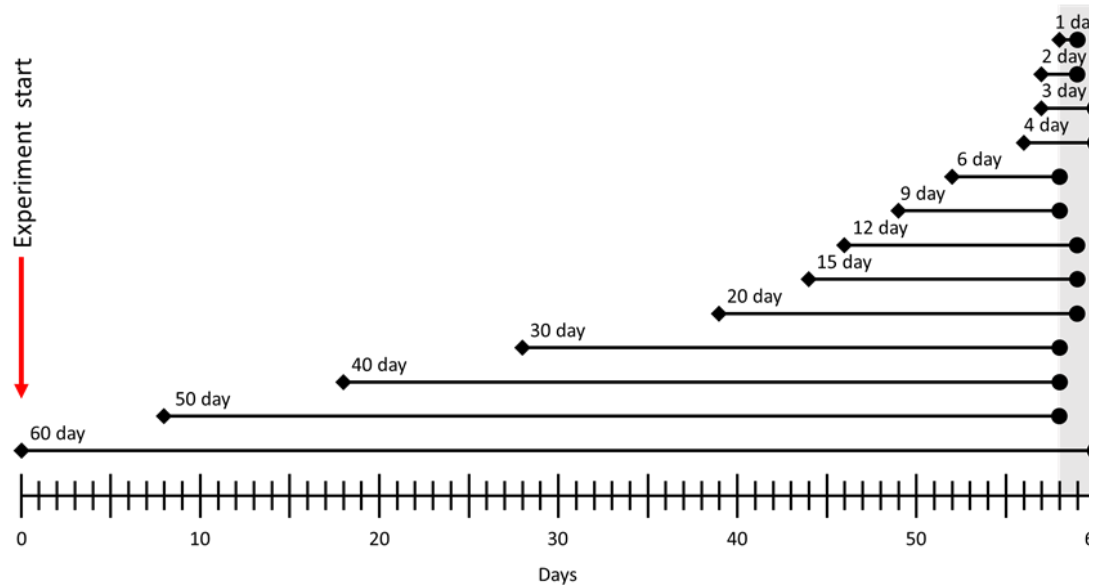
Figure 2.1. Timeline of heavy water injections and supplementation of water (♦) and termination (●) for each time-point. *Mice were injected at various time points and all culled over 3 days to avoid any issues related to long term storage of some samples.*

2.2.3 Dissection of individual muscles

For these experiments, different muscles were collected for various purposes. The EDL was taken for imaging purposes due to its small size being advantageous for imaging. *gastrocnemius* GTN muscles were used for western blotting, electromotility shift assay (EMSA) and quantitative polymerase chain reaction (qPCR) as they contain a lot of material. *Flexor digitorum brevis* (FDB) muscles were dissected for use in single fibre preparation as they contain short fibres which are able to be separated with ease. Careful dissection is important to maximise animal usage and good data production.

2.2.3.1 TA and EDL muscles

The mouse was laid on its back and the hind limb was positioned to allow access to the anterior, distal portion of the limb. An incision to the skin was made with microscissors and

94

the skin was removed to uncover the full TA muscle (**Figure 2.2A**). The epimysium was surrounding the muscle was then removed with curved forceps. The TA tendon was isolated using fine forceps and cut using microscissors. The TA could then be pulled away from the tissue and nerve beneath and cut at the proximal end. Through the removal of the TA, the EDL could now be isolated and removed at each tendon (**Figure 2.2B**). This was performed using curved forceps to isolate the distal EDL tendon. This was cut, the EDL was lifted and the proximal tendon was severed, freeing the muscle.

2.2.3.2 GTN and soleus muscles

After the anterior muscles were removed, the hind limb was repositioned to allow access to the posterior of the limb. The fat pad and epimysium covering the GTN was removed with scissors (**Figure 2.2C**). Curved forceps were then used to grip the Achilles tendon which was then severed. The muscles were then lifted to show the medial portion of the muscles. Through doing this the soleus could be removed using microscissors (**Figure 2.2D**). The GTN was then removed by cutting the muscle at the origin of the medial and lateral heads.

2.2.4 Isolation and culture of muscle fibres from the FDB muscle

FDB muscles were dissected from the base of the foot (**Figure 2.2E**). A scalpel was used to score the sides and the back of the foot and forceps were used to peel the skin from the base of the foot. A scalpel was positioned under the muscle and a cut was made to the proximal side of the muscle. The muscle was lifted and cut near the toes.
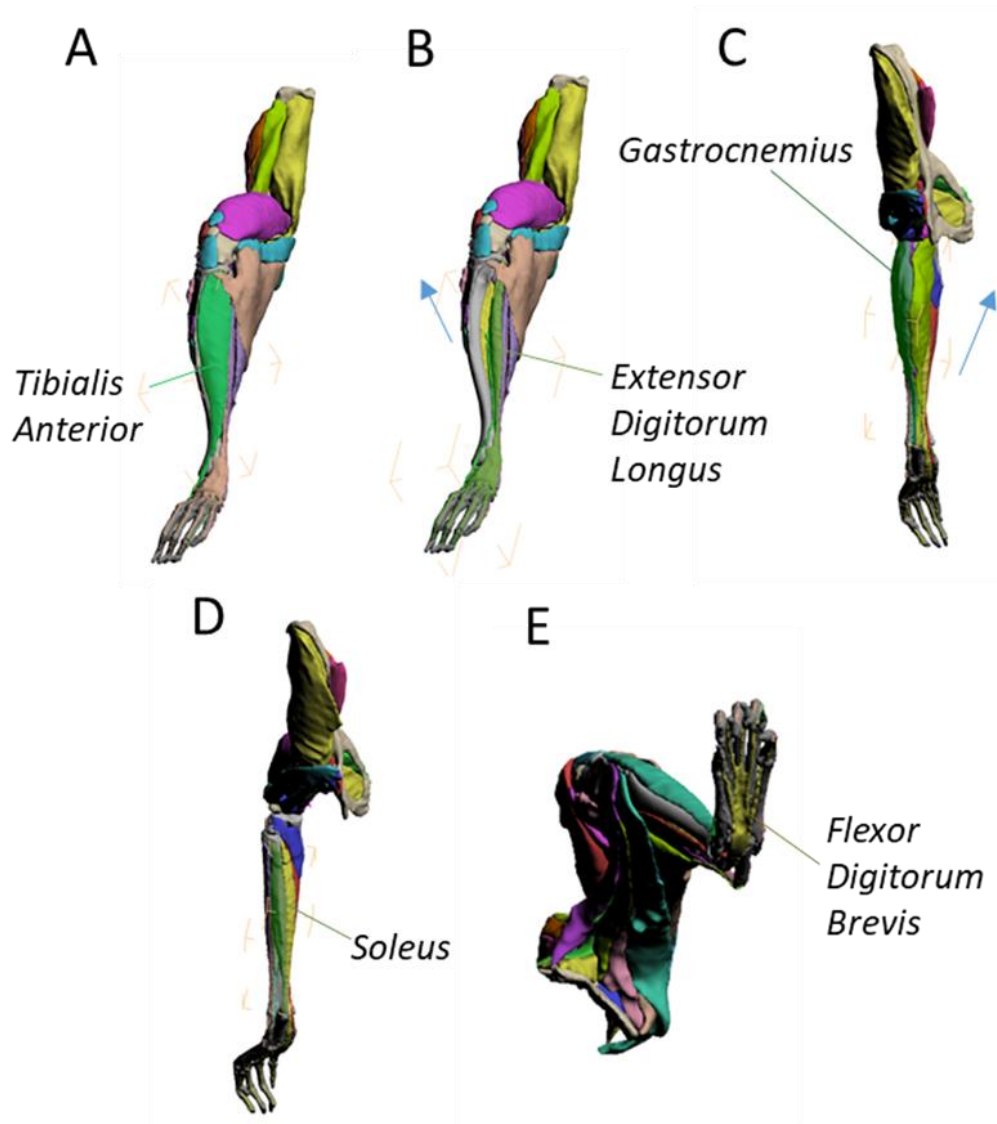
Figure 2.2: Representation of mouse hind limb muscle anatomy. *A) Tibialis anterior (TA; viewed from front of leg), B) extensor digitorum longus (EDL) muscle (viewed from front of leg), C) Gastrocnemius (GTN; viewed from rear of leg), D) soleus muscles (viewed from rear of leg), E) and the flexor digitorum brevis (FDB; viewed from base of foot) muscle. Images generated from* Charles et al. (2016).

2.2.4.1 Culture of fibres from the FDB muscle

Materials

Minimum essential media (MEM) (Sigma-Aldrich, Missouri, US)

Type I collagenase (Sigma-Aldrich, Missouri, US)

Foetal bovine serum (FBS) (Sigma-Aldrich, Missouri, US)

L-glutamine (Thermofisher, Massachusetts, US)

Penicillin-Streptomycin (Thermofisher, Massachusetts, US)

Engelbreth Holm Swarm murine sarcoma extracellular matrix (ECM) (Sigma-Aldrich, Missouri, US)

Protocol

FDB muscles were placed into 1 mL MEM containing 4 mg/mL type I collagenase, 10% FBS, 2mM L-glutamine, 100 units/mL penicillin and 100 µg/ml streptomycin and incubated at 37 ^{o}C, 5% CO_2 for 2 – 3 hours, agitated every 30 minutes (Selvin et al. 2015).

After digestion with collagenase intact fibres were separated from any debris and other cell types via two centrifugations at 600 g for 30s at room temperature. After each centrifugation, approximately 4 mL media was removed, leaving around 1 mL media containing the fibres, and replaced with around 4 mL fresh culture medium (Selvin et al. 2015).

Coverslips were coated with 3.4 mL ECM solution within 24 well plates by placing the coverslips into the bottom of the wells. Ice cold ECM (30 µL) was pipetted onto the cover slip. The ECM was then spread across the base using the edge of a bent pipette tip. This was allowed to settle for 2 minutes. Fibres prepared for imaging were plated into the ECM coated wells. The fibres were left for 30 minutes at 37 °C, 5% CO_2 to allow attachment to the base of the wells before the media was topped up with 200 µL to cover the fibres. These cells were left for overnight at 37°C and 5% CO_2 until use.

Fibres for media collection were plated directly onto 6 well plates coated with ECM. The same protocol for fibre attachment to the plates was performed as above.

2.2.4.2 Staining and imaging of FDB fibres

Materials

PBS (Sigma Aldrich, Missouri, US)

MEM (Sigma-Aldrich, Missouri, US)

Neutral Buffered Formalin 10% (NBF) (VWR, Pennsylvania, US)

Triton (Sigma Aldrich, Missouri, US)

Stock solution Rhodamine labelled Wheat Germ Agglutinin 5 mg/mL (WGA-Rhodamine) (Vector labs, California, USA)

Vectorshield hardset mounting media containing DAPI (Vector labs, California, USA)

Superfrost Plus slides (ThermoFisher, Massachusetts, US)

NBF 4%

- 40 mL NBF (10%)
- 60 mL 1x PBS

Protocol

The media was removed and the fibres were washed with 200 µL PBS. 200 µL serum free media was added, and the fibres were incubated at 37°C for 1.5 hours 37 °C, 5% CO_2. The fibres were then fixed in 4% NBF for 1 hour at room temperature. The NBF was removed and the fibres washed 3 times for 5 minutes in PBS containing 0.2% triton. WGA-Rhodamine was added to a final dilution of 1 in 1000 in PBS with 0.2% triton for 10 minutes at room temperature with gentle rocking.

The WGA rhodamine was removed, and fibres were washed 3x 5 minutes in PBS with 0.2% triton. This was then removed, and the coverslips were upturned and mounted on slides using Vectorshield hardset mounting media containing DAPI.

Fibres were imaged on a Zeiss LSM800 confocal microscope (Carl Zeiss AG, Oberkochen, Germany) with a 40x oil immersion objective lens (Carl Zeiss AG, Oberkochen, Germany). Z-stacking and image stitching were used to obtain a 3D representation of full isolated muscle fibres.

2.2.4.3 Media and fibre collection and preparation from isolated cultured FDB fibres

Materials

PBS (Sigma-Aldrich, Missouri, US)

MEM (Sigma-Aldrich, Missouri, US)

10 X Radioimmunoprecipitation assay (RIPA) buffer (Cell Signalling Technologies, Massachusetts, US)

cOmplete™ Protease Inhibitor Cocktail tablet (Roche, Basel, Switzerland)

Protocol

After overnight culture, the media was removed from the fibres and the fibres were washed 3 times for 5 mins each with PBS. 200 µL Serum free MEM was added to the fibres and the fibres were incubated for 3 hours at 37 °C, 5% CO_2. This media was removed and stored at -80 °C until future use. Twenty microlitres of RIPA buffer was added to the fibres in the remaining wells and the fibres were scraped. This lysate was centrifuged at 10,000 for 15 minutes before being transferred to a clean microcentrifuge tube and stored at -80 °C until use. Protein lysates concentration was were used to normalise the cytokine concentration in the media.

2.3 Histological analysis of muscles and isolated fibres

2.3.1 Cryosectioning of muscles

Materials

Shandon Cryomatrix embedding matrix (ThermoFisher, Massachusetts, US)

Cork discs (FisherScientific, New Hampshire, US)

Isopentane (ThermoFisher, Massachusetts, US)

SuperFrost Plus slides (ThermoFisher, Massachusetts, US)

Protocol

EDL muscles were cut transversely in the mid belly and positioned onto cork discs in a transverse orientation. Muscles were coated in Shandon Cryomatrix embedding matrix and frozen in isopentane cooled by liquid nitrogen. The EDLs were stored in -80 °C until used.

EDL muscles were cryosectioned to a thickness of 12 µM using a Leica CM1850 cryostat (Leica, Wetzlar, Germany) and transferred to SuperFrost Plus slides. Slides were stored at -20 °C until used.

2.3.2 Staining of muscle sections with Haematoxylin and Eosin

Materials

Harris Haematoxylin solution (Thermo Scientific, Massachusetts, US)

Eosin solution (Thermo Scientific, Massachusetts, US)

PBS Tablets (Sigma Aldrich, Missouri, US)

Tween-20 (Sigma Aldrich, Missouri, US)

1% Acid alcohol (Sigma Aldrich, Missouri, US)

Ethanol (EtOH) (Sigma Aldrich, Missouri, US)

Dibutylphthalate Polystyrene Xylene (DPX) (Sigma Aldrich, Missouri, US)

Protocol

Sections of EDL muscle were brought to room temperature before being washed with PBS with 1% tween. Sections were exposed to Harris Haematoxylin for 6 minutes and then washed in water. These were then dipped in acid alcohol and then transferred to eosin for 10 seconds. The slides were then washed in 70%, 90% and 100% EtOH for 1, 1 and 2 minutes respectively. Slides were allowed to air dry and then mounted with coverslips using DPX mountant. Images were captured on a Nikon Ci microscope using a 20x objective lens (Nikon, Kingston-upon-thames, UK).

2.3.3 Muscle fibre size analysis

Materials

ImmEdge hydrophobic marker (Vector labs, Ca, USA).

Rhodamine labelled Wheat Germ Agglutinin (WGA-Rhodamine) (Vector labs, California, USA)

Vectorshield hardset mounting media containing 4',6-diamidino-2-phenylindole (DAPI) (Vector labs, California, USA)

PBS (Sigma-Aldrich, Missouri, US)

Triton (Sigma Aldrich, Missouri, US)

Protocol

Transverse sections of EDL muscles were surrounded with a hydrophobic marker pen and PBS containing 0.2 % triton was added to the slides for 10 minutes to remove the tissue resin. The PBS was removed and 1 in 1000 of stock rhodamine-WGA solution in PBS was added for 15 minutes at room temperature. The rhodamine-WGA was removed and muscle sections washed 3 x 5-mins in PBS containing 0.2% triton. The sections were dipped into distilled water to remove any salts. Coverslips were then mounted in Vectorshield hardset mounting media containing DAPI (Kostrominova et al. 2010).

The muscle sections were imaged on a Zeiss LSM800 confocal microscope (Carl Zeiss AG, Oberkochen, Germany) with a 20x objective lens (Carl Zeiss AG, Oberkochen, Germany). The scan area was manually set to include the entire EDL section and focus was achieved by manually setting focus support points across the section. Images were exported as TIFF files.

Images were analysed to determine the total fibre number and Minimal Feret's diameter were analysed using the tissue cell geometry plugin on FIJI (U.S. National Institutes of Health, USA).

2.3.4 Analysis of centrally positioned nuclei in transverse muscle sections

Materials

Rhodamine labelled Wheat Germ Agglutinin (Rhodamine-WGA) (Vector labs, California, USA)

Vectorshield hardset mounting media containing DAPI (Vector labs, California, USA)

PBS (Sigma-Aldrich, Missouri, US)

Triton (Sigma Aldrich, Missouri, US)

Protocol

Transverse muscle sections were stained WGA-Rhodamine and DAPI as described above in **Section 2.3.3**. Images were captured using a Zeiss Axio Scan Z1 (Carl Zeiss AG, Oberkochen, Germany) using the settings detailed in **Figure 2.3**.

	Channel 1	Channel 2	Channel 3

Acquisition Information

Scan Profile	3chan DAPI 488 RHOD fluo 20x-.czspf
Acquisition Start	12/07/2019 11:57:40
Microscope	Axio Scan.Z1
Objective	Plan-Apochromat 20x/0.8 M27
Filters	412 - 438, 501 - 527, 583 - 601, 662 - 756, 507 - 543, 578 - 640

	Channel 1	Channel 2	Channel 3
Beam Splitter	405, 493, 575, 653	498	568
Filter Em. Wavelength	412 - 438, 501 - 527, 583 - 601, 662 - 756	507 - 543	578 - 640
Contrast Method	Fluorescence	Fluorescence	Fluorescence
Light Source	LED-Module 385nm	LED-Module 475nm	LED-Module 555nm
Light Source Intensity	20.57 %	60.05 %	75.00 %
Illumination Wavelength	370-400	450-488	505-605
Channel Name	DAPI	AF488	Rhoda
Channel Description			
Dye Name	DAPI	AF488	Rhoda
Channel Color			
Excitation Wavelength	353	493	558
Emission Wavelength	465	517	575
Effective NA	0.8	0.8	0.8
Imaging Device	Axiocam 506	Axiocam 506	Axiocam 506
Camera Adapter	1x Camera Adapter	1x Camera Adapter	1x Camera Adapter
Exposure Time	1.8 ms	50 ms	70 ms
Depth of Focus	1.45 μm	1.62 μm	1.80 μm
Binning Mode	2,2	2,2	2,2

Figure 2.3: Settings for the imaging of transverse muscle sections for the analysis of centrally positioned nuclei in fibres.

All fibres with peripheral nuclei were filtered out of images by an ImageJ macro created in-house (**Figure 2.4**). The resulting images were analysed using MyoVision (University of Kentucky, USA) to further identify the size of fibres with and without centrally positioned nuclei (Wen et al. 2018).

The resulting data was analysed to produce grouped fibre sizes, median minimum Feret's diameter and the percentage of fibres with centrally and peripherally located nuclei using R markdown.

The numbered steps in the figure:

1. Split channels into WGA and DAPI
2. Filter and reduce WGA background
3. Auto-local threshold
4. Analyse particles to extract debris in centre of fibres
5. Blur the central debris
6. Generate image from central debris subtracted from thresholded WGA
7. Binarise and dilate by 8 pixels
8. Gaussian blur (Sigma = 4)
9. Create new image from DAPI subtract the Gaussian blurred binary
10. Overlay central nuclei extracted and original WGA

Figure 2.4: Macro for filtering out fibres with peripheral nuclei.

2.3.5 Immunostaining of p65

2.3.5.1 Immunostaining for p65 localisation in transverse muscle sections

Materials

ImmEdge hydrophobic marker (Vector labs, Ca, USA).

Rhodamine labelled Wheat Germ Agglutinin (WGA-Rhodamine) (Vector labs, California, USA)

Vectorshield hardset mounting media containing DAPI (Vector labs, California, USA)

PBS (Sigma-Aldrich, Missouri, US)

Triton (Sigma Aldrich, Missouri, US)

Recombinant Anti-NF-κB p65 antibody (ab32536) (Abcam, Cambridge, UK)

Goat anti-Rabbit IgG (H+L) Cross-Adsorbed Secondary Antibody, Alexa Fluor 488 (Invitrogen, California, US)

Bovine serum albumin (Sigma Aldrich, Missouri, US)

Normal goat serum (Fisher Scientific, California, US)

Protocol

The EDL sections were surrounded with a hydrophobic marker and 100 µL PBS containing 0.2 % triton was added to the slides for 10 minutes to remove the tissue resin. The PBS was removed and 100 µL blocking buffer of PBS containing 1% triton, 1% BSA and, 10% normal goat serum was added and sections incubated for 1 hour at room temperature. The blocking buffer was removed and sections were washed 3 x 5-minute washes in 100 µL PBS with 0.2 % triton.

The primary p65 antibody (ab32536, Abcam) was diluted 1 in 1000 in PBS containing 0.2% triton, 1 % BSA and 100 µL added to the sections. These were incubated overnight at 4°C, loosely covered with a parafilm to prevent evaporation. The primary antibody was removed, and the sections washed 3 x 5-minute washes in 100 µL PBS containing 0.2 % triton.

The secondary antibody was diluted 1 in 1000 in PBS containing 0.2% triton, 1 % BSA and 100 μL added to the sections. This was incubated for 1 hour at room temperature. The secondary antibody was removed and the sections washed 3 x 5-minute washes in 100 μL PBS containing 0.2 % triton.

Stock solution of WGA-rhodamine was diluted 1 in 1000 in PBS and 100 μL added to the sections. This was incubated for 10 minutes at room temperature before being removed and the sections washed in 100 μL PBS containing 0.2 % triton.

The slides were placed into ddH$_2$O to remove any residual salts. The slides were dried, then mounted with coverslips using Vectorshield hardset mounting media containing DAPI.

2.3.5.2 Immunostaining of p65 in isolated FDB muscle fibres

Materials

Rhodamine labelled Wheat Germ Agglutinin (Rhodamine-WGA) (Vector labs, California, USA)

Vectorshield hardset mounting media containing DAPI (Vector labs, California, USA)

PBS (Sigma-Aldrich, Missouri, US)

Triton (Sigma Aldrich, Missouri, US)

Recombinant Anti-NF-κB p65 primary antibody (ab32536) (Abcam, Cambridge, UK)

Goat anti-Rabbit IgG (H+L) Cross-Adsorbed Secondary Antibody, Alexa Fluor 488 (Invitrogen, California, US)

Bovine serum albumin (Sigma Aldrich, Missouri, US)

Normal goat serum (Fisher Scientific, California, US)

Protocol

The fibres were prepared as described previously (Section 2.2.4). Media was removed from the fibres and the fibres were washed with PBS. Serum free media was added (200 μL), and the fibres were incubated for 1.5 hours 37 °C, 5% CO_2. The fibres were fixed in 200μL 4% NBF for 1 hour at room temperature. The NBF was removed and the fibres washed 3 times in 200 μL PBS with 0.2% triton.

The PBS was removed and 200 μL blocking buffer of PBS containing 1% triton, 1% BSA and, 10% normal goat serum added and fibres were incubated for 1 hour at room temperature. The blocking buffer was removed, and fibres were washed 3 x 5-minute washes in 200 μL PBS with 0.2 % triton.

The primary p65 antibody (ab32536, Abcam) was diluted 1 in 1000 in PBS containing 0.2% triton, 1 % BSA and 200 μL added to the fibres. These were incubated overnight at 4 °C in high humidity. The primary antibody was removed, and the fibres washed 3 x 5-minute washes in 100 μL PBS containing 0.2 % triton.

The secondary antibody was diluted 1 in 1000 in PBS containing 0.2% triton, 1 % BSA and 200 μL added to the fibres. This was incubated for 1 hour at room temperature. The secondary antibody was removed, and the fibres washed 3 x 5-minute washes in 200 μL PBS containing 0.2 % triton.

Stock WGA-rhodamine was diluted 1 in 1000 in PBS, 200 μL added to the fibres and these were then incubated for 10 minutes at room temperature before this solution was removed and the fibres washed in 200 μL PBS containing 0.2 % triton. A final two washes with ddH_2O was performed to remove any salt residues. The coverslips were removed from the wells, upturned and mounted on slides using Vectorshield hardset mounting media containing DAPI.

Fibres were imaged on a Zeiss LSM800 confocal microscope (Carl Zeiss AG, Oberkochen, Germany) with a 40x oil immersion objective lens (Carl Zeiss AG, Oberkochen, Germany). Z-stacking and image stitching were used to obtain a 3D representation of full fibres using the Zen imaging software (Carl Zeiss AG, Oberkochen, Germany).

2.4 Biochemical Analyses

2.4.1. GTN muscle sample preparation for all assays

Materials

Liquid nitrogen

Protocol

GTN muscles were recovered from -80 °C storage in liquid nitrogen. A pestle and mortar were pre-cooled with liquid nitrogen. The frozen muscle was placed into the mortar with additional liquid nitrogen. The GTN muscle was ground into a fine powder with the cooled pestle. Once ground to powder, the muscle was resuspended in liquid nitrogen and transferred to microcentrifuge tubes for future analyses described below.

2.4.1.1 Preparation of GTN muscle samples for Luminex assay

Materials

Bio-Plex Cell Lysis Kit (BioRad, California, US)

Phenylmethylsulfonyl fluoride (PMSF) (Sigma Aldrich, Missouri, US)

Dimethyl sulfoxide (DMSO) (Sigma Aldrich, Missouri, US)

Protocol

Bioplex lysing solution was prepared from mixing factor 1: factor 2: lysing buffer: PMSF (2:4:990:4) following manufcturer's instructions. To ~75 mg ground GTN muscle powder, 500

µL lysing solution was added and the muscle was homogenised using a pellet pestle (Sigma Aldrich, Missouri, US). The sample was then sonicated on ice for 30 seconds in short bursts. The samples were centrifuged at 4,500 g for 4 minutes at 4 °C. The supernatant was collected and stored at -80°C, and the pellet was disposed of.

2.4.1.2 Preparation of GTN muscle samples for western blotting

Materials

10 x RIPA Buffer (Cell signalling Technologies, Massachusetts, United States)

cOmplete™ Protease Inhibitor Cocktail (Roche, Basel, Switzerland)

Protocol

RIPA buffer was prepared by adding 10x RIPA buffer to ddH$_2$O 1:9. To this, one cOmplete protease inhibitor cocktail was added per 10 mL solution. RIPA buffer (500 µL) was added to ~75 mg ground GTN powder and the mixture was further homogenised using a pellet pestle. The sample was sonicated on ice for 30 seconds in short bursts. The samples were centrifuged at 4,500 g for 4 minutes at 4 °C. The supernatant was collected, and pellet was disposed of. Supernatants were stored at -80 °C.

2.4.1.3 Preparation of GTN muscle samples for EMSA

Materials

Glycerol (Sigma Aldrich, Missouri, US)

NaCl (Sigma Aldrich, Missouri, US)

Ethylenediaminetetraacetic acid (EDTA) (Sigma Aldrich, Missouri, US)

1,4-Dithiothreitol (DTT) (Sigma Aldrich, Missouri, US)

4-(2-hydroxyethyl)-1-piperazineethanesulfonic acid (HEPES) (Sigma Aldrich, Missouri, US)

cOmplete™ Protease Inhibitor Cocktail tablet (Roche, Basel, Switzerland)

NP-40 (Igepal) (Sigma Aldrich, Missouri, US)

500 mM PMSF:

- 0.436 g PMSF
- 5 mL DMSO
- Store as 0.5 mL aliquots at -20 °C and don't thaw more than 5 times

1 M NaOH

- 29.22 g NaCl
- 500 mL ddH$_2$O

0.5 M EDTA

- 73.06g EDTA
- Add 400 mL ddH$_2$O
- Adjust pH until stable at pH 8 using NaOH pellets
- Add water so total volume is 500 mL

1M DTT

- 1.54 g DTT
- 10mL ddH$_2$O

EMSA extraction buffer (25 % glycerol, 0.42 M NaCl, 1.5 mM MgCl$_2$, 0.2 mM EDTA, 0.5 mM

DTT, 20 mM HEPES, 0.1 % NP-40, pH 7.9):

- 2.5 mL glycerol
- 4.2 mL 1M NaCl
- 15 μL 0.5M EDTA
- 5 μL 1M DTT
- 48 mg HEPES
- 3.3 mL ddH$_2$O
- Adjust pH to 7.9
- Add 1 cOmplete™ Protease Inhibitor Cocktail tablet
- 10 μL NP-40 (Igepal)

Protocol

EMSA extraction buffer (0.5mL) was added to ~75 mg GTN muscle powder. The samples were

then homogenised using a bench top rotary homogeniser. The samples were then sonicated

on ice for 30 seconds in short bursts. The samples were centrifuged at 4,500 g for 4 minutes at 4 °C. The supernatant was collected, and pellet was disposed of. Samples were stored at -80 °C.

2.4.1.4 Bradford assay for protein content analysis

Materials

BradfordUltra reagent (Expedion, Cambridge, UK)

2 mg/mL Bovine serum albumin (BSA) standard (ThermoFisher, Massachusetts, US)

Protocol

BSA standards were prepared from the 2mg/mL stock BSA as detailed in **Table 2.1**.

Table 2.1: Preparation of a standard curve to be used with BradfordUltra reagent from a stock BSA solution of 2 mg/mL.

Tube	Concentration of BSA (ug/mL)	µL standard from previous dilution	µL Water
A	500	50	150
B	250	100	100
C	125	100	100
D	50	120	80
E	25	100	100
F	0	0	100

Twenty µL of standards and samples were added to each well of a 96 well plate. One hundred and eighty µL of BradfordUltra assay was added to each of the wells. Any bubbles on the surface were removed and the plate was analysed immediately using a SpectroStar plate reader (BMG Labtech, Aylesbury, UK) measuring absorbance at 595 nm (Staunton et al. 2019).

A linear line of regression was fit to the standard values and concentrations of the unknown samples were computed from the equation of this line using the MARS Data Analysis Software (BMG Labtech, Aylesbury, UK).

2.4.2 Cytokine protein analysis of muscle and plasma samples

Materials

Bioplex assay kit (BioRad, California, US) containing:

- Coupled magnetic beads
- Detection antibodies
- Cytokine standard mix
- Sample diluent
- Detection antibody diluent
- Standard diluent
- Assay buffer
- Wash buffer
- Streptavidin-PE
- Assay plate
- Sealing tape

Bioplex protein lysate buffer (BioRad, California, US)

Protocol

Bioplex is a bead based multiplex immunosorbent assay based on luminex xMap technology. This system uses the same concepts as a sandwich enzyme linked immunosorbent assay (ELISA) where captured antibodies capture target proteins were an enzyme linked detection antibody is used to measure the concentration of the intended target protein. In the Luminex xMap system, distinctly dyed magnetic microspheres (beads) are coupled to different capture antibodies. The magnetic beads can be immobilised through the use of a strong magnetic stand allowing washing of unbound proteins. Detection is facilitated by a biotinylated antibody bound to streptavidin - Phycoerythrin (PE). Streptavidin fluoresces upon excitation by a 488 nm laser light.

Plasma samples were diluted 1:3 in sample diluent. GTN muscle lysate samples were diluted to a final concentration of 500 µg/mL in sample diluent with BSA added to a final concentration of 0.5%. Serum free media samples were diluted 7:1 in 4% BSA to a final concentration of 0.5% BSA to stabilise protein targets and to block against non-specific binding.

All reagents in the kit were warmed to room temperature. The included cytokine standard was reconstituted in 250 µL cytokine standard diluent (**Table 2.2**).

This was then used to produce a 7-point curve using fourfold dilutions each step. This is shown in **Table 2.3**.

Table 2.2: Cytokine stock concentrations from the cytokine standard included in the Bioplex kit for use with the concentration curve.

Cytokine	S1 Value pg/mL		Chemokine	S1 Value pg/mL
GM-CSF	13,446		CCL1	6,811
IFN-γ	7,263		CCL2	124,144
IL-1β	33,329		CCL3	9,473
IL-2	6,025		CCL4	58,085
IL-4	1,011		CCL5	14,245
IL-6	12,954		CCL7	2,921
IL-10	106,983		CCL11	7,976
IL-16	4,691		CCL12	8,767
TNF-α	10,092		CCL17	11,197
			CCL19	25,967
			CCL20	12,684
			CCL22	9,678
			CCL24	168,737
			CCL25	46,758
			CXCL1	22,531
			CXCL2	22,854
			CXCL5	95,630
			CXCL10	176,583
			CXCL11	68,806
			CXCL12	16,748
			CXCL13	146,200
			CXCL16	7,979
			CXCL27	115,024
			CX3CL1	28,804

Table 2.3: Volumes used to produce a 7-point standard curve as part of the Bioplex 33-plex cytokine assay

Standard	Volume from previous standard (µL)	Volume diluent (µL)
S1	250	0
S2	50	150
S3	50	150
S4	50	150
S5	50	150
S6	50	150
S7	50	150
Blank	200	0

The coupled beads were diluted 1 in 10 in assay buffer and vortexed for 30 seconds. A multichannel pipette was used to add 50 µL diluted beads to each of the wells. Wash buffer was prepared by diluting the 10X stock wash buffer 1 in 10 in ddH$_2$O. Plate washing was

performed twice by first placing the plate on the magnetic holder to attract the magnetic beads to the bottom of the well, and tapping the holder on the table. The plate and magnetic holder were then inverted over a sink and replaced with 100 µL wash buffer. This was repeated once more and the wash buffer was once again, expelled from the wells. Fifty µL of samples and standards were added into each appropriate well of the assay plate. The plate was covered with sealing tape and was incubated for 30 min on a plate shaker at room temperature.

The plate was washed three times as previous with 100 µL wash buffer. The detection antibodies were prepared by diluting the 10X detection antibody stock 1:9 in detection antibody diluent and vortexed for 5 seconds. Twenty five µL detection antibody was added to each well on the assay plate. This was sealed with sealing tape and incubated on a plate shaker for 30 min at room temperature.

The plate was washed 3 further times with 100 µL wash buffer. The 100X stock streptavidin-PE was diluted 1 in 100 in assay buffer, 50 µL of which was added to each well. The plate was covered with sealing tape and incubated on a plate shaker for 10 min at room temperature. The plate was washed 3 times in 100 µL wash buffer. The beads were resuspended in 125 µL assay buffer and placed on a plate shaker for 30 seconds at room temperature.

The plate was placed into a calibrated and validated Bioplex 200 (BioRad, California, US) using the low photomultiplier tube (PMT) setting, with the doublet discriminator (DD) gates set to 5,000 and 25,000 and the bead events set to 50.

2.4.3 RNA analysis of muscle samples

2.4.3.1 RNA extraction from GTN muscles

Materials

Trizol reagent (Invitrogen, California, US)

Chloroform:Isoamyl alcohol (24:1), (Sigma Aldrich, Missouri, US)

Glycogen, RNA grade (Thermofisher, California, US)

Isopropanol (Sigma Aldrich, Missouri, US)

EtOH (Sigma Aldrich, Missouri, US)

RNAse free water (Invitrogen, California, US)

Protocol

GTN muscles were ground to a fine powder under liquid nitrogen using a pestle and mortar as described in **Section 2.4.1**. Approximately 0.2g of the resulting powder was added to 500 mL trizol.

Chloroform (100 µL) was added and the sample tubes were shaken vigorously for 1 minute. The mixture was then left at room temperature for 10 minutes before being centrifuged at 12,000 g for 15 minutes at 4 °C. The upper aqueous phase was collected and transferred to another microcentrifuge tube.

Glycogen (0.5 µg; co-precipitates with RNA) was added to the upper aqueous phase, followed by 250 µL isopropanol to precipitate the RNA at room temperature for 10 minutes. This was then centrifuged at 12,000 g for 10 minutes at 4 °C and the supernatant was completely removed.

EtOH (500 µL) was added to the pellet, and mixed. Samples were then centrifuged at 12,000 g for 5 minutes at 4 °C. The supernatant was removed and the pellets were left to air dry for 5 – 10 minutes at room temperature.

RNAse free water (30 µL) was added to the pellet and mixed by pipetting. RNA samples were heated to 55 °C for 10 minutes. Quantity and quality of RNA samples was measured using a nanodrop (Thermofisher; Winsford, UK). RNA was stored at -20 °C until use.

2.4.3.2 Complementary (cDNA) synthesis

Materials

iScript revese transcription kit (BioRad, California, US)

RNAse free water (Invitrogen, California, US)

Protocol

One µg of the isolated RNA was reverse transcribed using iScript cDNA Synthesis Kit from in the volumes detailed in **Table 2.3**.

Table 2.3: Reaction volumes for cDNA synthesis with iScript reagents.

Reagent	Volume (µL)
iScript Reverse transcription	1
iScript reaction mix	4
RNA	Volume for 1 µg RNA
Water	To final volume 25 µL

The reaction mixture was incubated in a thermocycler using the following protocol: 5 minutes at 25 °C, 1 minute at 46 °C and 1 minute at 95 °C as shown in **Table 2.4**. Synthesised cDNA was stored at -20 °C until used.

Table 2.4: Times and temperatures used for reverse transcription of RNA from muscle samples using iScript reagents

Step	Time	Temperature (°C)
Priming	5 Minutes	25
Reverse transcription	20 Minutes	46
Inactivation	1 Minute	95
Stop	Hold	4

Materials

Brilliant Multiplex qPCR mastermix (Agilent, California, US)

Nuclease free water (Invitrogen, California, US)

Fam conjugated experimental taqman probe (Thermofisher, California, US)

Vic conjugated housekeeping taqman probe (Thermofisher, California, US)

Reference dye (Agilent, California, US)

Microseal 'B' PCR Plate Sealing Film (Biorad, California, US)

Protocol

A mastermix was prepared containing reagents for the qPCR reaction to a total volume of 25 µL per well (**Table 2.5**). This mastermix was vortexed and 24 µL was added to each well.

Table 2.5: Reagent volumes for duplex TaqMan qPCR reaction

Reagent	Volume per reaction (µL)
Brilliant multiplex qPCR mastermix	12.5 µL
Fam experimental taqman probe	1 µL
Vic housekeeping taqman probe	1 µL
Reference dye	0.375 µL
Nuclease free water	9.125 µL

One µL cDNA was added to each well. The plate was sealed with sealing film and vortexed for 30 seconds. The plate was centrifuged and then placed in an Agilent Mx3005P qPCR thermocycler (Agilent, California, US). The two-step PCR cycling protocol used is detailed in **Table 2.6**.

Table 2.6: Cycle temperatures and durations for duplex taqman qPCR performed on an Agilent Mx3005P thermocycler

Cycles	Duration of Cycle	Temperature
1	10 Minutes	95 °C
40	15 seconds	95 °C
40	1 minute	60 °C

2.4.4 Measuring NF-κB DNA binding activity in muscles using EMSA

Materials

1M NaCl

40% Acrylamide (29:1), Acrylamide: bis-Acrylamide solution (Biorad, California, US)

Tris-base (Sigma Aldrich, Missouri, US)

Glycine (Sigma Aldrich, Missouri, US)

0.5M EDTA

1M DTT

Ammonium persulphate (APS) (Sigma Aldrich, Missouri, US)

Tetramethylethylenediamine (TEMED) (Biorad, California, US)

Potassium chloride (KCl) (Sigma Aldrich, Missouri, US)

Magnesium chloride (MgCl$_2$) (Sigma Aldrich, Missouri, US)

Glycerol (Sigma Aldrich, Missouri, US)

Orange G (Sigma Aldrich, Missouri, US)

Boric Acid (Promega, Wisconsin, US)

Tween-20 (Sigma Aldrich, Missouri, US)

Poly (dI-dC) 1 µg/µL in 10 mM Tris, 1mM EDTA; pH 7.5 (Licor, Cambridge, UK)

NF-κB p65 (D14E12) XP® Rabbit mAb (Cell Signalling Technologies, Massachusetts, United States)

50 nM NFκB Oligo (IRDye 700) (Licor, Cambridge, UK)

Unlabelled NF-κB probe (Licor, Cambridge, UK)

AP-1 consensus region oligo (IRDye 700) probe (Licor, Cambridge, UK)

1 M Tris-HCl, pH 7.5

- 60.57 g Tris-base
- Add 400 mL ddH$_2$O
- Adjust pH to 7.5 using concentrated HCl
- Add water so total volume is 500 mL

1M Glycine

- 37.54g Glycine
- Add 500 mL ddH$_2$O

10% APS

- 5g APS
- 50 mL ddH$_2$O

1M KCl

- 7.46g KCl
- 100 mL ddH$_2$O

1M DTT

- 1.54 g DTT
- 10mL ddH$_2$O

10x EMSA binding buffer - 100 mM Tris, 500 mM KCl, 10 mM DTT; pH 7.5

- 10 mL 1M Tris-HCl, pH 7.5
- 50 mL 1M KCl
- 1 mL 1 M DTT
- 39 mL ddH$_2$O

EMSA gel solution

- 5 mL 40% Acrylamide (29:1), Acrylamide: bis-Acrylamide solution
- 2 mL 1 M Tris, pH 7.5
- 7.6 mL 1 M Glycine
- 160 μL 0.5 M EDTA, pH 8.0
- 26 mL ddH$_2$0
- 200 μL 10% APS
- 30 μL TEMED

10X Orange G loading dye

- 100 mg Orange G
- 25 mL ddH$_2$O
- 25 mL glycerol

10X TBE solution

- 121.1 g Tris base
- 61.8 g Boric acid
- 20 mL 1M EDTA, pH 7.5
- Dissolve all in 700 mL ddH$_2$O
- Make up to 1 L with ddH$_2$O

25 mM DTT, 2.5% Tween-20

- 0.25 mL 1M DTT
- 0.25 mL Tween 20
- 9.5 mL ddH$_2$O

100 mM MgCl$_2$

- 95.211 mg MgCl$_2$
- 10 mL ddH$_2$O

200 mM EDTA, pH 8.0

- 4 mL 1M EDTA
- 6 mL ddH$_2$O

Protocol

The protein content of EMSA samples was measured by a Bradford assay to determine the loading volume for 100 μg protein of the individual samples as described in S**ection 2.4.1.4**.

The following protocol was performed using a Hoefer SE400 Air-cooled Vertical Protein Electrophoresis assembly. The EMSA gel solution was prepared as described in Table 2.6. The gel solution was gently pipetted between two clamped glass plates and a 1.5 mm, 15 well gel comb was inserted into the top of the gel solution. The gel was allowed to set for ~3 hours.

Muscle samples were prepared as shown in **Table 2.7**. The samples were incubated at room temperature for 30 minutes in the dark as to prevent photobleaching of the IRDye 700 probe. Two µL 10X orange g loading buffer was added to each sample and mixed. The samples were then loaded into the gel. Electrophoresis was performed at °C, 160V for ~2.5 hrs. The gel was imaged on a Licor Odyssey CLx system (Licor, Cambridge, UK).

Table 2.6: Reagent volumes for EMSA reaction mixtures using Licor fluorescent probes

Reagent	Volume uL
10X binding buffer	2
25 mM DTT, 2.5 % tween-20	2
Poly (dI-dC) 1 µg/µL in 10 mM Tris, 1mM EDTA; pH 7.5	1
100 mM MgCl$_2$	1
200 mM EDTA, pH 8.0	1
50 nM NFκB Oligo (IRDye 700)	1
ddH$_2$O	2
100 µg Protein extract in ddH$_2$O	10

Supershift and inhibition experiments

For the supershift experiments, 20 µL chromatin immunoprecipitation (ChIP) grade p65 antibody was added to the protein extract and ddH$_2$O prior to the reaction mixture. This was then incubated for 20 minutes at room temperature in the dark before adding to the reaction mixture.

The competitive probe was an unlabelled NF-κB probe of the same nucleotide sequence. The non-competitive inhibitor was an AP-1 consensus region oligo (IRDye 700) probe. To perform the competitive and non-competitive inhibitor experiments, 2 µL of the inhibitor was added to the reaction mixture prior to the NF-κB oligo probe.

2.4.5 SDS-PAGE and western blotting

Materials

0.1% Ponceau S solution (Sigma Aldrich, Missouri, US)

Sodium dodecyl sulphate (SDS) (Thermofisher, California, US)

Bromophenol blue (Sigma Aldrich, Missouri, US)

1M Tris-hydrochloride (tris-HCl)

Glycerol (Sigma Aldrich, Missouri, US)

0.5 M EDTA

β-mercaptoethanol (Thermofisher, California, US)

Tris-base (Sigma Aldrich, Missouri, US)

Methanol (Sigma Aldrich, Missouri, US)

6-Aminocaproic acid (Sigma Aldrich, Missouri, US)

NaCl (Sigma Aldrich, Missouri, US)

Sodium hydroxide (NaOH) pellets (Sigma Aldrich, Missouri, US)

Concentrated HCl (Sigma Aldrich, Missouri, US)

Tween-20 (Sigma Aldrich, Missouri, US)

45 % Fish scale gelatine (FSG) (Sigma Aldrich, Missouri, US)

Acrylamide/Bis (30%, 37.5:1) (Biorad, California, US)

TEMED (Biorad, California, US)

PageRuler prestained protein ladder (ThermoScientific, California, US)

10% APS **4X Loading buffer**

- 0.8 g SDS
- 4 mg bromophenol blue
- 2 mL 1M Tris-HCl
- 4 mL glycerol
- 1 mL 0.5 M EDTA
- 0.4 mL β-mercaptoethanol
- 2.6 mL ddH$_2$O

10% SDS

- 5 g SDS powder
- 50 mL ddH$_2$O

10X Running buffer

- 14.4 g glycine
- 3.02 g tris base
- 10 mL 10 % SDS
- 990 mL ddH$_2$O

1X Running buffer

- 100 mL 10X running buffer
- 900 mL ddH$_2$O

Anode 1 buffer

- 36.34 g tris base
- 100 mL Methanol
- 800 mL ddH$_2$O
- Adjust pH to 10.4
- Add water to total volume 1 L

Anode 2 buffer

- 3.03 g tris base
- 100 mL Methanol
- 800 mL ddH$_2$O
- Adjust pH to 10.4
- Add water to total volume 1 L

Cathode buffer

- 3.03 g tris base

- 5.25 g 6-Aminocaproic acid
- 100 mL Methanol
- 800 mL ddH$_2$O
- Adjust pH to 9.4
- Add water to total volume of 1 L

10X tris-buffered saline (TBS)

- 24.22 g tris HCl
- 87.66 NaCl
- Dissolve in 900 mL ddH$_2$O
- Adjust pH to 7.6 using HCl
- Add water to total volume of 1 L

TBS-tween (TBS-T)

- 100 mL 10X TBS
- 1 mL Tween 20
- 899 mL ddH$_2$O

5% FSG

- 111.1 mL 45 % FSG (warmed in microwave to decrease viscosity; 700W ~2 minutes)
- 888.9 mL ddH$_2$O

Blocking buffer – 1% FSG in TBS

- 100 mL 5% FSG
- 400 mL ddH$_2$O

Primary – 1% FSG in TBS-Tween

- 100 mL 5% FSG
- 50 mL 10X TBS
- 350 mL ddH$_2$O

Secondary – 1% FSG in TBS-Tween with 0.01% SDS.

- 100 mL 5% FSG
- 50 mL 10X TBS
- 0.5 mL 10% SDS
- 350 mL ddH$_2$O

Protocol

The protein content of lysate samples was measured by Bradford assay to determine the loading volume of the individual samples as described in **Section 2.4.1.4**. Protein lysates were diluted to contain 20 µg of total protein in ddH$_2$O to a volume of 11.5 µL. To these diluted samples, 3.5 µL 4X loading buffer was added and the samples were heated to 95°C for 5 minutes.

A 10 % SDS-PAGE gel was cast using a mini-Protean tetra handcast system (Biorad, California, US) using the reagents described in **Table 2.7** to make the 10% acrylamide resolving gel and **Table 2.8** to make the 4% acrylamide stacking gel. The resolving gel was poured into the cast and add approximately 1 mL ethanol to the top to remove any bubbles. After 20 minutes the ethanol was removed, and the stacking gel was added and comb fitted. The gel was allowed to set for ~30 minutes and either used immediately or stored at 4 °C wrapped in wet tissue overnight. Once ready to use, the gels were loaded into a mini-Protean tetra vertical gel tank, filled, and surrounded by running buffer.

Table 2.7: Reagents and volumes used to make 10 mL 10% SDS-PAGE resolving gel

Reagent	Volume for 10 mL 10% resolving gel
ddH$_2$O	2.8 mL
Acrylamide/Bis (30%, 37.5:1)	3.3 mL
Tris-HCl 1M	3.75 mL
10% SDS	100 µL
TEMED	10 µL
10% APS	32 µL

Table 2.8: Reagents and volumes used to make 10 mL 10% SDS-PAGE stacking gel

Reagent	Volume for 10 mL 4% stacking gel
ddH$_2$O	4.7 mL
Acrylamide/Bis (30%, 37.5:1)	1.3 mL
Tris-HCl 1M	3.75 mL
10% SDS	100 µL
TEMED	10 µL
10% APS	100 µL

Pageruler pre-stained protein ladder (4 µL) was placed into the first well of the gel and 20 µg of the samples were added to the remainder of the wells being careful not to have any liquid spill out of the wells. The lid of the tank was placed in position, and electrophoresis was performed for 15 minutes at 30V for the proteins to reach the border of the stacking and resolving gels. The voltage was raised to 120V and the electrophoresis was continued until the bromophenol blue front was close to the bottom of the gel (~50 minutes).

The gel was removed from the chamber, the glass plates separated, and the stacking gel was cut and disposed of from the resolving gel. To the lower anode plate of the semi-dry transfer system, a stack of 2 filter papers soaked in anode 1 buffer were placed followed by a filter paper and square of nitrocellulose membrane soaked in anode 2 buffer. The gel was placed on top of the nitrocellulose membrane and 3 sheets of filter paper soaked in cathode buffer. After each addition to the stack, the stack was rolled over with a roller to ensure no bubbles had formed between stacks. The completed stack is shown in **Figure 2.5**. The transfer was performed at 60 mA per stack for 1 hour.

Figure 2.5: Diagram of the semi dry transfer step of a western blot.

The membrane was recovered from the stack and Ponceau (0.1%) was added to the membrane which was agitated on a rocker for 5 minutes. The ponceau was removed and ddH$_2$O was used to rinse off the excess ponceau. The membrane was imaged on a Biorad Chemidoc XRS+ (Biorad, California, US) using Image Lab software (Biorad, California, US) to determine whether transfer had occurred evenly.

The ponceau was removed from the membrane through 3 x 5 minutes of washing using TBS-T at room temperature with agitation. The TBS-T was removed, and the membrane was covered with blocking buffer for 1 hour at room temperature with agitation.

The blocking buffer was removed, and the membrane was washed 3 x 5 minutes at room temperature. The primary antibody was diluted 1 in 1000 in the primary incubation buffer and incubated with the membrane overnight at 4°C with agitation.

The primary antibody was removed. The membrane was washed 3 x 5 minutes at room temperature. The secondary (IRDye 800CW) antibody was diluted 1:15,000 in secondary incubation buffer and incubated with the membrane for 1 hour at room temperature with gentle agitation.

The secondary antibody was removed, and the membrane was washed 5 x 5 minutes at room temperature. The membrane was imaged using a Licor Odyssey CLx system (Licor, Cambridge, UK). Pixel densitometry was performed in Image studio lite (Licor, Cambridge, UK) to quantify the images obtained.

2.4.6 Sample preparation for proteomics

2.4.6.1 Sample preparation of GTN muscles

GTN muscles (unlabelled and ^2H_2O dosed) were homogenised in 10-volumes of 25 mM ammonium bicarbonate containing a protease inhibitor cocktail. The sample was homogenised via a TissueRuptor (Qiagen, Hilden, Germany) set to the lowest setting. Further homogenisation was achieved using a bead beating homogeniser. 37.5U benzonase nuclease was added to each sample to reduce viscosity.

Fifty μg protein was diluted to be 80 μL in volume with 25 mM ammonium bicarbonate. Five μL of 1% Rapigest SF was added and the samples were brought to 80 °C for 10 minutes. Five μL 46.6 mg/mL iodoacetaide in 25 mM ammonium bicarbonate was added in the dark at room temperature for 30 minutes for alkylation to take place. This reaction was quenched using 4.7 μL DTT. Five μL trypsin was added to samples and samples were incubated overnight at 37 °C. Rapigest was removed through acidification with 1 μL trifluoroacetic acid (TFA) and incubation at 37 °C for 45 minutes. Samples were centrifuged at 17,200 g and supernatants were transferred to fresh tubes.

2.4.6.2 Liquid chromatography – tandem mass spec (LC-MSMS) analysis

Data-dependent LC-MSMS analyses were conducted on a QExactiveHF quadrupole-Orbitrap mass spectrometer coupled to a Dionex Ultimate 3000 RSLC nano-liquid chromatograph (Hemel Hempstead, UK). Sample digest (0.4mL, 200ng protein equivalent) was loaded onto a trapping column (Acclaim PepMap 100 C18, 75 μm x 2 cm, 3 μm packing material, 100 Å) using a loading buffer of 0.1% (v/v) TFA, 2 % (v/v) acetonitrile in water for 7 min at a flow

rate of 12 µL min-1. The trapping column was then set in-line with an analytical column (EASY-Spray PepMap RSLC C18, 75 µm x 50 cm, 2 µm packing material, 100 Å) and the peptides eluted using a linear gradient of 96.2 % A (0.1 % [v/v] formic acid):3.8 % B (0.1 % [v/v[formic acid in water:acetonitrile [80:20] [v/v]) to 50 % A:50 % B over 55 min at a flow rate of 300 nL min-1, followed by washing at 1% A:99 % B for 6 min and re-equilibration of the column to starting conditions. The column was maintained at 40°C, and the effluent introduced directly into the integrated nano-electrospray ionisation source operating in positive ion mode. The mass spectrometer was operated in data dependent acquisition mode with survey scans between m/z 350-2000 acquired at a mass resolution of 60,000 (FWHM) at m/z 200. The maximum injection time was 100 ms, and the automatic gain control was set to 3e6. The 16 most intense precursor ions with charges states of between 2+ and 5+ were selected for MS/MS at a resolution of 30,000 with an isolation window of 2 m/z units. The maximum injection time was 45 ms, and the automatic gain control was set to 1e5. Fragmentation of the peptides was by higher-energy collisional dissociation using a normalised collision energy of 30 %. Dynamic exclusion of m/z values to prevent repeated fragmentation of the same peptide was used with an exclusion time of 20 sec.

2.4.6.3 Quantification of protein abundance

For the protein abundance from the unlabelled samples, Individual data files were searched against the UniProt mouse reviewed database (16,966 sequences) using the Mascot search engine (Version 2.6.2). Between 900-1050 proteins were identified in each sample. A precursor and fragment ion mass tolerance of 10ppm and 0.01Da was used respectively. A fixed modification of carbamidomethyl cysteine and a variable modification of oxidation of methionine was included. Label free quantification was performed automatically on Progenesis QI.

2.4.6.4 Determination of Relative Isotope Abundance (RIA) and protein turnover rates (k)

The software d2ome (Sadygov et al. 2018) was used to automate in vivo protein turnover analysis from the acquired LC-MS data of heavy water metabolic labelling. Each Thermo raw MS data file, from each animal muscle tissue sample over the labelling trajectory, was initially converted into mzML format, using the MSConvert tool within Proteowizard (Chambers et al. 2012). mzML files were then searched using Mascot (version 2.7.0, Matrix Science, UK) against a UniProt Mus genus database (dated April 25, 2018) containing 16,966 reviewed entries. The search parameters allowed for a single trypsin missed cleavage and carbamidomethylation of cysteine residues as a fixed modification. Oxidation of methionine was allowed as variable modification. A peptide tolerance of 15 ppm was set, with an MS/MS tolerance of 0.01 Da. Following database searching, each search result was exported in mzIdentML format for use in d2ome which uses the mass spectral data (mzML files) and the corresponding protein identification results (mzIdentML files) and analyses all proteins/peptides that pass pre-defined identification thresholds (here, mass accuracy = 15 ppm; minimum protein score = 40; minimum peptide score = 20; maximum peptide expectation = 0.05; elution time window = 1 min; minimum number of experiments for protein consistency = 4; minimum number of experiments for a peptide consistency = 4). Mass isotopomer quantification is done in three-dimensional space (chromatographic time, m/z, and abundance). Increases in heavy peptide mass isotopomers (m1, m2, m3, m4, etc.) due to 2H-incorporation are reflected by a parallel decline in the monoisotopic mass spectral peak (m0) envelope, with time. Protein turnover rate constants (k) were determined based on the RIA data at each time point, t, using the default fitting process in d2ome (Sadygov et al. 2018), with the maximum achievable Relative isotopic abundance (RIA) set as a fixed value, the body water enrichment level, measured from plasma acetone exchange to be 4.64% (adult) and 4.71% (old).

2.4.6.5 Data analysis

All graphs were produced using "ggplot2" unless otherwise stated. The R packages "factorMineR" and "factoextra" were implemented for principle component analysis (PCA) and the "heatmap.2()" function from "gplots" was used (Lê et al. 2008). Kyoto encyclopedia of genes and genomes (KEGG) and gene ontology (GO) pathways were annotated and visualised using the "enrichKEGG()" and "enrichGO()" functions from the "clusterProfiler" package (Yu et al. 2012). Protein lengths and masses were annotated to each protein using the "UniprotR" package. Protein datasets and RNAseq datasets were merged through annotating the RNAseq dataset with Uniprot IDs according to their ensembl gene IDs and merging the datasets.

2.5 Statistics

All statistics were performed using Graphpad prism 8.4.3 (GraphPad Software, Inc, California, USA) unless otherwise stated. Statistical test performed is Analysis of variance (ANOVA) with post hoc Dunnet's test unless otherwise stated.

Combined -omics including dynamic proteomics, label-free proteomics and transcriptomics analysis were performed on R and all graphs and figures in Chapter 6 have been produced using ggplot2 unless stated otherwise.

Chapter 3: Alterations in inflammatory processes in plasma and muscles of old WT and adult SOD1KO mice

3.1 Introduction

3.1.1 There are dramatic changes in inflammatory status with ageing in humans and mice

Inflammaging is observed in a number of diseases including dementia, diabetes and chronic kidney disease (Ferrucci & Fabbri 2018). These diseases are characterised by high circulatory levels of inflammatory mediators, induction of disability and cellular senescence (Ferrucci & Fabbri 2018). Changes in a number of cytokines and chemokines have been reported during ageing, thus, there is an increase in the plasma concentration of G-CSF, GM-CSF, MIP-1/CCL2, TGF-α, IL-8, IL-12, IP-10/CXCL10, IL-6, IL-10, IFN-γ, Eotaxin/CCL11, IL-13, IL-1β, TNF-α, IL-1α, CCL2, CCL5, and CXCL10 in humans (Kim et al. 2011; Wang et al. 2017; Hoefer et al. 2017; Valdez et al. 2010; Rea et al. 2018; Tung et al. 2015; Gerli et al. 2001; Bonfante et al. 2017). Alongside the increase of these proinflammatory factors, there is also a decrease in the antagonist IL-1RA in the plasma of humans (Kinn et al. 2015). High plasma levels of several cytokines and chemokines, including IL-6 and CRP, are highly correlated with a loss of muscle strength and frailty in humans (Barbieri et al. 2003; Schaap et al. 2006; Westbury et al. 2018).

Similar changes in inflammatory cytokines and chemokines are observed in plasma of old WT compared with adult WT mice. Thus, changes in plasma concentrations of IL-6, IL-18, TNF-α, IL-4, IL-5, IL-22, CXCL1, and CCL7 are reported (Mahmoudi et al. 2019). Some reports of changes in mRNA expression levels have also been reported in cells and tissues. For example, the mRNA expression of IP-10/CXCL10, MIP-1α/CCL3, MIP-1β/CCL4, and RANTES/CCL5 was higher in CD4+ T-cells derived from old WT mice when compared with that of adult WT mice. Transgenic modification of cytokines and chemokines provides a link between inflammation and frailty. Thus, mice with a knockout of the gene for the anti-inflammatory cytokine IL-10, are a model of frailty showing an accelerated decrease in muscle strength with ageing when

compared with WT mice (Walston et al. 2008). These mice also show an increase in plasma IL-6 demonstrating the known network interactions of cytokines (Walston et al. 2008).

3.1.2 Muscle may be a major contributor to systemic increases in cytokines and chemokines

Human muscle has been shown to express many cytokines and chemokines including IL-1β, IL-4, IL-6, IL-7, IL-8, IL-10, IL-12p35, IL-15, IL-18, IFN-γ, TNF-α, MCP-1/CCL2 and TGFβ (Peake et al. 2015). Muscle fibres have also been shown to produce and secrete IL-1β, IL-6, IL-8, IL-18 TNF-α, MCP-1/CCL2, IFN-γ, CCL2, CXCL10, CCL5, CCL1, CCL19, CCL22, CXCL1, CXCL2 (Peake et al. 2015; Podbregar et al. 2013; Johnson et al. 2014; Chen et al. 2019; Catoire et al. 2014). *In-vitro*, mouse myotubes undergoing electric pulse stimulation produce a number of chemokines including CCL19, CCL22, CXCL5, and CXCL1 (Chen et al. 2019). In addition, cytokines possibly produced by other cells impact on muscle function - CXCL12 aids with muscle tissue regeneration as shown by an increase in rat muscle mass upon injection with the chemokine (Brzoska et al. 2012); CXCL10 mRNA expression is significantly increased following lengthening contractions (Deyhle et al. 2018) and exercise can result in an increase in the plasma content of IL-6 by as much as 100 fold (Steensberg et al. 2000). Muscle fibres from humans with Duchenne Muscular Dystrophy (DMD) have high levels of expression of CCL11, a chemokine known for its eosinophil attracting properties (De Paepe & De Bleecker 2013). An increase in TNFα and IL-6 expression and secretion is also observed in muscle biopsies of patients with DMD (Messina et al. 2011).

There is some evidence that there is an upregulation of cytokine or chemokine production or secretion from muscle or muscle fibres with increasing age, but data are sparce.

An increase in NF-κB DNA binding activity and p65 levels in the nucleus has been observed in the muscle of humans with Duchenne muscular dystrophy (DMD) (Messina et al. 2011). An increase in p65 levels has also been reported in humans (Cuthbertson et al. 2005)

although whether this reflects increased activity is unclear. Our laboratory has previously shown a chronic increase in NF-κB DNA binding activity in muscles of old WT mice using EMSA (**Figure 3.1**) and demonstrated that p65 was a major component of the activity, suggesting activation of the canonical NF-κB pathway (**Figure 3.1**). This published work also showed that this chronic activation was associated with a diminished acute NF-κB activation following a period of non-damaging exercise in old WT compared to adult WT mice (**Figure 3.1**; Vasilaki et al. 2006). The same study showed no significant difference in IκBα, p50 or p65 protein content in the muscle of old WT mice (Vasilaki et al. 2006b). If this chronic activation of NF-κB results in increased production of cytokines and chemokines by muscle, this has the potential to contribute to the systemic inflammation seen in old WT mice.

Mice lacking Cu,Zn superoxide dismutase (SOD1) show an accelerated, age-related loss of muscle mass and function (**Section 1.2.2.1**). Previously published work determined that adult mice lacking SOD1 in full body (SOD1KO mice) show a premature failure of adaptive responses to contractions in a similar manner to old WT mice. Adult SOD1KO mice (6–8 months of age) had a ∼30% reduction in muscle mass compared with age-matched WT mice and this was also associated with a chronic activation of DNA binding of NF-κB in muscle and a failure to activate NF-κB in response to non-damaging contractions (**Figure 3.1**; Vasilaki et al. 2010).
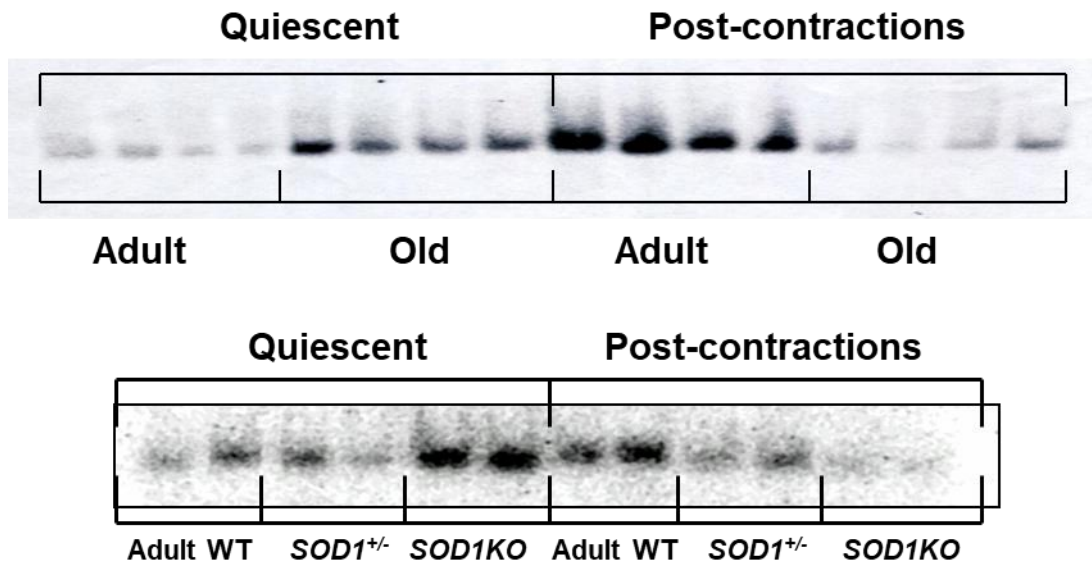
Figure 3.1. Electromotility shift assay showing *NF-kB binding activity of whole cell extracts from AT muscle of quiescent adult and old male mice and AT muscles immediately following a period of isometric contractions*. *There is a higher chronic basal level in the muscles of old WT and adult SOD1KO mice when compared with the adult mice and there is a decrease in the response to contractions in the muscles of SOD1KO mice and old WT mice when compared with the adult WT mice. Reproduced from Vasilaki et al. 2016 and* Vasilaki et al. 2010.

3.1.3 Hypothesis and aims

The hypothesis examined in this chapter was that the chronic activation of NF-κB in skeletal muscles of old WT and of adult SOD1KO mice results in a significant increase in the levels of cytokines and chemokines within muscles from both. This then influences systemic levels of cytokines and chemokines contributing to inflammaging. To test this hypothesis, the aims were as follows:

1. Determine the plasma concentrations of cytokines in old WT and adult SOD1KO mice compared with those of adult WT mice.

2. Determine whether NF-κB is activated in muscle fibres *per se* by determining the translocation of the NF-κB transcription component, p65 to nuclei within muscle fibres.

3. Determine the extent and number of cytokines in muscle tissue in old WT and adult SOD1KO mice compared with those of adult WT mice and whether these cytokines and chemokines were released by isolated muscle fibres from all cohorts.

3.2 Methods

3.2.1 Animals

Male C57BL6 mice adult (8-12 months) and old (22-26 months) WT mice and adult (8-12 months) SOD1KO mice were maintained in a temperature-controlled room (22-25°C) with food and water provided *ad libitum* on a 12-h light/dark cycle in the University of Liverpool Biomedical Services Unit. Numbers of mice in each group are given in the figure legends. All experimental procedures were performed under a UK Home Office licence (Home Office licence number P391895CA, approved 15/06/17) and complied with the UK Animals (Scientific Procedures) Act 1986 and were ethically approved by the University of Liverpool Animal Welfare Committee (AWERB) (Ethical approval number AWC0066, approved 23/3/17).

3.2.2 Sample preparation

3.2.2.1 Preparation of plasma samples for cytokine analysis

Blood samples were obtained via aortic bleed from adult WT, old WT and adult SOD1KO mice following an overdose of pentobarbital. Blood was collected into sodium heparin tubes which were then centrifuged at 10,000 g for 10 minutes at 4 °C. The plasma was then collected from the top layer into a clean microcentrifuge tube.

3.2.2.2 Preparation of muscle lysate samples for cytokine analysis

Muscle lysates were produced from adult WT, old WT and adult SOD1KO mice using the method described in **Section 2.4.1.1**.

3.2.2.3 Preparation of FDB muscle fibres for analysis of cytokine release

Fibres of FDB muscles were cultured overnight on ECM coated 6 well plates in MEM with serum as described in **Section 2.2.4**. The MEM was replaced with serum free MEM the following day. After 3 hours, the media was collected into microcentrifuge tubes and centrifuged at 1,000 g for 15 minutes at 4 °C to remove any crude debris. This time point was chosen as there is no evidence of cytokine degradation in media from muscle cells at 37°C (Lightfoot et al, unpublished). The total protein concentration of the supernatant was determined using a Bradford assay (**Section 2.4.1.4**). A stock of 4% BSA was then added to the samples 1:7 to produce a final concentration of 0.5% BSA in the sample following Luminex manufacturer's instructions for cytokine analysis.

3.2.3 Luminex assay to determine cytokine and chemokine levels in plasma, muscle lysate, and media from isolated muscle fibres

The cytokine protein assay was then performed according to **Section 2.4.2** using a Bioplex 200 (Biorad, California, US). Data are normalised to protein content of muscle fibres. Statistical analysis of cytokine levels was performed using a one-way ANOVA with post hoc

Dunnett's test for multiple comparisons in Graphpad Prism 8.4.3. Data are presented as mean ± SD.

Throughout this chapter, chemokines will be referred to with their systematic names (**Table 3.1**).

Table 3.1: List of systematic and common names for chemokines

Systematic name	Other name
CCL1	I-309
CCL2	MCP-1
CCL3	MIP-1a
CCL4	MIP-1b
CCL5	RANTES
CCL7	MCP-3
CCL11	Eotaxin
CCL12	MCP-5
CCL17	TARC
CCL19	MIP-3b
CCL20	MIP-3a
CCL22	MDC
CCL24	Eotaxin-2
CCL25	TECK
CCL27	CTACK
CXCL1	KC
CXCL2	MIP-2
CXCL5	ENA-78
CXCL10	IP-10
CXCL11	I-TAC
CXCL12	SDF-1a
CXCL13	BCA
CXCL16	SCYB16
CX3CL1	Fractalkine

3.2.4 Western blotting for components of the canonical and non-canonical NF-κB transcription factor family

Protein was extracted from the GTN muscles from adult WT and old WT, and adult SOD1KO mice as described in **Section 2.2.3.2** and protein concentration was determined by a Bradford assay (**Section 2.4.1.4**). These protein concentrations were used to perform SDS-

PAGE and western blotting to determine the content of NF-κB signalling proteins where equal amounts of proteins were loaded on to the gel (**Table 3.2**)

Table 3.2: Antibodies and dilutions used for western blotting.

Target	Antibody	Product code	Company	Antibody dilution	Protein loaded (ug)
p65	Anti-NF-kB p65 antibody	ab32536	Abcam	1:1000	20
RelB	RelB (D7D7W) Rabbit mAb	#10544	Cell Signalling technology	1:1000	20
IkBb	Recombinant Anti-IKB beta antibody	ab109509	Abcam	1:1000	20
p100/52	NF-κB2 p100/p52 Antibody	#4882	Cell Signalling technology	1:1000	20
p105/50	Recombinant NF-κB p105/p50 Antibody	ab32360	Abcam	1:1000	20

The membranes were imaged on a Licor Odyssey CLx system (Licor, Cambridge, UK), and pixel densitometry was performed using Image studio lite (Licor, Cambridge, UK).

Statistical analysis was performed using a one-way ANOVA with post hoc Dunnett's test for multiple comparisons in Graphpad Prism 8.4.3. Data are presented as mean ± SD.

3.2.5 qPCR to determine relative gene expression levels of proteins of the NF-κB family and associated proteins in muscles of adult WT, old WT and adult SOD1KO mice

Analysis of mRNA levels for the full panel of cytokines and chemokines was not possible within this project but a select number of mRNAs were analysed. RNA was extracted from the GTN muscles from adult WT, old WT, and adult SOD1KO mice as described in **Section 2.4.3.1**. The RNA was reverse transcribed (**Section 2.4.3.2**), and the resulting cDNA was used to determine the relative expression of genes (**Table 3.3**) using qPCR (**Section 2.4.3.3**).

Table 3.3: Taqman probe assays used for qPCR

Target	Probe	Assay ID	Efficiency
IkBb	FAM	Mm00456853_m1	92.91
IL-6	FAM	Mm00446190_m1	92.86
CCL11	FAM	Mm00441238_m1	78.43
CXCL10	FAM	Mm00445235_m1	87.47
PPIA (houskeeping)	VIC	Mm02342430_g1	94.97

Statistical analysis was performed using a one-way ANOVA with post hoc Dunnett's test for multiple comparisons in Graphpad Prism 8.4.3. Data are presented as mean ± SD.

3.2.6 Analysis of p65 localisation in transverse sections of GTN muscle from adult WT, old WT and adult SOD1KO mice

- Sections of 12 μM were cut from EDL muscles from adult WT, old WT, and adult SOD1KO mice using the method described in **Section 2.2.3.1**. Immunohistochemistry was then performed using the method described in **Section 2.3.5** with Abcam anti-NF-κB p65 antibody (ab32536; Abcam, Cambridge, UK) as the primary antibody.

- Sections were imaged on a Zeiss LSM800 confocal microscope using a 20x lens.

3.2.7 Analysis of p65 localisation in isolated fibres from adult WT, old WT and adult SOD1KO mice

Muscle fibres from FDB muscles of adult WT, old WT and adult SOD1KO mice were isolated and cultured overnight in 24 well plates containing 15 mm round coverslips coated with ECM as described in **Section 2.2.4.1**.

After 24 hours, immunocytochemistry was performed on the isolated fibres (**Section 2.3.5.2**) with the Abcam anti-NF-κB p65 antibody (ab32536; Abcam, Cambridge, UK). Fibres were imaged on a Zeiss LSM800 confocal microscope using a 20x lens.

3.3 Results

3.3.1 There was an increase in cytokine/chemokine concentration primarily in the plasma of old WT compared with adult SOD1 and adult WT mice

Figures 3.2 - 3.3 and **Table 3.4** show cytokine and chemokine concentrations of plasma from adult WT, old WT and adult SOD1KO mice. Of 33 cytokines examined, 28 were present at concentrations which were within the range of the standard curve.

There was an increase in the cytokines IL-6, IL-10, and TNFα in plasma of old WT mice when compared to the plasma of adult WT mice (**Figure 3.2; Table 3.4**). In contrast, no significant changes were seen in cytokine concentrations in the plasma of adult SOD1KO mice when compared with the plasma of adult WT mice (**Figure 3.2; Table 3.4**).

The concentrations of the chemokines CCL5, CCL7, CCL11, CXCL2, CXCL12 were all approximately 2-fold higher in the plasma of old WT mice compared with that of adult WT mice. CXCL5 was 4-fold higher in concentration in the plasma of old WT mice compared with plasma of adult WT. CXCL2 was the only chemokine seen to be elevated (2-fold higher) in the plasma of adult SOD1KO mice in comparison with the plasma of adult WT mice (**Figure 3.3; Table 3.4**).
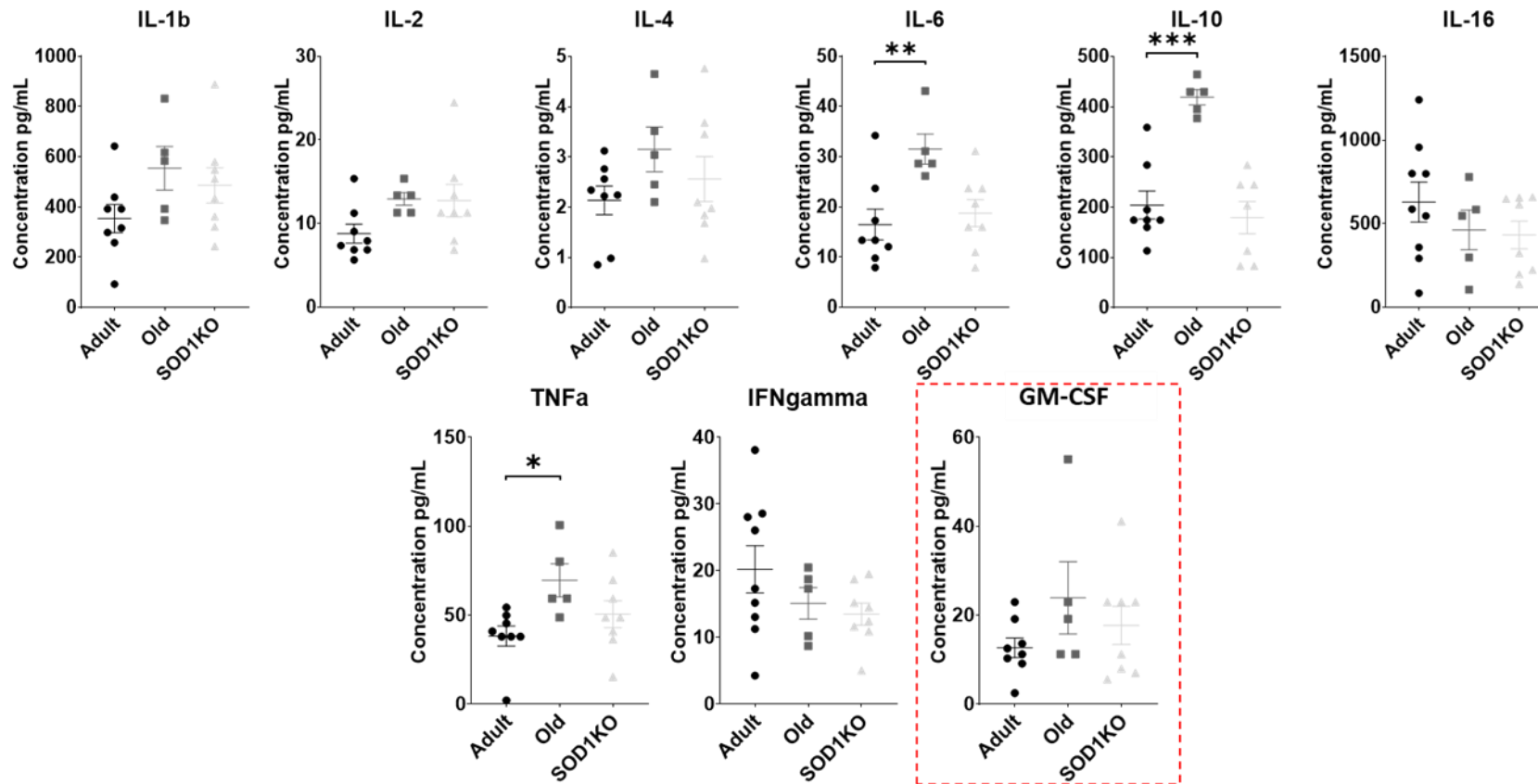
Figure 3.2: Plasma cytokine concentrations of adult WT (n=8-9), old (n=5), and SOD1KO (n=7-8) mice determined using the Bioplex assay. *Interleukin (IL), Tumour necrosis factor α (TNF-α), interferon γ (IFN-gamma), granulocyte-macrophage colony-stimulating factor (GM-CSF). Cytokines with dashed border had datapoints below the bottom standard of the standard curve. *p < 0.05, ***p < 0.005, ****p < 0.0001. (One-way ANOVA with Dunnet's post-hoc test).*
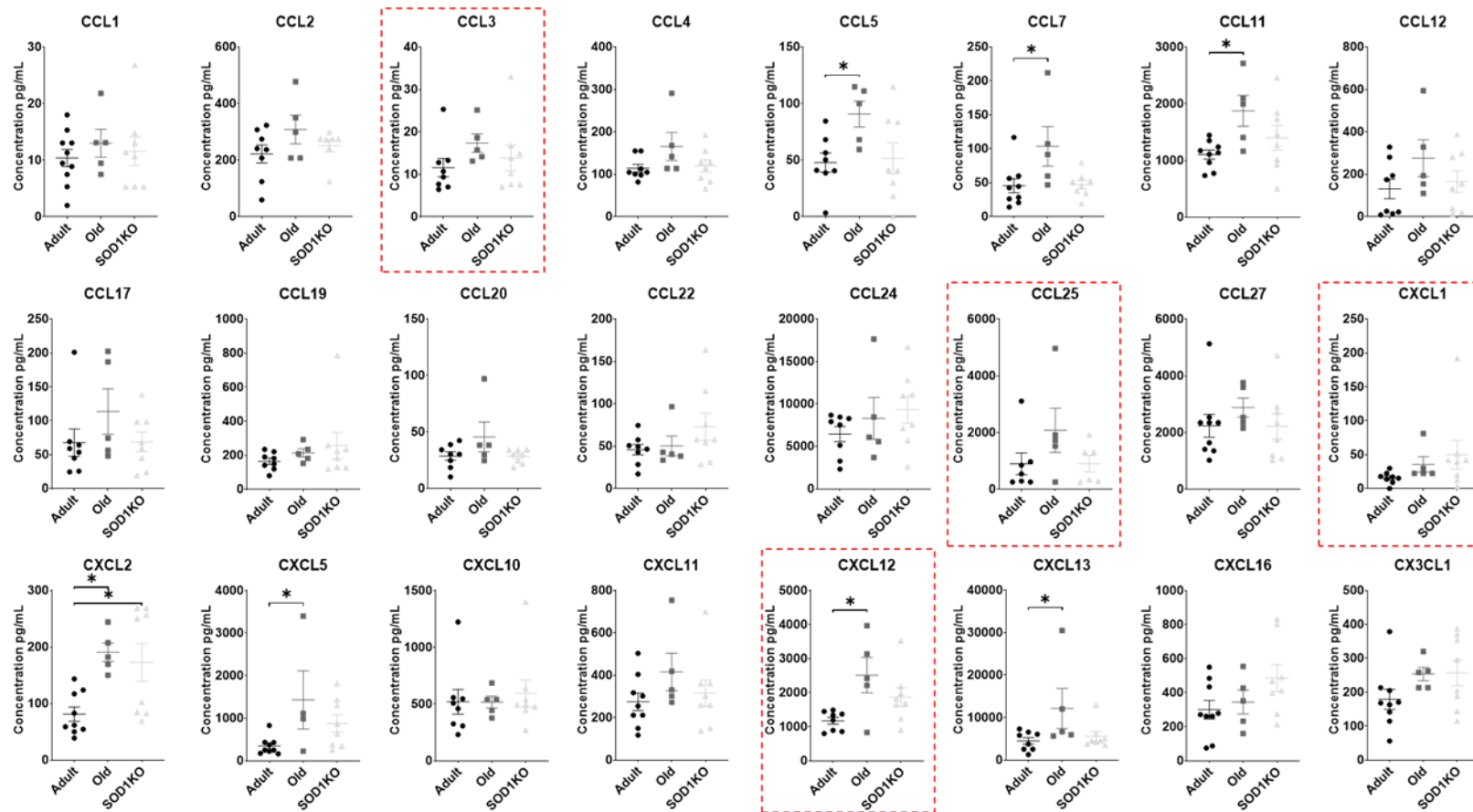
Figure 3.3: Plasma chemokine concentrations of plasma from adult WT (n=8-10), old (n=4-5), and SOD1KO (n=7-8) mice determined using the Bioplex assay. Cytokines with dashed border had datapoints below the bottom standard of the standard curve. *p < 0.05, **p < 0.01, ***p < 0.005 (One-way ANOVA with Dunnet's post-hoc test).

Table 3.4: Summary table for the cytokine and chemokine concentrations observed in the plasma of adult WT, old WT, and SOD1KO mice. Adjusted p values generated via one-way ANOVA with Dunnett's post-hoc test. *p < 0.05, **p < 0.01, ***p < 0.005, ****p < 0.0001

	Cytokine/ chemokine	Mean concentration adult (ug/ug)	Mean concentration old (ug/ug)	P value Old vs Adult	Significance Old Vs Adult	Mean concentration SOD1KO (ug/ug)	P value SOD1KO vs Adult	Significance SOD1KO Vs Adult
Cytokines	IL-10	204	418.9	0.0002	***	179.1	0.7468	ns
	IL-6	16.44	31.51	0.0064	**	18.72	0.7919	ns
	TNFa	38.21	69.57	0.0198	*	50.45	0.3659	ns
	IL-2	8.784	12.94	0.1533	ns	12.75	0.1157	ns
	IL-1B	353.6	554.2	0.1275	ns	485.9	0.2836	ns
	IFN-gamma	20.19	15.06	0.4208	ns	13.46	0.1664	ns
	IL-4	2.134	3.15	0.1868	ns	2.559	0.6454	ns
	GM-CFS	12.63	23.89	0.2076	ns	17.68	0.6273	ns
	IL-16	629.4	462.5	0.5222	ns	432.6	0.3228	ns
Chemokines	CXCL12	1172	2514	0.0113	*	1869	0.1453	ns
	CXCL2	81.2	190.5	0.0133	*	172.6	0.0174	*
	CCL11	1104	1875	0.0209	*	1400	0.3834	ns
	CCL7	45.37	103.4	0.0236	*	46.83	0.9956	ns
	CXCL5	345.5	1429	0.0309	*	875.7	0.2225	ns
	CXCL13	4473	12160	0.0468	*	5575	0.8951	ns
	CCL5	47.75	90.57	0.0473	*	51.48	0.9597	ns
	CXCL16	300.1	344.6	0.8829	ns	485.8	0.1008	ns
	CCL4	113.8	165.2	0.1206	ns	199.4	0.9592	ns
	CCL20	28.74	45.68	0.1365	ns	28.61	0.9998	ns
	CX3CL1	178.8	253.3	0.2627	ns	256.9	0.1578	ns
	CXCL1	15.68	35.64	0.5956	ns	49.99	0.1752	ns
	CCL2	221.4	307.8	0.1755	ns	250.7	0.7506	ns
	CCL25	895.2	2077	0.1877	ns	904.1	0.9999	ns
	CCL12	130.2	275.3	0.1938	ns	164.5	0.8675	ns
	CCL22	45.89	50.3	0.9616	ns	72.82	0.2061	ns
	CXCL11	274.5	415.5	0.2325	ns	315.7	0.8285	ns
	CCL3	11.57	17.35	0.2758	ns	13.84	0.7481	ns
	CCL17	67.73	113.5	0.2858	ns	68.62	0.9993	ns
	CCL24	6442	8286	0.6611	ns	9305	0.3059	ns
	CCL19	164.3	213.8	0.7782	ns	257	0.354	ns
	CCL27	2237	2879	0.5232	ns	2215	0.9988	ns
	CCL1	10.38	12.98	0.6518	ns	11.57	0.8832	ns
	CXCL10	519	516.1	0.9998	ns	593.3	0.8368	ns

3.3.2 There was an increase in of cytokine/chemokine content of muscles of SOD1KO and old WT compared with adult WT mice although the pattern of changes was different.

Figures 3.4 - 3.5 and **Table 3.5** show cytokine and chemokine content of muscle lysates from adult WT, old WT and adult SOD1KO mice. Of 33 cytokines examined, 26 were present at concentrations which were within the range of the standard curve.

GM-CSF was significantly increased approximately 2-fold in muscles of old WT mice when compared with the muscle lysates of adult WT mice although the detected levels remained low (**Figure 3.4; Table 3.5**). IL-16 was significantly increased (approximately 2.5-fold) in the muscle lysates of SOD1KO mice compared with those of adult WT mice (**Figure 3.4; Table 3.5**). For the chemokine analysis, CXCL2 was significantly increased (~2-fold) in muscle lysate

from old WT relative to adult WT mice (**Figure 3.5; Table 3.5**). CCL7 and CCL11 were increased

~1.5-fold and ~2-fold respectively in muscles of SOD1KO mice when compared with lysates

from adult WT mice (**Figure 3.5; Table 3.5**).
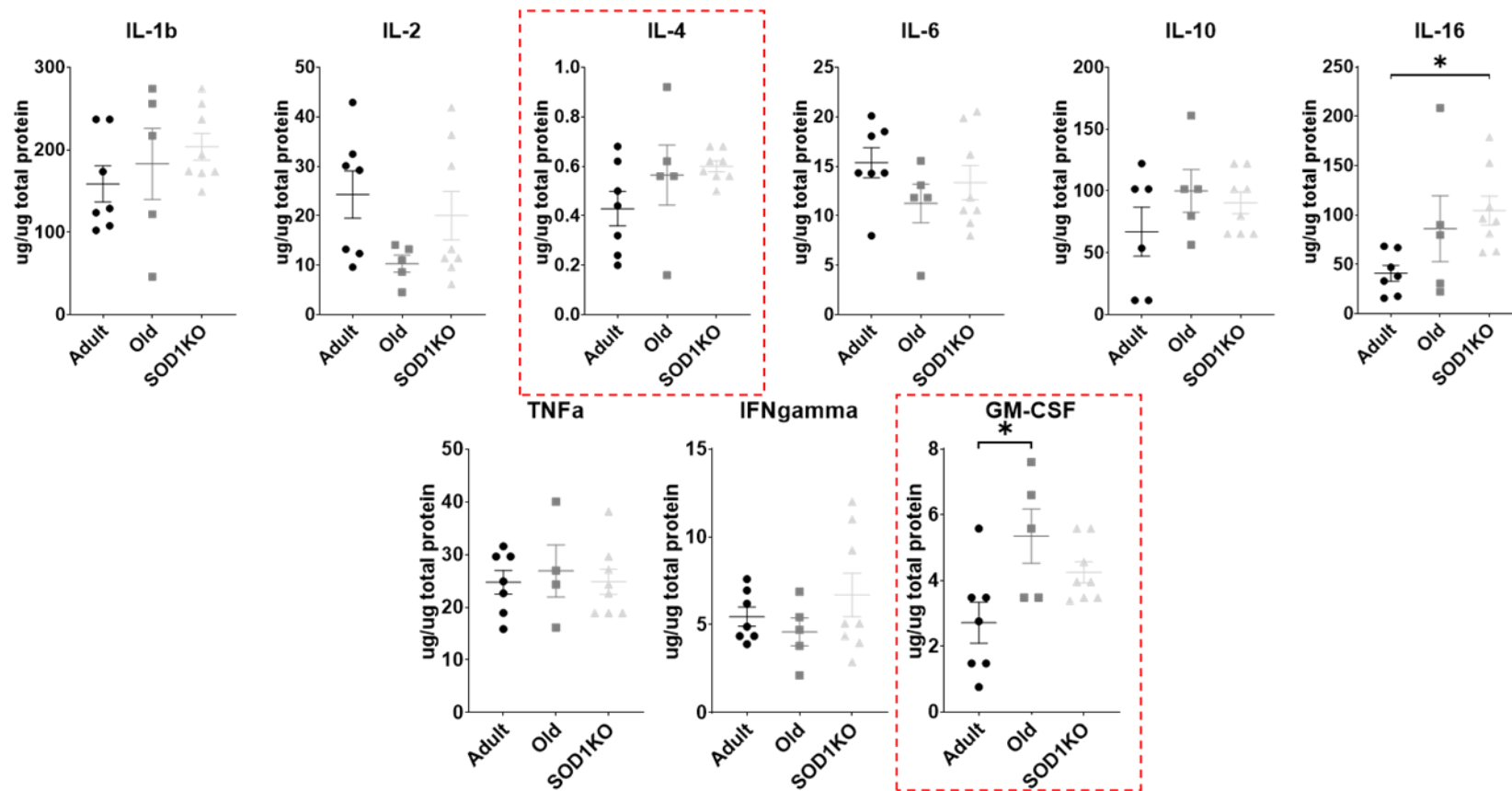
Figure 3.4: Lysate cytokine content of muscles from adult WT (n=6-7), old WT (n=4-5), and SOD1KO (n=7-8) mice determined via Bioplex assay. *Cytokines with dashed border had datapoints under the standard curve. Interleukin (IL), Tumour necrosis factor α (TNF-α), interferon γ (IFN-gamma), granulocyte-macrophage colony-stimulating factor (GM-CSF). **p < 0.01. (One-way ANOVA with Dunnet's post-hoc test).*
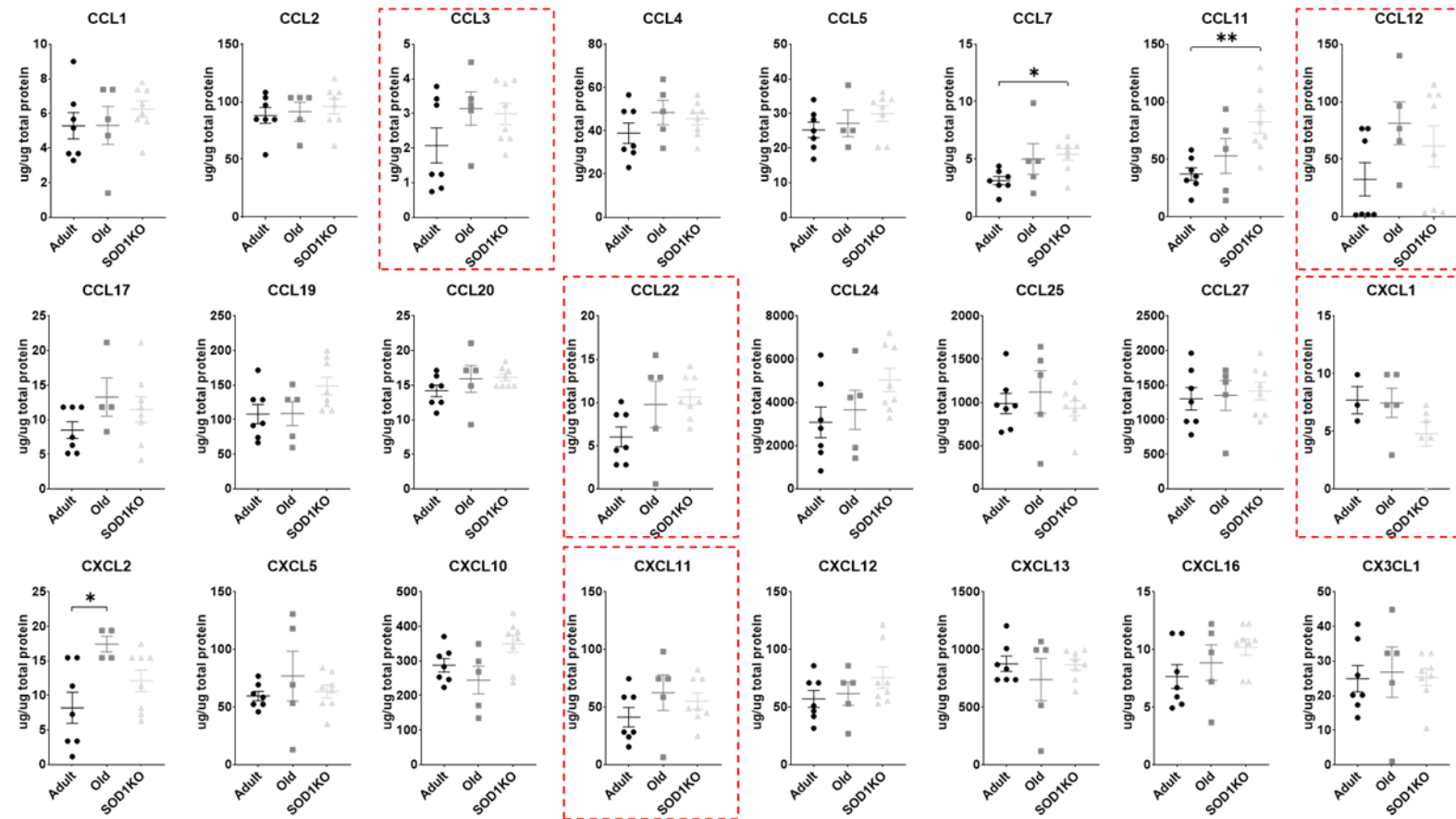
Figure 3.5: Lysate chemokine content of muscles from adult WT(n=6-7), old WT (n=4-5), and SOD1KO (n=7-8) mice determined via Bioplex assay. *Cytokines with dashed border had datapoints below the bottom point of the standard curve. *p < 0.05, **p < 0.01. (One-way ANOVA with Dunnet's post-hoc test)*

*Table 3.5: Summary table for the cytokine and chemokine concentrations observed in the muscle lysates of adult WT, old WT, and SOD1KO mice. Adjusted p values generated via one-way ANOVA with Dunnett's post-hoc test.   *p < 0.05, **p < 0.01.*

	Cytokine/ chemokine	Mean concentration adult (ug/ug)	Mean concentration old (ug/ug)	P value Old vs Adult	Significance Old Vs Adult	Mean concentration SOD1KO (ug/ug)	P value SOD1KO vs Adult	Significance SOD1KO Vs Adult
Cytokines	GM-CFS	2.717	5.348	0.0122	*	4.248	0.1021	ns
	IL-16	41.01	86.24	0.2006	ns	104.5	0.0324	*
	IL-2	24.26	10.31	0.1044	ns	20.03	0.717	ns
	IL-4	0.4286	0.564	0.341	ns	0.6	0.1354	ns
	IL-6	15.36	11.24	0.2281	ns	13.35	0.6008	ns
	IL-10	67.07	100.1	0.2688	ns	90.45	0.4162	ns
	IL-1B	158.5	182.9	0.7543	ns	203.6	0.3305	ns
	IFN-gamma	5.469	4.592	0.7877	ns	6.703	0.5619	ns
	TNFa	24.73	26.88	0.8539	ns	24.83	0.9995	ns
Chemokines	CCL11	37.24	52.98	0.4965	ns	82.41	0.0069	**
	CXCL2	8.206	17.43	0.0133	*	12.12	0.2292	ns
	CCL7	3.131	5.016	0.1563	ns	5.405	0.0456	*
	CCL22	6.026	9.772	0.1891	ns	10.62	0.0574	ns
	CCL24	3078	3654	0.8086	ns	5037	0.0876	ns
	CCL19	108.1	109	0.9989	ns	148.7	0.0894	ns
	CCL12	32.56	81.38	0.1361	ns	61.38	0.3706	ns
	CXCL16	7.669	8.856	0.6742	ns	10.22	0.1444	ns
	CXCL10	287.7	244.6	0.4834	ns	349.7	0.1798	ns
	CCL3	2.071	3.14	0.2021	ns	2.99	0.2177	ns
	CCL17	8.523	13.29	0.2114	ns	11.48	0.3893	ns
	CXCL1	7.7	7.472	0.9881	ns	4.787	0.2238	ns
	CXCL12	57.03	61.55	0.923	ns	75.61	0.2353	ns
	CCL4	38.81	48.38	0.2598	ns	45.51	0.4094	ns
	CXCL11	41.16	62.48	0.2731	ns	55.17	0.4653	ns
	CCL20	14.19	15.91	0.4518	ns	16.12	0.2961	ns
	CCL5	25.23	27.14	0.8553	ns	29.93	0.2981	ns
	CXCL5	59.56	75.87	0.4445	ns	63.48	0.9424	ns
	CCL1	5.286	5.308	0.9997	ns	6.25	0.5309	ns
	CXCL13	876.2	739.4	0.5333	ns	867.7	0.9966	ns
	CCL2	88.14	91.44	0.9341	ns	96.05	0.6234	ns
	CCL25	986.5	1119	0.7572	ns	930.6	0.9367	ns
	CCL27	1303	1351	0.972	ns	1417	0.8226	ns
	CX3CL1	24.91	26.82	0.9374	ns	25.34	0.9958	ns

3.3.3 Muscle fibres of old WT mice produced a large proportion of chemokines

Figures 3.6 - 3.7 and **Table 3.6** show cytokine and chemokine levels in media from isolated FDB muscle fibres from adult WT, old WT and adult SOD1KO mice. Of 33 cytokines examined, 26 were present at concentrations which were within the range of the standard curve.

No significant differences in cytokine concentrations were detected in the media from isolated muscle fibres between any of the groups studied (**Figure 3.6; Table 3.6**), however significant increases were seen in chemokine content of the media collected from isolated muscle fibres from old WT mice where the levels of CCL11, CXCL5, and CXCL12 were all approximately doubled. CCL2 was increased by 100-fold in the media of muscle fibres from

old mice (959788 ± 10686 ug/ug total protein; p = 0.0069) when compared with that of adult

WT mice (7402 ± 6673 ug/ug total protein) (**Figure 3.7; Table 3.6**).
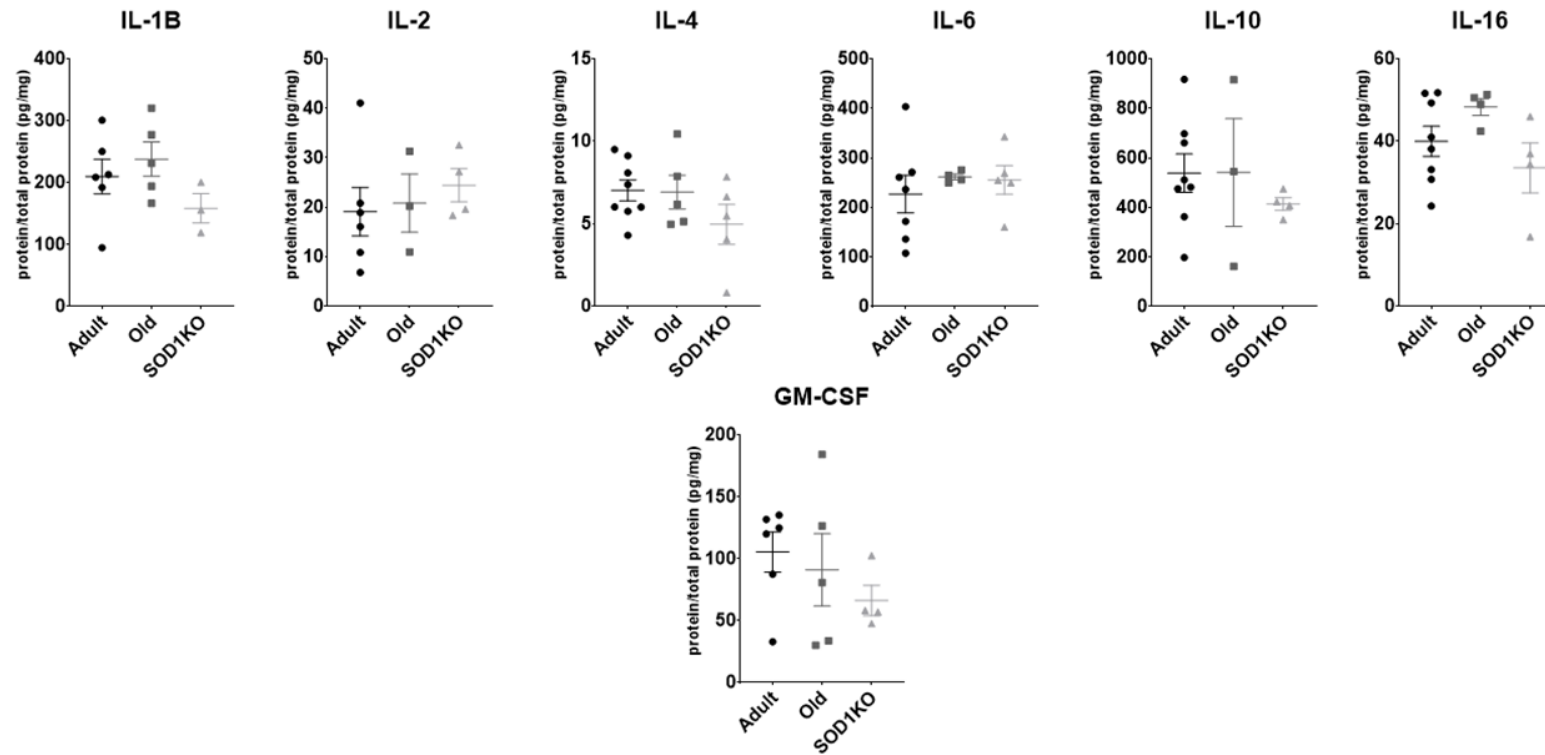
Figure 3.6: Cytokine concentrations in media of FDB fibres from adult WT (n=6-8), old WT (n=3-5), and SOD1KO (n=7-8) mice determined via Bioplex assay. *Interleukin (IL), Tumour necrosis factor α (TNF-α), interferon γ (IFN-gamma), granulocyte-macrophage colony-stimulating factor (GM-CSF). Cytokines with dashed border had datapoints under the standard curve. (One-way ANOVA with Dunnet's post-hoc test).* Values are normalised to the protein content of the lysed fibres.
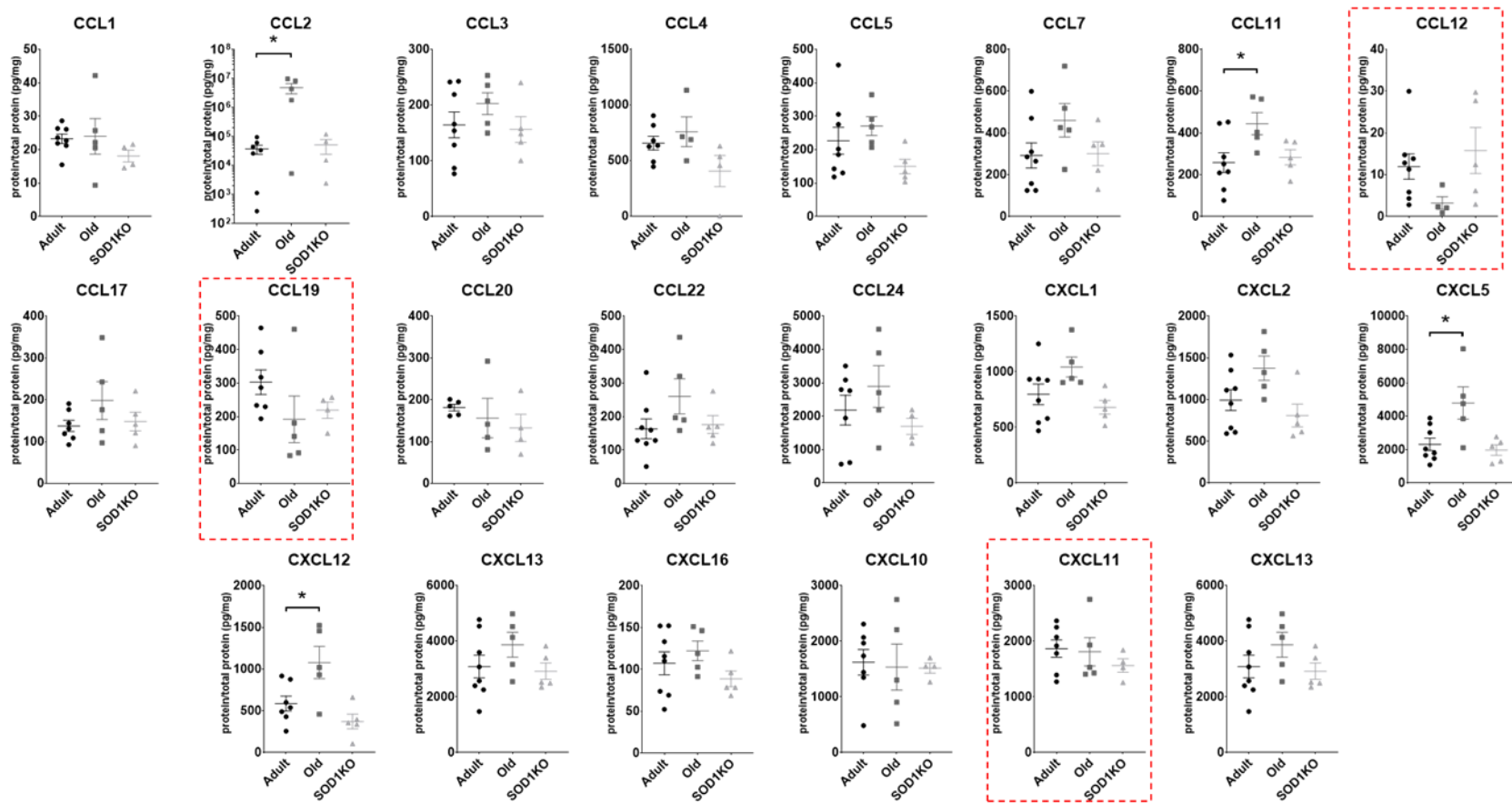
Figure 3.7: Chemokine concentrations in media of FDB fibres from adult WT(n=6-8), old WT (n=4-5), and SOD1KO (n=4-5) mice determined via Bioplex assay. *Cytokines with dashed border had datapoints below the bottom point of the standard curve. *p < 0.05. (One-way ANOVA with Dunnet's post-hoc test).* Values are normalised to the protein content of the lysed fibres.

Table 3.6: Summary table for the cytokine and chemokine concentrations observed in the media of FDB fibres from adult WT, old WT, and SOD1KO mice. *Adjusted p values generated via one-way ANOVA with Dunnett's post-hoc test. *p < 0.05, **p < 0.01.*

	Cytokine/ chemokine	Mean concentration adult (pg/mL)	Mean concentration old (pg/mL)	P value Old vs Adult	Significance Old Vs Adult	Mean concentration SOD1KO (pg/mL)	P value SOD1KO vs Adult	Significance SOD1KO Vs Adult
Cytokines	IL-4	1.404	1.383	0.9959	ns	0.9923	0.2309	ns
	IL-16	8	9.666	0.3386	ns	6.712	0.5116	ns
	GM-CFS	21.08	18.21	0.8588	ns	13.26	0.3964	ns
	IL-1B	41.99	47.6	0.7198	ns	31.7	0.4596	ns
	IL-10	107.6	108.2	0.9998	ns	82.69	0.6316	ns
	IL-2	3.817	4.116	0.9659	ns	4.884	0.6861	ns
	IL-6	45.33	52.28	0.7345	ns	51.05	0.7845	ns
Chemokines	CCL2	7402	959800	0.0069	**	10167	>0.9999	ns
	CXCL5	463	958.1	0.0128	*	394.4	0.8893	ns
	CXCL12	117.5	215.7	0.0276	*	74.35	0.4188	ns
	CCL11	51.61	88.78	0.029	*	56.58	0.92	ns
	CXCL2	198.5	274.8	0.1236	ns	161.6	0.5751	ns
	CXCL1	159.3	208.3	0.1315	ns	136	0.5968	ns
	CCL22	32.61	52.05	0.1398	ns	35.17	0.9608	ns
	CCL7	58.42	92.03	0.1706	ns	60.07	0.9951	ns
	CCL19	60.49	38.29	0.2117	ns	43.77	0.4404	ns
	CCL17	27.51	39.6	0.2435	ns	29.59	0.9543	ns
	CCL12	2.392	0.647	0.2565	ns	3.158	0.7188	ns
	CCL5	45.331	54.07	0.6326	ns	29.95	0.2683	ns
	CXCL13	617.3	773.8	0.3426	ns	584	0.9487	ns
	CCL4	131.1	151.5	0.6258	ns	104	0.4464	ns
	CCL3	32.86	40.49	0.4479	ns	31.22	0.9615	ns
	CCL1	4.648	4.794	0.9803	ns	3.62	0.4504	ns
	CCL20	36.25	31.24	0.8151	ns	26.56	0.4857	ns
	CXCL11	373.2	362.3	0.9727	ns	312.9	0.4977	ns
	CCL24	436.4	577.8	0.5239	ns	339.1	0.7591	ns
	CXCL16	21.45	24.43	0.6643	ns	17.74	0.5336	ns
	CX3CL1	69.48	72.08	0.973	ns	56.91	0.5643	ns
	CXCL10	324.6	307.2	0.9698	ns	303.3	0.606	ns

3.3.4 The relative expression of CXCL10 was increased in old and SOD1KO mice

There was no significant difference in the gene expression of IL-6, or CCL5 in mRNA extracted from muscle tissue. There was, however, a significant increase in CXCL10 muscle mRNA expression in old WT (15.96 ± 10.10 AU; p = 0.0196) and adult SOD1KO mice (11.87 ± 10.94 AU; p = 0.0196) when compared with adult WT mice (1.208 ± 0.8722 AU) (**Figure 3.8**).
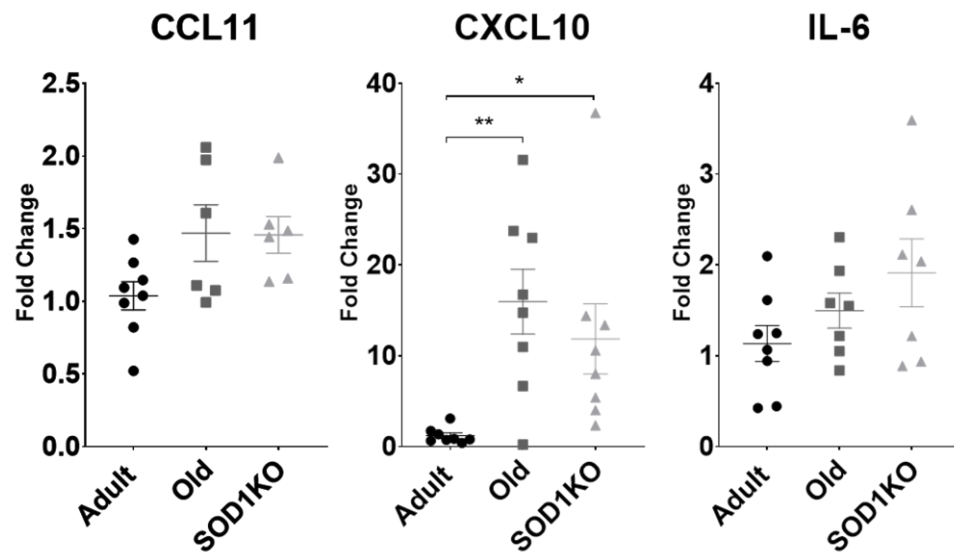
Figure 3.8: Relative mRNA levels of genes in the muscle tissue of adult WT, old WT and adult SOD1KO mice. *Data shown as mean ± SEM. * p<0.05, **p < 0.01 (One-way ANOVA with Dunnet's post-hoc test).*

3.3.5 Muscles of old mice display an increase in p65 levels in peripherally located nuclei compared with centrally positioned nuclei in muscles of adult SOD1KO mice.

In measuring the levels of subunits of the NF-κB pathway, the detected levels of p105, RelB and p100 were low and so were not able to be quantified. The absolute protein levels of p65, p50 and p52 were unchanged in muscles from all three groups, although the level of IκB was significantly reduced in muscles of old WT mice, supporting a role for activation of NF-κB in these muscles (**Figure 3.9**). Interestingly, no difference was observed in the level of IκBβ mRNA between any of the groups examined although data were very variable (**Figure 3.9**).

Though detecting levels of NF-κB proteins was difficult via immunoblotting and qPCR, observing the location of p65 in transverse sections of muscle from old WT mice, there was a clear visual increase in the levels of p65 in muscle fibres within peripherally positioned nuclei compared with nuclei of adult WT mice whereas in the muscles of adult SOD1KO mice there was an increase in the level of p65 in the muscle fibres with centralised nuclei (**Figure 3.10**). The p65 was detected in a punctate pattern in nuclei in all instances.
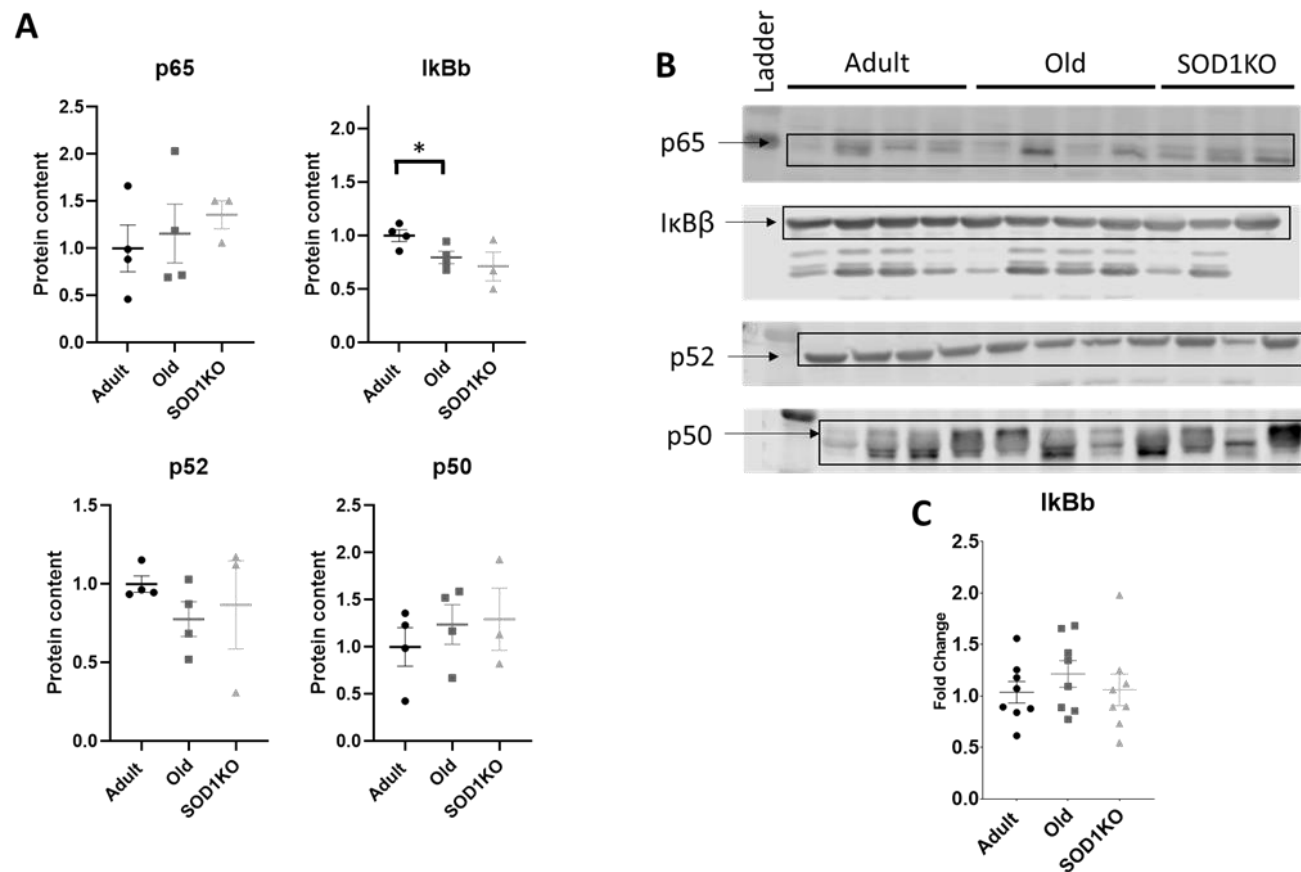
Figure 3.9: Measurements of NF-κB protein and mRNA levels via western blotting and qPCR. *A) Content of proteins in lysates of muscles from adult WT, old WT and adult SOD1KO mice as quantified by densitometry following normalisation to loading control and the mean value from adult WT mice. B) Images of the immunoblotting with black outlines showing the band of interest. C) The mRNA level of IκBβ in the muscle tissue of adult WT, old and SOD1KO mice. * p<0.05. Data shown as mean ± SEM.*
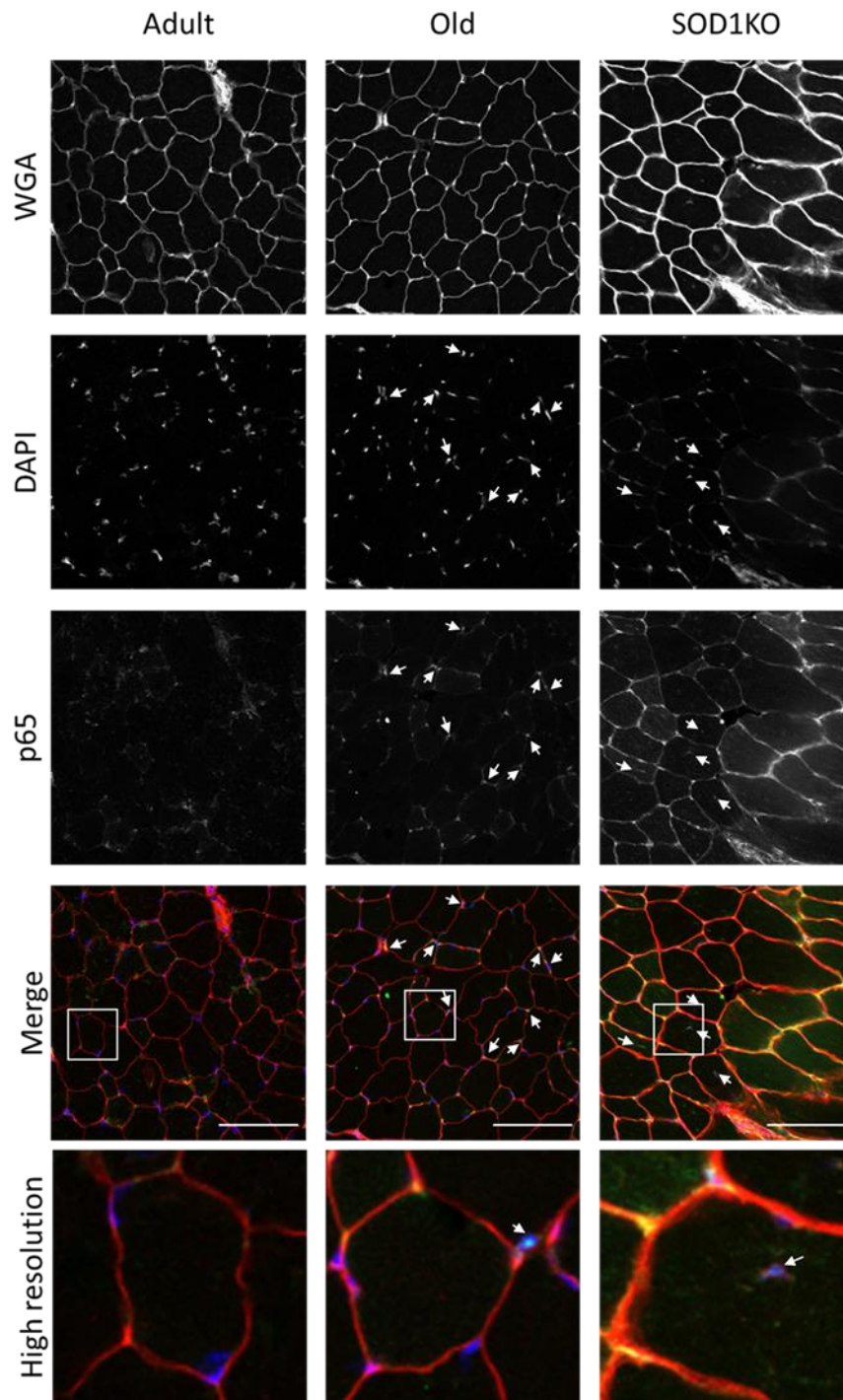
Figure 3.10: Confocal microscopy of immunohistochemistry of EDL muscles to determine nuclear localisation of p65 (green) to the nuclei (blue). *Sections are counterstained with wheat germ agglutinin (WGA; red). Scale bar = 100 µm.*

In isolated fibres, diffuse staining for p65 was observed in the cytosol of fibres from all groups, with some evidence of concentration of staining around all nuclei. There was some evidence of increased p65 localisation in centrally positioned nuclei in fibres of adult SOD1KO mice, although the incidence of centrally positioned nuclei in fibres of adult and old WT mice was too low to examine in these groups. No discernible difference was seen in the level of p65 in the peripherally positioned nuclei in fibres of old (**Figure 3.12**) or SOD1KO mice (**Figure 3.13**) when compared with isolated fibres of adult WT mice (**Figure 3.11**).

To determine whether this pattern of staining was representative of the maximum activation of NF-κB, isolated muscle fibres from adult WT mice were treated with relatively high concentrations of TNFα and IL-1β for 1.5 hours. The pattern of p65 localisation in fibres was examined (**Figure 3.14**). In the FDB muscle fibres of adult mice, the 8 cytokines analysed were not significantly different following 3 hours treatment with TNF-α and IL-1β (**Figure 3.15**). The patterns of release of cytokines by these fibres also demonstrated substantial increases in the release of CCL2, CCL3, CCL22, CXCL2 and CXCL5. CCL2 specifically was 100-fold higher in response to the cytokine treatment (**Figure 3.16**). The other measured cytokines were all at least 2-fold higher relative to the fibres from the adult controls (**Figure 3.16**).
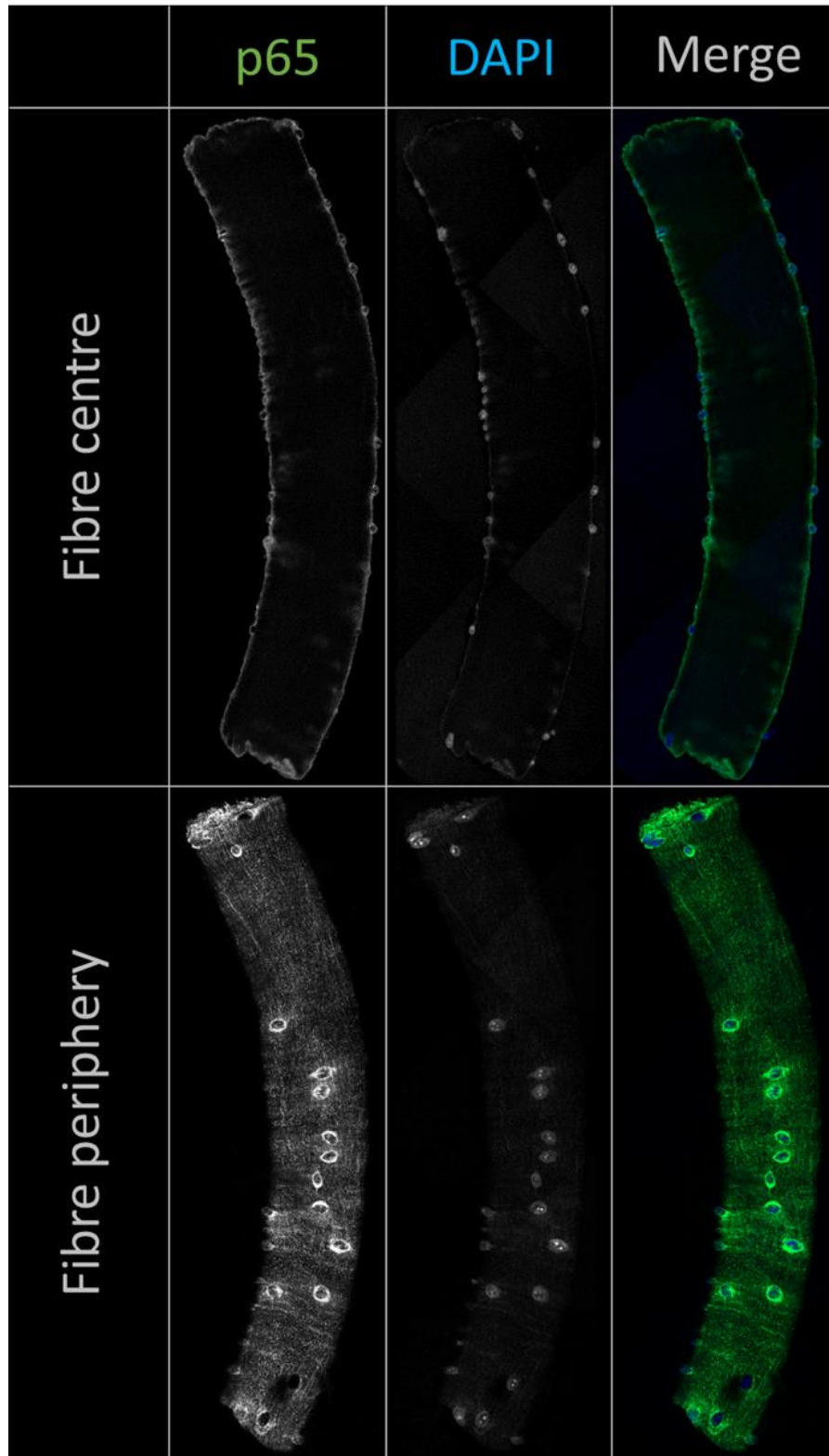
Figure 3.11: Confocal microscopy of immunocytochemistry for p65 localisation in FDB fibres from an adult WT mouse to observe the level of p65 (green) in the nuclei (blue). Image shows the fibre periphery to observe peripheral nuclei and mid slice depth of the fibre (Fibre centre) to show centrally located nuclei.
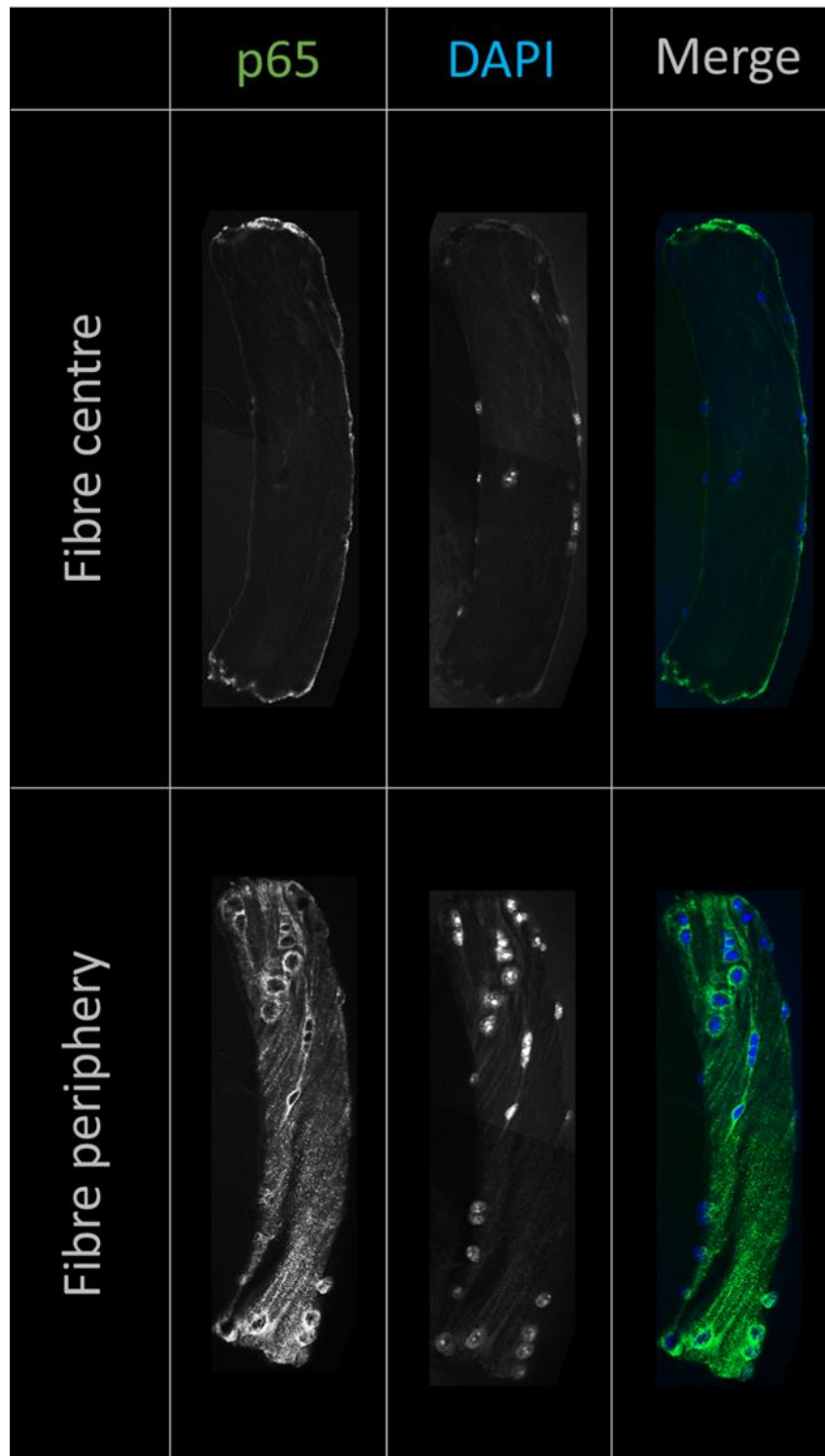
Figure 3.12: Confocal microscopy of immunocytochemistry for p65 localisation in FDB fibres from an old WT mouse *to observe the levels of p65 (green) to the nuclei (blue). Image shows the fibre periphery to observe peripheral nuclei and mid slice depth of the fibre (Fibre centre) to show centrally located nuclei.*
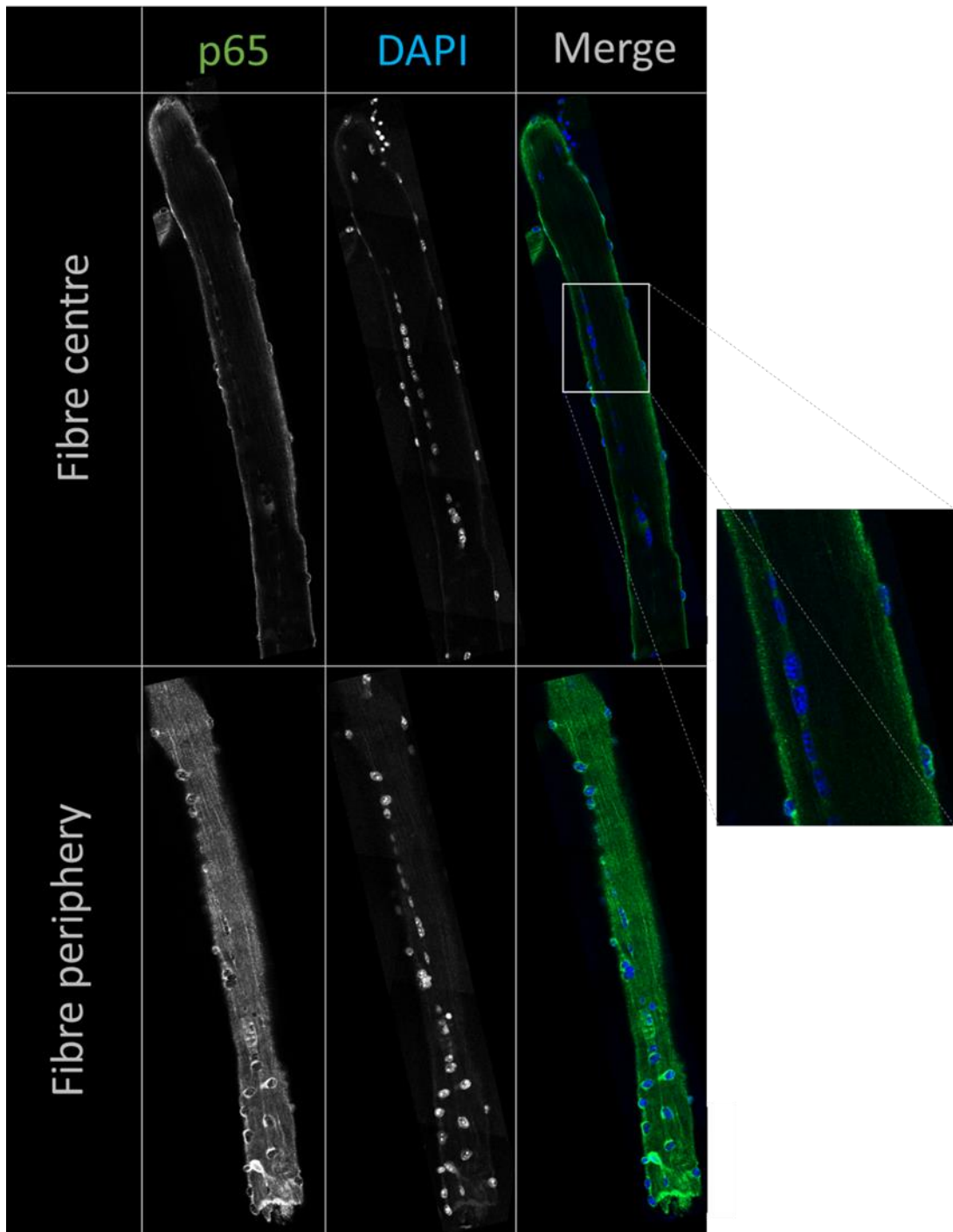
Figure 3.13: Confocal microscopy of immunocytochemistry of p65 levels in FDB fibres from an adult SOD1KO mouse to observe the level of p65 (green) to the nuclei (blue). Image shows the fibre periphery to observe peripheral nuclei and mid slice depth of the fibre (Fibre centre) to show centrally located nuclei. High resolution image on the right shows a trail of centrally located nuclei which are positive for p65 staining.
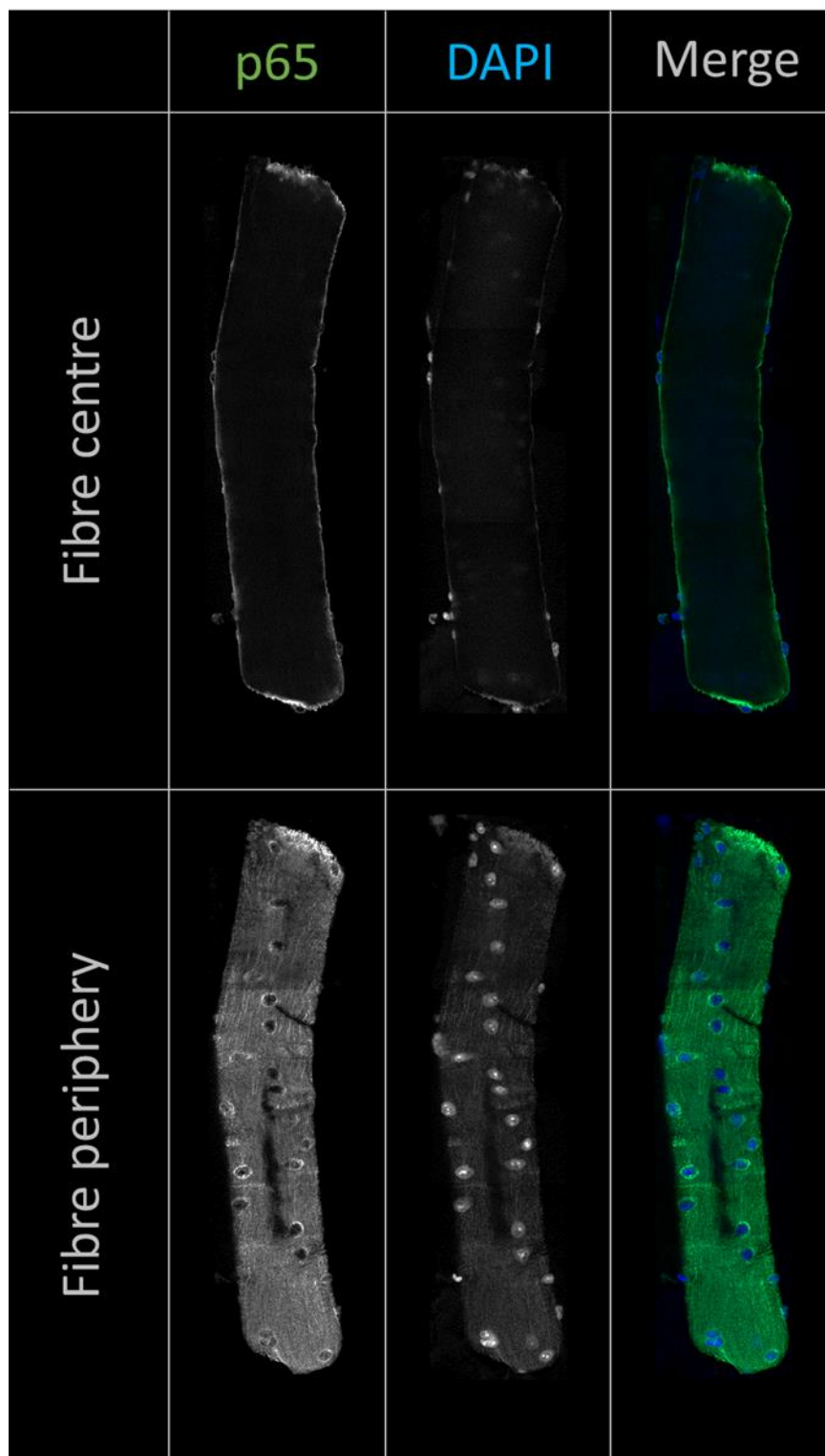
Figure 3.14: Confocal microscopy of immunocytochemistry of an FDB fibre from an adult WT mouse following treatment with TNF-α (25 ng/mL) and IL-1β (25 ng/mL) to observe the translocation of p65 (green) to the nuclei (blue). Image shows the fibre periphery to observe peripheral nuclei and mid slice depth of the fibre (Fibre centre). Here there are no centrally located nuclei as the fibre is from an adult WT mouse
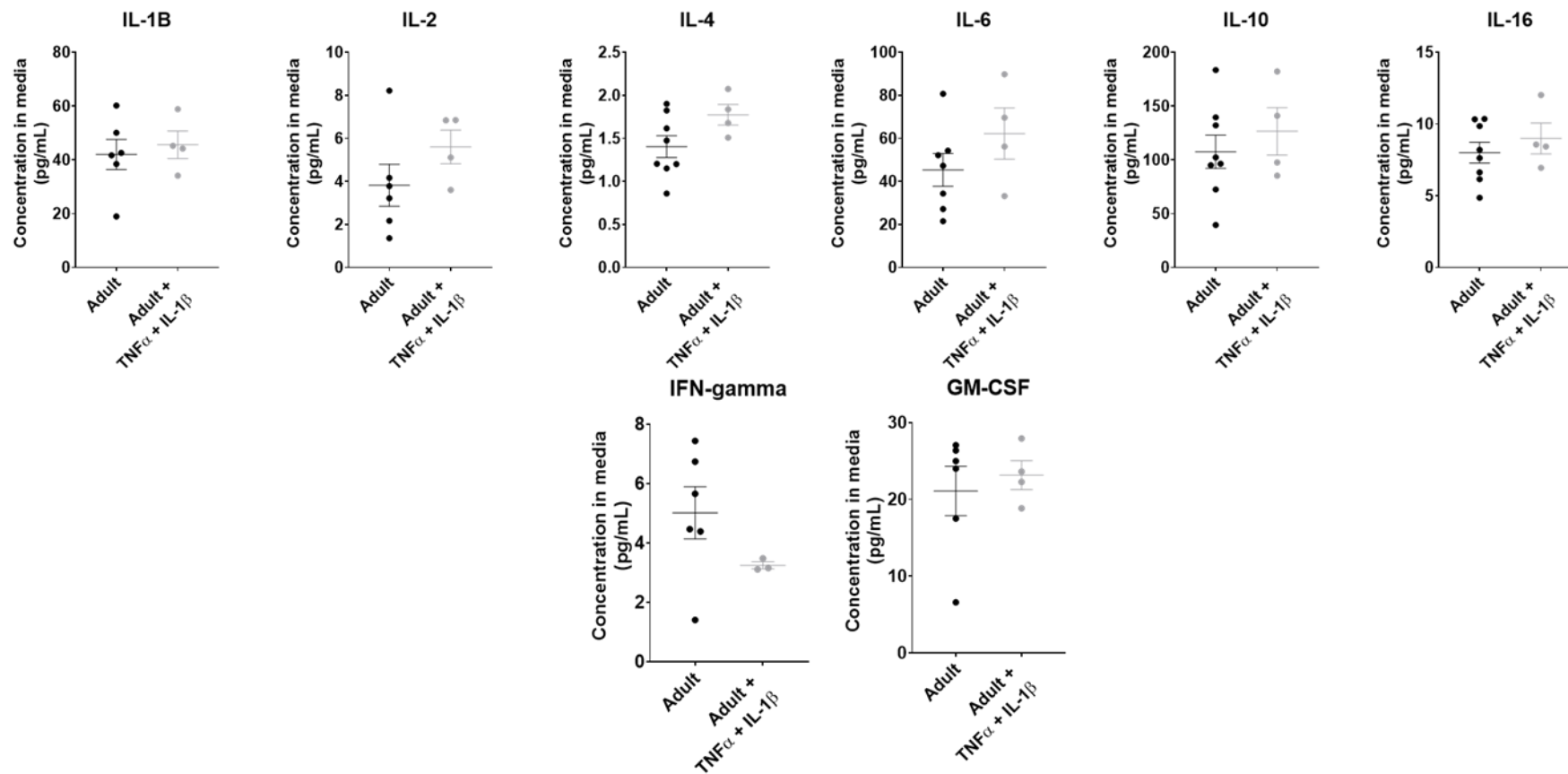
Figure 3.15: Cytokine concentrations of media from isolated fibres from adult WT mice with and without addition of TNFα (25 ng/mL) and IL-1β (50 ng/mL) determined via Bioplex assay. Interleukin (IL), Tumour necrosis factor α (TNF-α), interferon γ (IFN-gamma), granulocyte-macrophage colony-stimulating factor (GM-CFS). Data presented as mean±SEM. Values normalised to the protein content of the lysed fibres.
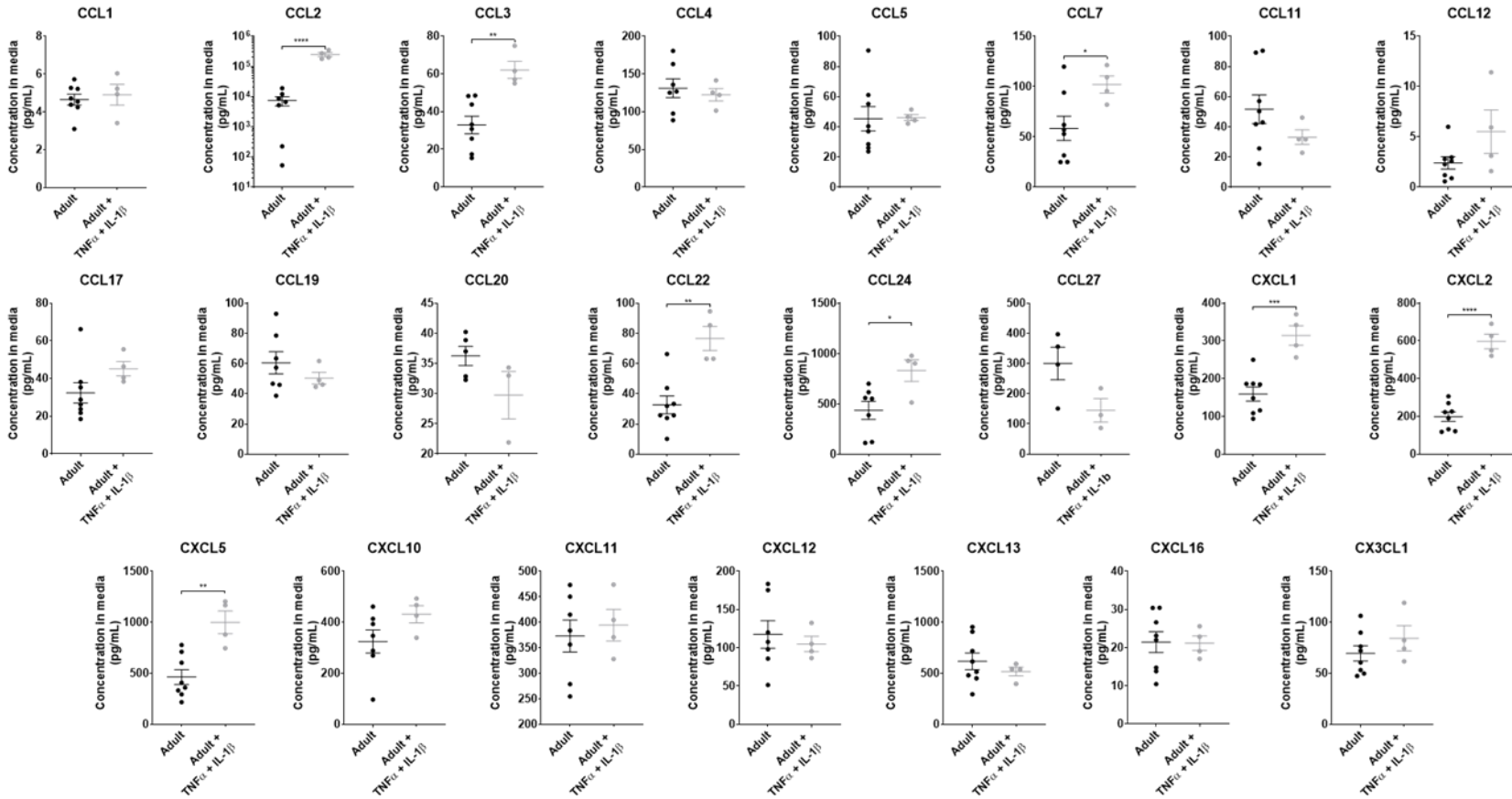
Figure 3.16: Chemokine concentrations of media from isolated fibres from adult WT mice with and without addition of TNFα (25 ng/mL) and IL-1β (50 ng/mL) *determined via Bioplex assay. Data presented as mean±SEM. *p < 0.05, **p < 0.01, ***p < 0.005, ***p < 0.001 (*One-way ANOVA with Dunnet's post-hoc test). *Data presented as mean±SEM. Values normalised to the protein content of the lysed fibres.*

Table 3.7: Summary of findings from the analysis of cytokines/chemokines in various samples. *Green shading represents a significant difference compared with adult WT mice, darker green shading indicates a lower p value when compared with adult WT mice. White boxes demonstrated no significant difference when compared with adult WT mice. Grey boxes represent that the cytokine/chemokine had not been measured.*

	Plasma		Lysate		Fibre media			Gene expression	
	Old	SOD1KO	Old	SOD1KO	Old	SOD1KO	Cytokine	Old	SOD1KO
IL-1B								grey	grey
IL-2								grey	grey
IL-4								grey	grey
IL-6	green								
IL-10	dark green								
IL-16				light green					
TNFa	light green				grey	grey		grey	grey
IFN-g								grey	grey
GM-CFS			light green					grey	grey
CCL1								grey	grey
CCL2					green		dark green	grey	grey
CCL3							green	grey	grey
CCL4								grey	grey
CCL5	light green							grey	grey
CCL7	light green			light green			light green	grey	grey
CCL11	light green		green	light green	light green				
CCL12								grey	grey
CCL17								grey	grey
CCL19								grey	grey
CCL20								grey	grey
CCL22							light green	grey	grey
CCL24								grey	grey
CCL25					grey	grey		grey	grey
CCL27					grey			grey	grey
CXCL1							green	grey	grey
CXCL2	light green	light green	light green				dark green	grey	grey
CXCL5	light green				light green			grey	grey
CXCL10								light green	light green
CXCL11								grey	grey
CXCL12	light green				light green			grey	grey
CXCL13								grey	grey
CXCL16								grey	grey
CX3CL1								grey	grey

3.4 Discussion

3.4.1 The activation of NF-κB in muscle fibres of old WT and SOD1KO mice are distinctly different

No detectable change in the levels of the majority of protein components of the NF-κB pathway using immunoblotting, although levels of some proteins remained poorly detected in all samples, but IκB protein levels were significantly reduced in muscles of old WT mice, consistent with a chronic increase in canonical NF-κB activation in these muscles. Interestingly, this was not the case in muscles of SOD1KO mice.

A higher level of p65 in some peripheral nuclei was seen as punctate transverse staining of the muscle sections of old WT compared with adult WT mice (**Figure 3.10**), suggesting that the canonical pathway of NF-κB was activated and supporting data showing increased NF-κB DNA binding activity in muscles of old compared with adult WT mice (Vasilaki et al, 2006). This indicated that there was likely to have been proteolysis of IκB, allowing for translocation of p65 (Nelson et al. 2004). The same increased localisation of p65 to nuclei was observed in the muscles of adult SOD1KO mice; however, this was only seen in centrally located nuclei (**Figure 3.13**). As centrally located nuclei are an indicator of fibre regeneration, this could be evidence that NF-κB activation is involved in the regeneration of muscle fibres (Spiro et al. 1966), commonly seen in muscles of SOD1KO mice (Nagahisa et al. 2016).

An alternative approach to staining muscle sections, was to examine p65 localisation to nuclei in isolated muscle fibres. This provides a number of advantages to the examination of intact muscles. Analysis of p65 localisation to nuclei of muscle fibres is complicated by the multinuclear nature of muscle fibres. Thus, it is possible within a single muscle fibre to have both peripherally and centrally located nuclei. There was no evidence for p65 being present in the nuclei of isolated fibres though this may be due to a lack of permeability in the centrally positioned nuclei of the fibres isolated from adult SOD1KO mice (**Figure 3.13**). In fibres isolated from the FDB muscles of adult and old WT mice, however, there was no evidence of p65 in nuclei of either peripherally located or centrally located nuclei (**Figures 3.11-3.12**). As the nuclear and fibres membranes are more "intact" in isolated fibres than in the cryosectioned tissues, the nuclear membranes required further permeabilisation to allow antibody entry. To improve this, a different permeabilisation solution could be used such as Igepal or methanol. Another factor which could be impeding the detection of p65 translocation to the nucleus is that the fibres have been removed from their inflammatory environment before staining. There is, however, staining evident around the nuclei of these fibres suggesting p65 shuttling into and outside of the nucleus is taking place. During this

extended time, NF-κB signalling may have ceased (Hoffmann et al. 2002). In an attempt to increase activation of NF-κB to maximum, fibres were also treated with a cocktail of pro-inflammatory cytokines. Interestingly, no additional p65 was seen in nuclei in this instance, with punctate patterns of p65 localisation still evident in the nuclei of these fibres (**Figure 3.14**).

3.4.2 Old WT and SOD1KO mice have varying levels and patterns of inflammatory cytokines and chemokines in plasma and muscle

Data examining plasma chemokines and cytokines (**Figures 3.2-3.3**) shows an elevated inflammatory environment within the old WT and to a lesser extent in adult SOD1KO mice as previously reported (Michaud et al. 2013; Tung et al. 2015) with elevations in 10 cytokines and chemokines in plasma of old WT mice but only one in the plasma of adult SOD1KO mice (Table 3.7). The only chemokine that was significantly altered in the plasma of SOD1KO was CXCL2, a chemokine shown to be transcriptionally controlled by NF-κB (Burke et al. 2014). This may suggest that there is a lower level of inflammation in SOD1KO mice. It also raises the question: from which tissues do these cytokines originate, particularly in old WT mice?

An increase in the cytokine GM-CSF and the chemokine CXCL2 was seen within the muscle tissue lysates of old WT mice and the mean level of CXCL2 was approximately double that of muscle lysates of adult SOD1KO mice although these data were more variable and so did not reach statistical significance (**Figures 3.4 - 3.5**). Thus, production of CXCL2 by muscle tissue could be contributing to systemic inflammation in the plasma of old WT and possibly adult SOD1KO mice. CXCL2 is recognised as an atrophy gene and is upregulated during bed rest induced atrophy in human studies (Mahmassani et al. 2019). Elevated levels of other cytokines/chemokines (IL-16, CCL11 and CCL7) were seen in muscle lysates from SOD1KO but not old WT compared with adult WT mice. There are several reasons that may explain the increase of these cytokines/chemokines in muscle lysates of the SOD1KO mice including,

a different state of the muscle (more evidence of actively regenerating muscle) or a higher proportion of non-muscle cells such as immune cell infiltration into the muscles of SOD1KO mice. No gross evidence of immune cell infiltration was seen in these muscles, but this was not examined in detail in this study. The difference in cytokines and chemokines observed to be significantly increased in plasma and muscle from old WT and adult SOD1KO mice may be indicative of a difference in the factors driving inflammation in muscle.

3.4.3 Isolated muscle fibres from old WT mice appear to produce significantly increased levels of chemokines compared with fibres from adult WT or SOD1KO mice.

The benefit of isolating muscle fibres is that this analysis is in the absence of any other cell type, and so these secreted proteins must originate from the muscle fibres themselves. Despite some limitations of the examination of cytokine production by isolated muscle fibres, there were some notable chemokines which were secreted at significantly higher levels by isolated fibres of old WT compared with adult WT mice (**Figure 3.7**). As two of the chemokines seen to be increased in the media of fibres from old WT mice were also increase in the plasma of old WT mice (CCL11, and CXCL5), muscle fibres may be a major source of these chemokines. This is particularly pertinent if we consider the total mass of muscle contributing to plasma cytokine/chemokine levels where muscle tissue comprises a large proportion of the total body tissue. One limitation of this isolated fibre approach is the limited time over which media cytokine/chemokine data can be collected. Previous (unpublished) data suggest that cytokine/chemokine levels are relatively stable for up to 3 hours in culture conditions. Thus, data represent cytokine/chemokine secretion over a relatively short time-period. The function of these increased chemokines in muscle is unclear. CCL11 is a potent eosinophil attractant and as such may increase the number of eosinophils trafficked to the muscle (Kodali et al. 2004). Invasion of eosinophils is a characteristic of myopathies which present with necrosis (Schröder et al. 2013) although overt necrosis is not evident in muscles of old WT mice. CXCL5 promotes the recruitment and

activation of neutrophils (Yang et al. 2016). Neutrophils are recruited to skeletal muscle to promote tissue repair and may be an attempt by muscles of old WT mice to maintain tissue repair processes (Toumi et al. 2006).

There was no evidence of changes in secretion of cytokines or chemokines by fibres from adult SOD1KO mice. This provides further evidence that although these two models of sarcopenia are comparable in some instances, they have discrete pathophysiological differences, particularly related to inflammation. One of the differences is the increased regeneration in the muscles of SOD1KO mice as shown by the occurrence of centrally located nuclei when compared to that of adult and old WT mice and this will be examined in more detail in Chapter 4 (Sakellariou et al. 2014a)

The response of isolated muscle fibres of adult mice to treatment with high levels of the cytokines TNF-α and IL-1b provide some insight into the effect of maintaining a fibre in a pro-inflammatory environment. Treatment of these fibres resulted in a significant increase in the release of a number of cytokines/chemokines, of note this also included CXCL2.

3.4.4 Cytokine/chemokine mRNA expression was altered in the muscles of old WT and adult SOD1KO mice when compared with those of adult WT

In order to gain a more detailed understanding of the nature of production and release of cytokines and chemokines by muscle, mRNA levels of a select few were examined. Although a thorough analysis of cytokine/chemokine mRNA levels was not undertaken. Thus, several cytokines/chemokines shown to be either elevated or unchanged in plasma of old WT mice were selected for further analysis of mRNA levels in muscle tissue. It is interesting to note that the mRNA level of CXCL10 was increased in muscles of old WT and adult SOD1KO mice but not in the plasma of either (**Figure 3.8**), demonstrating that the muscle tissue had a higher level of expression of this cytokine but that this did not impact on muscle protein or plasma levels, possibly suggesting a more rapid turnover of this chemokine, although further

analysis of this was outside the scope of this study. IL-6 mRNA was not altered in muscles of either old WT or adult SOD1KO mice compared with adult WT mice and this was reflected in no difference in muscle protein levels of this cytokine. Thus, it is likely that the increased levels of IL-6 seen in plasma of old mice is from a non-muscle source. CCL11 (eotaxin) mRNA was also unaltered in muscles of old WT and adult SOD1KO mice (and the lack of difference in old vs adult WT mice confirmed by RNASeq data shown in Chapter 6) whereas there was some evidence of increased production by muscles of both old WT and SOD1KO mice and elevated levels in the plasma of old WT mice. Despite the increased plasma levels of IL-6, IL-10, TNF-α, CCL5, CCL7, and CXCL13 in old WT mice, no evidence of muscle as a major source of these cytokines/chemokines was evident using any of the approaches described above. Little evidence suggests that muscle is a major source of the elevated CXCL2 seen in plasma of adult SOD1KO mice.

3.5 Conclusion

Data presented in this Chapter shows that there were significant and detectable differences in the inflammatory profile in the plasma of old WT mice which was mostly not reflected in the SOD1KO mice. Likewise, there were considerable increases in different cytokines and chemokines in the lysates of muscle from both old WT and adult SOD1KO mice. This may be due to the difference in p65 activation in the fibres detailed in **Figure 3.10** whereby increased p65 localisation appears to be evident primarily in centrally positioned nuclei in muscle fibres of adult SOD1KO mice and in some peripherally positioned nuclei in muscle fibres of old WT mice. To conclude these results, the muscle of old WT and SOD1KO mice both show differential indices of inflammation which appears to be associated with differences in the position of nuclei, and so potentially as a response to muscle fibre regeneration or other structural or compositional changes. When scaled to the full muscle content of the body, one chemokine in particular, CXCL2 may be, at least in part, contributing to the inflammaging experienced with ageing.

It is also worth noting that determination of cytokine/chemokine protein content of muscle, mRNA content and release by isolated fibres produce differing data and interpretation of such individual findings should be carried out with caution. Such differences are addressed in more detail in Chapter 6.

Further examination of the role of differences in the structure of muscles between these models, particularly regeneration with the positioning of nuclei to the centre or periphery of the fibres is required to fully understand this and so the next Chapter will focus on the effects of damage subsequent regeneration of skeletal muscle on adult WT, old WT, and adult SOD1KO mice in the context of inflammation.

Chapter 4: Changes in skeletal muscle morphology with ageing

4.1 Introduction

4.1.1 Age related loss of muscle mass and function

As humans age, they experience a loss of muscle mass, referred to as muscle atrophy. This, alongside the loss of muscle function, is one of the key criteria in the diagnosis of sarcopenia. By the age of 70, skeletal muscle cross sectional area (CSA) is reduced by 25-30% alongside a 30-40 % decrease in muscle strength (Porter et al. 1995). A reduction is also seen in the CSA of total and individual thigh muscles in humans from 60-80 years of age (Frontera et al. 2000). In *vastus lateralis* muscles isolated from adults (~20 years) and aged (~70 years) humans, the loss of muscle CSA was accompanied by a loss of total fibre number (Lexell & Henriksson-Larsen 1983; Porter et al. 1995).

There are common intrinsic and extrinsic alterations which regulate muscle ageing in mice, rats and humans, highlighting that rodents are a relevant model of sarcopenia (Demontis et al. 2013; Cobley et al. 2015). Rodent muscles age in a similar way to humans. Loss of muscle mass is evident in mice with a decrease in EDL and TA muscle mass by 20-30% between 10 and 26 months of age (Brooks & Faulkner 1988; McArdle et al. 2004). There is a loss in CSA of the EDL muscle of mice of around 10 % from the age of 10 months to 28 months old (eg Kayani et al. 2010).

The loss of muscle mass usually occurs in tandem with a loss of muscle function and a reduction of both is referred to as sarcopenia (Cruz-Jentoft & Sayer 2019). Men and women show a significant decrease in strength when performing grip, back extensor, hip flexor, and knee extensor measurements showing that the extent of sarcopenia is evident throughout skeletal muscle in all of the body (Kasukawa et al. 2017; Frontera et al. 2000). In older, mixed sex populations, isometric, concentric and eccentric knee extensions are reduced to 60 – 70% of those of young adults (Porter et al. 1995).

The loss of muscle function has also been measured in mice and shown to be decreased in fore limb muscles with *in-vivo* grip tests (Ge et al. 2016). This has also been shown in hind limb muscles with measurements of tetanic, specific forces, maximal and twitch of EDL muscles *in-vivo* and *ex-vivo* (Brooks & Faulkner 1988; Sheth et al. 2018; McArdle et al. 2004).

4.1.2 Age-related changes in the size of muscle fibres

Early measurements of muscle fibre size showed there to be no significant difference between muscles of adult and old humans, however this was performed on only small sections of muscles (Lexell & Henriksson-Larsen 1983). In contrast, muscle fibre size has now been shown to be reduced with ageing in humans which is most pronounced in the type II fibres but is also observed in type I fibres in *vastus lateralis muscle*(Evans & Grimby 1995; Nilwik et al. 2013; Porter et al. 1995; Verdijk et al. 2007; Scelsi et al. 1980). It has also been noted that in muscles of aged populations, there exists distinct grouped populations of atrophied fibres (Porter et al. 1995).

A reduction in CSA and minimum Ferets diameter has been reported in fibres of GTN muscles and a reduction of minimum Ferets diameter has been shown in the EDL and TA muscles from old mice (Walsh et al. 2015; Sakellariou et al. 2016; Messa et al. 2019; Zhu et al. 2019) A reduction in the size of all fibre types, the number of IIB fibres, and average fibre size is also apparent in mice with a loss of fibres of a larger size and abundance of smaller fibres, although the majority of muscle fibres in mice are Type II (Sakellariou et al. 2016; Kayani et al. 2010). There are also reports of reductions in total fibre number in muscles of old compared with adult mice although this isn't a consistent finding (eg Sayed et al. 2016; Sakellariou et al. 2016; Tang et al. 2019).

The SOD1KO mouse displays some of the physical aspects of frailty in ageing (**Section 1.2.2.1**) and, therefore, adult SOD1KO mice can be used as a model of accelerated muscle ageing. These mice show a decrease in various hind limb muscle strength, mass, maximum tetanic

force, maximum specific force and grip strength (Sakellariou et al. 2014a; Deepa et al. 2017; Muller et al. 2006) in a similar manner to muscles of old WT mice. A decrease in the total number of fibres, apparent reduction in fibre size, and loss of larger fibre sizes was also seen in muscles of this mouse model when compared to age matched WT controls (Larkin et al. 2011; Jang et al. 2010).

4.1.3 The prevalence of muscle fibres with centrally located nuclei observed at old age

In healthy muscle fibres of adult mice and humans, nuclei are typically positioned at the periphery of muscle fibres with transcriptional control over set myodomains (Pavlath et al. 1989), thus maximising space between the nuclei (Bruusgaard et al. 2003). It is thought that the nuclei are positioned here to offer them protection from contractile forces and to not impede the action of the contractile machinery (Folker & Baylies 2013).

Centrally located nuclei, originally thought to be a feature only of embryonic development, have been associated with myopathies since the 1960s (Spiro et al. 1966). Centrally located nuclei are now an index of various diseases of the muscle and nervous system including Duchenne Muscular Dystrophy (DMD) where it is thought to be a remnant of degeneration and ongoing regeneration (Wang et al. 2000).

The role of centrally located nuclei is not currently defined in muscle of old mice and it is not yet known of the effects of these on the force generation by individual fibres. A higher prevalence of centrally located nuclei in older muscle may indicate ongoing degeneration and regeneration, alternatively, it may indicate a halted state of regeneration in some fibres. Regardless of the purpose, this central position in an area known to contain the contractile machinery may be a possible reason for lower force generation by disruption of efficient interactions of the contractile machinery. In humans, the prevalence of centrally located nuclei have been shown to be elevated in some fibres types (Joanisse et al. 2013).

In old WT mice, centrally located nuclei are reported to be increased in TA and GTN muscles when compared to adult WT controls (Sakellariou et al. 2016; Sayed et al. 2016; Tang et al. 2019). The number of centrally located nuclei is also significantly increased in muscles of SOD1KO mice (Nagahisa et al. 2016). It is unclear whether the fibres with centrally positioned nuclei are entirely populated with centrally positioned nuclei or if they contain a mix of centrally and peripherally positioned nuclei.

The hypothesis for this study was that there will be observable morphological differences (including evidence of degeneration, denervation and regeneration) in the muscle fibres of old WT and adult SOD1KO mice when compared with adult WT mice, particularly those related to a chronic increase in activation of NF-κB.

In order to explore this hypothesis, the aims of this chapter were to:

- Characterise the extent of loss of muscle mass and function in old WT and adult SOD1KO mice compared with adult WT mice.

- Determine the size of individual fibres in EDL muscles from adult and old WT and adult SOD1KO mice by observing the median fibre diameter and the distributions of fibre diameters.

- Determine the prevalence of centrally positioned nuclei along isolated fibres and in whole EDL transverse muscle sections from muscles of adult and old WT and adult SOD1KO mice as an index of the state of regeneration of the individual muscle fibres.

4.2 Methods

4.2.1 Dissection of adult and old mice

All mice used were male and on a C57BL6/J background. Mice were culled by overdose of pentobarbital and death was confirmed by cessation of circulation unless otherwise stated.

Following this, body weights were measured. The GTN muscles were removed and snap frozen in liquid N_2. EDL muscles were mounted onto corks in a transverse orientation and coated in Shandon™ Cryomatrix™ embedding resin (Thermofisher, UK). This was frozen in isopentane cooled in liquid N_2.

4.2.2 Measurement of force generation from the muscles of adult WT, old WT and adult SOD1KO mice

The protocol was adapted from McArdle et al. (2004). Mice were anaesthetised with isoflurane and maintained under anaesthesia throughout the procedure. The knee of the right hind-limb was fixed. The distal tendon of the EDL muscle was exposed and attached to the lever arm of a servomotor (Cambridge Technology). The lever served as a force transducer. The peroneal nerve was exposed, and electrodes were placed across the nerve. The EDL muscle of the contralateral limb served as a non-exercised control. Stimulation voltage and muscle length were each adjusted to produce maximum twitch force. The optimal length for maximum twitch force is also the optimal length for the development of maximum tetanic force (Brooks & Faulkner 1988). With the muscle at optimal length, the maximum tetanic force was determined during 300msec of voltage stimulation (10V) with a frequency of 100 Hz. The maximum tetanic force was identified by increasing the frequency of stimulation at 2-min intervals until the maximum force plateaued. Muscle fibre length and cross-sectional area were calculated (Brooks & Faulkner 1988).

4.2.3 FDB fibre isolation and culture

FDB fibres were dissected and isolated as described in **Section 2.2.4**

4.2.4 Staining to observe position of nuclei in single fibres

The media was removed from the isolated muscle fibres and the fibres were washed with PBS. The fibres were fixed in 4% neutral buffered formalin (NBF) for 1 hour at room temperature. The NBF was removed and the fibres washed 3 times in PBS with 0.2% triton.

WGA-Rhodamine was added to a final dilution of 1 in 1000 in PBS with 0.2% triton for 10 minutes at room temperature with gentle rocking.

The WGA rhodamine was removed and fibres were washed 3x 5 minutes in PBS with 0.2% triton. This was then removed and the coverslips with fibres attached were removed from the wells, upturned and mounted on slides using Vectorsheild hardset mounting media containing DAPI (Vector labs, California, USA).

Fibres were imaged on a Zeiss LSM800 confocal microscope with a 40x oil immersion objective lens (Carl Zeiss AG, Oberkochen, Germany). Z-stacking and image stitching were used to obtain a 3D representation of full fibres which could be represented as both transverse and transverse images.

4.2.5 Fibre size analysis of isolated EDL muscles

The EDL muscles prepared for sectioning were cryosectioned transversely at -20 °C at a thickness of 12 µM as described in **Section 2.3.1** onto superfrost plus slides. These slides were stored at -20 °C until use.

Muscle sections were stained with DAPI and WGA and imaged on a LSM800 confocal microscope with a 20x objective lens (Carl Zeiss AG, Oberkochen, Germany) as described in **Section 2.3.3.**

Images were analysed to determine the total fibre number and the minimum Ferets diameter of each fibre using the 'Automated Multicellular Tissue Analysis' macro in FIJI.

4.2.6 Determination of size and abundance of fibres with centrally positioned nuclei in EDL muscles of adult WT, old WT and adult SOD1KO mice.

Slides were stained as described above and in **Section 2.3.4**. Images were captured using a Zeiss axio scan Z1 using the settings detailed in **Figure 2.3**.

First, the peripheral nuclei were masked out through thresholding these nuclei with using the WGA channel. This was performed using the image j macro in **Figure 2.4**. The resulting images were analysed using MyoVison (University of Kentucky) to further characterise the size of fibres with and without centrally positioned nuclei.

The resulting data were analysed to produce grouped fibres sizes, median minimum Ferets diameter and the percentage centrally located nuclei using R.

4.2.7 Statistics

All comparisons between the adult WT, old WT and adult SOD1KO groups were performed by one-way ANOVA with Dunnet's multiple comparisons test. For the comparisons between adult WT, old WT and adult SOD1KO mice for fibre size distribution, two-way ANOVA with Tukey's multiple comparison test was performed to observe differences in fibre size thresholds. These analyses were performed using Graphpad Prism 8.3.0.

4.3 Results

4.3.1 Muscle mass decreases with ageing and in SOD1KO mice
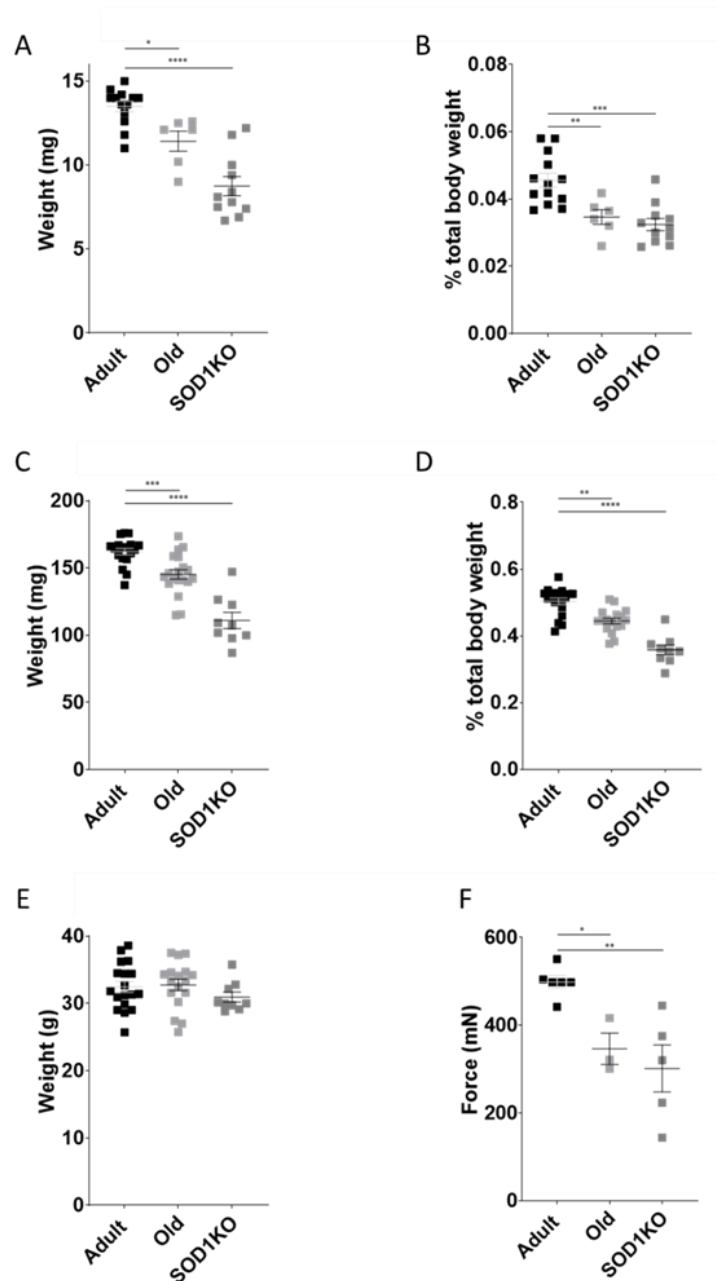
Figure 4.*1: Characterisation of quiescent muscles from adult and old WT and adult SOD1KO- mice. *Absolute EDL (A) and GTN (C) muscle weight of adult WT, old WT, and adult SOD1KO mice and normalised to body weight (B & D respectively). Body weights of the mice (E) and maximum tetanic force generation (F) of EDL muscles. Data presented as mean ± SEM. *p<0.05, **p<0.01, ***p<0.005, ****p<0.001 (one-way-ANOVA with Dunnett's multiple comparison test).*

There was no significant difference in body weight between adult WT, old WT and adult

SOD1KO mice (**Figure 4.1E**). In contrast, a significant decrease was seen in EDL muscle weight

of old WT mice (11.4 ± 0.6 mg; p = 0.0183) and adult SOD1KO mice (8.8 ± 0.6 mg; p < 0.0001) when compared with EDL weights of adult WT mice (13.5 ± 0.3 mg) (**Figure 4.1A**). When data were normalised to body weight, the EDL muscle weights of old WT mice and adult SOD1KO mice remained lower (0.0346 ± 0.0022 %; p = 0.0046; 0.3240 ± 0.0181 %; p < 0.0001) when compared with those of adult WT (0.0456 ± 0.0021 %). **(Figure 4.1B)**. Similarly, the weights of GTN muscles from old WT (145.2 ± 3.5 mg; p = 0.0021) and adult SOD1KO (111.0 ± 6.1 mg; p < 0.0001) mice were significantly reduced relative to those of adult WT mice (162.1 ± 2.4) **(Figure 4.1C)** and this reduction remained when data were normalised to body mass (0.442 ± 0.009 %; p = 0.0003 and 0.3578 ± 0.015 %; p < 0.0001 for old WT and adult SOD1KO respectively) **(Figure 4.1D)**.

The reduced muscle mass was associated with a decrease in the maximum tetanic force generation by the EDL muscle of old WT mice (346.3 ± 35.6 mN; p = 0.396) and the adult SOD1KO mice (301.6 ± 53.5 mN; p = 0.0036; a 39% reduction) compared with that of EDL muscles of adult WT mice (498.5 ± 14.1mN). The reduction in muscle mass did not fully account for the reduced muscle force generation, so the specific force generation of the remaining muscle was reduced by ~14% in old WT compared with adult WT mice (152 mN/mm^2 ± 22 cf. 176 ± 11) and by 10% (159 mN/mm^2 ± 47 cf. 47) in adult SOD1KO compared with adult WT mice.
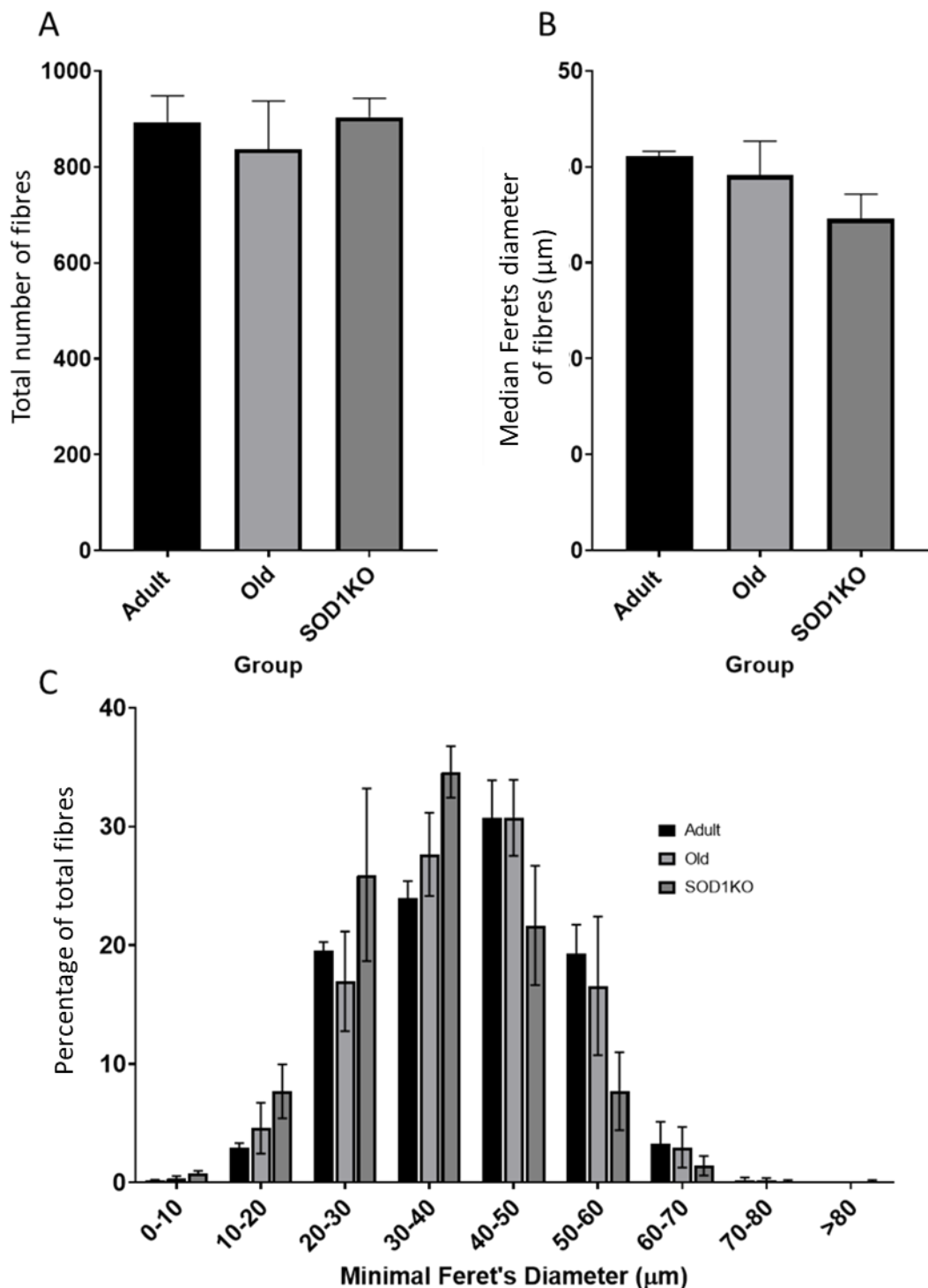
Figure 4.2: **Comparison of the muscle fibre number, median ferets diameter and fibre size distribution of muscles from adult WT, old WT, and adult SOD1KO mice.** *Total number of fibres (A) median fibre size (B), fibre size distribution (C) from EDL muscles of adult WT, old WT and adult SOD1KO mice. Data presented as mean ± SEM.*

There was no difference in the average number of fibres of the EDL muscles from old WT and adult SOD1KO mice compared with those from adult WT mice. A similar result was seen for the median fibre size although there was a non-significant 12.5% decrease in average diameter in the fibres of adult SOD1KO mice when compared to fibres of the adult WT mice. While there was no significant difference in the median of the fibre size, an apparent decrease in the percentage of larger fibres (40-80 μm) and increase in number of smaller fibres (0-40 μm) with 70% of fibres smaller than 40μm (the average muscle fibre diameter in adult WT mice seen in muscles of adult SOD1KO mice. This was not evident in muscles of old WT mice **(Figure 4.2C)**.

4.3.3 The prevalence of centrally located nuclei increased in muscles of SOD1KO mice but is unchanged with ageing

The FIJI macro used for filtering out the fibres with peripherally located nuclei was able to accurately quantify the presence and number of fibres with centrally located nuclei **(Figure 4.4**. Little difference was observed in the presence of fibres with centrally located nuclei in EDL muscles from old compared with adult WT mice (0.917 ± 0.445% vs 0.241 ± 0.109% for old vs adult respectively, p = 0.5113). In contrast to this, the percentage of fibres with centrally located nuclei in muscles of adult SOD1KO mice remained small (4.68 ± 0.706%) but was significantly higher than in adult WT mice (p = 0.0003). Thus, as anticipated from the above data, the prevalence of fibres with central nuclei was significantly lower in EDL muscles from old WT mice when compared with muscles of adult SOD1KO mice.

Muscles of adult and old WT mice contained very few fibres with centrally positioned nuclei when examined on transverse sections **(Figure 4.3)**. Muscles of SOD1KO mice showed an increased number of fibres with centrally positioned nuclei although again the percentage of fibres remained relatively low (~5%) **(Figure 4.3)**. Analysis of isolated muscle fibres (which could be viewed in any orientation and in 3-dimensional imaging) demonstrated that such

centrally positioned nuclei were relatively focal in nature along the length of the muscle (**Figure 4.5**). Thus, individual FDB fibres that contained at least one centrally positioned nucleus (as documented through transverse sectioning), contained a mix of centrally and normally (peripheral) positioned nuclei (**Figure 4.5**).
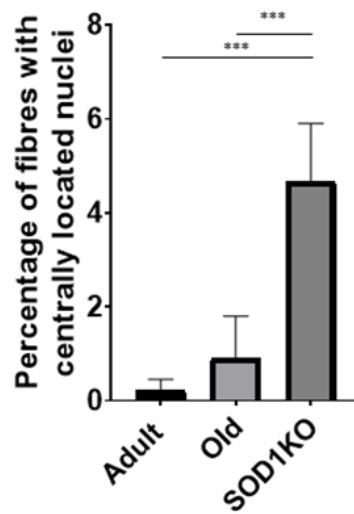
Figure 4.3: Percentage of fibres containing centrally located nuclei in EDL muscles from adult WT, old WT, and adult SOD1KO mice. Data acquired via an automated tissue analysis tools as to be unbiased. Data represented as mean ± SEM. *** $p < 0.0005$ (One-way ANOVA with Tukeys multiple comparisons correction; n = 3-4).
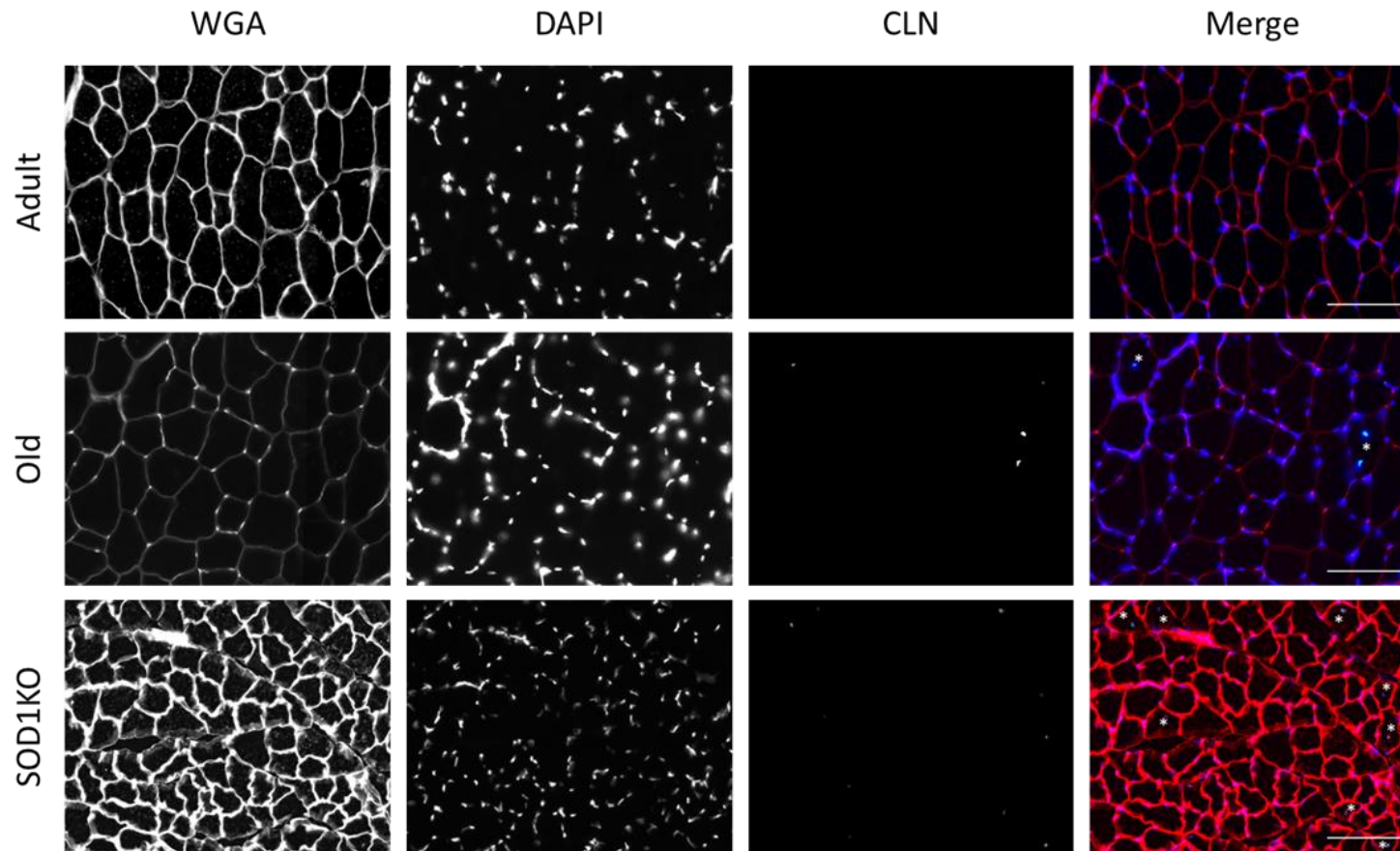
Figure 4.4: Images showing the prevalence of centrally located nuclei within fibres in transverse sections of extensor EDL muscles from adult WT, old WT, and adult SOD1KO mice. *The centrally positioned nuclei image was generated using a macro for FIJI to remove peripheral nuclei. The merged image depicts WGA staining the plasma membrane (red), DAPI staining nuclei (blue) and centrally located nuclei denoted by green. * Centrally located nuclei in fibres detected using the FIJI macro.*
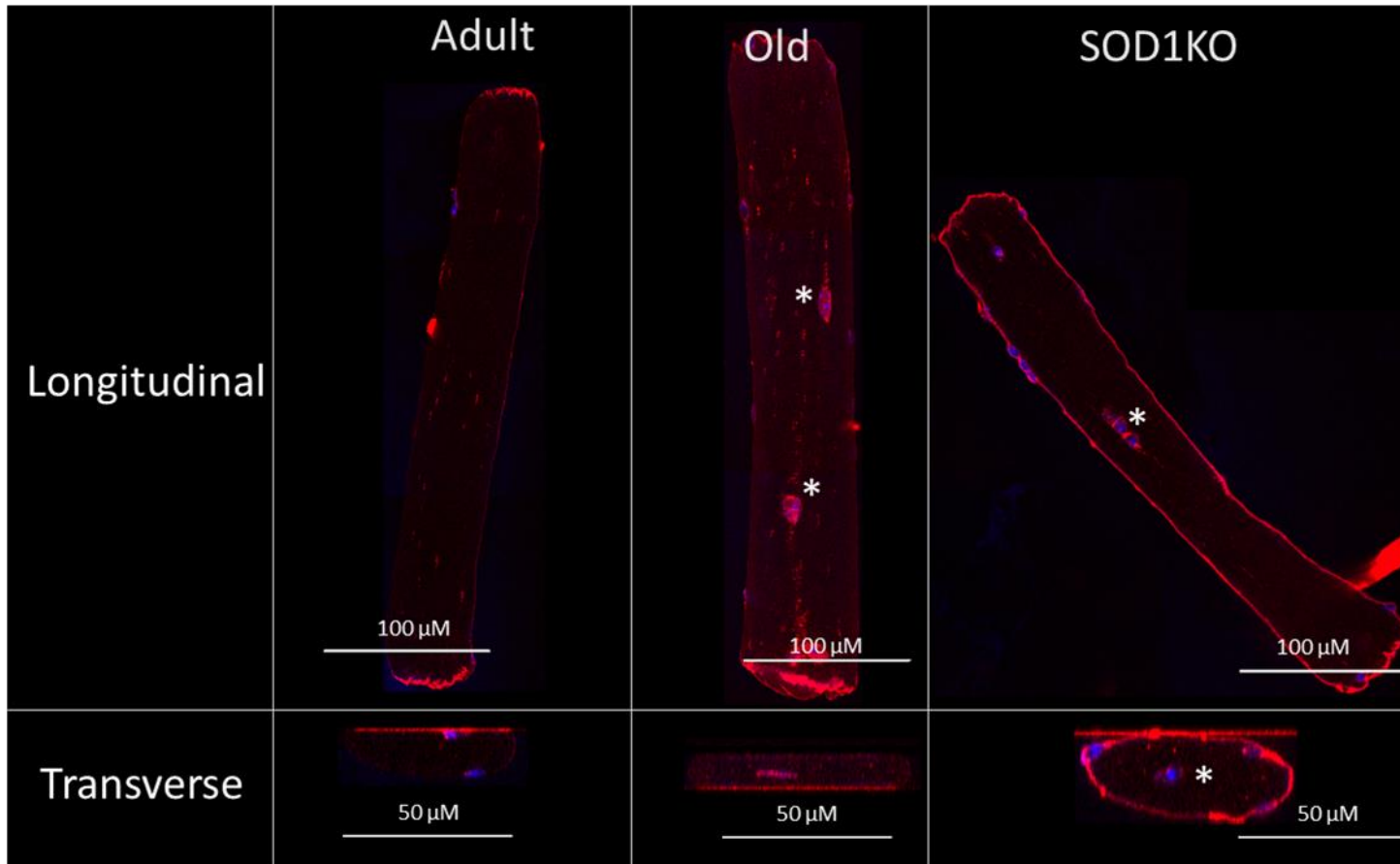
*Figure 4.5: 3D images showing centrally located nuclei in individual fibres isolated from the FDB muscles of adult WT, old WT, and adult SOD1KO mice shown as longitudinal and transverse orientation. * Centrally located nuclei within fibres. The flattened shape of the transverse orientated images is due to the fibres being between a coverslip and slide.*

4.3.4 Size comparisons of fibres containing centrally located and peripherally located nuclei in muscles of old WT and adult SOD1KO mice

Despite the lack of difference in the average fibre sizes in muscles of old WT and adult SOD1KO mice compared with adult WT mice, some differences were observed when the distributions of fibre sizes for those with centrally and peripherally positioned nuclei were analysed. It is more appropriate to compare the distribution of fibre sizes compared with the average size of all fibres in that group although it is important to remember that in some instances, the comparisons represent only a small proportion of total fibres (i.e. for fibres with centrally located nuclei, ~1% in old WT mice and ~5% in adult SOD1KO mice). This comparison would identify whether the fibres with centrally positioned nuclei were smaller, therefore potentially actively regenerating, or of similar or greater size than average, suggesting a completion of regeneration or persistent central positioning of the nuclei.

There was no significant difference in the size of the fibres with centrally located fibres in all cases. (**Figure 4.6**).
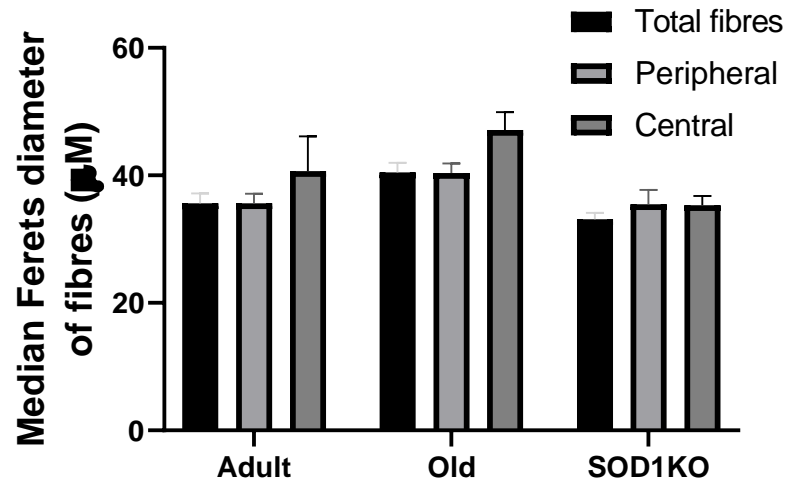
Figure 4.6: Median minimum Ferets diameter of fibres with centrally or peripherally located nuclei from adult WT, old WT and SOD1KO mice compared with the median average size of all fibres. Data are represented mean ± SEM. * p<0.05 (2-way ANOVA with Tukeys multiple comparisons correction, n = 3-4).
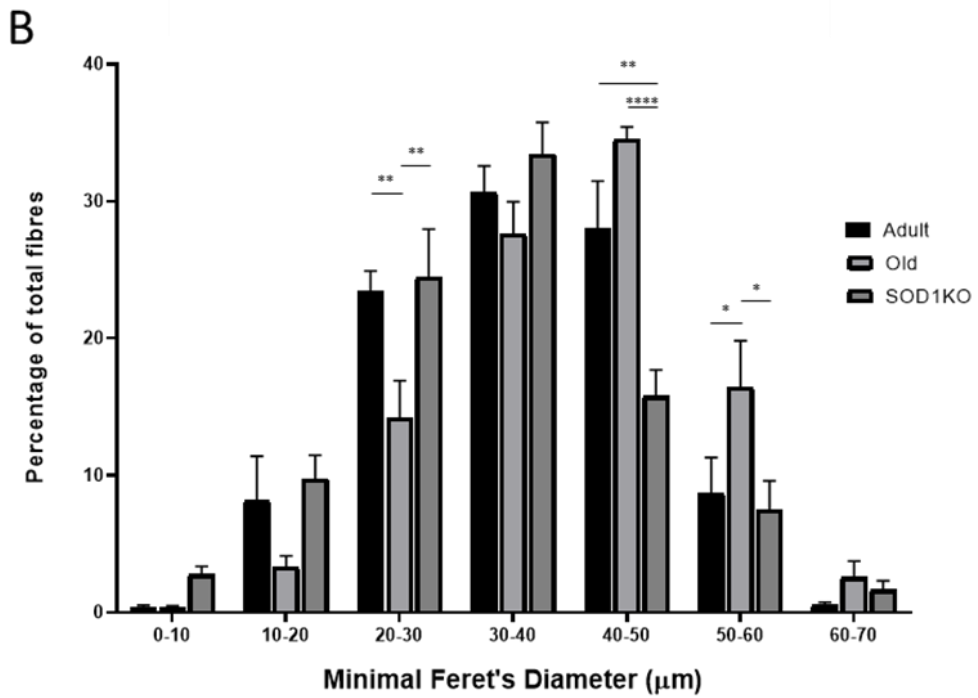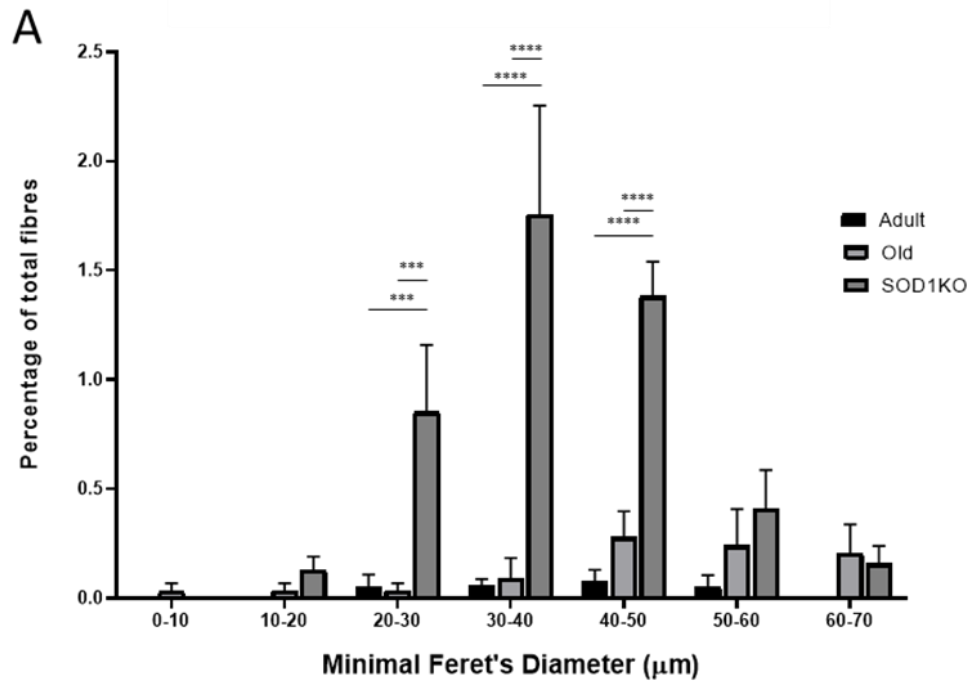
Figure 4.7: Size distribution of fibres containing centrally located nuclei (A) and peripheral located nuclei (B) in EDL muscles from adult WT, old WT and adult SOD1KO mice. *Data represented as mean ± SEM. *p< 0.05, **p<0.01, ***p< 0.0005, ****p<0.0001 (Two-way ANOVA with Tukey's multiple comparisons correction; n = 3-4).*

4.4 Discussion

4.4.1 Muscles from old WT and SOD1KO mice have decreased function and mass

This data demonstrated a decrease in EDL muscle weights of old WT mice which is what has been seen in previous studies (Brooks & Faulkner 1988; Kayani et al. 2010; McArdle et al. 2004). This was also true when accounting for the total mass of the animals. There is also a decrease in both the GTN raw mass and the mass normalised to body weight with age. The adult SOD1KO mice have a decrease in raw and normalised mass in the GTN muscles. Tying into this, muscle forces are reduced in the muscles of old WT and adult SOD1KO mice. These results confirm that there is a loss of muscle mass and function in the old WT and the adult SOD1KO animals which can be described as sarcopenia. They also confirm that the EDL muscle is a muscle effected by the loss of muscle mass and function with ageing in mice in matching of what is seen in humans (Frontera et al. 2000; Nilwik et al. 2013; Porter et al. 1995).

4.4.2 There is no difference in fibre number and diameter in EDL muscles of old mice

No change was seen in fibre number or fibre diameter in either the adult SOD1KO or old WT mice. Previous reports of a reduced fibre number have only been shown in TA and GTN muscles and not in EDL muscles (Sakellariou et al. 2016; Sayed et al. 2016; Tang et al. 2019). Due to the much smaller size of the EDL muscle, significant differences may be more difficult to observe, and this result is consistent with other experiments performed on EDL muscles (Brooks & Faulkner 1990).

This chapter has also shown there to be no significant change in the diameter in the EDL muscle fibres in both the old WT and adult SOD1KO mice. This is not what has been observed in other muscles, but we can see a slight loss in the larger sized fibres and an increase in number of the smaller fibres in both groups through the fibre size distributions (**Figure 4.2**). This was similar to what has been detected in other studies in GTN and TA (Sakellariou et al.

2016; Zhu et al. 2019) and EDL muscles of old WT mice when compared with adult WT mice (Brooks & Faulkner 1988). Although non-significant, there was a 12.5% decrease change in the fibre size of SOD1KO mice when compared with adult WT mice.

4.4.3 Centrally located nuclei are more prevalent in EDL muscles of SOD1KO compared with adult and old WT mice

An increase in the percentage of centrally located nuclei by 4% was seen in the EDL muscles of adult SOD1KO mice through central nuclei analysis at a proportion comparable to that observed by Nagahisa *et al* (2016). In contrast, no significant increase in percentage of centrally positioned nuclei was observed in the EDL muscles of old compared with adult WT mice. This is in contrast to previous observations in GTN and TA muscles of old WT mice (Sakellariou et al. 2016) which may be due to the position of the EDL muscle being deeper in the leg and as such, less exposed to physical injury. This suggests that the centrally positioned nuclei in SOD1KO mice is likely directly due to the increase in oxidative stress known to be present in skeletal muscle fibres of these mice, which may also be a contributor to the accelerated loss of function and mass in the muscle of these mice.

Interestingly, via staining of the full length of single fibres isolated from EDL muscles, this study demonstrated that fibres could contain a mix of centrally and peripherally located nuclei (**Figure 4.3**). This result means that it is more likely that individual myodomains, rather than full fibres, undergo regeneration and the response is localised to injury.

Due to the low percentage of fibres containing centrally located nuclei in all models (<5%) it is important to remember that the data representing fibres with central nuclei represent a small proportion of the total fibre pool. When examining median Feret's diameter the few fibres with central nuclei in muscles of old and adult WT mice alongside the adult SOD1KO were were not significantly different from the Ferets diameter of both the total fibre pool

and those fibres with only peripherally located nuclei (both of which represented 100% or ~99% of total fibres in the muscle) **(Figure 4.6)**.

When observing the size distribution of these fibres presenting with centrally positioned nuclei **(Figure 4.7)**, the data demonstrated that size distribution of fibres with central nuclei in muscles of old WT mice was skewed towards larger fibres in agreement with the data in Figure 4.6 and in contrast with the size distribution in muscle fibres from adult WT and SOD1KO mice.

4.5 Conclusion

In conclusion, muscles from old WT and SOD1KO mice showed a decrease in muscle mass and force generation in fitting with what would be considered as sarcopenia. In EDL muscles, it appears that the change in muscle mass with age cannot be fully explained by a change in fibre number, diameter, or presence of regenerating fibres. In adult SOD1KO mice, a loss of force generation by EDL muscles was observed which could be, at least in part due to the increase in the presence of fibres with centrally located nuclei. These data highlight subtle differences between the muscles of old WT mice and the muscles of our model of ageing, the adult SOD1KO mouse and the role that degeneration and regeneration may play in muscle atrophy. The effect of muscle regeneration on muscle force generation will be explored further in a later chapter where a chemical insult will be administered directly to EDL muscles of mice.

Chapter 5: The role of an inflammatory environment on muscle at rest and during regeneration

5.1 Introduction

5.1.1 Poor muscle regeneration contributes to an aged phenotype

Injury to muscle occurs every day due to normal daily activity (Armstrong 1984). This can be partially attributed to the effects of contraction involving muscle fibre lengthening (Brooks & Faulkner 1990). Previous studies have shown that the recovery of muscle of old mice following damage is not as efficient/successful as the recovery of adult mice following damage leading to the development of a permanent deficit in muscle function in old mice (Brooks & Faulkner 1990; McArdle et al. 2004). It is possible that the failure to regenerate muscle during ageing is a major factor in the development of weakness and loss of muscle mass observed in sarcopenia. The mechanisms by which such regeneration fails in muscles of old mice is unclear. Regeneration is accompanied by a defined progression of changes in gene expression, including expression of embryonic and mature forms of myosin and other proteins under the control of a number of transcription factors.

Activation of NF-κB is undoubtedly required for successful regeneration of muscle and IKKβ-mediated canonical NF-κB signalling has been implicated in the regulation of myogenesis and skeletal muscle mass and the correct regulation of canonical NF-κB signalling is important for the regeneration of adult skeletal muscle (Straughn et al. 2018). It is therefore crucial to determine whether there are any changes in the patterns of NF-κB activation in muscles of old WT and adult SOD1KO mice and whether these are associated with alterations in gene expression, particularly of cytokines, poor muscle regeneration and the development of sarcopenia.

5.1.2 Models of muscle regeneration and the role of cytokines in regeneration

5.1.2.1 Regeneration following a period of damaging lengthening contractions.

There are several models of regeneration in muscles which start with the initiation of an injury. A lengthening (eccentric/damaging) contraction is where the muscle fibres are

lengthened using force. Previous studies have shown that following 450 repeated bouts of lengthening contractions in the EDL muscles of adult WT mice, there was a force deficit after 3 hours which persists for up to 28 days while regeneration of muscle fibres occurs (McCully & Faulkner 1985; McArdle et al. 2004; Pizza et al. 2005). At 3 days post-lengthening contraction causing substantial contraction-induced damage, there was an increase in macrophage and neutrophil infiltration into the EDL muscles causing secondary damage to muscle primarily by additional ROS generation by the infiltrating immune cells (Pizza et al. 2005; Pizza et al. 2002). This was also at the time where there was the highest percentage of injured muscle fibres (Pizza et al. 2005). By 14 days following damage, there was a recovery in the CSA of muscle fibres and a significant increase in fibres with centrally positioned nuclei (Pizza et al. 2005) suggesting active regeneration of muscle fibres. Muscle regeneration following contraction-induced damage is associated with changes in a number of cytokines and chemokines. An increase in CXCL10 levels were seen at 24 to 72 hours following lengthening contractions in humans (Deyhle et al. 2018). There was also an increase in cytokines CXCL10/IP-10, CCL2/MCP1 concentration in the lysates of TA muscles of adult mice at 2 days following a second bout of lengthening contractions (Deyhle et al. 2016). This model however is complicated due to the different susceptibilities of different models to lengthening contraction – mediated damage. Different levels of damage across models (e.g. adult and old mice) would complicate interpretation of the regenerative process following damage. Thus, due to NMJ disruption in adult SOD1KO mice and old WT mice, a lengthening contraction protocol initiated by neuronal activation of muscle may not produce equivalent functional damage. In addition, the second phase of damage seen in muscles of mice at ~ 3 days following initiation of damage does not always occur to similar extents in muscles of adult and old WT mice, further complicating this as a model of regeneration (Zerba et al. 1990).

5.1.2.2 Regeneration following treatment with myotoxins/venoms.

Myotoxin venoms such as cardiotoxin (CTX) or notoxin (NTX) have also been used to injure muscle in a controlled way and cause a regenerative response and such toxins are used to provide an equivalent and extensive amount of damage to muscles in different models. Treatment with NTX results in increased expression of TNFα, IL-6, CCL2, CCL7 and CCL3 in muscle after injury (Liu et al. 2015) associated with an increased activation of resident muscle macrophage cells (Brigitte et al. 2010). In contrast, following CTX-induced injury of the TA muscle, there was no increase in inflammatory cell infiltration into the area which included pro-inflammatory macrophages (Hu et al. 2019). Increased levels of several cytokines, including TNFα and CCL2 were seen at 1-2 days following damage (Sun et al. 2018). Both forms of damage were followed by infiltration of anti-inflammatory macrophages at ~5 days following toxin injection (Sun et al. 2018). As such, these approaches may be used to cause equivalent levels of damage to muscles otherwise showing different susceptibilities to contraction-induced injury. However, in our hands, use of these toxins in mice produces very variable levels of damage (McArdle et al. 1994 and unpublished findings).

5.1.3 Muscle directed Barium Chloride ($BaCl_2$) injection as a model of muscle damage and regeneration

Muscle-directed injection of $BaCl_2$ is a well characterised model of muscle damage and subsequent regeneration. It is proposed that the mechanism of this damage is due to Ca^{2+} dependent proteolysis and membrane depolarisation (Morton et al. 2019). In this model of regeneration, there is extensive necrosis at ~18 hours post injection. 1 month after injury, the fibre diameters are larger than fibres in uninjured TA muscles (McArdle et al. 1994; Hardy et al. 2016). These measures persist for at least 6 months post injury in adult TA muscles (Hardy et al. 2016). The production of cytokines during regeneration are poorly described, but some evidence shows that during the month following injury, increases in cytokines were

seen in the lysates of injured muscle which included IL-6, IL-10, MCP-1, MIP-1α and MIG, however these may include cytokines from resident and invading immune cells (Hardy et al. 2016). There was also an acute increase in IL-1β, IL-17, IFN-γ, and CCL2 within the lysate of the TA muscle, peaking at 3 days post-injection and associated with an increased presence of inflammatory cells (Mosele et al. 2020). It is not known whether NF-κB mediated pathways within the fibres themselves are active.

5.1.4 Hypothesis and aims

This chapter addressed the hypothesis that NF-κB is active to a higher degree than basal levels in muscle fibres undergoing regeneration (identified by the presence of centrally positioned nuclei), this in turn causes an inflammatory response by muscle fibres driven by the release of cytokines by muscle. In addition, that the apparent chronic presence of regenerating fibres identified by the central position of the nuclei, particularly in the muscles of SOD1KO mice is responsible for the increase in some systemic cytokines and chemokines seen in plasma of adult SOD1KO mice.

In this study, $BaCl_2$ injection was used to induce an equivalent and substantial amount of muscle damage in adult and old WT mice and adult SOD1KO mice and to examine the process of regeneration in these models. NMJ disruption in the old WT and adult SOD1KO mice means that a lengthening contraction protocol via nerve activation may not produce equivalent damage to these muscles.

The hypotheses were examined by a number of aims to determine:

1. The morphological and physiological changes observed in muscle fibres during damage and regeneration following chemical damage using $BaCl_2$ in the EDL muscles of adult WT, old WT and adult SOD1KO mice.

2. The occurrence and pattern of muscle fibres containing centrally located nuclei in adult WT, old WT and adult SOD1KO mice in response to injury via injection of $BaCl_2$ into the EDL muscles.

3. The nuclear localisation of p65 throughout degeneration and regeneration in muscles of adult WT, old WT and adult SOD1KO mice.

4. The plasma concentrations of cytokines and chemokines through the process of regeneration in adult WT, old WT and adult SOD1KO mice.

5.2 Methods

5.2.1 Induction of damage and regeneration in muscles of adult WT, old WT and adult SOD1KO mice using $BaCl_2$

$BaCl_2$ injections were administered directly into the EDL muscle belly (IM) as described in **Section 2.2.1**. The adult WT and old WT mice were allowed to recover for 3, 14, 28, and 60 days post injection and then culled via lethal injection of pentobarbital and confirmatory cervical dislocation. SOD1KO mice were studied prior to and 28 days post $BaCl_2$ injection as the number of mice available was limited and this time point was where a failure to recover contractile force in adult WT and old WT mice was apparent. Upon cessation of circulation and loss of eye and toe pinch twitch, whole blood was extracted via aortic bleed and a cervical dislocation was performed. This was collected into tubes containing sodium heparin to prevent clotting, centrifuged at 10,000g for 10 min at 4°C and the plasma was collected into clean microcentrifuge tubes. EDL muscles were dissected using the protocol described in **Section 2.2.3.1**.

Maximum tetanic force generation was determined in a sub-set of mice. The protocol was adapted from McArdle et al. (2004). Mice were anaesthetised with isoflurane and maintained under anaesthesia throughout the procedure. The knee of the right hind-limb was fixed. The distal tendon of the extensor digitorum longus (EDL) muscle was exposed and

attached to the lever arm of a servomotor (Cambridge Technology). The lever arm served as a force transducer. The peroneal nerve was exposed, and electrodes were placed across the nerve. A separate group of mice provided control muscles.

Stimulation voltage and muscle length were each adjusted to produce maximum twitch force. The optimal length for maximum twitch force is also the optimal length (L0) for the development of maximum tetanic force (P0; (Brooks & Faulkner 1988)). With the muscle at L0, the P0 was determined during 300msec of voltage stimulation. The P0 was identified by increasing the frequency of stimulation at 2-min intervals until the maximum force plateaued. Muscle fibre length and cross-sectional area were calculated (Brooks & Faulkner 1988). Following the final measurement, the mouse was removed from the platform. The mouse was weighed, and the EDL muscles were removed immediately. The muscle length was measured, and mass weighed. Mice were sacrificed by cervical dislocation.

5.2.2 H&E staining of damaged and regenerating muscle sections from adult WT, old WT, and adult SOD1KO mice

EDL muscles were mounted onto corks in a transverse orientation and mounted into embedding matrix (**Section 2.3.1**). The muscle blocks were then sectioned at a thickness of 12μm using a Leica CM1850 cryostat (Leica, Wetzlar, Germany) and transferred to SuperFrost Plus slides (**Section 2.3.1**).

The EDL sections were stained using haematoxylin and eosin as in **Section 2.3.2**. The sections were then mounted in DPX mountant and images were captured on a Nikon Ci microscope (Nikon, Kingston-upon-thames, UK).

5.2.3 Fibre size analysis of regenerating muscles from adult WT, old WT, and adult SOD1KO

Analysis of the Feret's diameter of fibres in the EDL muscle sections was performed as described in **Section 2.3.3**.

5.2.4 Analysis of morphology of fibres with centrally compared with peripherally positioned nuclei. regenerating muscles from adult WT, old WT, and adult SOD1KO mice

Central nuclei analysis was performed as shown in **Section 2.3.4**. The images were captured on a Zeiss axio scan Z1 using the settings detailed in **Figure 2.3**.

The images were pre-processed using the macro in **Figure 2.4** and the resulting images were analysed in the MyoVision software.

The data produced was processed to demonstrate fibre size densities, median minimum Feret's diameter of fibres with central versus peripheral nuclei and the percentage centrally located nuclei using R.

5.2.5 P65 staining of sections of regenerating muscles from adult WT, old WT, and adult SOD1KO

Transverse sections of EDL muscles following damage with $BaCl_2$ from adult WT, old WT, and adult SOD1KO mice were prepared using the method described in **Section 2.3.1**. Immunohistochemistry was then performed using the method described in **Section 2.3.5.1** using the Abcam anti-NF-κB p65 antibody (ab32536; Abcam, Cambridge, UK) as the primary antibody.

Sections were imaged for p65 localisation using a Zeiss LSM800 confocal microscope (Carl Zeiss AG, Oberkochen, Germany) using a 20x lens.

5.2.6 Cytokine analysis of plasma samples from adult WT, old WT and adult SOD1KO mice following injection of EDL muscles with $BaCl_2$

Plasma samples were diluted 1:3 in Bioplex sample diluent and the Luminex-based assay for 33 cytokines was performed as described in **Section 2.4.2**.

5.3 Results

5.3.1 The mass and function of muscles from adult WT, old WT, and adult SOD1KO of mass following regeneration

A significant increase in the weight of the EDL muscles normalised to the total body weight of adult mice was seen at both 3 days and 28 days post injection (**Figure 5.1D**). No observed change was detected in the normalised weight of the EDL muscles from old and SOD1KO mice at any time-point when compared to their uninjected controls (**Figure 5.1B; Figure 5.1C**). There was no significant changein the body weight of adult WT, old or SOD1KO mice at any of the time-points examined (**Figure 5.1G; Figure 5.1H; Figure 5.1I**).

The maximum tetanic force of uninjected muscles SOD1KO mice was significantly decreased when compared with the uninjected muscles of adult WT mice. The maximum tetanic force was not significantly different post 28 days of the muscles of both the adult and old WT mice when compared to their uninjected controls (**Figure 5.2**). The force experienced by the old WT mice 28 days post injection was significantly lower than that of the adult WT mice (**Figure 5.2**). Undamaged EDL muscles from the adult SOD1KO mice showed a significant reduction in tetanic force generation compared with adult WT mice (**Figure 4.1F**) but this force generation recovered fully to undamaged levels by 28 days following damage (**Figure 5.2**) The deficit in maximum tetanic force generation in muscles of old WT mice at 28 days following damage was accompanied by a 30% deficit in specific force generation (**Table 5.1**). In contrast, no deficit in specific force generation was seen in muscles of adult WT or adult SOD1KO mice at this time point.
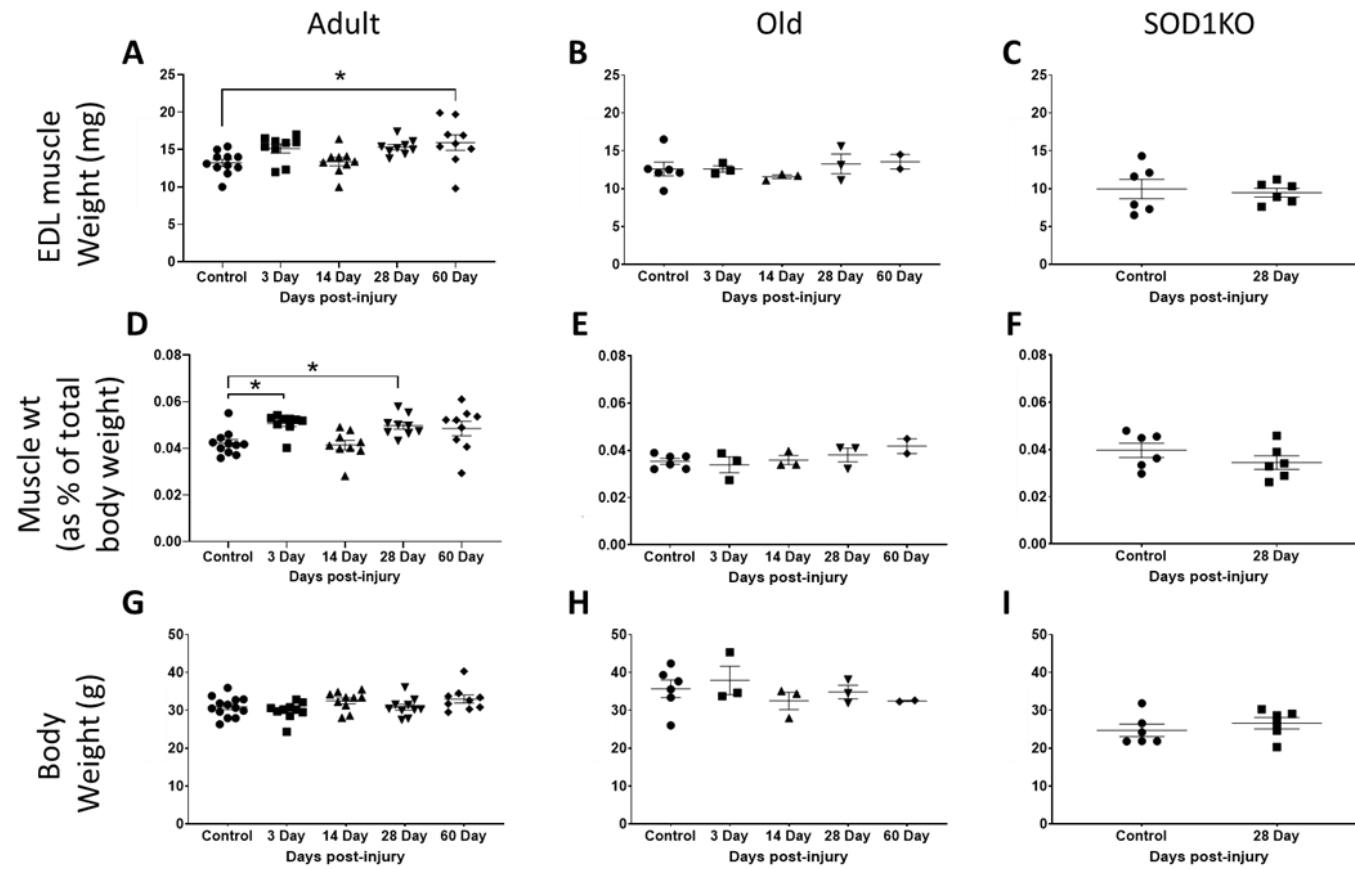
Figure 5.1: Measurements of muscle mass throughout degeneration and regeneration in adult WT, old WT and adult SOD1KO mice following injury with Barium Chloride. *A-C) The weights of EDL muscles, D-E) muscle weight as a percentage of body weight and G-I) body weight of adult and old WT, and adult SOD1KO mice prior to and 3-, 14-, 28- and 60-days following injection with BaCl₂. Data presented as mean ± SEM. * p<0.05. (One-way ANOVA with Dunnet's Post-hoc correction).*
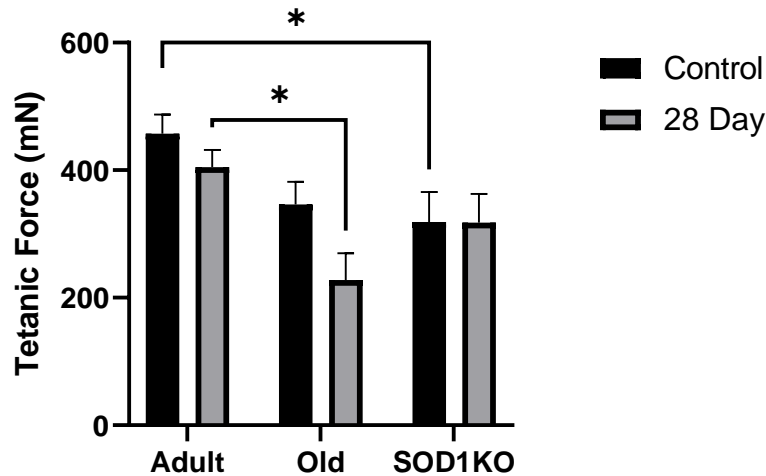
Figure 5.2: Muscle force generation prior to and following damage to the muscles of adult WT. old WT and adult SOD1KO mice following the injection of barium chloride. Maximal tetanic force generated by EDL muscles of adult WT, old WT and, adult SOD1KO mice in un-injected and at 28 days post-injection with $BaCl_2$. Data shown as mean ± SEM. * p<0.05. (Two-way ANOVA with Benjamini-Hochberg-hoc correction)

Table 5.1: Specific force generation by EDL muscles of adult and old WT and adult SOD1KO mice. *P<0.05 cf Baseline values.

	Adult WT	Old WT	Adult SOD1KO
Quiescent	176 (11)	152 (22)	159 (47)
28 days post-BaCl$_2$	150 (8)	99 (19) *	180 (28)

In transverse sections from un-injected EDL muscles from adult WT, old WT and adult SOD1KO mice stained with H&E, the fibres appeared regularly spaced with little evidence of gross necrosis and had no large open spaces in the muscles. There was a significant amount of damage at the 3-day time-point following injection with $BaCl_2$, evidenced by the presence of infiltrating immune cells and this was followed by a sustained period of regeneration as shown by the centrally located nuclei which were present for at least to 60 days following damage. Although still substantial, a lower amount of damage and oedema (as shown by an apparently empty space between fibres) seemed evident in muscles of old WT mice although this time point was not quantified and there was a reduced number of centrally located nuclei throughout the time course studied (**Figure 5.3A**). The EDL muscles of the adult

SOD1KO mice showed a similar proportion of centrally located nuclei to the adult WT mice at 28 days post-injection **(Figure 5.3B)**.
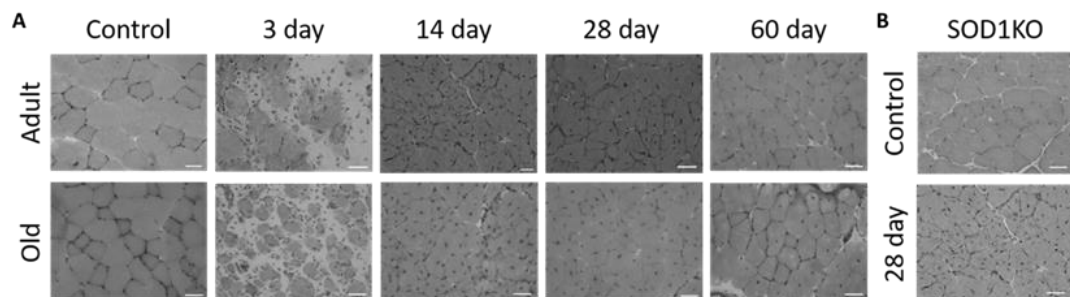
Figure 5.3: Representative images of time course of changes in muscle morphology and location of nuclei following BaCl$_2$ injection in adult WT, old WT and adult SOD1KO mice. Representative images of H&E stained muscle fibres from (a) adult and old WT mice prior to and 3, 14, 28, and 60 days post BaCl$_2$ injection, (b) *SOD1KO* mice prior to and 28 days post BaCl$_2$ injection.

5.3.2 Changes in muscle morphology during regeneration

No loss of fibres was seen in any of the groups studied at any time-point compared with pre-damage values **(Figure 5.4A)**. No difference was seen in the minimum Feret's diameter at any time point and the fibre size distribution revealed a general increase in the number of smaller muscle fibres in muscles of all three groups of mice (**Figure 5.4B; Figure 5.4C** (**Figure 5.4D; Figure 5.4E**).
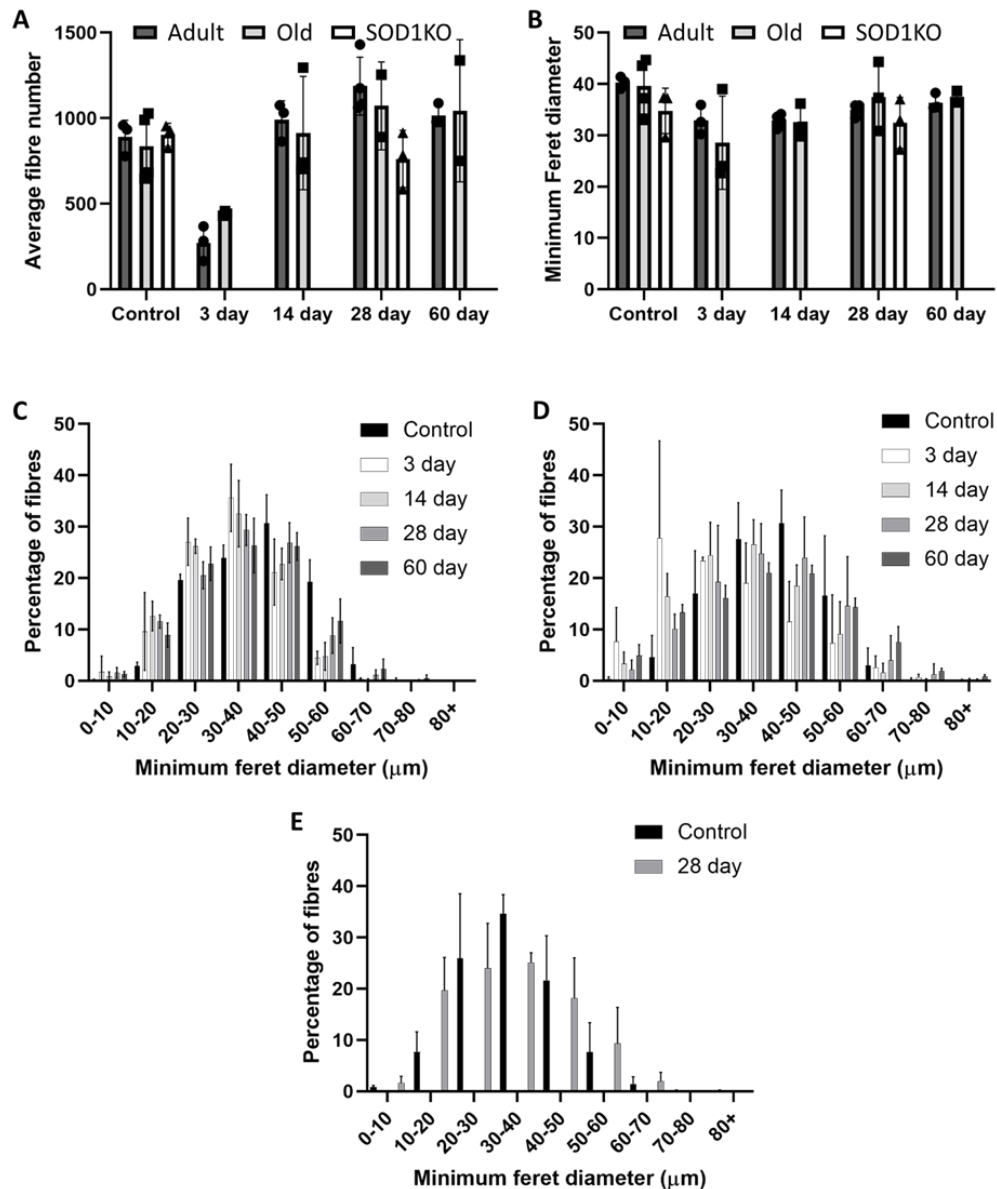
Figure 5.4: Time course of changes in muscle structure and function induced by BaCl₂ injection in the muscles of adult WT and old WT and adult SOD1KO mice. *EDL muscle characteristics, (A) mean fibre number and (B) mean fibre Feret's diameter in EDL muscles from adult (dark grey) and old (light grey) WT mice prior to and 3, 14, 28 and 60 days post BaCl₂ injection and from adult SOD1KO mice (white) prior to and 28 days post BaCl₂ injection. Fibre size distribution in EDL muscles from (C) adult and (D) old WT mice prior to and 3, 14, 28, and 60 days post BaCl₂ injection. (E) Fibre size distribution in EDL muscles from adult SOD1KO mice prior to and 28 days post BaCl₂ injection. p<0.05*, p<0.05**, p<0.001*** p<0.0001**** (One-way ANOVA with Dunnet's post-hoc test).*

Fibres with centrally located nuclei were evident in the muscles of both adult and old WT and adult SOD1KO mice from 14-days onwards following injection with BaCl₂ up to 60 days following injection (**Figure 5.5A; Figure 5.5B**). In EDL muscles of adult WT mice, the

percentage of fibres with centrally located nuclei remained stable at around 70% from 14 to 60 days (**Figure 5.5A**). In the EDL muscles from old WT mice, the percentage reached the same peak of 70 % at 14 days but reduced to around 55% at 60 days showing a premature return to the periphery since the total number of fibres remained the same (**Figure 5.5B**). Seventy percent of fibres from adult SOD1KO mice contain centrally located nuclei 28 days post injection with BaCl$_2$ (**Figure 5.5C**). The fibre size of muscle fibres with centrally located nuclei were not significantly different from fibre sizes of uninjured muscle for all the groups at all time points (**Figure 5.5G-I**). In contrast to this, the minimum Feret's diameter was significantly decreased in fibres with peripherally located nuclei in muscles of adult WT, old WT and adult SOD1KO mice at all time points following damage. This was not evident when all fibres were analysed together as these fibres only account for around 30 percent the total fibres in the muscle (**Figure 5.5D-F**).
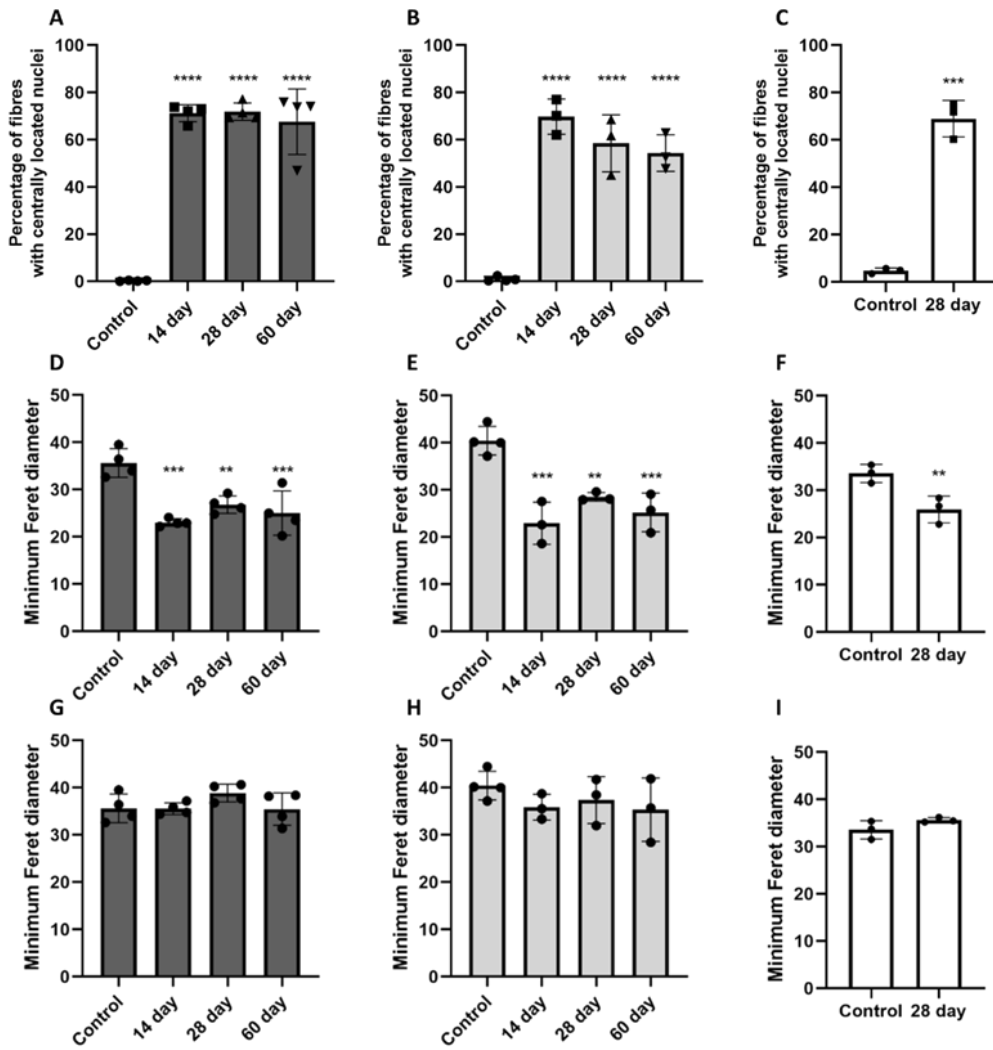
Figure 5.5: Time course of changes in muscle morphology and location of nuclei following BaCl₂ injection in adult WT, old WT and adult SOD1KO mice. The percentage of fibres containing centrally located nuclei in EDL muscle from (A) adult WT and (B) old WT mice prior to and 3, 14, 28, and 60 days post BaCl₂ injection. (C) The percentage of fibres containing centrally located nuclei in EDL muscle from adult SOD1KO mice prior to and 28 days post BaCl₂ injection. The minimum Feret's diameter of fibres with peripheral nuclei only in EDL muscle from (D) adult WT and (E) old WT prior to and 3, 14, 28, and 60 days post BaCl₂ injection. (F) The minimum Feret's diameter of fibres with peripheral nuclei in EDL muscle from adult SOD1KO mice prior to and 28 days post BaCl₂ injection. The minimum Feret's diameter of fibres with one or more centrally positioned nuclei in EDL muscle from (G) adult WT and (H) old WT mice prior to and 3, 14, 28, and 60 days post BaCl₂ injection. The minimum Feret's diameter of fibres with one or more centrally positioned nuclei in EDL muscle from (I) adult SOD1KO mice prior to and 28 days post BaCl₂ injection. Data are presented as means ± SD. Symbols represent significant differences compared with adult WT p<0.05*, p<0.05**, p<0.001*** p<0.0001**** (One-way ANOVA with Dunnet's post-hoc test).

5.3.3 NF-κB localisation following regeneration in the muscles of adult WT, old WT and adult SOD1KO mice

No observable p65 was evident within the nuclei in the transverse sections of EDL muscles from adult mice prior to damage. In the transverse muscle sections from the old WT mice however, there was an increase in p65 content within the peripherally located nuclei as described in **Chapter 3**. Quiescent muscles from adult SOD1KO mice demonstrated an increase in p65 content of centrally located nuclei, as described in Chapter 3. p65 localisation to nuclei in the muscles of all groups showed increased levels of p65 associated with the centrally located nuclei for up to 60 days although the levels and time course appeared different between the groups (**Figure 5.6; Figure 5.7; Figure 5.8**). Thus, there was a higher content of p65 within the centrally located nuclei of muscles of old WT mice 14 days post injection with $BaCl_2$ in comparison with that of adult WT muscles although this decreased at later time points (**Figure 5.6; Figure 5.7**). Muscles of adult SOD1KO mice showed a persistent localisation of p65 to the muscle nuclei for up to 28 days following damage (Figure 5.8).
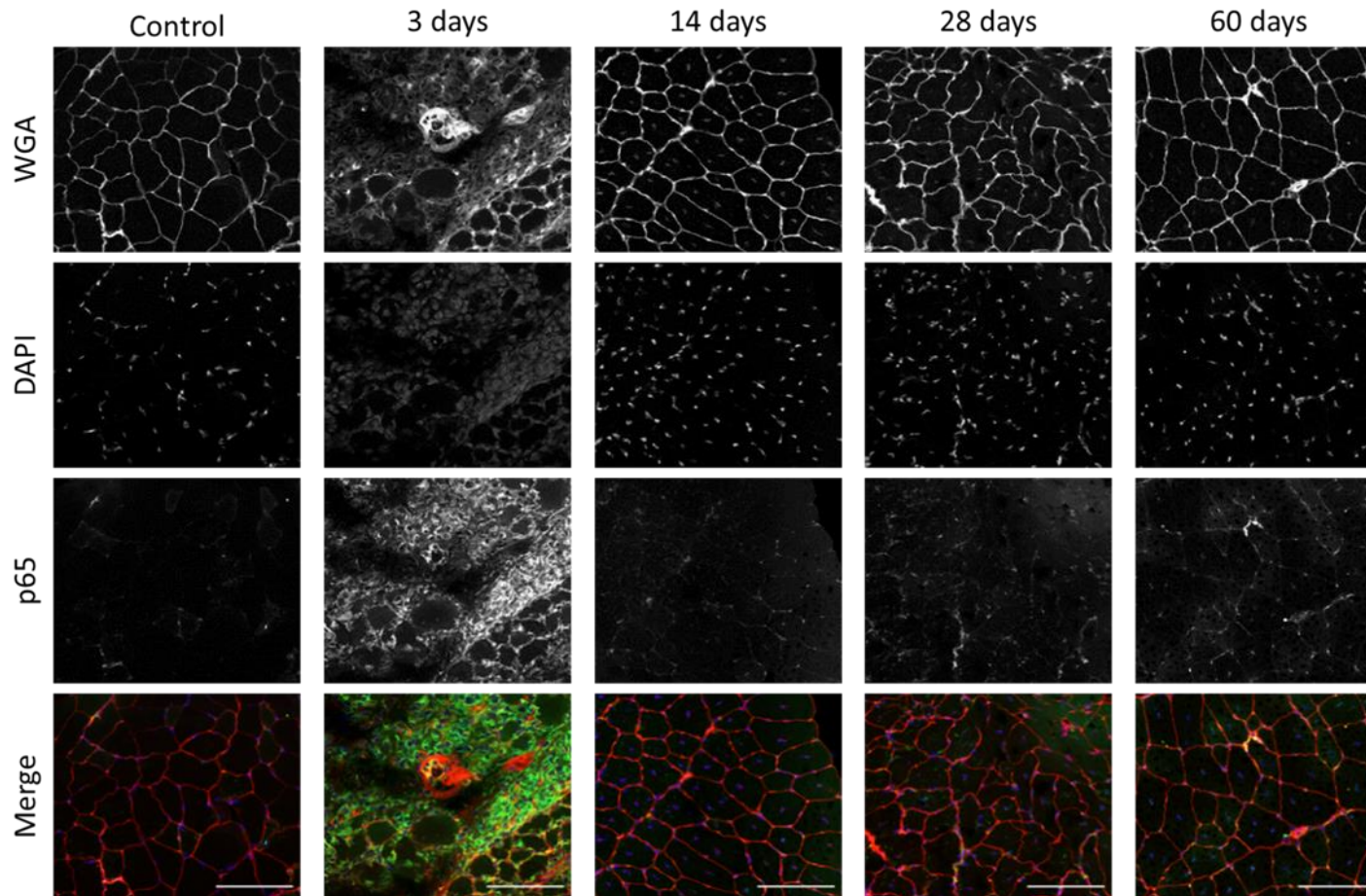
Figure 5.6: p65 nuclear translocation during regeneration in EDL muscles of adult WT mice following the injection of barium chloride. *Confocal microscopy of immunohistochemistry of EDL muscles of adult WT mice during regeneration following injection of BaCl$_2$ demonstrating increased p65 (green) localisation of p65 to the nuclei (blue). Sections are counterstained with wheat germ agglutinin (WGA; red). Scale bar = 100 μm.*
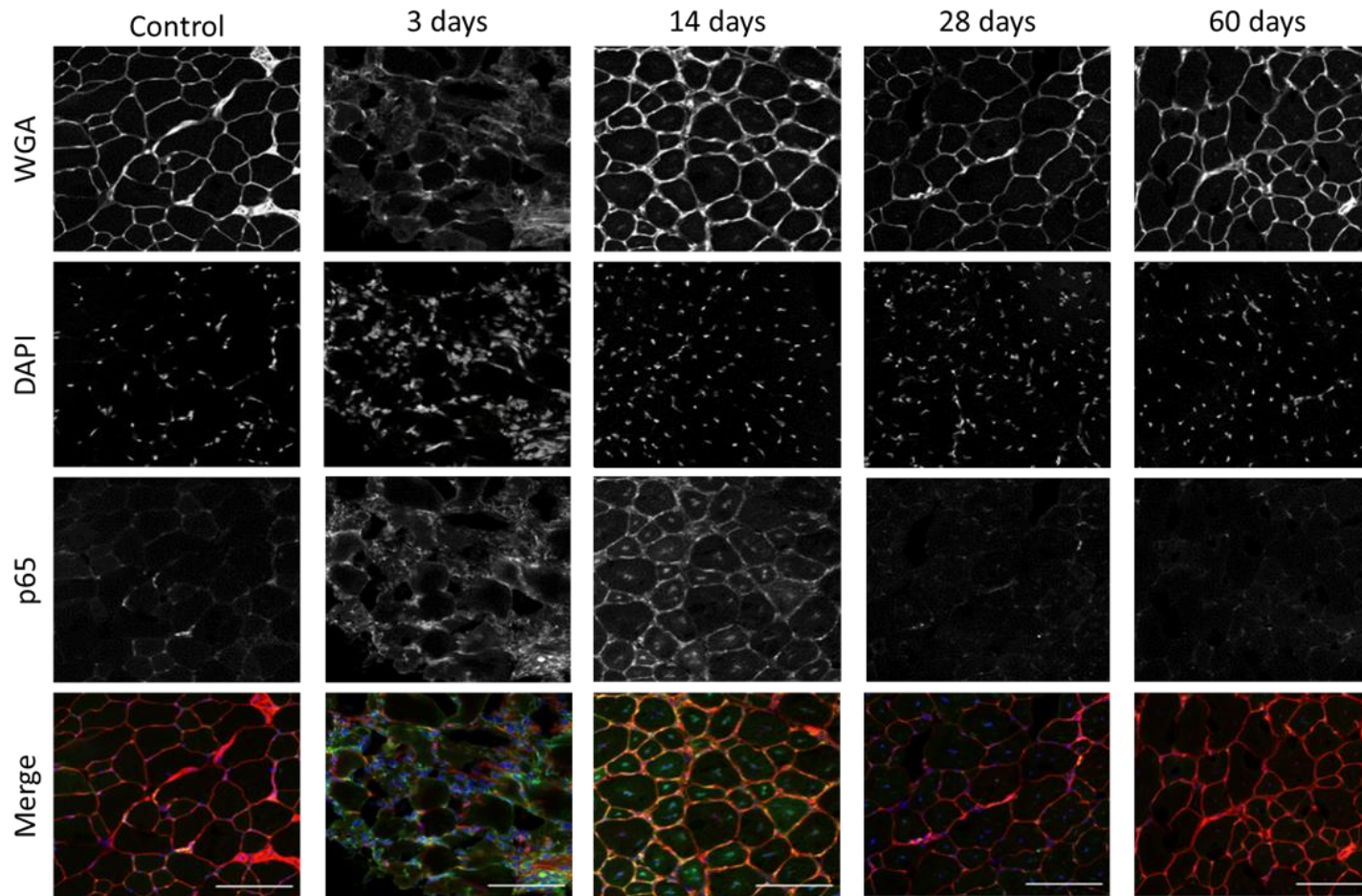
Figure 5.7: p65 nuclear translocation during regeneration in the muscles of old WT mice following the injection of barium chloride. *Confocal microscopy of immunohistochemistry of EDL muscles of old mice during regeneration following injection of BaCl₂ to observe the translocation of p65 (green) to the nuclei (blue). Sections are counterstained with wheat germ agglutinin (WGA; red). Scale bar = 100 μm.*
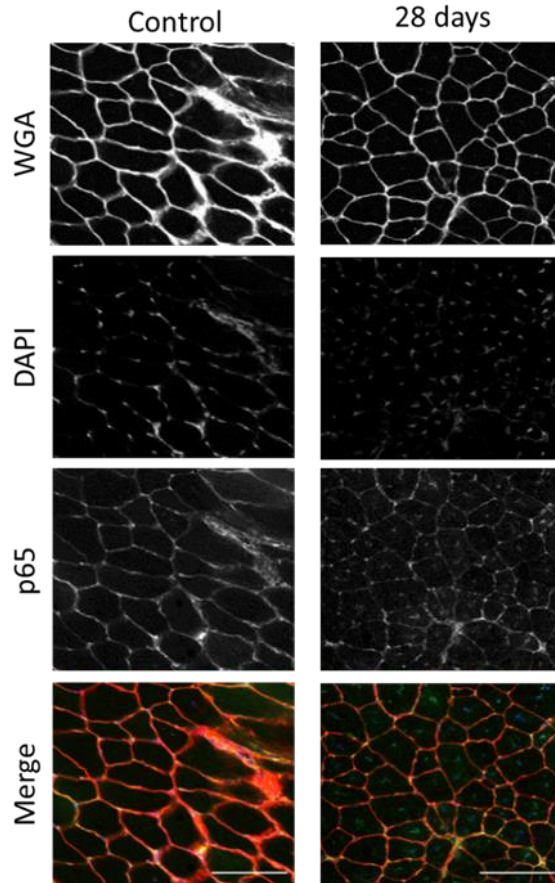
Figure 5.8: p65 nuclear translocation during regeneration in the muscles of adult SOD1KO mice following the injection of barium chloride. Confocal microscopy of immunohistochemistry of EDL muscles of SOD1KO mice during regeneration following injection of BaCl$_2$ to observe the translocation of p65 (green) to the nuclei (blue). Sections are counterstained with wheat germ agglutinin (WGA; red). Scale bar = 100 µm.

5.3.4 Plasma cytokine and chemokine levels during regeneration

In **Chapter 3**, data showed there was a significant increase in the plasma content of 3 cytokines, and 7 chemokines in old WT mice compared with adult WT mice and 1 chemokine in the plasma of adult SOD1KO mice (**Table 3.7**). Data also demonstrated an increase in 1 cytokine and 1 chemokine in quiescent muscle lysates from old WT mice and 1 cytokine and 2 chemokines from adult SOD1KO mice (**Figure 3.14**). Muscle fibres isolated from old WT mice produced 4 chemokines at a higher level that fibres isolated from adult WT mice (**Figure 3.14**).

Cytokine content of the plasma of adult WT, old WT and adult SOD1KO mice prior to and 3, 14, 28, and 60 post intramuscular BaCl$_2$ injection is shown in **Figures 5.9 – 5.14**. Of the 33 chemokines/cytokines examined, 15 were at levels within the detection limits of the assay although a number of these were below the value for the lowest standard for that cytokine/chemokine.

In adult WT mice, the plasma concentration of CXCL1 was reduced 14 days post injection (**Figure 5.10**). No significant changes were seen in any other detectable cytokines/chemokines. In the plasma of the old WT mice, CCL2 and CCL5 were both reduced in concentration at 3 days following damage (**Figure 5.12**). CCL5 was also at a lower concentration in the plasma, 28 days post-injury (**Figure 5.12**). CXCL2 was increased in the plasma of adult mice at 28 days post-injection (**Figure 5.14**). All other cytokines and chemokines measured were not significantly changed for up to 60 days following injection (**Figure 5.10 - Figure 5.14**).
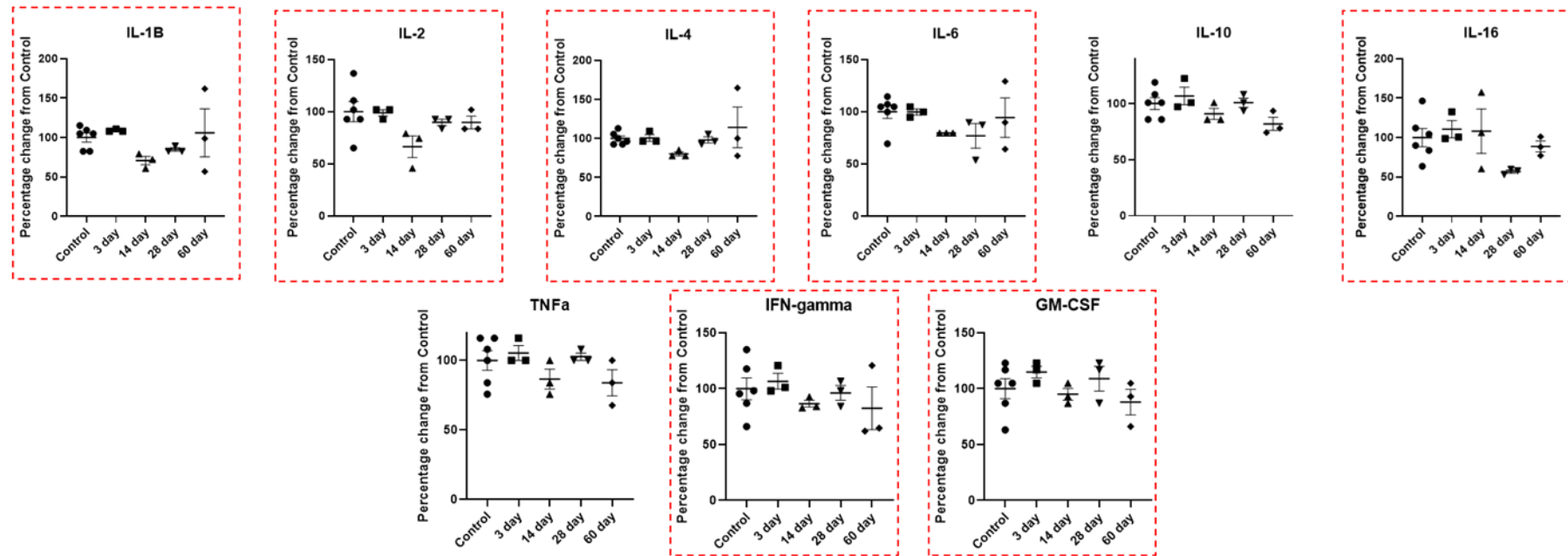
Figure 5.9: Cytokine concentrations of plasma from adult WT mice during regeneration following IM injection with barium chloride determined via Bioplex assay. *Interleukin (IL), Tumour necrosis factor α (TNF-α), interferon γ (IFN-gamma), granulocyte-macrophage colony-stimulating factor (GM-CFS). Cytokines with dashed border had data points under the standard curve. Data presented as mean±SEM. (One-way ANOVA with Dunnet's post-hoc test).*
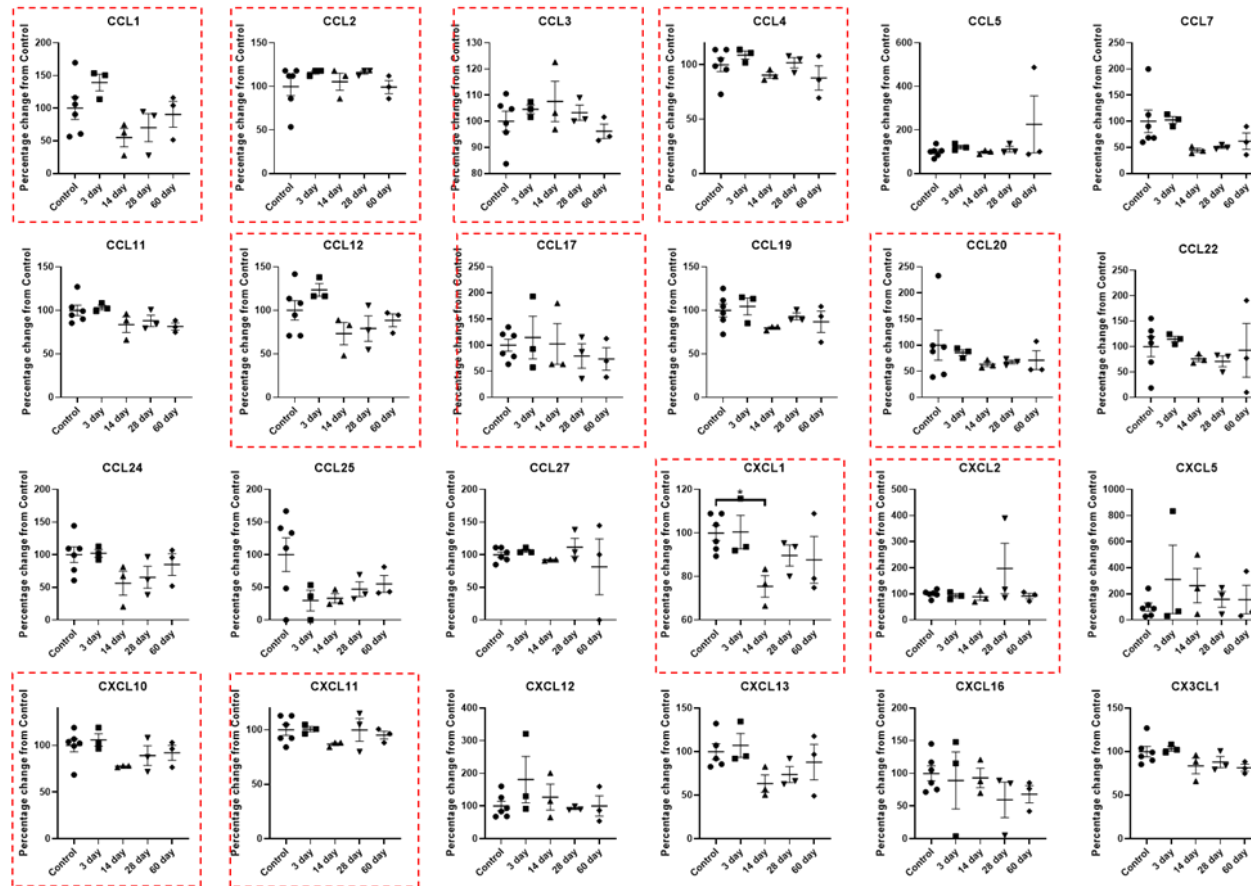
Figure 5.10: Chemokine concentrations of plasma from adult WT mice during regeneration following IM injection with barium chloride determined via Bioplex assay. *Chemokines with dashed border had datapoints under the standard curve. Data presented as mean±SEM. *p < 0.05 (One-way ANOVA with Dunnet's post-hoc test)*
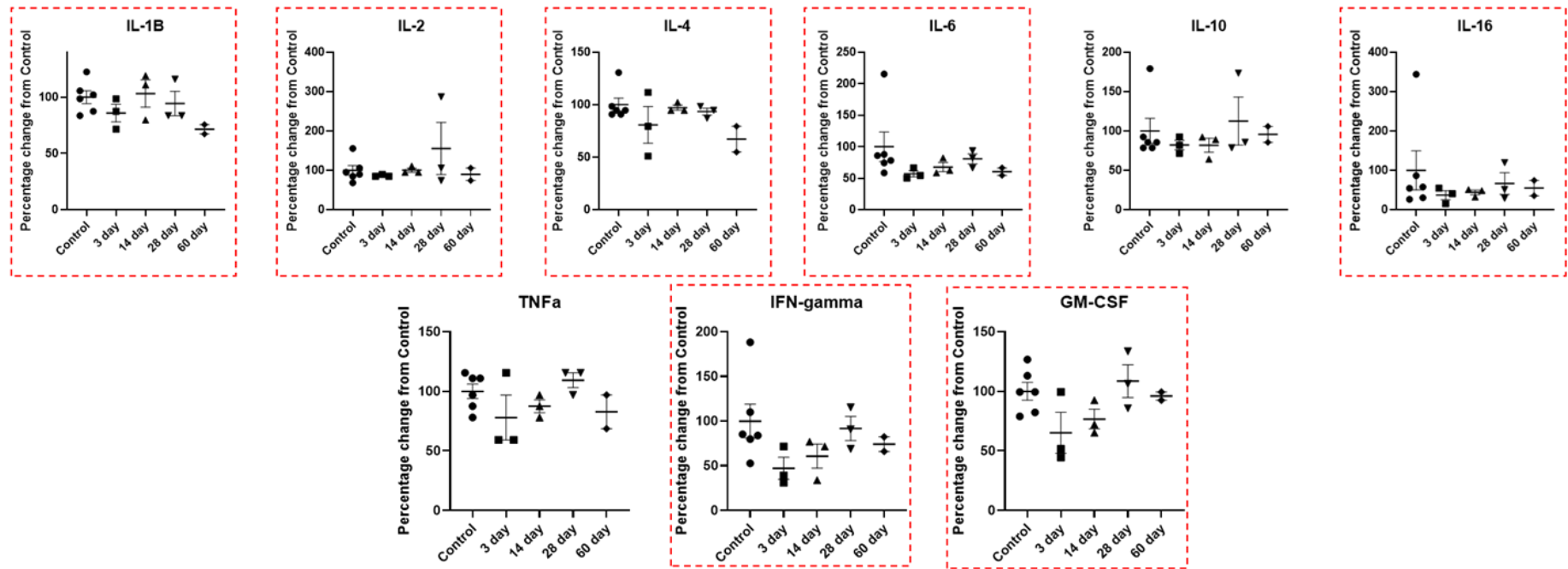
Figure 5.11: Cytokine concentrations of plasma from old WT mice during regeneration following IM injection with barium chloride determined via Bioplex assay. *Interleukin (IL), Tumour necrosis factor α (TNF-α), interferon γ (IFN-gamma), granulocyte-macrophage colony-stimulating factor (GM-CFS). Cytokines with dashed border had datapoints under the standard curve. (One-way ANOVA with Dunnet's post-hoc test).*
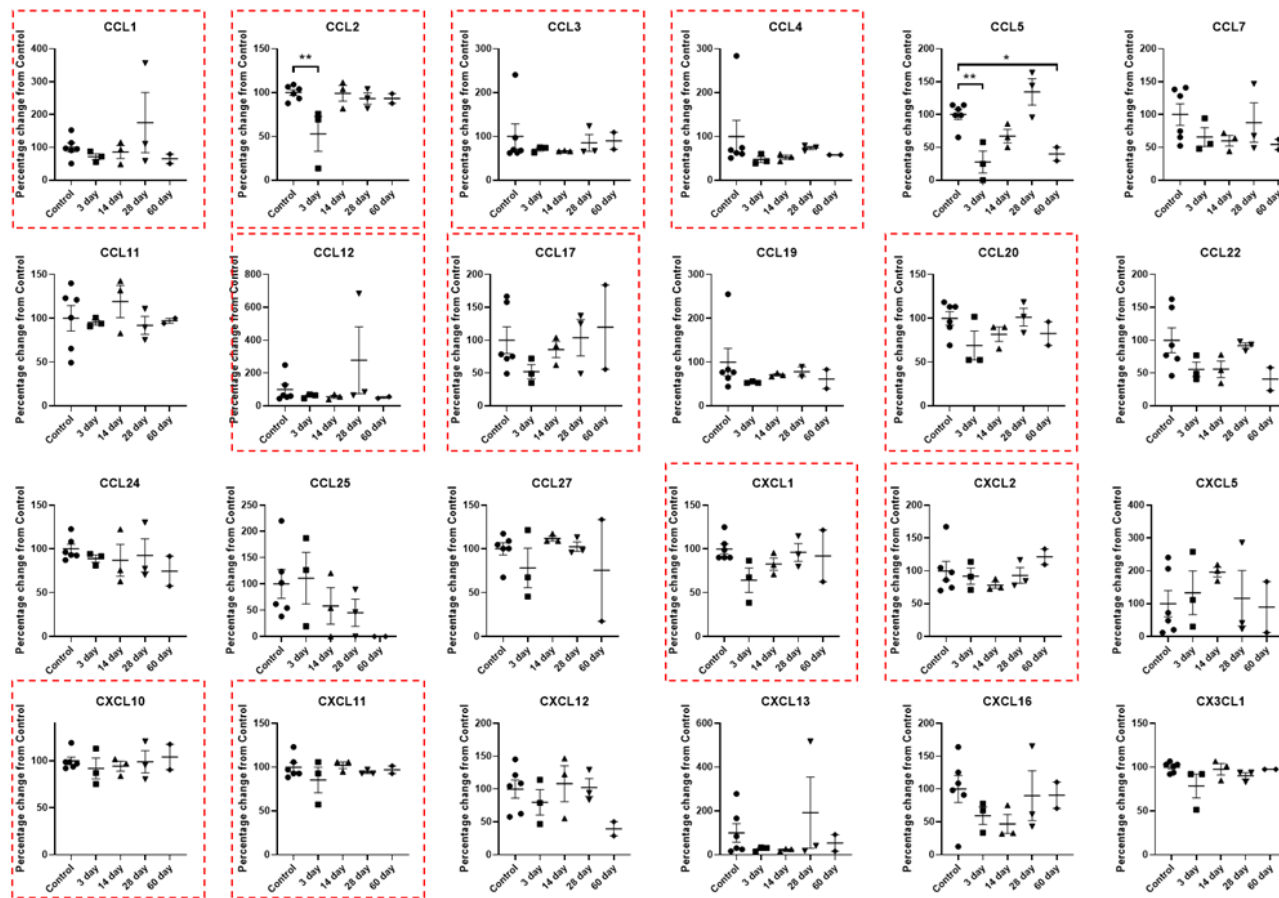
Figure 5.12: Chemokine concentrations of plasma from old WT mice during regeneration following IM injection with barium chloride determined via Bioplex assay. *Chemokines with dashed border had datapoints under the standard curve. Data presented as mean±SEM. *p < 0.05, **p < 0.01 (One-way ANOVA with Dunnet's post-hoc test)*
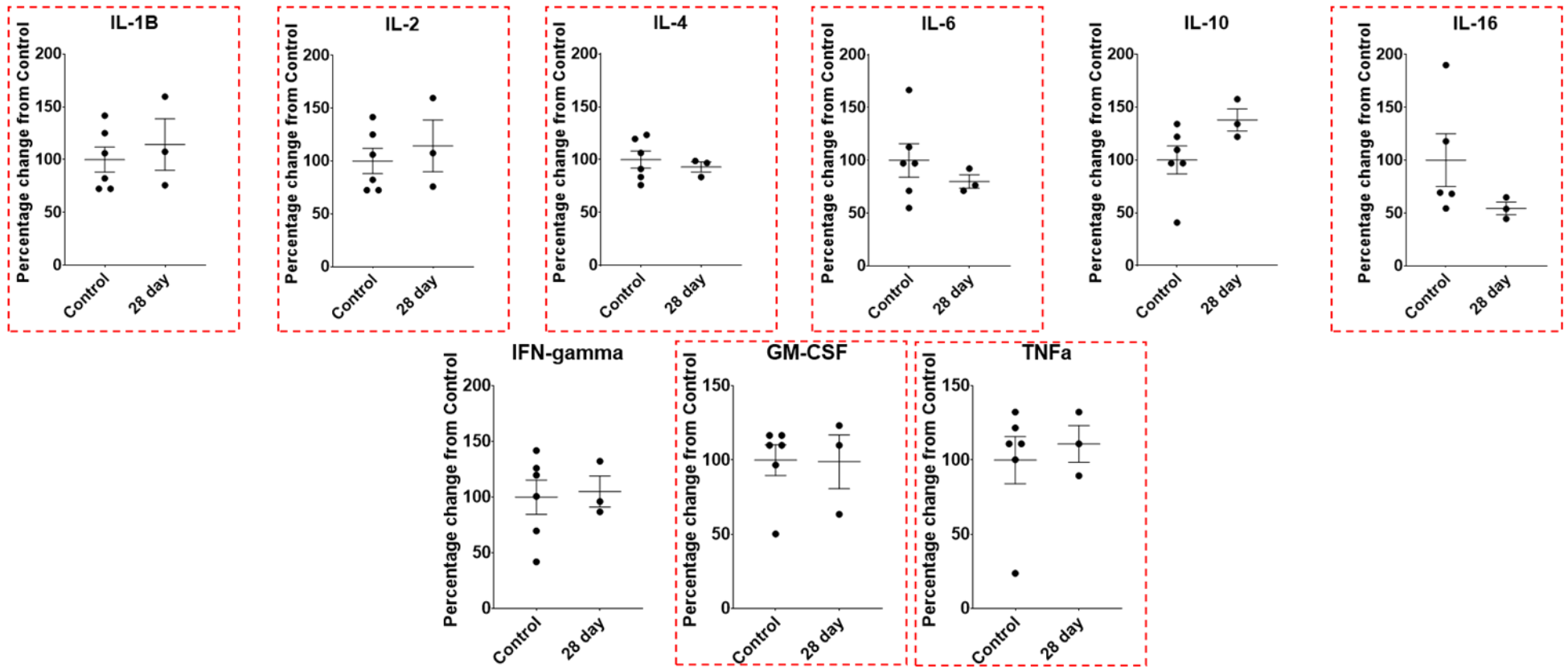
Figure 5.13: Cytokine concentrations of plasma from adult SOD1KO mice during regeneration following IM injection with barium chloride determined via Bioplex assay. *Interleukin (IL), Tumour necrosis factor α (TNF-α), interferon γ (IFN-gamma), granulocyte-macrophage colony-stimulating factor (GM-CFS) Cytokines with dashed border had datapoints under the standard curve. (One-way ANOVA with Dunnet's post-hoc test).*
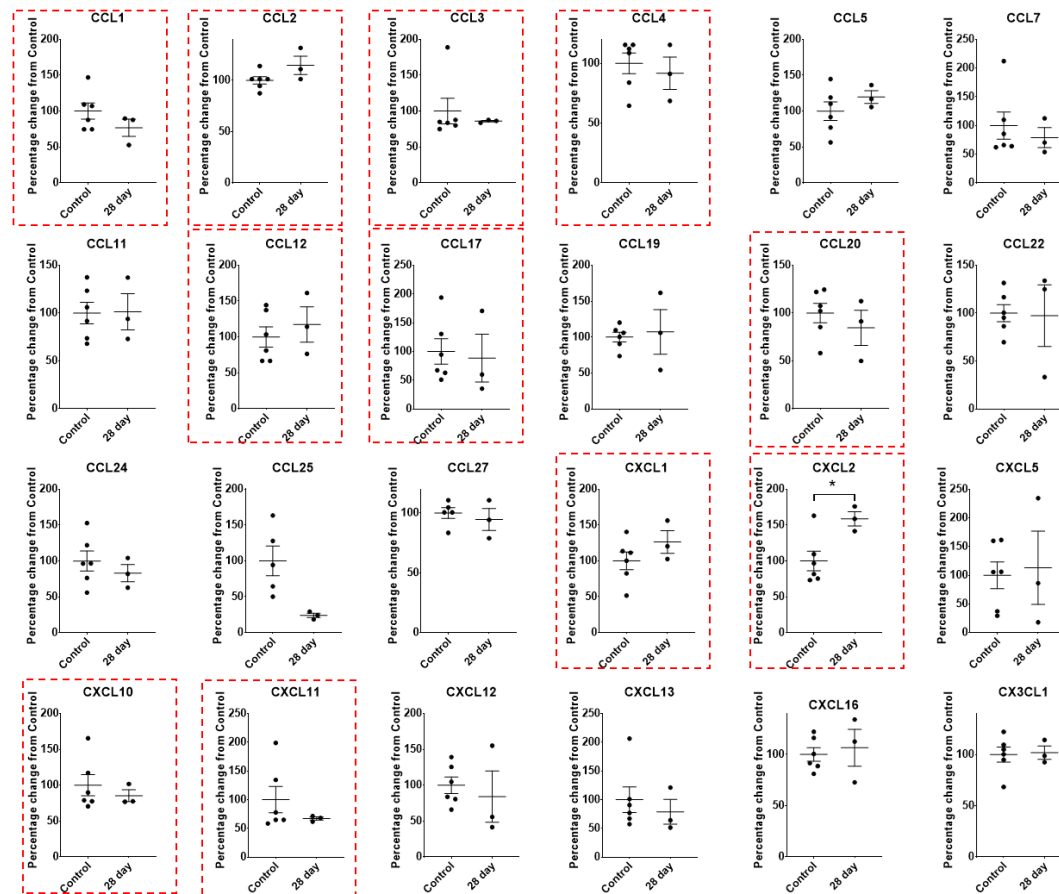
Figure 5.14: Chemokine concentrations of plasma from adult SOD1KO mice during regeneration following IM injection with barium chloride determined via Bioplex assay. *Chemokines with dashed border had datapoints under the standard curve. Data presented as mean±SEM. *p < 0.05 (One-way ANOVA with Dunnet's post-hoc test).*

5.4 Discussion

This chapter addressed the hypothesis that NF-κB was active in muscle fibres undergoing regeneration (identified by the presence of centrally positioned nuclei) in both old WT and adult SOD1KO mice and that this in turn results in the increased release of cytokines by muscle. In addition, that the apparent chronic presence of regenerating fibres identified by the central position of the nuclei, particularly in the muscles of adult SOD1KO mice is responsible for the increase in some systemic cytokines and chemokines seen in the plasma of adult SOD1KO mice.

Incomplete recovery of function in muscles of old WT mice following damage is not due to altered muscle fibre size or number.

Data indicated that injury by intramuscular injection of $BaCl_2$ was followed by a full recovery of the muscles of adult WT mice and the muscles of old WT mice. However the muscles of the old WT mice 28 days post recovery were 50 % the maximum strength of the muscles of adult mice 28 days post injection. The poor recovery observed in muscles of old WT mice cannot be attributed to substantial loss of fibre number or decrease in the average muscle fibre size, in agreement with data from Brooks and Faulkner (1990) and suggests that other factors are playing a role in the functional deficit seen in quiescent muscles of old mice. Examination of the position of the nuclei in muscle fibres during regeneration revealed that fibres which had recently regenerated (containing one or more centrally positioned nuclei) had recovered to pre-damage diameter by 14 days following damage in both adult and old WT mice. Fibres with peripherally located nuclei (perceived as undamaged) which represent around 30 % of all fibres across cohorts following damage, were substantially smaller than pre-damaged fibres for up to 60 days following damage. Interestingly, this was not evident when analysing all fibres together as the fibres with peripherally located nuclei represent a small subset of the whole population of fibres. The mechanisms responsible for the poor

recovery of these muscle fibres are unclear, however may suggest a longer timeframe is required to fully repair rather than replace the damaged muscle fibres. There is, however, no difference observed between the adult and old WT mice suggesting that this does not play a role in the functional deficit in the muscles of old WT mice following damage with $BaCl_2$.

It is possible that the muscle fibres may remain injured at other locations other than the cross section that was examined as there is evidence from longitudinal analysis of muscles following damage which demonstrates focal adhesions, though this is unlikely to account for such a large deficit in muscle function recovery (Brooks & Faulkner 1990). Previously, it has been thought that poor reinnervation or revacularisation are responsible for the loss of muscle function in old mice following injury (Carlson & Faulkner 1989) but this was outside of the scope of this study.

In contrast to the muscles of old WT mice, muscles from adult SOD1KO mice demonstrated a complete recovery in force generation like that of adult WT mice. The return of muscles adult WT and SOD1KO mice to their pre-damage mass and strength following damage is intriguing since muscles of SOD1KO mice return to the pre-damage value for tetanic force generation, a value which was significantly less than that of quiescent adult WT mice. These data seem to suggest that there is a pre-determined limit to the functional recovery of muscle, at least in this model.

5.4.1 Inflammation in response to muscle regeneration does not affect systemic inflammation.

Immunofluorescent localisation of p65 in muscles during the regeneration process demonstrate the temporal translocation to the nuclei in muscles of adult and old WT and adult SOD1KO mice (**Figures 5.6 – 5.8**). The time course and extent of nuclear localisation of p65 appeared different in the three groups, with some evidence of increases in nuclear

localisation in adult muscles that peaked around 28 days post injection but greater increases in muscles of old WT mice that peaked at 14 days following damage and in adult SOD1KO mice that remained elevated at 28 days following damage. We know that temporal changes in p65 have drastic effects on the downstream gene expression. If muscle was the source for the cytokines/chemokines seen to be increased in the plasma of quiescent old WT or adult SOD1KO mice, it is surprising how few cytokines were observed to be increase in the plasma of mice following damage, given that the percentage of regenerating fibres in this model is likely to be similar to the total evident in the whole body of old WT or adult SOD1KO mice although it may be that the lack of substantial changes in plasma cytokine levels was likely due to the low muscle mass of the muscles injected. No significant changes were seen in the concentrations of any of the cytokines measured. If the presence of regenerating fibres *per se* was responsible for such changes in plasma cytokine concentration, one would expect those to be elevated at least at one of the time points during regeneration in adult WT mice, but this was not the case. Interestingly, the cytokines/chemokines seen to be elevated in plasma of quiescent old WT mice appeared to remain elevated. There was a transient decrease in the plasma level of CXCL1 at 14 days post injury in the plasma of adult WT mice (**Figure 5.10**). There was also a transient but significant decrease in both CCL2 and CCL5 at 3 days post-injection in old WT mice and CCL5 returned to reduced levels at 60 days post injection in the plasma of old WT mice (**Figure 5.12**). In the plasma of adult SOD1KO mice, there was an increase in CXCL2 at 28 days following injury (**Figure 5.14**). These cytokines are associated with the loss of grip strength with age in humans. CCL2 in particular is associated with control over macrophages which would be essential in the recovery of muscle post injury (Gschwandtner et al. 2019). Higher CCL5 levels in the heart muscle of mice is associated with a lower amount of damage following tissue damage (Braunersreuther et al. 2010). This could in part account for the difference in muscle damage experienced from these mice following muscle injury. The difference in chemokines between adult WT, old WT

and adult SOD1KO mice shows that there are alterations in the regenerative response to damage between these groups of mice, but interpretation of these data is complicated on an already modified plasma cytokine background in these models.

Table 5.2: Summary of the results from the Luminex on various samples and qPCR from Chapters 4 and 5. *Green represents an increase in cytokine/chemokine content whereas red represents a decrease in cytokine content. Darker shading indicates a lower p value when compared to adult WT mice. White boxes have no significant difference when compared to adult WT mice. Grey boxes show there has been not measurement for this cytokine/chemokine.*

| | Quiescent | | | | | | | | | Regeneration | | | | | | | | |
| | Plasma | | Lysate | | Fibre media | | | Gene expression | | Adult | | | | Old | | | | SOD1KO |
	Old	SOD1KO	Old	SOD1KO	Old	SOD1KO	Cytokine	Old	SOD1KO	3 day	14 day	28 day	60 day	3 day	14 day	28 day	60 day	28 day
IL-1B								grey	grey									
IL-2								grey	grey									
IL-4								grey	grey									
IL-6	green																	
IL-10	dark green							grey	grey									
IL-16				light green				grey	grey									
TNFa	light green				grey	grey		grey	grey									
IFN-g					grey	grey		grey	grey									
GM-CSF			light green					grey	grey									
CCL1								grey	grey									
CCL2					green		dark green	grey	grey					red				
CCL3							green	grey	grey									
CCL4								grey	grey									
CCL5	light green							grey	grey					red			light red	
CCL7	light green			light green			light green	grey	grey									
CCL11	light green			green	light green													
CCL12								grey	grey									
CCL17								grey	grey									
CCL19								grey	grey									
CCL20								grey	grey									
CCL22							light green	grey	grey									
CCL24							light green	grey	grey									
CCL25					grey	grey		grey	grey									
CCL27					grey	grey		grey	grey									
CXCL1							green	grey	grey		light red							
CXCL2	light green	light green	light green				dark green	grey	grey									light green
CXCL5					light green		green	grey	grey									
CXCL10								light green	light green									
CXCL11								grey	grey									
CXCL12	light green				light green			grey	grey									
CXCL13	light green							grey	grey									
CXCL16								grey	grey									
CX3CL1								grey	grey									

5.5 Conclusion

Data in this chapter have demonstrated that treatment of muscles of adult WT mice with BaCl$_2$ resulted in a characteristic pattern of necrosis and regeneration, providing a robust model to study the process of muscle regeneration. Muscles of old WT mice displayed a relatively permanent force deficit following chemical damage compared with the complete recovery of muscles of adult WT mice, in a similar manner to contraction-induced damage. Data demonstrated that this deficit in muscles of old WT mice was not due to altered muscle fibre number or size. In contrast, muscles of adult SOD1KO mice recovered to their pre-damage (reduced) levels of maximal force generation by 28 days following damage. p65 translocation to the nucleus occurred readily in the regenerating muscle fibres of WT adult, WT old, and adult SOD1KO mice. There was no overwhelming increase in cytokines or chemokines in response to injury that were able to explain the substantial changes seen in plasma levels of cytokines and chemokines in these models. Interestingly, temporal differences in p65 translocation were evident in the different models during regeneration. It may be that such differences may represent different functions of NF-κB since it is known that temporal changes in p65 localisation can result in differential gene expression unrelated to cytokine production.

Chapter 6: Protein synthesis in muscle during ageing: A heavy water approach

6.1 Introduction

It is axiomatic that muscle atrophy is the consequence of changes in protein synthesis or breakdown but the nature and extent of these changes is controversial, in part arising from differing technical approaches and confounding effects of 'immobility/disuse' in both caged mice and sedentary older humans (Jackson et al. 2012).

6.1.1 Crosstalk between the NF-κB pathway and protein turnover in muscles

Activation of NF-κB pathway is involved in protein turnover within muscles. Activation in muscle is associated with an increase in the E3 ligases atrogin-1 and MuRF-1, the translation initiation faction eukaryotic translation factor 4E binding protein 1 (elF4EBP1), and the transcription factor foxhead box protein O1 (FOXO1) in myotubes (Fry et al. 2016; Wu et al. 2014). Reduction of p65 using small interfering RNA protects against muscle atrophy (Yamaki et al. 2012). Transgenic increase in constitutively active IKKβ in muscle resulted in a loss of muscle mass and fibre atrophy in muscles of mice via an upregulation of MuRF1, an E3 Ligase which mediates muscle atrophy via proteolysis (Cai et al. 2004) and muscle specific knockout of IKKβ in mice protected a number of muscles from a loss in muscle weight, tetanic force, reduction in fibre size, and promoted regeneration in denervated mouse muscles in response to denervation (Mourkioti et al. 2006). The specificity of responses to NF-κB activation are likely to reflect subtle differences in NF-κB dimers that regulate expression of specific genes (Bakkar et al. 2013) and recent evidence suggests that the control of differential gene expression is also dependent on the frequency of NF-κB movement between the cytoplasm and nucleus and this may be modulated through environmental factors such as oxidative stress, hypoxia and temperature. In skeletal muscle, NF-κB modulates expression of genes associated with myogenesis (Bakkar et al. 2013; Dahlman et al. 2009), catabolism (Bar-Shai et al. 2005; Peterson & Guttridge 2008; Gammeren et al. 2009), and cytoprotection (Vasilaki et al. 2006b). Thus,

control of such diverse transcriptional responses is undoubtedly under additional control and it is important to characterise such responses.

Thus, there is some evidence that changes in activation of NF-κB are consistent with changes in muscle protein turnover resulting in loss of muscle mass. Several studies have examined changes in protein synthesis and degradation in muscles of adult and old humans using stable isotope approaches.

6.1.2 Muscle protein synthesis

The loss of muscle mass with age accompanies a parallel loss of total muscle proteins. There has been a major focus on protein synthesis rates in muscles of aged populations to identify whether this is a major factor in the negative net protein balance experienced. Initial attempts at characterising protein synthesis rates gave hope to the notion reduction of synthesis may be at the heart of muscle loss with ageing. Several studies have shown that an increase in protein intake and exercise leads to an increase in hypertrophy over time (eg Biolo et al. 1997). The relevance of this to elderly populations and sarcopenia being that older humans tend to have insufficient protein intake (Ten Haaf et al. 2018) and live a more sedentary lifestyle (Harvey et al. 2013).

There is some controversy regarding the rates of basal muscle protein synthesis in older people, with some studies reporting reduced basal muscle protein synthetic rate in older people compared with younger subjects (Balagopal et al. 1997; Rooyackers et al. 1996b; Short et al. 2004; Welle et al. 1993; Yarasheski 2003; Yarasheski et al. 1993) and others suggesting no difference in healthy old compared with younger people (Cuthbertson et al. 2005; Volpi et al. 1998; Volpi et al. 2001). Measurement of fractional synthesis rates (FSRs) of protein by infusion of an isotopic tracer (e.g. ^{13}C leucine) and subsequent analysis via gas chromatography is a common method of measuring total protein synthesis rates. A decrease in the FSR of mitochondrial proteins and mixed proteins was reported in muscle biopsies

from older people (Rooyackers et al. 1996a). Subsequent studies showed a lower fractional synthesis r of myosin heavy chain in muscle of old humans which correlated with an increase in insulin – like growth factor I (IGF-1) and a decline in muscle strength (Balagopal et al. 2017; Short et al. 2004; Katsanos et al. 2006). In contrast with this, muscle biopsies taken from adult and old humans have been shown to not be significantly different in terms of FSR (Volpi et al. 2001). There were, however, several problems with the Volpi et al study including taking biopsies from the same area of muscle repeatedly, diet and exercise were not controlled, and the arterial – ventricular balance experiment was problematic as it didn't account for the change in muscle with age (Yarasheski et al. 2002). Further to this, there is increasing evidence that basal muscle protein synthesis (MPS) may not be altered in muscle during ageing (Cuthbertson et al. 2005; Kumar et al. 2009; Yarasheski et al. 2017).

More recently, focus has shifted away from basal rates of MPS and towards adaptive responses to stress such as exercise and/or diet as a means by which muscle mass and function are not maintained. Ingestion of essential amino acids has been shown to stimulate MPS, but this occurs to a lesser extent in muscle of old humans (Cuthbertson et al. 2005; Volpi et al. 1999). Post-prandial synthesis rates have been observed to be 16 % lower in muscle of older than in that of younger humans and MPS can be more than three times more responsive to protein digestion in younger compared with older groups (Wall et al. 2015). Increasing dietary leucine can reverse the reduction in protein synthesis rate in the elderly population but not in adults (Katsanos et al. 2006).

Resistance exercise has been shown to increase both MyHC and mixed muscle protein synthesis rates with no change in actin synthesis (Short et al. 2004; Volpi et al. 2000; Yarasheski et al. 2017). This blunted response could be due to a loss of signalling and protein synthesis through p70 ribosomal S6 kinase (p70s6K) and initiation factor 4E binding protein 1 (4EBP1) leaving synthesis rates 'decoupled' from protein synthesis (Kumar et al. 2009). This

can be exacerbated by elderly humans being prone to living a more sedentary lifestyle. Protein mass can be reduced following 14 days of reduced physical activity. This also leads to increased systemic inflammatory markers, increased insulin signalling and a blunted response of postprandial MPS (Breen et al. 2013).

In summary, there are some concerns with the above studies that need to be addressed. 1) the studies examine global protein synthesis, pooling in slowly turned over proteins with those that are turned over quickly and differences in single proteins may be overshadowed by the change in very few muscle proteins. 2) Exercise and food intake were different in all the studies and may have had an impact 3) regarding the MHC protein FSRs, the approach is flawed since varying MHC isoforms were not identified and compared, which may account for the difference in ageing as the ratios of isoforms change with age.

6.1.3 Muscle protein breakdown

A negative net protein balance can also be initiated through an increase in muscle protein breakdown (MPB) although protein degradation has been less extensively studied.

Gene expression profiling has resulted in the identification of the ubiquitin ligases 'atrogenes' which are involved in muscle atrophy (Bodine et al. 2001; Gomes et al. 2001; Sacheck et al. 2007). The genes induced most strongly encode two muscle-specific ubiquitin ligases, atrogin-1 and MuRF1 (Bodine et al. 2001; Gomes et al. 2001). In catabolic states, the expression of atrogin-1 and MuRF1 accelerate protein turnover in muscle via the ubiquitin proteasome system (Bonaldo & Sandri 2013; Demontis et al. 2013).

During ageing, the muscle proteasome demonstrates some changes in function. An increase in total catalytic subunit protein content has been described as well as a larger amount of the inducible, immune-proteasome catalytic subunits: low molecular mass peptide 2 (LMP2), Multicatalytic Endopeptidase Complex Subunit (MECL), and LMP7 which replace beta 1, 2 and 5 respectively (Ferrington et al. 2005). This alteration can be induced by the presence of

TNFα and is mainly used by antigen presenting cells to process antigens efficiently (Hallermalm et al. 2001; Murata et al. 2018). Calorie restriction rescues this increase in subunit expression (Altun et al. 2010).

With an increase in protein oxidation, as is seen in muscles during ageing, substrate proteins are not as readily degraded by the proteasome. This is unless the subunits in the proteasome itself are oxidised (Ferrington et al. 2005). When oxidised, the lid and base structures of the proteasome dissociate and allow the breakdown of oxidised proteins rather than ubiquitinated proteins (Grune et al. 2011; Hugo et al. 2018).

An increase in ubiquitination of substrate proteins is one of the factors which could be driving an increase in proteolysis. Free ubiquitin and ubiquitinated proteins and deubiquitinating enzymes (DUBs) are reported to be higher in muscle during ageing (Altun et al. 2010). Atrogin-1 and MuRF1 are induced in a number of models of muscle atrophy, including surgical denervation of muscle (Sacheck et al. 2007) which may be representative of muscle during ageing and have been shown to be elevated in muscles of old mice (Schiaffino et al. 2013).

An increase in MPB has been observed in muscle with ageing using other approaches, for example through the measurement of 3-methylhistidine, a metabolite of actin/myosin breakdown in muscles using microdialysis probes (Trappe et al. 2004).

MPB has been analysed following resistance exercise in adults but studies concluded that no change can be observed over the 24 hours following the exercise. Here, regulators of protein breakdown, E3 ligases and autophagy markers were measured with muscle protein breakdown rates calculated using an infused isotopic tracer. However, this study was proposed to be limited as there was an assumption that there was no tracer recycling (Fry et al. 2013).

6.1.4 Analysis of protein turnover using heavy water proteomics

Determination of protein abundance can only ever be a snapshot of the current situation in a dynamic process. However, the proteome is dynamically active where proteins are constantly synthesised and metabolised.

Metabolic labelling of proteins is a method which, when combined with unlabelled proteomics, can be used to determine protein dynamics, potentially of the full proteome (Claydon et al. 2012). Metabolic labelling can be achieved *in-vivo*, through dosing the animal with the use of stable isotope labelling in mammals (SILAM). Amino acids, their precursors, or a mixture of amino acids can be labelled with a stable isotope and given to the animal through injection, diet, or drinking water for a range of time periods which, when measured by Mass Spectrometry, give two separate spectra of which a ratio can be calculated. Most commonly, these are amino acids with substitutions of carbon-13 or hydrogen-2 (Beynon & Pratt 2005).

The use of deuterated (heavy; ^2H_2O) water has a number of advantages to the use of labelled amino acids. ^2H_2O is safe to supplement in humans and animals for longer periods of time (years). ^2H_2O is quick to equilibrate through the body via osmosis and so constant enrichment levels are very easily maintained. ^2H_2O is also much cheaper than other methods of metabolic labelling (Kim et al. 2012a; Busch et al. 2006).

6.1.5 Hypothesis and aims

The hypothesis for this chapter was that there are alterations in the fractional synthesis rates of individual proteins in muscles of old WT mice when compared with those of adult mice that are lost when looking at large protein pools. Further, that changes in protein synthesis/degradation related to NF-κB activation can be identified by examination of the major pathways altered in muscles of old compared with adult mice. To explore this hypothesis, the aims of this chapter were to:

1. Functionally annotate the proteins in an unlabelled protein dataset to identify the major pathways which are altered in the muscles of old WT mice.

2. Describe the fractional synthesis rates of proteins from the muscles of adult and old WT mice.

3. Compare the fractional synthesis to the relative levels of unlabelled proteins and expression of the mRNA from an RNAseq dataset from quiescent muscles of adult and old mice.

6.2 Methods

6.2.1 Dosing and dissections

For the unlabelled proteomics, 4 adult mice and 5 old WT mice were used. For the heavy water experiments, 14 adult and 14 old WT mice were dosed for different time periods and culled over 3 days (**Section 2.2.2**). For the RNAseq experiments, 5 adult and 5 old WT mice were used.

Adult and old WT mice were given drinking water with heavy water to an enrichment of 4.5% in plasma as described in **Section 2.2.2** for between 1 and 60 days. Mice were weighed intermittently. Mice were culled via overdose of pentobarbital (IV) and blood was collected. The bloods were centrifuged at 10,000g for 10 minutes at 4 $^\text{O}$C and the plasma was collected into clean microcentrifuge tubes. The muscles were dissected, weighed and placed into liquid nitrogen and stored at -80$^\text{o}$C until use.

6.2.2 Sample preparation of GTN muscles

Sample preparation was performed by the centre for proteome research (CPI). GTN muscles (unlabelled and ^{2}H$_2$O dosed) were homogenised in 10-volumes of 25 mM ammonium bicarbonate containing a protease inhibitor cocktail. The sample was homogenised via a TissueRuptor (Qiagen, Hilden, Germany) set to the lowest setting. Further homogenisation

was achieved using a bead beating homogeniser. 37.5U benzonase nuclease was added to each sample to reduce viscosity.

50μg protein was diluted to be 80 μL in volume with 25 mM ammonium bicarbonate. 5μL of 1% Rapigest SF was added, and the samples were brought to 80°C for 10 minutes. 5 μL 46.6 mg/mL iodoacetaide in 25 mM ammonium bicarbonate was added in the dark at room temperature for 30 minutes for alkylation to take place. This reaction was quenched using 4.7 μL DTT. 5μL trypsin was added to samples and samples were incubated overnight at 37°C. Rapigest was removed through acidification with 1 μL TFA and incubation at 37°C for 45 minutes. Samples were centrifuged at 17,200 g and supernatants were transferred to fresh tubes.

6.2.3 LC-MSMS analysis of labelled proteins

LC-MSMS was performed by the centre for proteome research (CPI). Data-dependent LC-MSMS analyses were conducted on a QExactiveHF quadrupole-Orbitrap mass spectrometer coupled to a Dionex Ultimate 3000 RSLC nano-liquid chromatograph (Hemel Hempstead, UK). Sample digest (0.4mL, 200ng protein equivalent) was loaded onto a trapping column (Acclaim PepMap 100 C18, 75 μm x 2 cm, 3 μm packing material, 100 Å) using a loading buffer of 0.1% (v/v) TFA, 2 % (v/v) acetonitrile in water for 7 min at a flow rate of 12 μL min-1. The trapping column was then set in-line with an analytical column (EASY-Spray PepMap RSLC C18, 75 μm x 50 cm, 2 μm packing material, 100 Å) and the peptides eluted using a linear gradient of 96.2 % A (0.1 % [v/v] formic acid):3.8 % B (0.1 % [v/v[formic acid in water:acetonitrile [80:20] [v/v]) to 50 % A:50 % B over 55 min at a flow rate of 300 nL min-1, followed by washing at 1% A:99 % B for 6 min and re-equilibration of the column to starting conditions. The column was maintained at 40°C, and the effluent introduced directly into the integrated nano-electrospray ionisation source operating in positive ion mode. The mass spectrometer was operated in data dependent acquisition mode with survey scans between

m/z 350-2000 acquired at a mass resolution of 60,000 (full width at half maximum) at m/z 200. The maximum injection time was 100 ms, and the automatic gain control was set to 3e6. The 16 most intense precursor ions with charges states of between 2+ and 5+ were selected for MS/MS at a resolution of 30,000 with an isolation window of 2 m/z units. The maximum injection time was 45 ms, and the automatic gain control was set to 1e5. Fragmentation of the peptides was by higher-energy collisional dissociation using a normalised collision energy of 30 %. Dynamic exclusion of mass top charge ratio (m/z) values to prevent repeated fragmentation of the same peptide was used with an exclusion time of 20 sec.

6.2.4 Quantification of protein abundance

Quantification for protein abundance was performed by the centre for proteome research (CPI). For the protein abundance analysis from the unlabelled samples, individual data files were searched against the UniProt mouse reviewed database (16,966 sequences) using the Mascot search engine (Version 2.6.2). Between 900-1050 proteins were identified in each sample. A precursor and fragment ion mass tolerance of 10ppm and 0.01Da was used respectively. A fixed modification of carbamidomethyl cysteine and a variable modification of oxidation of methionine was included. Label free quantification was performed automatically on Progenesis QI.

6.2.5 Determination of Relative Isotope Abundance (RIA) and protein turnover rates (k)

Determination of RIA and turnover rates was performed by Dr. Dean Hamond. The software d2ome (Sadygov et al. 2018) was used to automate *in vivo* protein turnover analysis from the acquired Liquid chromatography-mass spec (LC-MS) data of heavy water metabolic labelling. Each Thermo raw MS data file, from each animal muscle tissue sample over the labelling trajectory, was initially converted into mzML format, using the MSConvert tool

within Proteowizard (Chambers et al. 2012). mzML files were then searched using Mascot (version 2.7.0, Matrix Science, UK) against a UniProt Mus genus database (dated April 25, 2018) containing 16,966 reviewed entries. The search parameters allowed for a single trypsin missed cleavage and carbamidomethylation of cysteine residues as a fixed modification. Oxidation of methionine was allowed as variable modification. A peptide tolerance of 15 ppm was set, with an MS/MS tolerance of 0.01 Da. Following database searching, each search result was exported in mzIdentML format for use in d2ome which uses the mass spectral data (mzML files) and the corresponding protein identification results (mzIdentML files) and analyses all proteins/peptides that pass pre-defined identification thresholds (here, mass accuracy = 15 ppm; minimum protein score = 40; minimum peptide score = 20; maximum peptide expectation = 0.05; elution time window = 1 min; minimum number of experiments for protein consistency = 4; minimum number of experiments for a peptide consistency = 4). Mass isotopomer quantification was done in three-dimensional space (chromatographic time, m/z, and abundance). Increases in heavy peptide mass isotopomers (m1, m2, m3, m4, etc.) due to 2H-incorporation were reflected by a parallel decline in the monoisotopic mass spectral peak (m0) envelope, with time. Protein turnover rate constants (k) were determined based on the RIA data at each time point, t, using the default fitting process in d2ome (Sadygov et al. 2018), with the maximum achievable RIA set as a fixed value, the body water enrichment level, measured from plasma acetone exchange to be 4.64% (adult) and 4.71% (old).

6.2.6 RNA sequencing of muscles from adult and old WT mice

RNA isolation, library preparation, data processing and initial bioinformatics analysis were performed, and data generously provided by Dr Caroline Staunton with methods described below.

6.2.6.1 RNA extraction from GTA muscles of adult and old mice

RNA extraction was performed by Dr Caroline Staunton. All RNA extraction was performed using the RNeasy Fibrous Tissues kit (Qiagen, UK) as per manufacturer's instruction. Approx. 30mg of tissue was lysed and homogenised using an ultra turrax (IKA Homogeniser, Sigma, UK) in buffer RLT before proteinase K digestion steps, total RNA bound followed by several washing steps and DNase digestion and total RNA eluted. Total RNA integrity was confirmed using the Bioanalyzer (Agilent Technologies, USA) and RIN values for all samples obtained with only those with a RIN ≥7 used. Ribosomal RNA (rRNA) was depleted from RNA samples by using the Ribo-Zero™ rRNA Removal Kit (Epicentre, USA) in accordance with the instructions of the manufacturer.

6.2.6.2 Bioinformatic Analysis and read alignment

Bioinformatics was performed by Dr Caroline Staunton. Base-scaling and de-multiplexing of indexed reads was performed by CASAVA version 1.8.2 (Illumina) to produce 20 samples in FASTQformat. The raw FASTQfiles were trimmed to remove Illumina adapter sequences using Cutadapt version 1.2.1 (Martin, 2011). The option "-O 3" was set, so the 3' end of any reads which matched the adapter sequence over at least 3bp was trimmed off. The reads were further trimmed to remove low quality bases, using Sickle version 1.200 with a minimum window quality score of 20. After trimming, reads shorter than 20bp were removed. Reads were then aligned to the genome sequences using Tophat version 2.1.0 and transcript assembly conducted using HTSeq2.

6.2.6.3 Differential gene expression analysis

Differential gene expression analysis was performed by Dr Caroline Staunton. Raw sequence counts were subsequently used as the input into using R (version 1.2.5042) to utilise the DESeq2 package for identifying differentially expressed genes. Data was assessed using

pairwise comparisons, correlation heatmaps and PCA plots generated from normalised count data and outliers removed accordingly using R.

Fold changes and the threshold of false discovery rate (FDR) adjusted p values < 0.05, generated using the Benjamini and Hochberg approach and in some cases a 1.4 log2 fold change (Log2FC) from the DEG were used to perform functional analysis, specifically enrichment analysis with Gene Ontology (GO) Biological Process using the Panther Classification System, Kyoto Encyclopedia of Genes and Genomes (KEGG) pathway enrichment analysis using the 'enrichKEGG' command from clusterProfiler v. 3.8.1 from Bioconductor v. 3.7 with mouse as the reference organism. The GO terms and KEGG pathways with FDR < 0.05 were considered to be significantly enriched.

6.2.7 Data analysis

ll graphs were produced using "ggplot2" unless otherwise stated. The R packages "factorMineR" and "factoextra" were implemented for principle component analysis (PCA) and the "heatmap.2()" function from "gplots" was used (Lê et al. 2008). Kyoto encyclopaedia of genes and genomes (KEGG) and gene ontology (GO) pathways were annotated and visualised using the "enrichKEGG()" and "enrichGO()" functions from the "clusterProfiler" package (Yu et al. 2012). Protein lengths and masses were annotated to each protein using the "UniprotR" package. Protein datasets and RNAseq datasets were merged through annotating the RNAseq dataset with uniprot IDs according to their ensembl gene IDs and merging the datasets.

6.3 Results

6.3.1 There was a significant loss of muscle mass with age

There was a significant loss of muscle mass in the GTN, quadriceps (Quad) and soleus (SOL) muscles of old mice when compared with the muscles of adult mice (**Figure 6.1A**). There was also little body weight change over the time following injection showing that there was likely no adverse effect of the heavy water dosing regimen.
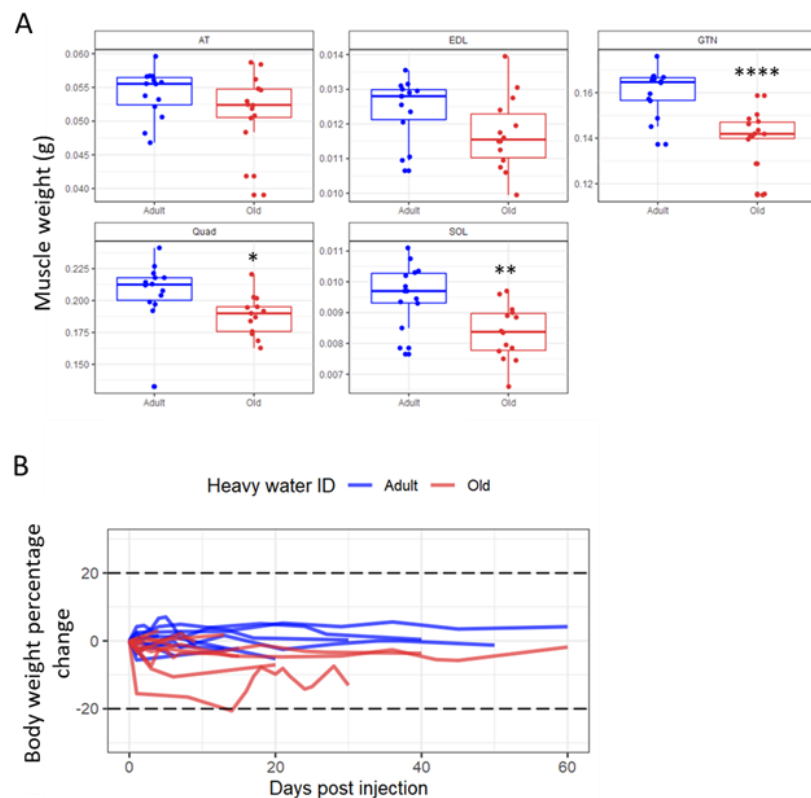
Figure 6.1: A) Weights of muscles from adult and old mice. B) Body weight percentage change over the heavy water dosing time-period. *Mice were culled at different times following the start of the experiment and so individual plots terminate at different times. Graphs were produced using the Ggplot2 package in R.*

6.3.2 There were major changes in the abundance of muscle proteins with ageing

With respect to protein abundance, a total of 1495 proteins were identified, 1124 proteins showed no significant difference between the GTN muscles from adult and old WT mice. Sixty-three proteins were of significantly higher abundance in the GTN muscles of adult WT mice and 208 were significantly higher in the muscles of old WT mice (**Figure 6.2A**). 16

proteins had a $-\text{Log}_{10}$(q value) over 1 and log_2(fold change) over 1.5. 2 proteins had a $-\text{Log}_{10}$(q value) over 1 and log_2(fold change) under -1.5. Hierarchical clustering of abundance of all detected proteins showed that the samples could be grouped by age (**Figure 6.2B-C**).
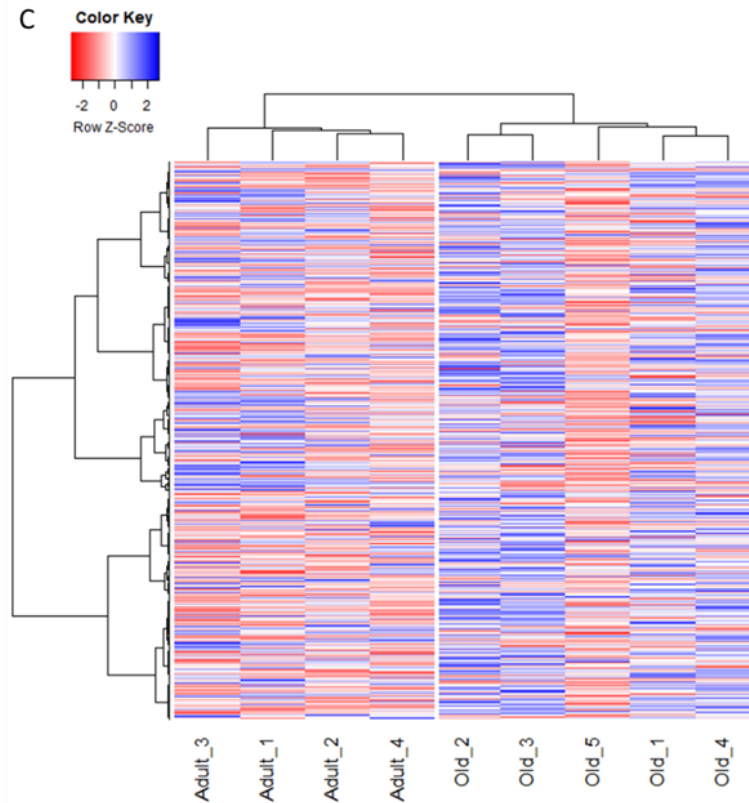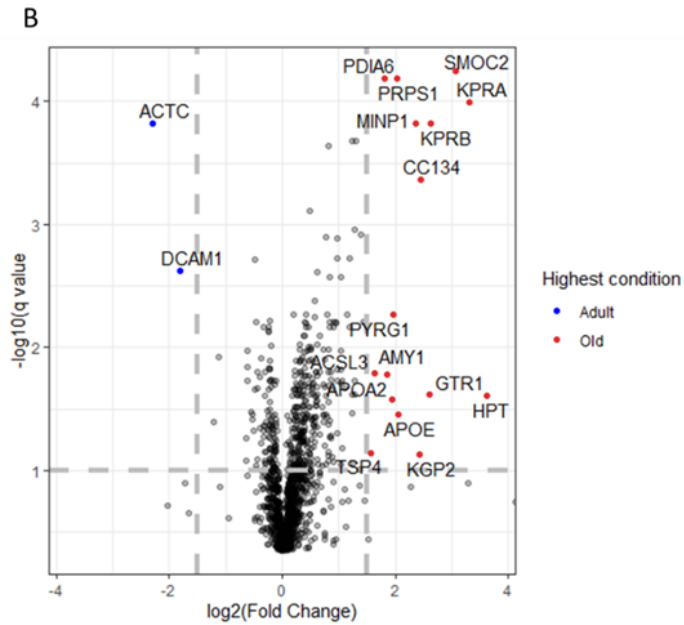
Figure 6.2: Visualisation of unlabelled protein abundance in the muscles of adult WT and old WT mice using a heatmap and volcano plot. A) The number of proteins detected to be significantly higher in each condition. B) Volcano plot of proteins detected with a log fold change cut off of ± 1.5 and a −log$_{10}$(q value) above 1. C) Heatmap of protein abundance in each sample z transformed by protein. Dendrograms show Euclidian distance.

The PCA revealed the groups to be separated in principle component (PC) 1 which accounted for 30.9% of the variability between the samples (**Figure 6.3A**). The top 20 contributors of PC1 included binding immunoglobulin protein (BIP), vinculin (VINC) and protein disulfide-isomorase (PDI)-A6 (**Figure 6.3C**). The samples from adult and old mice were able to be separated by k means clustering in the 1st and 2nd principal components showing the proteome of the adults and olds were observably distinct from each other (**Figure 6.3 A-B**).

6.3.2.1 Protein degradation via the unfolded protein response (UPR) and endoplasmic reticulum associated degradation (ERAD) pathways is associated with ageing

GO term enrichment highlighted alterations in proteins involved in a number of pathways. Those involved in actin binding were in the top term identified which was expected due to muscles high content of actin and cytoskeletal proteins. GO terms related to NF-κB activation and protein turnover included ubiquitin protein ligase binding of the ERAD system, and the unfolded protein response (UPR) (**Figure 6.4**) and these are presented in further detail. Related to the GO term for ubiquitin protein ligase, 4 proteins were significantly higher in abundance in the GTN muscles of old WT mice and 11 were significantly lower (**Figure 6.5**). Of these proteins, BIP and VINC were also high contributors to PC1 (**Figure 6.3C**). Ten proteins more abundant in the GTN muscles of old WT mice were related to the UPR (**Figure 6.6**). Endoplasmin (ENPL) was also a contributor to PC1 and BIP was also shared with this GO term (**Figure 6.3C, Figure 6.4, Figure 6.5**).
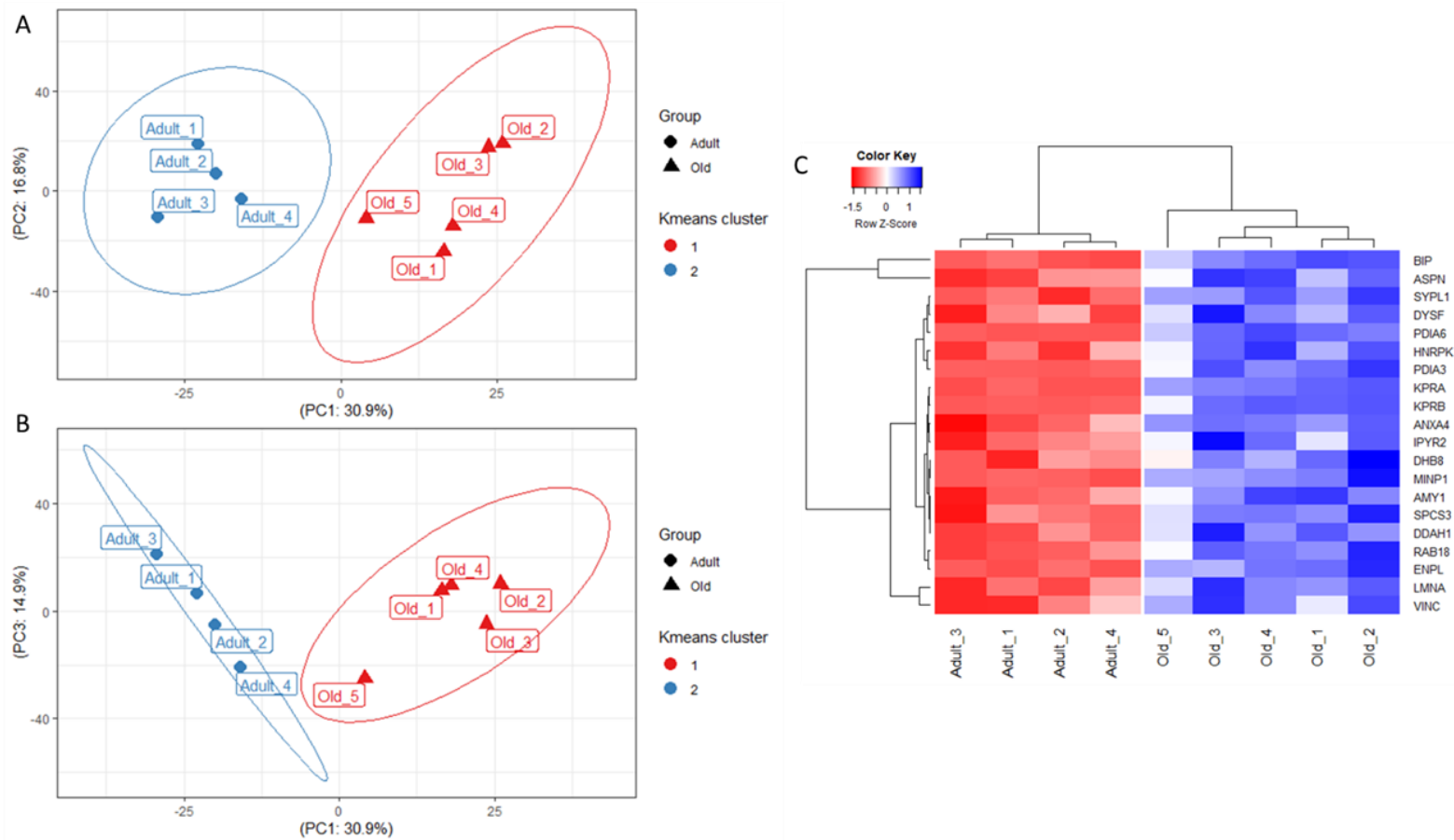
Figure 6.3: Principal component analysis of muscle proteomes of adult WT and old WT mice and clustering in principle components as well as by Euclidean distance. *PCA plots of A) PC1 vs PC3 and B) PC1 vs PC3. C) A heatmap showing the top 20 contributors to PC1 Z-transformed by protein. Dendrogram represent Euclidean distance. The two groups cluster by k-means in principle components 1, 2, and 3 and the top 20 contributors to PC1 cluster by Euclidean distance by age of animal.*
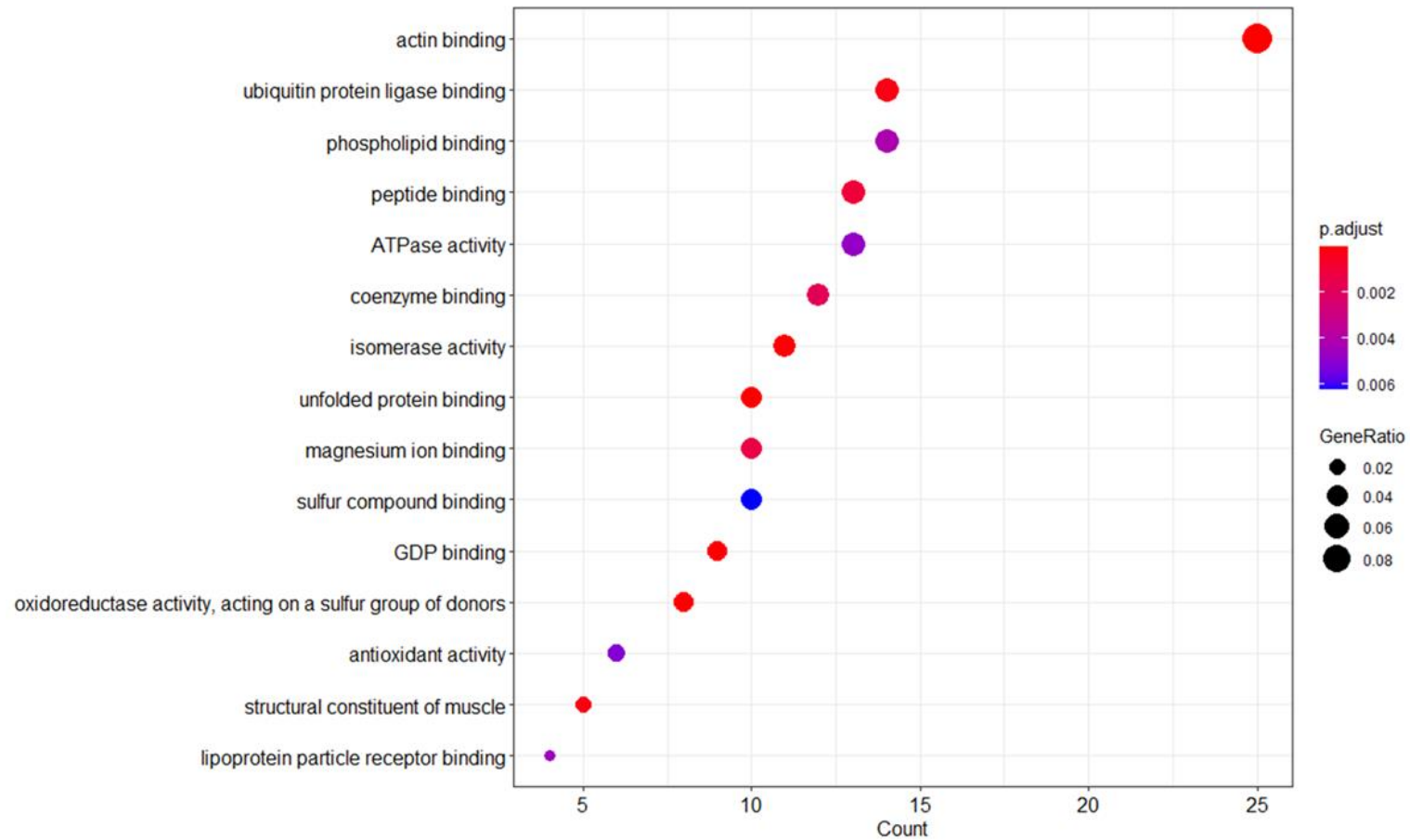
Figure 6.4: Top 15 enriched GO terms from the significantly different protein content in the muscles of old WT mice when compared those of adult WT mice. *Each GO term is plotted by count. Gene ratio is shown in the size of the point and adjusted p value is represented by the colour. GO enrichment was performed using the clusterProfiler package in R. Data was simplified using the "measure = Wang" with "cutoff = 0.6" to remove duplicate/similar GO terms*
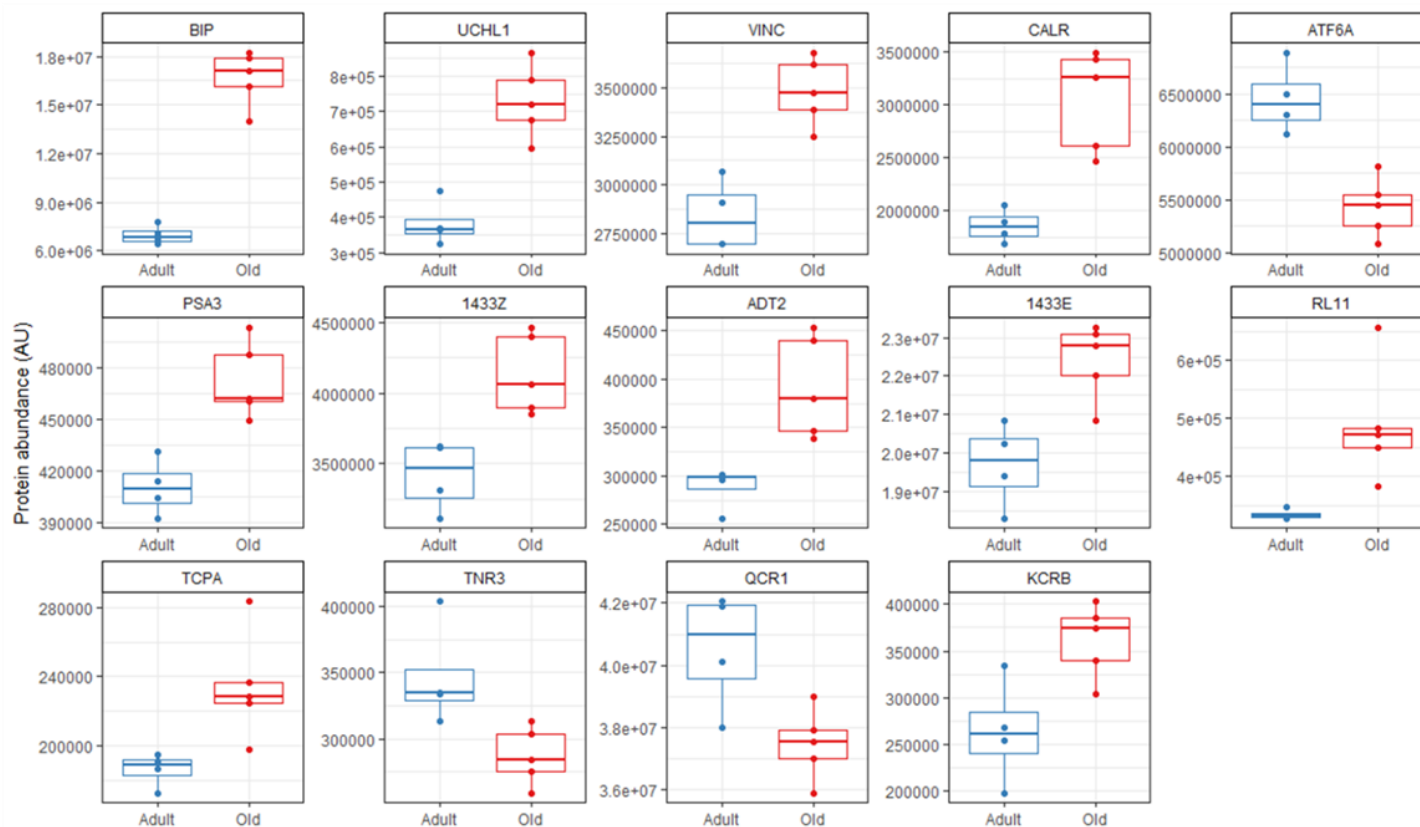
Figure 6.5: Abundance of proteins in the muscles of the muscles of old WT mice when compared with the muscles of adult WT mice which are associated with the GO term "ubiquitin protein ligase binding". Protein abundance is displayed in arbitrary units (AU). All proteins displayed are q<0.05. 11 of the proteins displayed here are of a significantly higher abundance in the muscles of old WT mice when compared with the abundance in adult WT mice whereas 3 of the proteins are significantly lower in abundance.
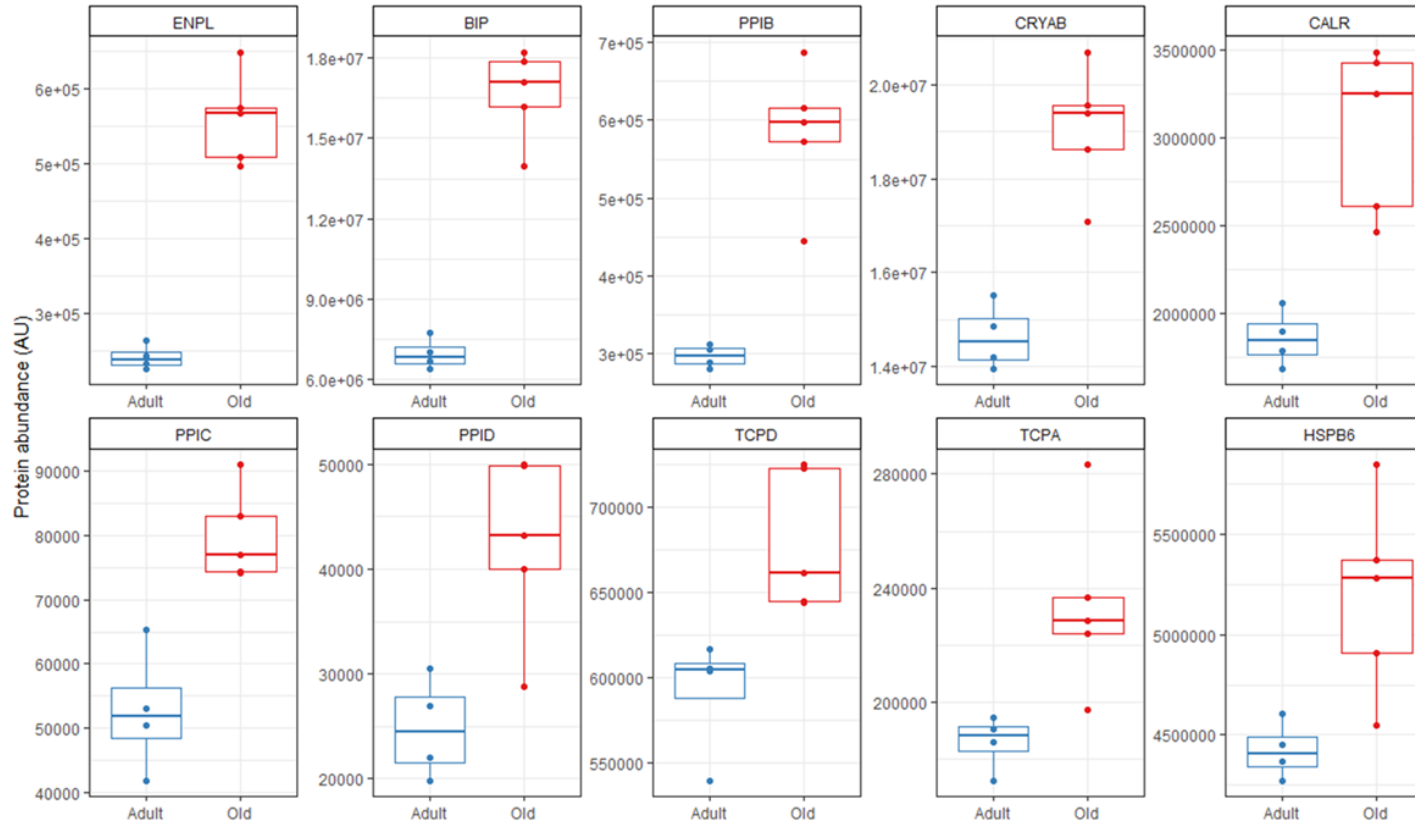
Figure 6.6: Abundance of proteins in the muscles of the muscles of old WT mice when compared with the muscles of adult WT mice from the enriched GO term "unfolded protein response". *Protein abundance is given as arbitrary units (AU). All proteins displayed are q<0.05. The proteins relating to this GO pathway are all significantly more abundant in the muscles of old WT mice when compared with that of adult WT mice which indicates a significant amount of alteration to this particular pathway.*

The top 4 enriched KEGG pathways from the unlabelled proteomics analysis were "protein misfolding diseases: amyotrophic lateral sclerosis, Alzheimer disease, Parkinson disease and prion disease (**Figure 6.8-6.9**), all associated with protein misfolding/altered degradation. The 6th most enriched KEGG pathway was protein processing in the endoplasmic reticulum of which 11 proteins were more abundant and one protein less abundant in the GTN muscles of old mice. ENPL, BIP and protein disulphide isomerase A3 also appear in PC1 and PDIA6 appeared in the volcano plot from the protein abundance (**Figures 6.2B and 6.3C**).

Nine proteins related to the KEGG pathway for leukocyte trans-endothelial migration were more abundant in muscles of old mice, whereas one protein was reduced in the muscles of old mice (**Figure 6.10-6.11**). One of these proteins, VINC was also a major PC1 contributor (**Figure 6.3C**).
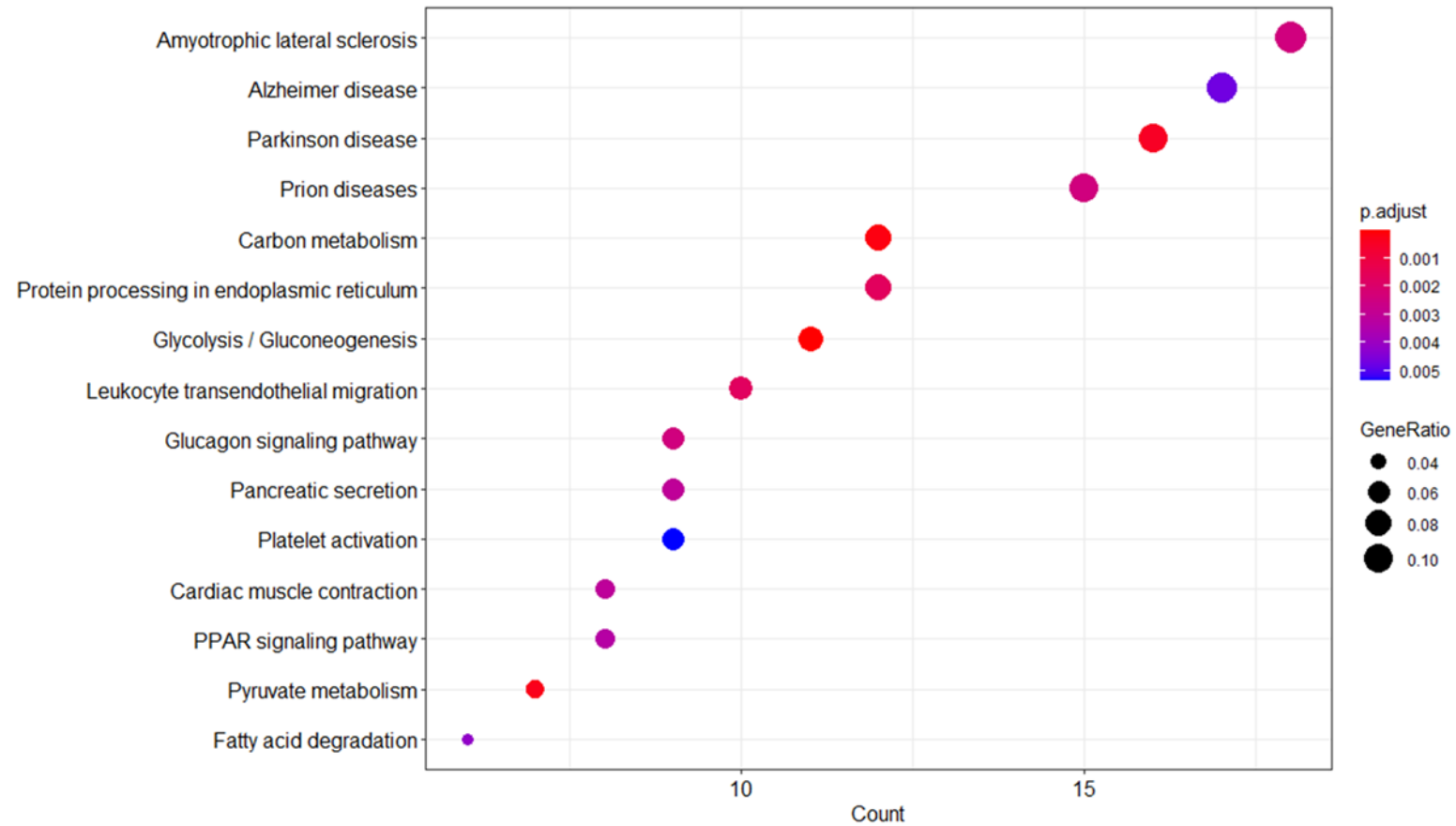
Figure 6.7: Top 15 enriched KEGG pathways terms from the significantly different protein content in the muscles of old WT mice when compared those of adult WT mice. *Each KEGG pathway is plotted by count. Gene ratio is shown in the size of the point and adjusted p value is represented by the colour. KEGG enrichment was performed using the clusterProfiler package in R*
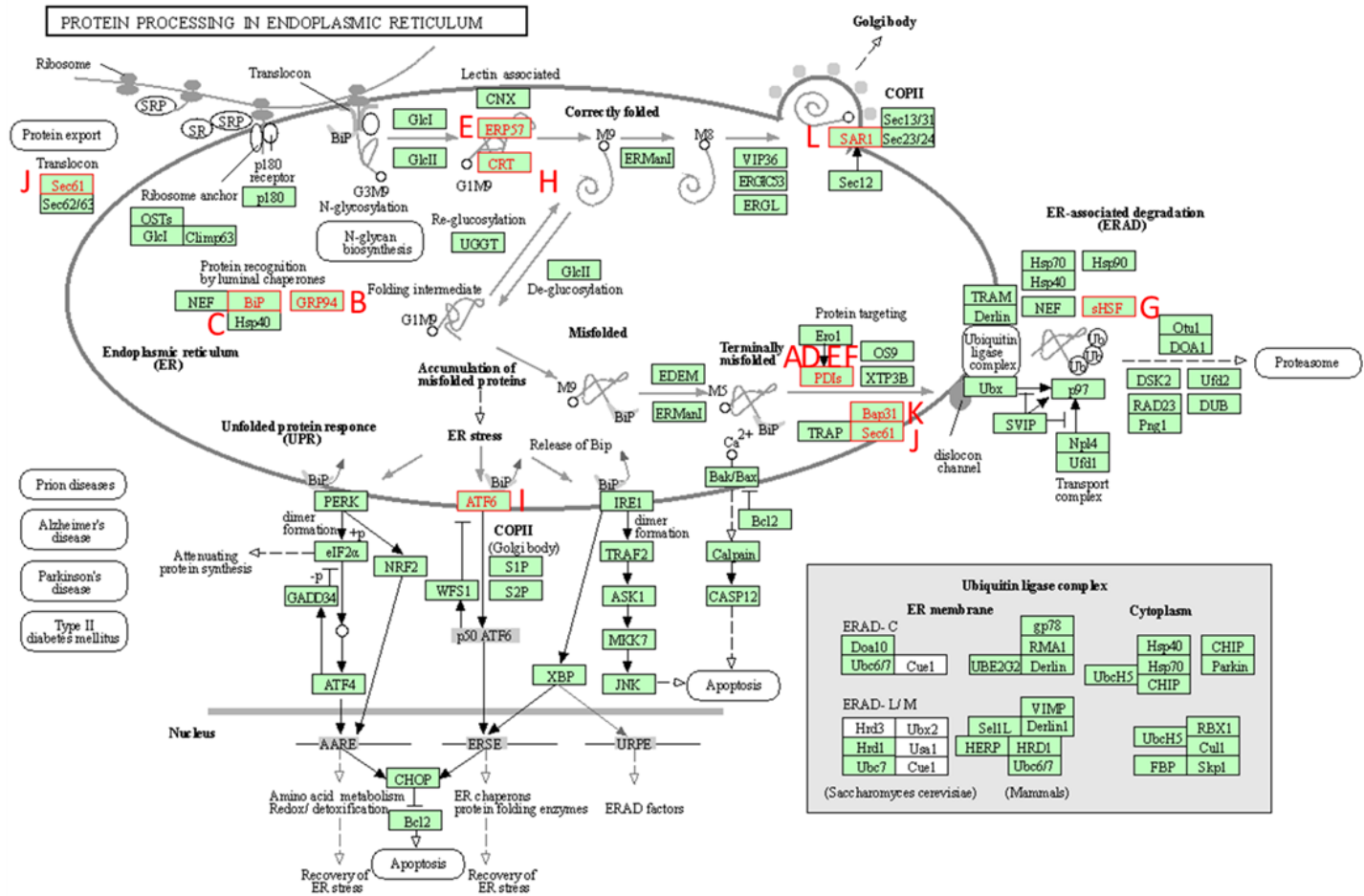
Figure 6.8: Proteins involved in the "protein processing in the endoplasmic reticulum" KEGG pathway. *Proteins with a red outline are those which are significantly different in the muscles of old mice when compared with the muscles of adult mice (Continued in **Figure 6.9**). Taken from Kanehisa & Goto 2000.*
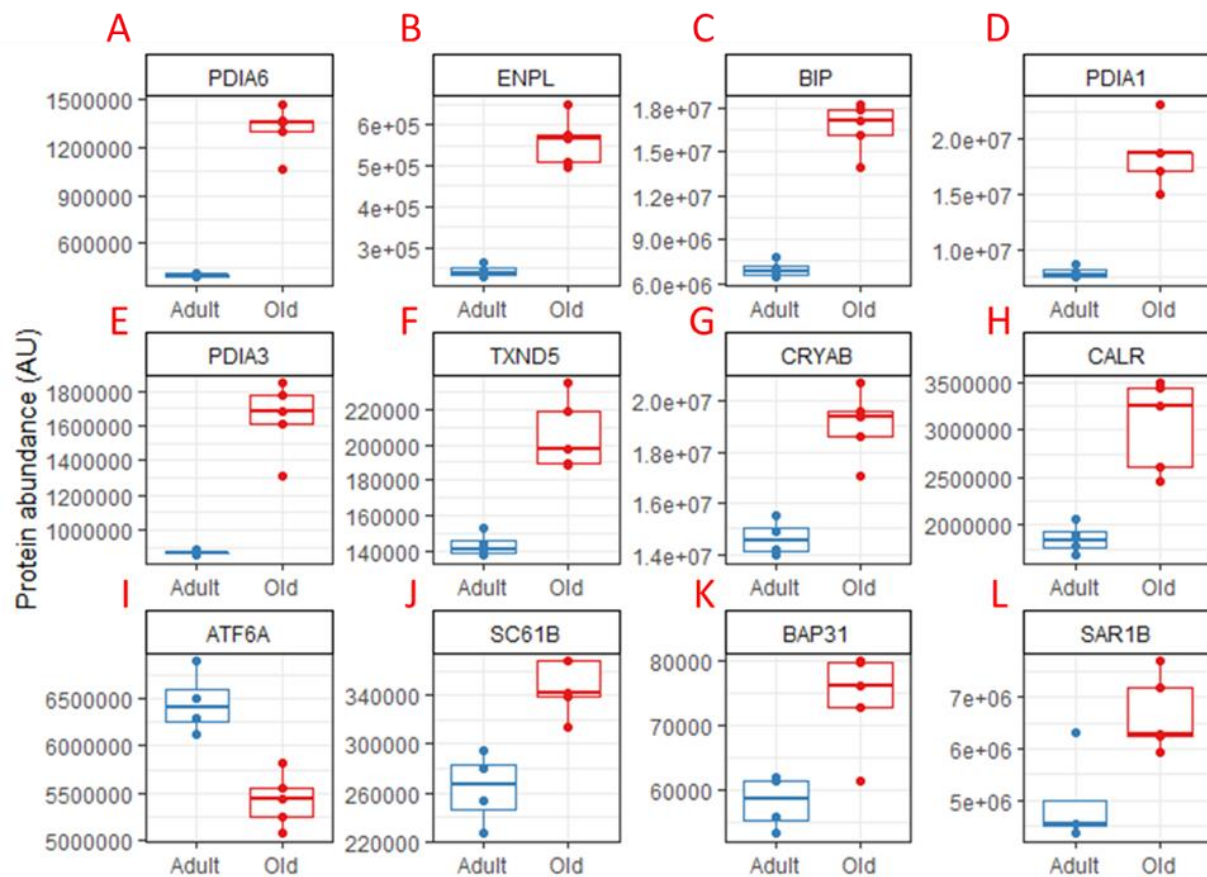
Figure 6.9: Abundance of proteins involved in the "protein processing in the endoplasmic reticulum" KEGG pathway in the muscles of old WT and adult WT mice. All proteins displayed are q<0.05. Protein abundance displayed in arbitrary units (AU). Data here demonstrates the increased abundance of proteins involved in the endoplasmic reticular degradation (ERAD) pathway in muscles of old WT mice when compared with those of adult WT mice
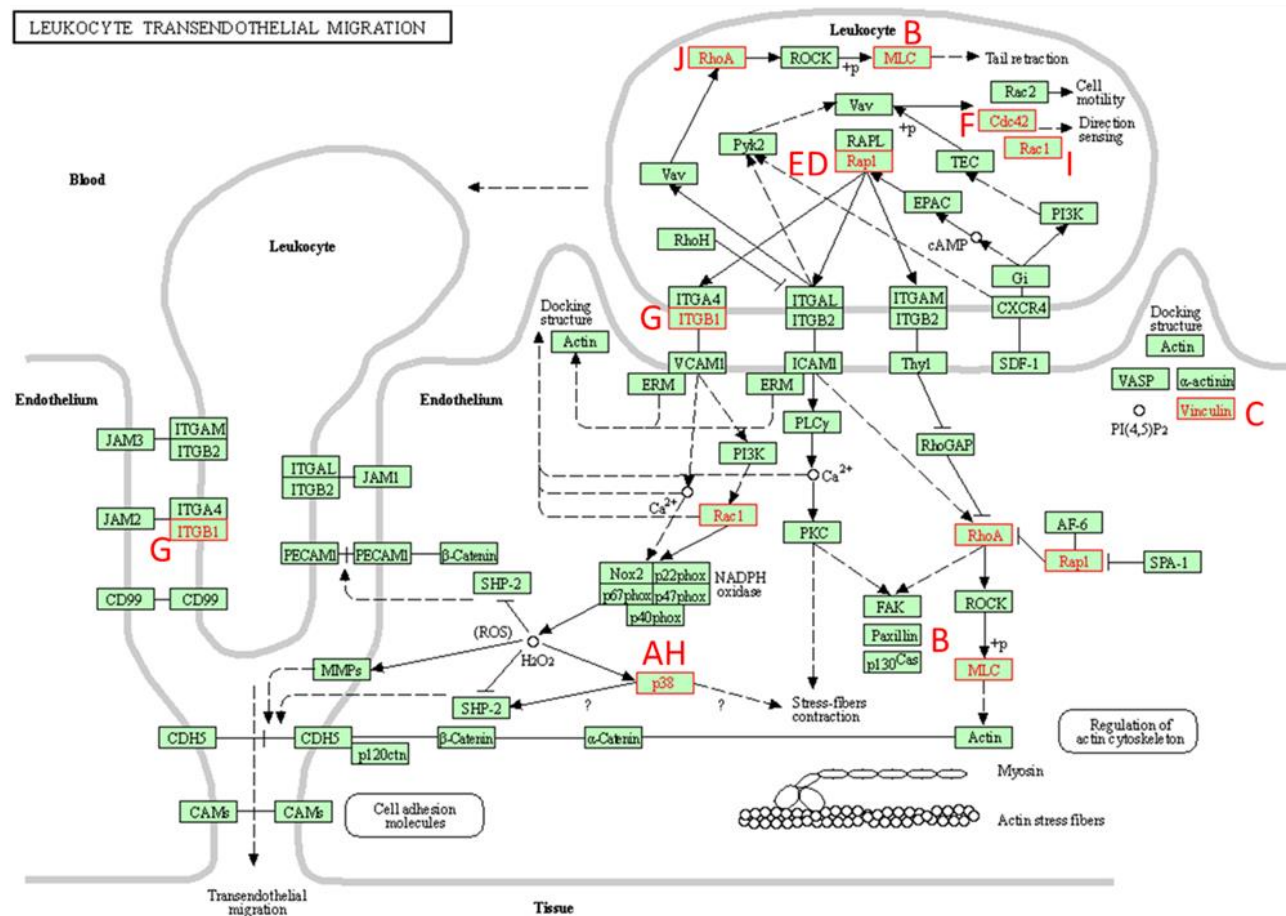
Figure 6.10: Proteins involved in the "Leukocyte transendothelial migration" KEGG pathway. *Proteins with a red outline are those which are significantly different in the muscles of old mice when compared with the muscles of adult mice (Continued in **Figure 6.11**).Taken from Kanehisa & Goto 2000.*
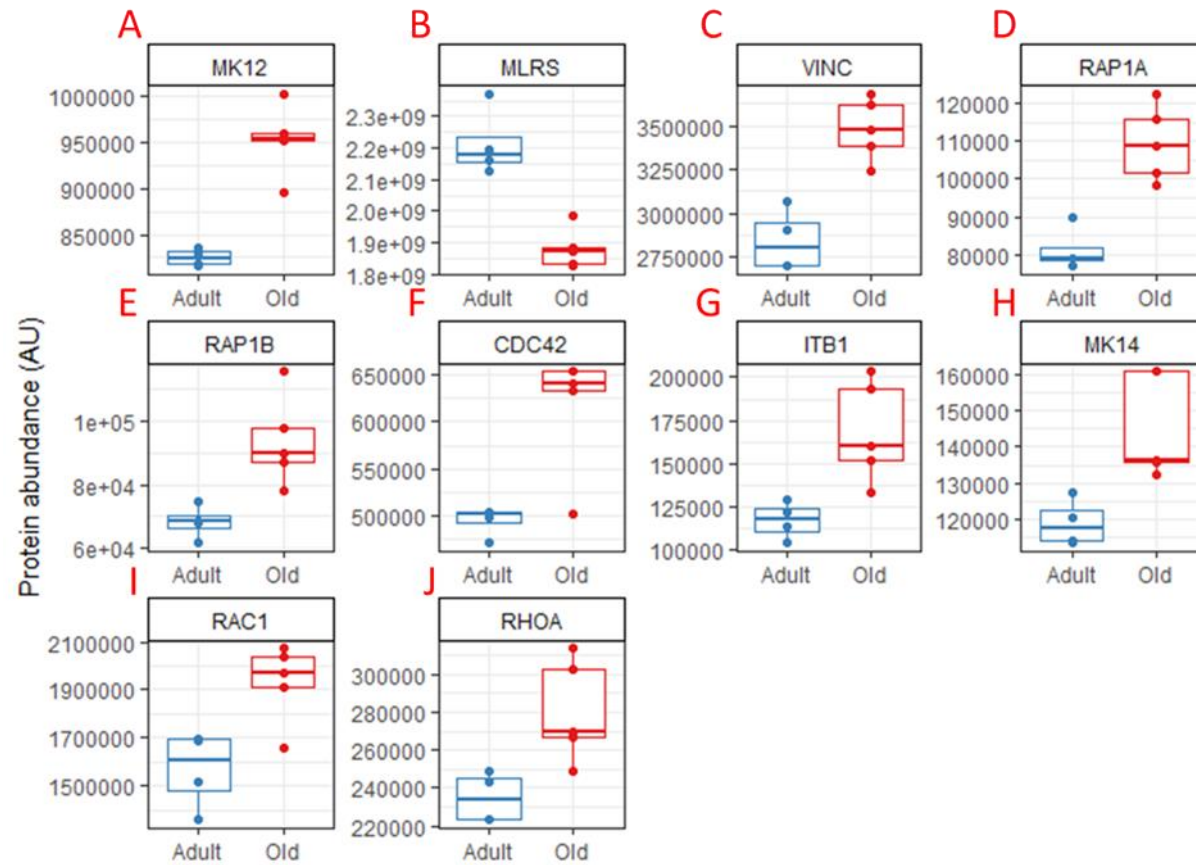
Figure 6.11: Abundance of proteins involved in the "Leukocyte transendothelial migration" KEGG pathway in old WT and adult WT mice. *All proteins displayed are q<0.05. Protein abundance displayed in arbitrary units (AU). Data here demonstrates the increase in protein abundance in muscles of old WT mice relating to leukocytes when compared with muscles from adult WT mice.*

6.3.3 Analysis of rates of synthesis of individual proteins show very little evidence of changes in overall protein synthesis in muscles with ageing

Data from the heavy water study examining the rates of synthesis of individual proteins suggest that overall, there was no obvious difference in the global rate of protein synthesis in muscles of old compared with adult WT mice (**Figure 6.12**) Differences in synthesis rates of individual proteins from muscles of adults and old WT mice were seen as an exception and these were not related to either the weight or mass of the individual proteins (**Figure 6.13A – B**). The mode value for the protein mass was around $10^{4.5}$ kDa and the mode protein length was around $10^{2.5}$ amino acids (**Figure 6.13C – D**). There was no observable difference between the synthesis rates of proteins from muscles of adult or old mice with length or mass of protein (**Figure 6.13 E – F**).

Despite the lack of change in global protein synthesis (**Figure 6.12**), there were some intriguing patterns of individual proteins showing increased or decreased rates of protein synthesis in muscles of old compared with adult WT mice (**Figure 6.14 & Figure 6.16 - 6.17**).

The full set of protein synthesis data are shown in Annex 1 and example plots are shown in **Figure 6.14**. Despite the majority of proteins showing little difference in synthesis rates when comparing muscles from adult and old WT mice, there were some individual proteins where the rates of synthesis were either elevated or reduced (**Figure 6.14**).
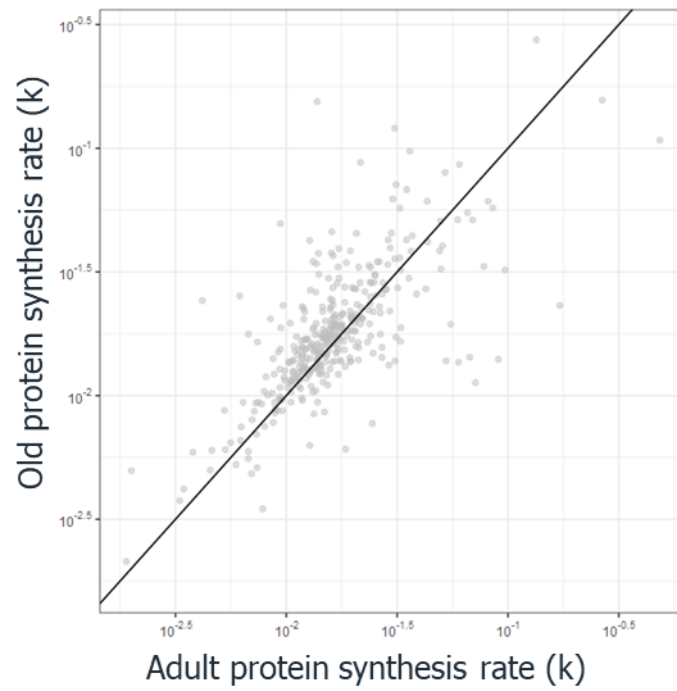
Figure 6.12: Log graph of synthesis rates (k) of individual proteins in adult WT and old WT mice. *Data here show a high degree of correlation between the synthesis rate of individual proteins in old WT mice when compared with that of adult WT mice. Each individual protein is represented by a grey circle. X = Y line is shown by a black line.*

.
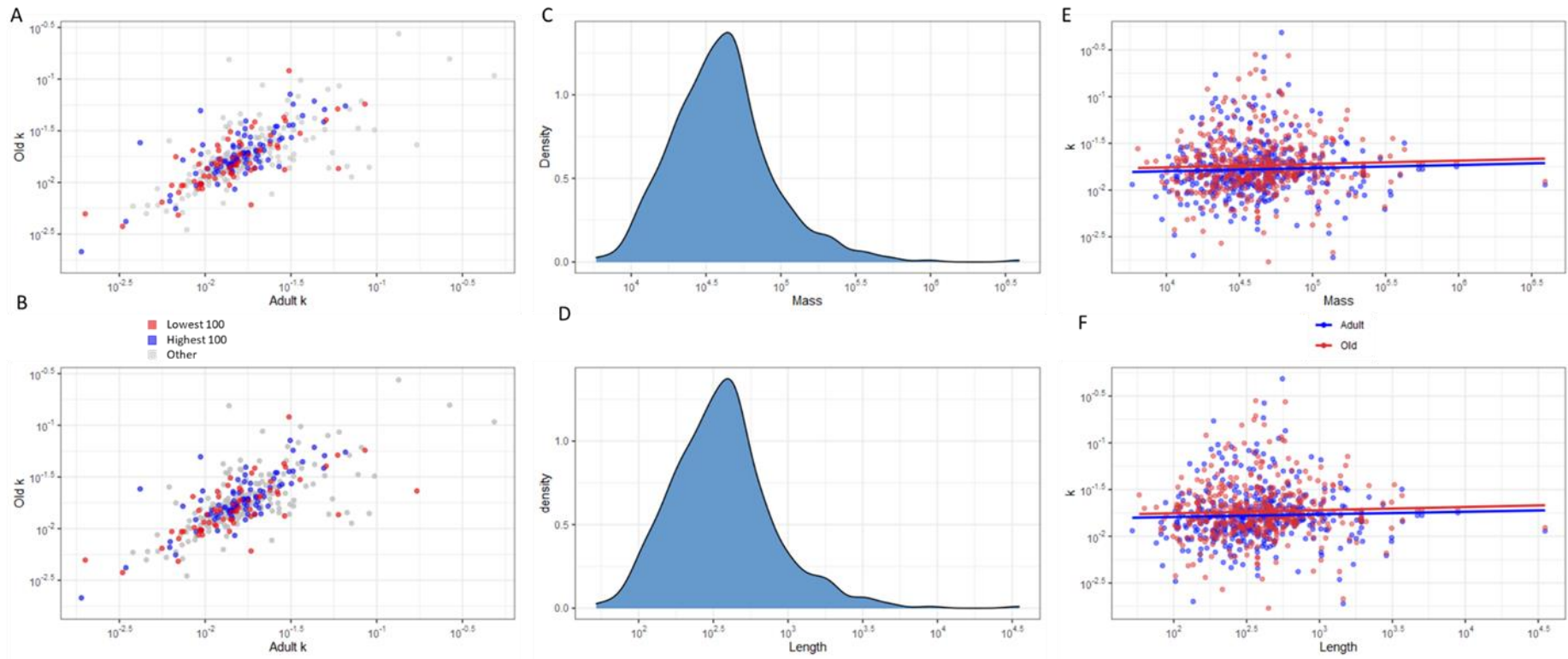
Figure 6.13: Synthesis rates of the highest and lowest mass and lengths of proteins found in the muscle proteome of adult WT and old WT mice*. the top and bottom 100 A) mass and B) length proteins and their protein synthesis rate (k) in the muscles of adult and old mice. The density of C) mass and D lengths of all proteins detected and the protein synthesis rate (k) in adult and old WT mice against protein E) mass and F) length.*
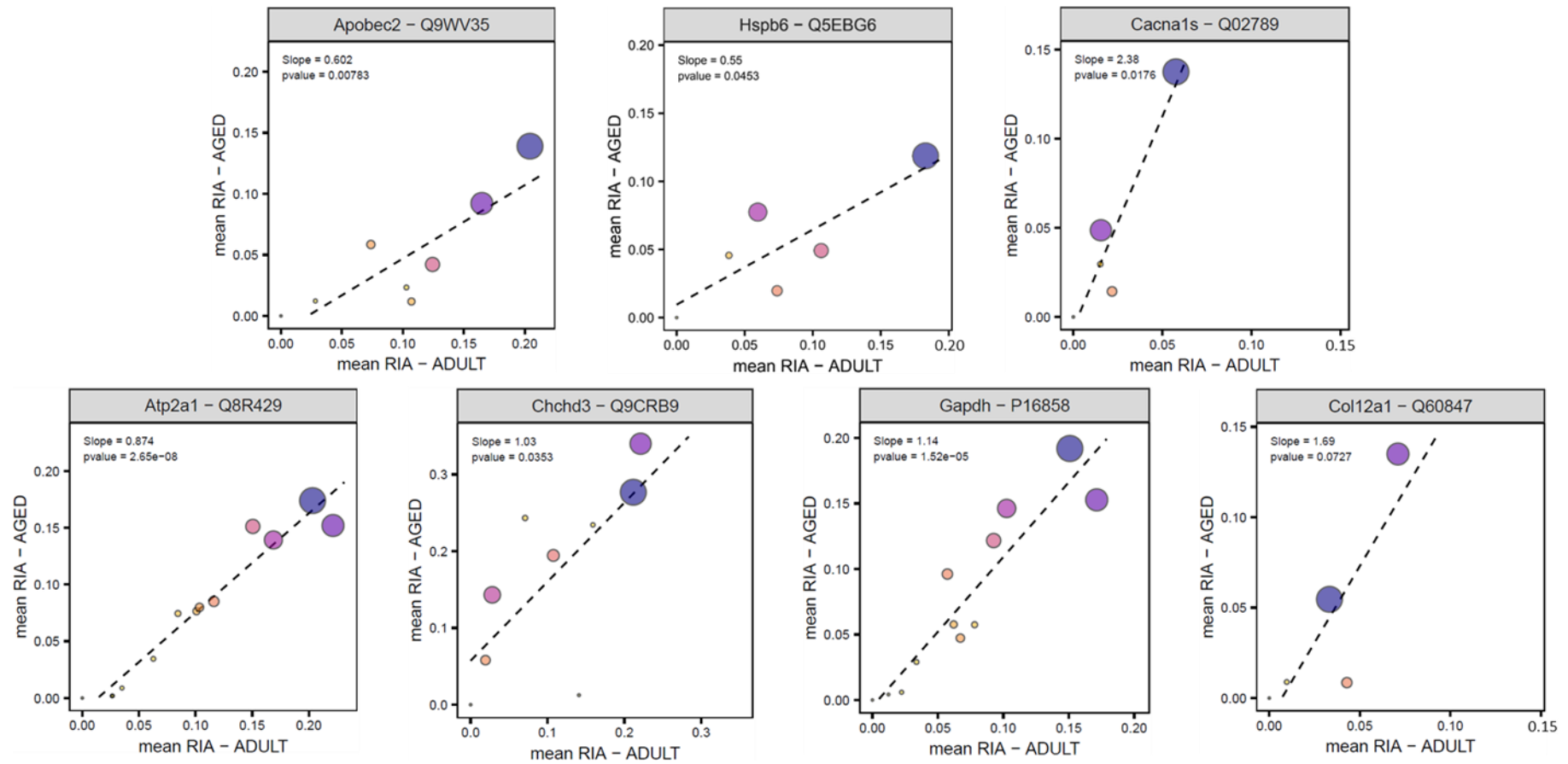
Figure 6.14: Comparison of synthesis rates of individual proteins from the GTN muscles of adult WT and old (Aged) WT mice. *A slope higher than 1 shows a protein which is synthesised at a higher rate in old mice, whereas a slope lower than 1 shows a protein which is synthesised slower in the muscles of old WT mice when compared with that of adult WT mice. Size and colour of points on the graph relates to the dosing period of heavy water of the individual mouse (i.e. 0 – 60 days). Relative isotope abundance (RIA).*

6.3.4 Comparison of protein abundance and synthesis rate with differential expression of mRNA from quiescent muscles from adult and old mice.

The ability to compare the rate of synthesis of individual proteins to static levels of proteins and mRNA determined by RNASeq provides a powerful analytical tool. The RNASeq data were kindly provided by Professor Malcolm J Jackson, Professor Richard Barrett-Jolley, and Dr Caroline Staunton at the University of Liverpool. There were 185 proteins that were common to the abundance proteomics, synthesis proteomics, and RNAseq datasets. All 268 proteins in the protein synthesis dataset were also observed in the protein abundance dataset. There were 757 proteins common to just the RNAseq and protein abundance datasets (**Figure 6.15**).

The RNAseq dataset contained 29,842 transcripts, 14,772 of which were not detected in the transcriptomes of all mice and 3,808 of which were not able to be annotated with Uniprot accession numbers. The unlabelled proteomics dataset contained abundance values for 1395 proteins and the protein synthesis dataset contained synthesis rates for 248 proteins (**Figure 6.15**).
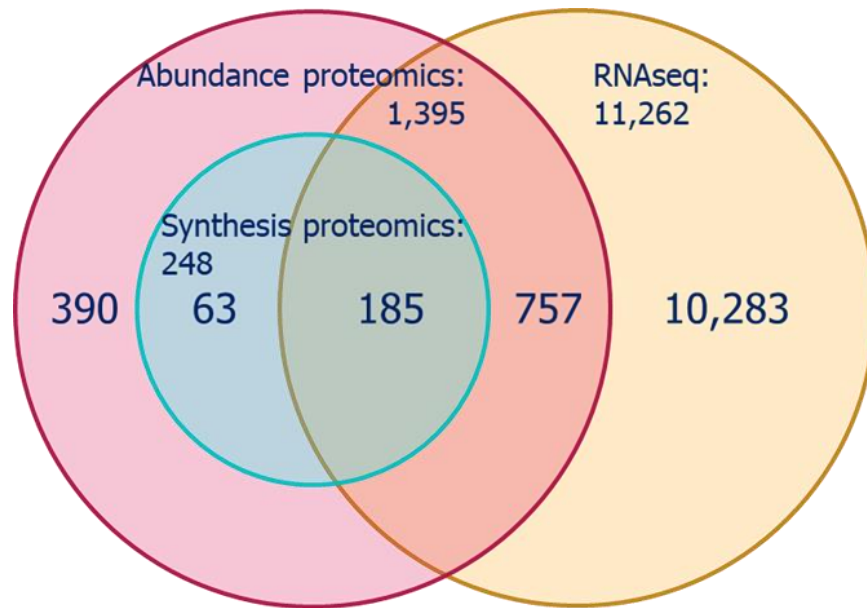
Figure 6.15: Venn diagram showing the overlap of detectable targets between unlabelled (abundance) proteomics, heavy water (synthesis) proteomics, and RNAseq data. *The abundance proteomics showed a total count of 1,395 analytes. The synthesis proteomics showed a total count of 248 analytes. The RNAseq showed a total count of 11,262 analytes. The synthesis proteomics showed a 100% overlap of analytes with the abundance data set due to the similarity in analytics technique.*

Upstream analysis of the abundance proteomics dataset revealed significant relations to master regulators Single Ig IL-1-related receptor (SIGIRR), IκBα, IKKε and p65 all with overlap p-values $< 2.2 \times 10^{-28}$. All of these regulators have key roles in the NF-κB pathway. The top canonical IPA pathways identified included the actin cytoskeleton including specific actin proteins ACTC1, ACTA1, Actn3 and ACRT2 which were all decreased in terms of protein abundance in the muscles of old WT mice. The rates of protein synthesis of ACTA1 and ACTC1 were both reduced in muscles of old compared with adult WT mice, although ACTA1 mRNA was shown to be increased via RNAseq. Likewise, the protein abundances of specific myosins MYLPF, MYLK2, MYL1 MYH4 and MYH3 were decreased and the rates of protein synthesis (with the exception of MYLPF) were also decreased in muscles of old compared with adult mice although the mRNA for these proteins determined by RNASeq were also generally increased.

In contrast for other proteins, in the muscles of old WT mice, the abundance of 7 NADH:ubiquinone oxidoreductase supernumerary (NDUF) subunits were all generally decreased in the muscles of old compared with adult WT mice besides NDUFB1, whereas two of these subunits had an elevated protein synthesis rate (NDUFS7 and NFUFS6) but notably a decreased mRNA expression level determined by RNASeq. These proteins appear in both the 2nd and 3rd canonical pathways as described via the IPA output. Canonical pathways are the most significant to the input data (Savli et al. 2008).

It is difficult to undertake a full comparison of the three datasets for several reasons including the availability of data in all datasets, and so the approach taken was to undertake a comparison across the three approaches for the top canonical pathways identified as modified by the protein abundance data. It is important to note that the levels of a large number of proteins remained unchanged and so the focus in this comparison is on those identified where the abundance was modified with age. The top IPA canonical pathways identified in the protein abundance dataset were actin cytoskeleton signalling, sirtuin signalling, mitochondrial dysfunction, glycolysis I and gluconeogenesis I. Within these top 5 IPA pathways, there was no clear pattern between the RNA expression, protein abundance and protein synthesis rates change between the muscles of adult and old WT mice (**Figure 6.16)**.
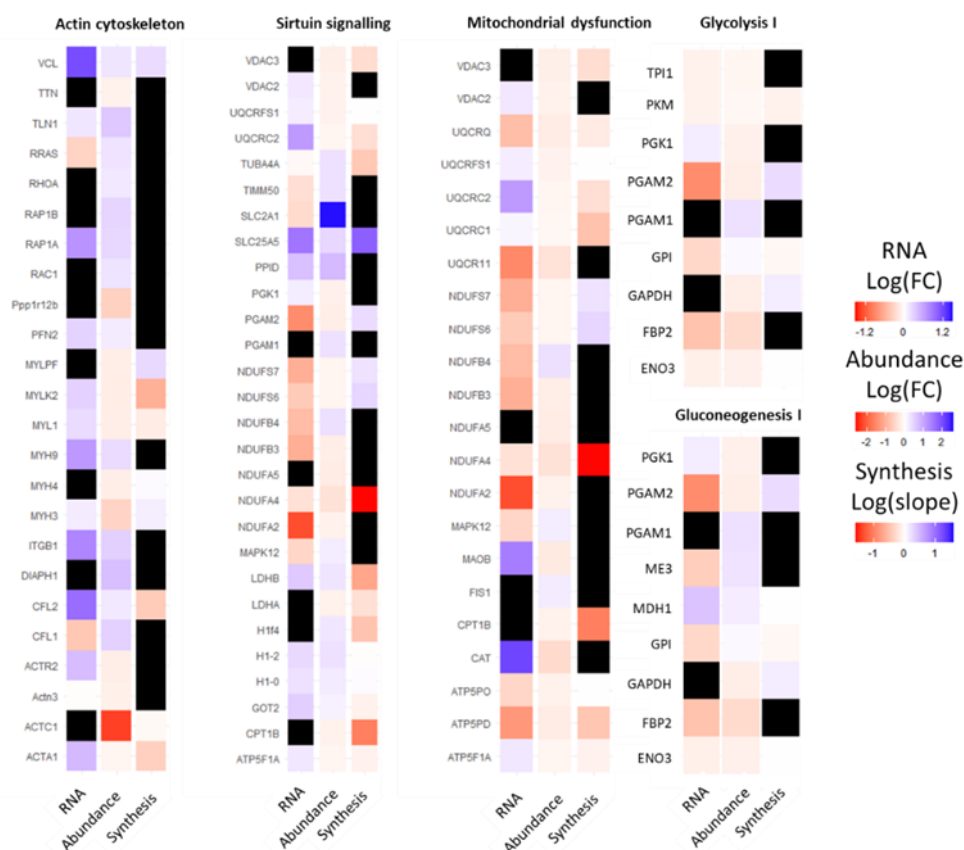
Figure 6.16: Relative RNA expression levels, protein abundance, and protein synthesis rates in the muscles of old WT mice for the top 5 IPA canonical pathways which differ in protein abundance between adult WT mice and old WT mice. All data is relative to values for muscles of adult WT mice.

Thus, selecting targets which were common to all three datasets revealed how differently the protein synthesis rates can vary from both the 'snapshot' RNA expression and the abundances of the proteins, suggesting that interpretation based on one of these measures should be treated with caution. As a further example, Myosin light chain 1 (MyL1) was less abundant in muscles of old WT mice, which may be explained by its decrease in protein synthesis, however, this was not reflected in the level of RNA expression where no difference was seen with respect to Myosin heavy chain 3 (MyH3), there was a decrease in protein abundance but a small increase in the rate of protein synthesis with age and little difference in RNA levels between the two age groups (**Figure 6.17**).
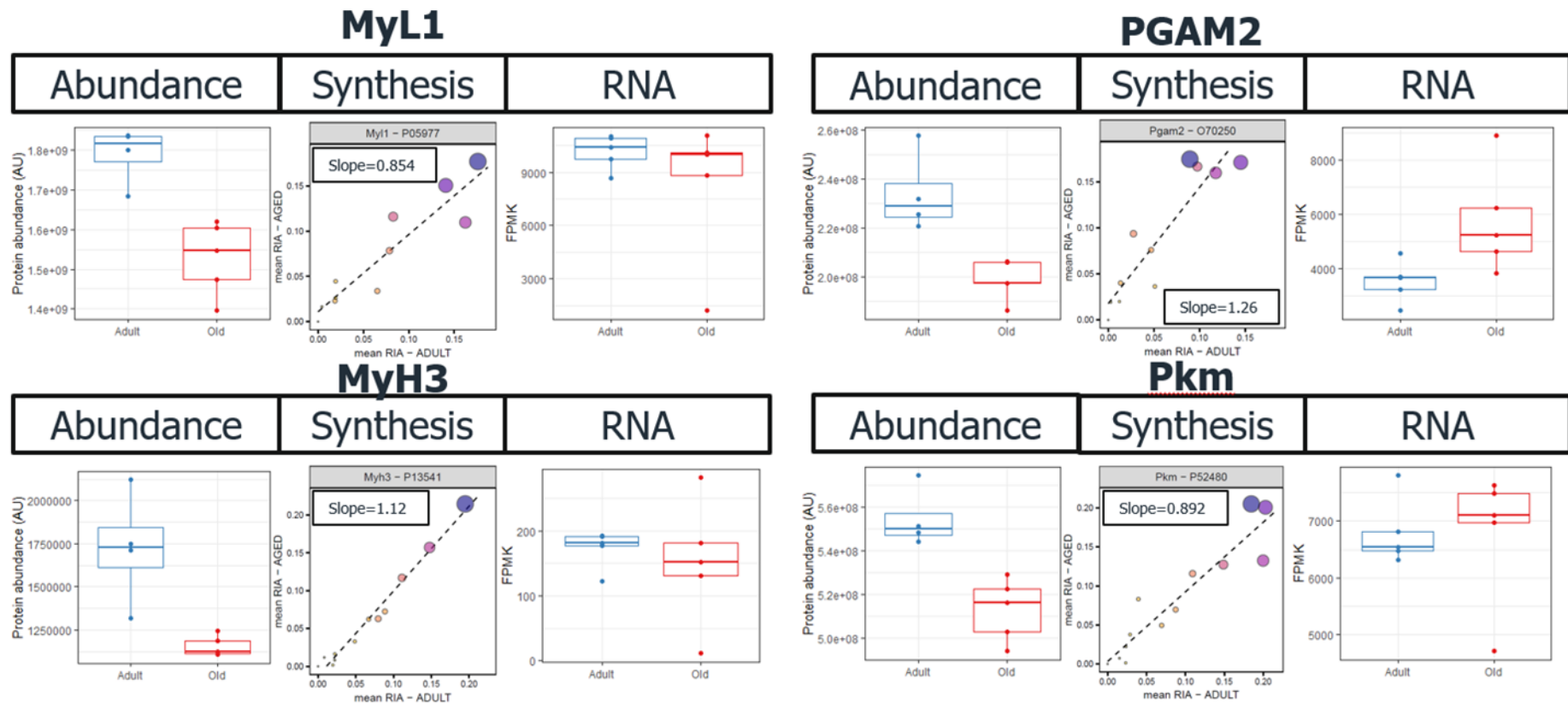
Figure 6.17: Examples of a number of select proteins where data are available for protein abundance, protein synthesis rate and mRNA expression datasets. *With respect to the proteins synthesis rates, a slope below 1 indicates that there was a decrease in synthesis rate in the muscles of old WT mice. A slope above 1 indicates there was an increase in the protein synthesis rate in the muscles of old WT mice. Myosin light chain 1 (MyL1); Myosin heavy chain 3 (MyH3); Phosphoglycerate mutase family protein 2 (PGAM2); Pyruvate kinase (Pkm).*

The abundance of phosphoglycerate mutase family protein (PGAM)2 was significantly decreased in muscles of old compared with adult mice, however the synthesis rate of the same protein was increased by ~26% with an increase in RNA expression too. The abundance of pyruvate kinase (PKM) in the muscles of old mice was decreased when compared with the muscles of adult mice, with a decrease in the synthesis of this protein too and this was accompanied by a no significant difference in the expression of RNA for this protein (**Figure 6.17**).

6.4 Discussion

6.4.1 Functional annotation of proteins in the unlabelled protein dataset demonstrated an upregulation of protein degradation pathways with ageing

Several GO terms which were enriched in the proteins significantly altered between old and adult WT mice were closely linked to protein degradation, namely ubiquitin protein ligase binding (which facilitates the targeted breakdown of proteins via the proteasome) and the UPR (which is in control of the systematic breakdown of misfolded proteins) (**Figures 6.4 – 6.6**). This agrees with other studies (Altun et al. 2010; Sacheck et al. 2007; Schiaffino et al. 2013; Sandri et al. 2013; Bonaldo & Sandri 2013) and suggests that there is a clear role of protein degradation as a major contributor to the loss of muscle mass with age. In addition to this, the top 4 KEGG pathways enriched when comparing protein abundance in the muscles of adult and old WT mice were all degenerative diseases caused or exacerbated by protein misfolding and accumulation (**Figure 6.6 – 6.7**). As sarcopenia is a degenerative disease, this provides evidence that sarcopenia may at least in part be exacerbated by protein misfolding and accumulation of misfolded proteins.

Underlying these changes is likely to be the increased oxidative stress reported in muscles of old compared with adult WT mice (Jackson & McArdle 2011). Such oxidation is known to result in activation of NF-κB and to cause protein misfolding similar to that observed in the protein misfolding diseases: ALS, Parkinson disease, Alzheimer disease and prion diseases and also underpins the accelerated muscle ageing observed in SOD1KO mice. Bioinformatics analysis predicted mitochondrial

dysfunction in muscles of old compared with adult WT mice and this is associated with the altered mitochondrial ROS generation reported previously (Van Remmen & Jones 2009).

Another highly enriched KEGG pathway identified was "leukocyte trans-endothelial migration, associated with an increase in 9 proteins of this pathway in muscles of old WT mice (**Figure 6.8-6.9**) (Neubauer et al. 2014). In addition, further upstream analysis of the proteomics using IPA revealed key regulators of the NF-κB pathway to play major roles in the variation of protein abundance in the muscles of old WT mice when compared with the muscles of adult WT mice. Data in Chapter 3 demonstrated an increase in NF-κB translocation to the nuclei of muscle fibres in old WT mice (**Section 3.3.5**), decrease in IκB, and increased secretion of chemokines from muscle fibres (**Section 3.3.3**) which are likely to play a role in this increased leukocyte infiltration. Muscles of old mice have been shown to contain a higher proportion of M2 macrophages than that of adult mice (Cui et al. 2019) and an increase in neutrophil infiltration is observed following acute tissue injury in mice (Nicholas et al. 2015). Some of the chemokines directly inducing neutrophil and macrophage infiltration and activation have been shown to be increasingly secreted by the muscles of old mice suggesting a mechanism by which this occurs.

Several proteins repeatedly appeared through several data reduction techniques such as ENPL, also referred to as HSP90b1 (**Figure 6.3C**). This protein is contained within the endoplasmic reticulum as a chaperone protein which can chaperone around 10% of all proteins. The transcription of ENPL is regulated by the XBP1 pathway which controls the UPR and ERAD responses. As the protein is more abundant in the muscles of old WT mice, the UPR and ERAD responses is likely to be upregulated in these muscles.

Another major protein of interest is VINC (**Figure 6.3C, Figure 6.5, Figure 6.11**). In previous studies on the ageing heart muscle of rat and macaque monkeys, there is an increase in the protein content of VINC (Kaushik et al. 2015). VINC is a protein which is essential for cell morphology and adhesion and is highly associated with cytoskeletal structure and proteins (Coll et al. 1995). The overexpression of

VINC within the heart muscle of drosophila increased longevity by 150 % (Kaushik et al. 2015). Data in this chapter show VINC to be increased in muscles of old mice in all three measures, gene expression, protein abundance and protein synthesis rates. It may therefore be that this is an attempt by the muscle to compensate to the stress of ageing by increasing cytoprotective proteins.

Interestingly, the length or mass of proteins did not have any influence on synthesis rates and as such, any observed difference in synthesis rate with ageing is not likely to be attributed to amino acid pool, ribosome number or protein elongation (**Figure 6.12**).

6.4.2 The overall synthesis rates of proteins from muscles of adult and old WT mice were unchanged although there was evidence of changes in individual proteins.

The possibility that reduced protein synthesis rates in muscles of aged populations were a major factor in the negative net protein balance seen remains controversial. Data presented here using deuterated water to examine synthesis of individual proteins demonstrate little evidence of global changes in protein synthesis at a level that would result in such loss of muscle mass. This suggests that the net negative protein balance within the muscles of old humans and mice, is more heavily influenced by an increase in protein degradation rather than a decrease in protein synthesis.

6.4.3 Comparison of protein synthesis rates with static protein and mRNA levels suggest that the levels of individual proteins are likely to be under different regulatory processes.

This is the first study we are aware of that has compared all of these indices or protein turnover. Data demonstrated that there was little consensus in the associations between rate of synthesis, static protein and mRNA levels. The reasons for this are likely to be complex and relate to the nature of the individual proteins. Thus, we have previously reported a constitutive increase in HSP content of skeletal muscle of old mice but a down-regulation of mRNA level (Kayani et al. 2008). Although HSP levels were elevated, it was hypothesised that the HSP was bound to oxidised proteins that were not degraded and so not 'available' to provide additional protection to the muscle. Further, HSPs have a feedback mechanism whereby high levels of HSPs result in a down-regulation of mRNA.

Of interest is that the rate of synthesis of a protein is rarely associated with an increase in mRNA and data suggest that caution should be taken in extrapolating the suggestion that static mRNA levels reflect the rate of synthesis or indeed the protein levels. Instead, the synthesis rate of proteins is likely to also be linked to translation dynamics, ribosomal alterations, and individual protein chemistries.

6.5 Conclusion

In summary, this study has demonstrated a clear upregulation of protein degradation processes and protein misfolding in the muscles of old WT mice. In contrast, there was little evidence of a global change in synthesis of proteins although there were some exceptions. As such, these findings suggest that the mechanisms by which muscle is lost with age in mice is primarily by protein degradation.

Chapter 7: General discussion and future directions

7.1 Hypothesis

The overall hypothesis of this thesis was that the increased activation of NF-kB reported in muscles of old WT and adult SOD1KO mice is associated with degenerated, denervated or regenerating muscle fibres and this results in an increased production of cytokines/chemokines by muscle which contribute to the chronic inflammation seen in old age (inflammaging). Further, such chronic activation of NF-kB activation will lead to modified protein turnover in muscles of old WT mice causing a net loss of muscle protein.

7.2 Overall aims of this thesis

The aims of the work reported in this thesis were:

1. To determine the localisation of nuclei with increased activation of the canonical pathway of NF-kB in quiescent muscles of old WT and adult SOD1KO compared with adult WT mice.

2. To identify whether any changes in the cytokine and chemokine levels in the plasma of old WT and adult SOD1KO mice are associated with altered cytokine/chemokine production by muscles and whether this is associated with the presence of degenerating/regenerating muscle fibres.

3. To examine and model differentially expressed proteins using unlabelled and deuterated water-based proteomics to determine whether activation or inhibition of protein turnover pathways are likely to be driven by changes in NF-kB activity in old compared with adult WT mice.

7.3 Summary of the findings of the thesis

The major findings of this work are:

1. Data demonstrated a reduction in muscle mass and function in old WT and adult SODKO mice when compared with muscles of adult WT mice generation in fitting with what would be considered as sarcopenia although subtle differences were seen between the muscles of old

WT mice and the muscles of our model of ageing, the adult SOD1KO mouse, particularly following damage.

2. Examination of p65 localisation in muscle fibres of adult and old WT and adult SOD1KO mice demonstrated a clear increase in the levels of p65 within peripherally positioned nuclei in muscle fibres of old mice compared with nuclei of adult WT mice whereas in the muscles of adult SOD1KO mice there was an increase in the level of p65 primarily in the muscle fibres with centralised nuclei, fibres that were more prevalent in muscles of SOD1KO mice. The p65 was detected in a punctate pattern in nuclei in all instances. These changes in p65 localisation were associated with a significant decrease in IkB levels in muscles of old WT but not SOD1KO mice.

3. The difference in p65 activation was reflected in differences in the cytokine/chemokine profile in these mice, whereby levels of a number of cytokines/chemokines were elevated in plasma of old WT compared with adult WT mice but this was not fully reflected in SOD1KO mice. There were increases in different cytokines and chemokines in the lysates of muscle from both old and SOD1KO mice and increased release of a number of cytokines/chemokines from isolated fibres from old WT mice, not evident from muscles of adult SOD1KO mice.

4. Following muscle damage, the nuclear localisation of p65 was strongly associated with degeneration and regeneration in muscles of adult WT, old WT and adult SOD1KO mice although the time course and extent of nuclear localisation of p65 appeared different in the three groups. Muscles of adult WT and adult SOD1KO mice recovered mass and function to pre-damage levels by 28 days following damage whereas a permanent functional deficit was evident in muscles of old WT mice. This did not appear to be due to any gross changes in cytokine/chemokine production at this time point, at least at the plasma level. In addition, there was no overwhelming increase in cytokines or chemokines when substantial numbers of regenerating muscle fibres are present, suggesting that presence of such fibres did not explain the substantial changes seen in plasma levels of cytokines and chemokines in these

models under quiescent conditions. It may be that temporal differences in p65 translocation in the different models during regeneration may represent different functions of NF-κB since it is known that temporal changes in p65 localisation can result in differential gene expression unrelated to cytokine production.

5. Analysis of unlabelled proteomic datasets demonstrated a clear upregulation of protein degradation and protein misfolding in muscles of old WT mice known to be, at least in part, under the control of NF-kB. Use of novel heavy water approaches demonstrated that there was little evidence of a global change in synthesis of proteins in muscles of old WT mice although there were some exceptions. As such, these findings suggest that the mechanisms by which muscle is lost with age in WT mice is primarily by increased protein degradation.

7.4 General Discussion

7.4.1 Inflammation in old WT mice: role of skeletal muscle

An increase in levels of inflammatory markers such as plasma IL-6, TNF-α, and CRP have been associated with a higher patient mortality and the onset of sarcopenia in a number of studies (Ferrucci et al. 2002; Bautmans et al. 2011). Elevated CRP is associated with low chair stand performance in men and women and loss of handgrip strength in men and women over 55 (Hamer & Molloy 2009). Administration of the common non-steroidal anti-inflammatory drug (NSAID) ibuprofen significantly decreased age related muscle mass in rats (Rieu et al. 2009) providing further evidence of a role for inflammation in the development of sarcopenia. The source of the systemic cytokines seen in old age is not known, however there are numerous proposed cells. Muscle accounts for around 40% of body mass, so an increase in cytokine production and release by muscle fibres would potentially result in a considerable contribution to systemic inflammation (da Silva et al. 2019).

Studies described in this thesis have identified a number of cytokines and chemokines that are elevated in plasma of old WT mice at a time when muscle loss is evident. These are IL-6, IL-10, TNF-a, CCL5, CCL7, CCL11, CXCL2, CXCL5, and CXCL12 and CXCL13. There is some evidence that a number of

these cytokines/chemokines, at sufficiently high concentration, will affect muscle mass and function. Studies described in Chapter 3 demonstrated the complex nature of determining cytokine synthesis, protein levels and secretion in the different models and comparison of the mRNA levels in the RNASeq dataset added to this complication. However, studies described in this thesis suggest that a number of cytokines are likely to be chronically produced by skeletal muscle and some of these, particularly CXCL2, CCL11, CXCL5 and CXCL12 may influence the plasma pool. In other instances, the increased production and release do not reflect changes in the plasma pool and so are likely to have a more local effect, potentially on the function of local cells and tissues such as peripheral nerve.

7.4.2 Structural and functional changes in muscles of old WT and adult SOD1KO compared with adult WT mice reflect sarcopenia but demonstrate some differences

Skeletal muscle atrophy and weakness plays a major role in the development of frailty in older people and is the major cause of the loss in mobility, the high incidence of falls, and the eventual move to assisted living conditions and nursing homes for the elderly (Faulkner et al. 2007; McArdle et al. 2019). In humans, by the age of 70, the cross-sectional area of skeletal muscle is reduced by 25-30% and muscle strength is reduced by 30-40% (Porter et al. 1995). A similar loss of muscle is seen in old mice, with a 20-30% loss of muscle mass and function by 24-26 months of age (Brooks & Faulkner 1990; McArdle et al. 2004) and this was replicated in studies in this thesis (**Chapter 4**) whereby muscles from old WT mice show a decrease in muscle mass and force in fitting with what would be considered as sarcopenia.

Data presented in **Chapter 4** demonstrated that the main cause of the reduction in tetanic force generated by quiescent muscles of old WT mice is unlikely to be due to an atrophy or loss of muscle fibres. Although the diameter of muscle fibres was more variable in old compared with adult WT mice, no significant difference was seen. The lack of difference in fibre number and fibre diameter observed in the present study for EDL muscles of old compared with adult WT mice compared with the small (8%) but significant decrease in muscle mass likely reflects the variability in fibre diameter in muscles

of old mice, although an 8% reduction in muscle mass would also not account for the substantial decrease in tetanic force generated by muscles of old compared with adult WT mice. Similarly, our research group have shown that ~5% of muscle fibres were fully denervated in muscles of the old WT mice although significant partial denervation was also observed. The lack of a substantial effect of measurement of force generation when muscles were activated via muscle surface electrodes compared with nerve activation (Larkin et al. 2011) suggests that other factors than structural changes are playing a role in the functional deficit seen in quiescent muscles of old WT mice, with the potential of a change in inflammatory environment playing a role. Centrally located nuclei, originally thought to be a feature only of embryonic development, have been associated with myopathies since the 1960s (Spiro et al. 1966). Centrally located nuclei are now an index of various diseases of the muscle and nervous system including Duchenne Muscular Dystrophy (DMD) where it is thought to be a remnant of degeneration and ongoing regeneration (Wang et al. 2000).

The role of centrally located nuclei is not currently defined in muscle of old WT mice and it is not yet known of the effects of these on the force generation by individual fibres. A higher prevalence of centrally located nuclei in older muscle may indicate ongoing degeneration and regeneration, alternatively, it may indicate a halted state of regeneration in some fibres. Regardless of the purpose, this central position in an area known to contain the contractile machinery may be a possible reason for lower force generation by disruption of efficient interactions of the contractile machinery.

7.4.3 SOD1KO mice as a model of inflammaging

SOD1KO mice display many of the functional losses associated with frailty in humans (Deepa et al. 2017). SOD1KO mice have an accelerated decrease in body mass, adult mice demonstrate a decrease in wheel running capacity and performance on a Rota-rod test, and increase in oxidative damage to macromolecules (Muller et al. 2006). A significant decrease in mass of all muscle types is also observed, with the exception of the postural *soleus* muscle (Muller et al. 2006; Jang et al. 2010; Larkin et al. 2011). Alongside the loss of muscle mass, is a loss of muscle force generation, even when

normalised to the cross sectional area of the muscle (Muller et al. 2006; Jang et al. 2010), suggesting a weakening of the remaining muscle in a similar manner to muscles of old mice and humans. The SOD1KO mice demonstrate a deterioration in the NMJs which is reflected in a parallel loss of synaptic function (Jang et al. 2010; Deepa et al. 2019; Larkin et al. 2011).

Data presented in **Chapter 3** shows that the significant and detectable differences in the inflammatory profile in the plasma of old WT mice was not reflected in the SOD1KO mice. Likewise, there were considerable increases in different cytokines and chemokines in the lysates of muscle from both old WT and adult SOD1KO mice. This may be due to the difference in p65 activation in the fibres detailed in **Chapter 3** whereby increased p65 localisation appears to be evident primarily in centrally positioned nuclei in muscle fibres of adult SOD1KO mice and in some peripherally positioned nuclei in muscle fibres of old WT mice. It may also be that there is a difference in the cell composition of the muscle in the two models, although this was out of the scope of the current study. To conclude these results, the muscle of old WT and SOD1KO mice both show differential indices of inflammation which appears to be associated with differences in the position of nuclei, and so potentially as a response to muscle fibre regeneration, suggesting that the SOD1KO mice are a poor model of inflammaging and that the mechanisms by which sarcopenia occur in adult SOD1KO mice and old WT mice are either a) different or b) unrelated to systemic inflammation.

7.4.4 Protein turnover in muscles of old WT mice. Protein synthesis vs degradation

There is some controversy regarding the rates of basal muscle protein synthesis in older people, with some studies reporting reduced basal muscle protein synthetic rate in older people compared with younger subjects (Balagopal et al. 1997; Rooyackers et al. 1996b; Short et al. 2004; Welle et al. 1993; Yarasheski 2003; Yarasheski et al. 1993) and others suggesting no difference in healthy old compared with younger people (Cuthbertson et al. 2005; Volpi et al. 1998; Volpi et al. 2001). Measurement of fractional synthesis rates (FSRs) of protein by infusion of an isotopic tracer (e.g. ^{13}C leucine) and subsequent analysis via gas chromatography is a common method of measuring total protein

synthesis rates. A decrease in the FSR of mitochondrial proteins and mixed proteins was reported in muscle biopsies from older people (Rooyackers et al. 1996a). Subsequent studies showed a lower FSR of myosin heavy chain in muscle of old humans which correlated with an increase in insulin – like growth factor I (IGF-1) and a decline in muscle strength (Balagopal et al. 2017; Short et al. 2004; Katsanos et al. 2006). In contrast with this, muscle biopsies taken from adult and old humans have been shown to not be significantly different in terms of FSR (Volpi et al. 2001). There were, however, several problems with the Volpi et al study including taking biopsies from the same area of muscle repeatedly, diet and exercise were not controlled, and the arterial – ventricular balance experiment was problematic as it didn't account for the change in muscle with age (Yarasheski et al. 2002). Further to this, there is increasing evidence that basal muscle protein synthesis (MPS) may not be altered in muscle during ageing (Cuthbertson et al. 2005; Kumar et al. 2009; Yarasheski et al. 2017).

Data presented in **Chapter 6** using deuterated water to examine synthesis of individual proteins demonstrate little evidence of global changes in protein synthesis at a level that would result in such loss of muscle mass although there were exceptions in some individual proteins of note. In contrast, Functional annotation of proteins in the unlabelled protein dataset demonstrated an upregulation of protein degradation pathways with ageing, fully supporting the hypothesis that the major factor in the loss of muscle mass with ageing in mice is via increased protein degradation although it is important to examine the effects on individual proteins.

7.4.5 Comparison and interpretation of 'omics' data

Determination of protein or mRNA abundance can only ever be a snapshot of the current situation in a dynamic process and the proteome is dynamically active where proteins are constantly synthesised and metabolised. Metabolic labelling of proteins is a method which, when combined with unlabelled proteomics, can be used to determine protein dynamics (Claydon et al. 2012). Metabolic labelling can be achieved *in-vivo*, through dosing the animal with the use of stable isotope labelling in mammals (SILAM). Amino acids, their precursors, or a mixture of amino acids can be labelled with a stable

isotope and given to the animal through injection, diet, or drinking water for a range of time periods which, when measured by Mass Spectrometry, give two separate spectra of which a ratio can be calculated. Most commonly, these are amino acids with substitutions of carbon-13 or hydrogen-2 (Beynon & Pratt 2005).

The use of deuterated (heavy; ^2H_2O) water has a number of advantages to the use of labelled amino acids. ^2H_2O is safe to supplement in humans and animals for longer periods of time (years). ^2H_2O is quick to equilibrate through the body via osmosis and so constant enrichment levels are very easily maintained. ^2H_2O is also much cheaper than other methods of metabolic labelling (Kim et al. 2012a; Busch et al. 2006).

Through comparing the results of the proteins synthesis dataset and the RNAseq dataset (**Chapter 6**), it is clear that there was no global correlation between transcription and translation rates. This could be due to the multifaceted nature of protein synthesis with the synthesis of protein being the end product of several regulatory steps and include multiple factors. These factors include but are not limited to the RNA stability, regulatory elements, protein stability and dynamics, protein modifications and general breakdown of the protein. Such findings stress the importance of caution when interpreting static protein and mRNA levels in tissues, particularly when examining secreted proteins, which add a further level of complexity.

7.5 Limitations of current studies

There are a number of limitations to the studies reported in this thesis that are worthy of consideration.

1. This study was only conducted in male mice. Thus, although sarcopenia is evident in both sexes in mice, hormonal and gender specific differences may influence the detailed findings (Blenck et al. 2016). In humans, sarcopenia appears more prevalent within the female population and as such it may be that we might expect differences in the mechanisms and processes of muscle loss with age in other mammals such as mice (Du et al. 2019). Expanding

this work to include female mice would involve increasing the number of mice considerably and was beyond the scope of the current study, but would allow for greater conclusions to be made on both genders.

2. NF-κB is proposed to be temporally controlled and it is proposed that fluctuation in oscillations between the nucleus and cytoplasm provide additional control of the nature of genes that are activated (Ashall et al. 2009; Zambrano et al. 2016). This study only confirmed canonical activation of NF-κB and its location in individual nuclei. Temporal changes to the NF-κB pathway may highlight further alterations to the regulation of the transcription of different genes.

3. Though the NF-κB pathway is highly conserved between species, there may be defined differences between inflammatory mediation both in terms of NF-κB pathway activation and in cytokines/chemokines. Although this is a contentious area, it is proposed that although mice are an excellent model of sarcopenia, there may be subtle differences in the immune system that need to be taken into consideration. For chemokines specifically, mice exhibit differences in their chemokine ligands compared with humans (Zlotnik & Yoshie 2012). In addition to differences in intracellular signalling, the murine and human immune systems are different in terms of cellular proportions and expression of some receptors (Mestas & Hughes 2004).

4. Data presented in **Chapter 6** have provided compelling evidence that increased protein degradation seems to be the major mechanism by which muscle is lost in old WT mice. However, previous studies in humans and mice have demonstrated the inability of muscles of old mice and humans to respond to an anabolic stimuli, known as anabolic resistance and this has been discussed as a possible cause for a decrease in acute protein synthesis with ageing (Burd et al. 2013). For this reason, it would be of interest to expand the heavy water study in **Chapter 6** to include an anabolic stress such as exercise.

7.6 Future directions

Clearly, reliance on datasets to predict targets for intervention is a powerful approach but given the concerns of the use of individual data sets to undertake such predictions, it is imperative to undertake mechanistic interventions to support these findings. Thus, in mouse models, knock out or knock in studies can be undertaken. In addition, more translational interventions can be undertaken in mice as proof-of-principle for human interventions.

Having gathered evidence that the NF-κB pathway and inflammation plays a potential role in the loss of proteostasis and is a contributing factor to the onset of sarcopenia in mice, being able to control the level of inflammation within the muscle (or systemically) through intervention studies might be a way to alleviate muscle loss with ageing. One non-specific method for this would be to use a non-steroidal anti-inflammatory such as aspirin or ibuprofen to treat mice at an old age and observe differences in muscle structure, muscle function, NF-κB signalling and the cytokines produced by muscle fibres. In place of non-steroidal anti-inflammatory drugs, specific small molecule NF-κB inhibitors could be used. One such example is YC-1 which reduces the translocation of p65 to the nucleus and thus diminishes inflammatory signalling (Lee et al. 2018). Likewise, the small molecule ubiquitination inhibitor Ro106-9920 has been shown to inhibit ubiquitination of IκBα and, in turn, stop NF-κB activation and cytokine expression (Swinney et al. 2002).

Through determining the production of cytokines/chemokines from muscle fibres, we have some potential targets to reduce immune cell mediation into the muscles of old WT mice. We showed that the chemokines CCL2, CCL11, CXCL5, and CXCL12 are produced in increased amounts by the muscles of old WT mice when compared with those of adult WT mice (**Chapter 3**). CCL2 was found to be produced at over 100x in muscle fibres of old WT mice when compared with fibres from adult WT mice. This chemokine can be specifically inhibited using an RNA oligonucleotide known as emapticap (NOX-E36) and has been shown to be effective against inflammatory diseases such as type 2 diabetes and liver fibrosis murine models (Menne et al. 2017; Ehling et al. 2014).

The study in **Chapter 6**, showed that protein degradation appears to be the major factor in the loss of muscle protein with age; more specifically protein quality control with the UPR and ERAD pathways are upregulated in these muscles. To reduce the amount of protein degradation, inhibitors of the ubiquitin-proteasomal pathways could be used. Proteasome inhibitors such as ixazomib are effective in treating multiple myeloma (Kumar et al. 2016). The downside to this is the ER becomes stressed by the blocking of breakdown of misfolded proteins leading to the unfolded protein response. This is one of the leading causes of side effects associated with protease inhibitors (Nunes & Annunziata 2016) and as we have shown the ER to already be in a stressed state, this would not be ideal for treatment of sarcopenia. An alternative to proteasomal inhibition could be to relieve the ER stress leading to the upregulation of the ERAD pathway, chemical chaperones could be of use. Two of these, tauroursodeoxycholic acid and 4- phenylbutyric acid are approved by the FDA for treatment of urea cycle disorders and biliary cirrhosis (Uppala et al. 2017).

Chapter 8: References

Abb J, Abb H & Deinhardt F (1983) Phenotype of human α-interferon producing leucocytes identified by monoclonal antibodies. *Clin. Exp. Immunol.* 52, 179–184.

Acuner Ozbabacan SE, Gursoy A, Nussinov R & Keskin O (2014) The Structural Pathway of Interleukin 1 (IL-1) Initiated Signaling Reveals Mechanisms of Oncogenic Mutations and SNPs in Inflammation and Cancer Y. Xia, ed. *PLoS Comput. Biol.* 10, e1003470. Available at: http://dx.plos.org/10.1371/journal.pcbi.1003470 [Accessed May 4, 2020].

Akdis M, Aab A, Altunbulakli C, Azkur K, Costa RA, Crameri R, Duan S, Eiwegger T, Eljaszewicz A, Ferstl R, Frei R, Garbani M, Globinska A, Hess L, Huitema C, Kubo T, Komlosi Z, Konieczna P, Kovacs N, Kucuksezer UC, Meyer N, Morita H, Olzhausen J, O'Mahony L, Pezer M, Prati M, Rebane A, Rhyner C, Rinaldi A, Sokolowska M, Stanic B, Sugita K, Treis A, van de Veen W, Wanke K, Wawrzyniak M, Wawrzyniak P, Wirz OF, Zakzuk JS & Akdis CA (2016) Interleukins (from IL-1 to IL-38), interferons, transforming growth factor β, and TNF-α: Receptors, functions, and roles in diseases. *J. Allergy Clin. Immunol.* 138, 984–1010.

Almaden J V., Tsui R, Liu YC, Birnbaum H, Shokhirev MN, Ngo KA, Davis-Turak JC, Otero D, Basak S, Rickert RC & Hoffmann A (2014) A Pathway Switch Directs BAFF Signaling to Distinct NFκB Transcription Factors in Maturing and Proliferating B Cells. *Cell Rep.* 9, 2098–2111.

Altun M, Besche HC, Overkleeft HS, Piccirillo R, Edelmann MJ, Kessler BM, Goldberg AL & Ulfhake B (2010) Muscle wasting in aged, sarcopenic rats is associated with enhanced activity of the ubiquitin proteasome pathway. *J. Biol. Chem.* 285, 39597–608. Available at: http://www.ncbi.nlm.nih.gov/pubmed/20940294 [Accessed July 8, 2019].

Anderson CF & Mosser DM (2002) A novel phenotype for an activated macrophage: the type 2 activated macrophage. *J. Leukoc. Biol.* 72, 101–6. Available at: http://www.ncbi.nlm.nih.gov/pubmed/12101268 [Accessed May 15, 2020].

Anfinsen CB (1973) *Principles that Govern the Folding of Protein Chains*,

Anisimova AS, Alexandrov AI, Makarova NE, Gladyshev VN & Dmitriev SE (2018) Protein synthesis and quality control in aging. *Aging (Albany. NY).* 10, 4269–4288.

Ansel KM, Ngo VN, Hyman PL, Luther SA, Förster R, Sedgwlck JD, Browning JL, Upp M & Cyster JG (2000) A chemokine-driven positive feedback loop organizes lymphoid follicles. *Nature* 406, 309–314.

Araki-Sasaki K, Tanaka T, Ebisuno Y, Kanda H, Umemoto E, Hayashi K & Miyasaka M (2006) Dynamic expression of chemokines and the infiltration of inflammatory cells in the HSV-infected cornea and its associated tissues. *Ocul. Immunol. Inflamm.* 14, 257–266.

Arend WP (2002) The balance between IL-1 and IL-1Ra in disease. *Cytokine Growth Factor Rev.* 13, 323–340.

Arimont M, Hoffmann C, de Graaf C & Leurs R (2019) Chemokine receptor crystal structures: What can be learned from them? *Mol. Pharmacol.* 96, 765–777.

Arinobu Y, Iwasaki H, Gurish MF, Mizuno SI, Shigematsu H, Ozawa H, Tenen DG, Austen KF & Akashi K (2005) Developmental checkpoints of the basophil/mast cell lineages in adult murine hematopoiesis. *Proc. Natl. Acad. Sci. U. S. A.* 102, 18105–18110.

Arizono N, Koreto O, Iwai Y, Hidaka T & Takeoka O (1984) MORPHOMETRIC ANALYSIS OF HUMAN NEUROMUSCULAR JUNCTION IN DIFFERENT AGES. *Pathol. Int.* 34, 1243–1249.

Armitage RJ (1994) Tumor necrosis factor receptor superfamily members and their ligands. *Curr. Opin. Immunol.* 6, 407–413.

Armstrong RB (1984) Mechanisms of exercise-induced delayed onset muscular soreness: A brief review. *Med. Sci. Sports Exerc.* 16, 529–538.

Aronica MA, Mora AL, Mitchell DB, Finn PW, Johnson JE, Sheller JR & Boothby MR (1999) Preferential role for NF-κB/Rel signaling in the type 1 but not type2 T cell-dependent immune response in

vivo. *J. Immunol.* 163, 5116–5124.

Ashall L, Horton CA, Nelson DE, Paszek P, Harper C V, Sillitoe K, Ryan S, Spiller DG, Unitt JF, Broomhead DS, Kell DB, Rand DA, Sée V & White MRH (2009) Pulsatile stimulation determines timing and specificity of NF-κB-dependent transcription. *Science (80-.).* 324, 242–246.

Asseman C, Mauze S, Leach MW, Coffman RL & Powrie F (1999) An essential role for interleukin 10 in the function of regulatory T cells that inhibit intestinal inflammation. *J. Exp. Med.* 190, 995–1003.

Attaix D, Mosoni L, Dardevet D, Combaret L, Mirand PP & Grizard J (2005) Altered responses in skeletal muscle protein turnover during aging in anabolic and catabolic periods. *Int. J. Biochem. Cell Biol.* 37, 1962–1973.

Attaix D & Taillandier D (1998) *The Critical Role of the Ubiquitin-Proteasome Pathway in Muscle Wasting in Comparison to Lysosomal and Ca2+-Dependent Systems*,

Au Y (2004) The muscle ultrastructure: A structural perspective of the sarcomere. *Cell. Mol. Life Sci.* 61, 3016–3033.

Axe EL, Walker SA, Manifava M, Chandra P, Roderick HL, Habermann A, Griffiths G & Ktistakis NT (2008) Autophagosome formation from membrane compartments enriched in phosphatidylinositol 3-phosphate and dynamically connected to the endoplasmic reticulum. *J. Cell Biol.* 182, 685–701.

Baker DJ, Childs BG, Durik M, Wijers ME, Sieben CJ, Zhong J, A. Saltness R, Jeganathan KB, Verzosa GC, Pezeshki A, Khazaie K, Miller JD & Van Deursen JM (2016) Naturally occurring p16 Ink4a-positive cells shorten healthy lifespan. *Nature* 530, 184–189. Available at: https://www.nature.com/articles/nature16932 [Accessed November 1, 2020].

Baker DJ, Wijshake T, Tchkonia T, Lebrasseur NK, Childs BG, Van De Sluis B, Kirkland JL & Van Deursen JM (2011) Clearance of p16 Ink4a-positive senescent cells delays ageing-associated disorders. *Nature* 479, 232–236. Available at: https://www.nature.com/articles/nature10600 [Accessed

November 1, 2020].

Bakkar N, Wang J, Ladner KJ, Wang H, Dahlman JM, Carathers M, Acharyya S, Rudnicki MA, Hollenbach AD & Guttridge DC (2013) IKK/NF-kB regulates skeletal myogenesis via a signaling switch to inhibit differentiation and promote mitochondrial biogenesis. *J. Cell Biol.* 202, 825.

Balagopal P, Ljungqvist O & Nair KS (1997) Skeletal muscle myosin heavy-chain synthesis rate in healthy humans. *Am. J. Physiol. - Endocrinol. Metab.* 272.

Balagopal P, Rooyackers OE, Adey DB, Ades PA & Nair KS (2017) Effects of aging on in vivo synthesis of skeletal muscle myosin heavy-chain and sarcoplasmic protein in humans. *Am. J. Physiol. Metab.* 273, E790–E800. Available at: http://www.physiology.org/doi/10.1152/ajpendo.1997.273.4.E790 [Accessed July 6, 2019].

Baldwin AS (1996) THE NF-κB AND IκB PROTEINS: New Discoveries and Insights. *Annu. Rev. Immunol.* 14, 649–681.

Bao M & Liu YJ (2013) Regulation of TLR7/9 signaling in plasmacytoid dendritic cells. *Protein Cell* 4, 40–52.

Bar-Shai M, Carmeli E, Coleman R, Rozen N, Perek S, Fuchs D & Reznick AZ (2005) The effect of hindlimb immobilization on acid phosphatase, metalloproteinases and nuclear factor-κB in muscles of young and old rats. *Mech. Ageing Dev.* 126, 289–297.

Bárány M (1967) ATPase activity of myosin correlated with speed of muscle shortening. *J. Gen. Physiol.* 50. Available at: https://rupress.org/jgp/article-pdf/50/6/197/593273/197.pdf [Accessed March 9, 2020].

Barbieri M, Ferrucci L, Ragno E, Corsi A, Bandinelli S, Bonafé M, Olivieri F, Giovagnetti S, Franceschi C, Guralnik JM & Paolisso G (2003) Chronic inflammation and the effect of IGF-I on muscle strength and power in older persons. *Am. J. Physiol. - Endocrinol. Metab.* 284, 481–487. Available at: http://www.ajpendo.org [Accessed September 23, 2020].

Barczewski AH, Ragusa MJ, Mierke DF & Pellegrini M (2019) The IKK-binding domain of NEMO is an irregular coiled coil with a dynamic binding interface. *Sci. Rep.* 9, 1–13.

Barlan K & Gelfand VI (2017) Microtubule-based transport and the distribution, tethering, and organization of organelles. *Cold Spring Harb. Perspect. Biol.* 9.

Barthlott T, Moncrieffe H, Veldhoen M, Atkins CJ, Christensen J, O'Garra A & Stockinger B (2005) CD25+CD4+ T cells compete with naive CD4+ T cells for IL-2 and exploit it for the induction of IL-10 production. *Int. Immunol.* 17, 279–288.

Bauernfeind FG, Horvath G, Stutz A, Alnemri ES, MacDonald K, Speert D, Fernandes-Alnemri T, Wu J, Monks BG, Fitzgerald KA, Hornung V & Latz E (2009) Cutting Edge: NF-κB Activating Pattern Recognition and Cytokine Receptors License NLRP3 Inflammasome Activation by Regulating NLRP3 Expression. *J. Immunol.* 183, 787–791.

Bautmans I, Onyema O, Van Puyvelde K, Pleck S & Mets T (2011) Grip work estimation during sustained maximal contraction: Validity and relationship with dependency and inflammation in elderly persons. *J. Nutr. Heal. Aging* 15, 731–736.

Berent-Maoz B, Piliponsky AM, Daigle I, Simon H-U & Levi-Schaffer F (2006) Human Mast Cells Undergo TRAIL-Induced Apoptosis. *J. Immunol.* 176, 2272–2278.

Bergqvist S, Croy CH, Kjaergaard M, Huxford T, Ghosh G & Komives EA (2006) Thermodynamics reveal that helix four in the NLS of NF-κB p65 anchors IκBα, forming a very stable complex. *J. Mol. Biol.* 360, 421–434.

Bernhagen J, Krohn R, Lue H, Gregory JL, Zernecke A, Koenen RR, Dewor M, Georgiev I, Schober A, Leng L, Kooistra T, Fingerle-Rowson G, Ghezzi P, Kleemann R, McColl SR, Bucala R, Hickey MJ & Weber C (2007) MIF is a noncognate ligand of CXC chemokine receptors in inflammatory and atherogenic cell recruitment. *Nat. Med.* 13, 587–596.

Beynon RJ & Pratt JM (2005) Metabolic labeling of proteins for proteomics. *Mol. Cell. Proteomics* 4,

857–872. Available at: http://www.mcponline.org [Accessed September 14, 2020].

Bianchi M, Giacomini E, Crinelli R, Radici L, Carloni E & Magnani M (2015) Dynamic transcription of ubiquitin genes under basal and stressful conditions and new insights into the multiple UBC transcript variants. *Gene* 573, 100–109.

Bicer S & Reiser PJ (2004) Myosin Light Chain 1 Isoforms in Slow Fibers from Global and Orbital Layers of Canine Rectus Muscles. *Investig. Ophthalmol. Vis. Sci.* 45, 138–143.

Biolo G, Tipton KD, Klein S & Wolfe RR (1997) An abundant supply of amino acids enhances the metabolic effect of exercise on muscle protein. *Am. J. Physiol.* 273, E122-9. Available at: http://www.ncbi.nlm.nih.gov/pubmed/9252488 [Accessed July 6, 2019].

Biswas SK & Mantovani A (2010) Macrophage plasticity and interaction with lymphocyte subsets: Cancer as a paradigm. *Nat. Immunol.* 11, 889–896.

Blenck CL, Harvey PA, Reckelhoff JF & Leinwand LA (2016) The importance of biological sex and estrogen in rodent models of cardiovascular Health and Disease. *Circ Res* 118, 1294–1312.

Bodine SC, Latres E, Baumhueter S, Lai VK, Nunez L, Clarke BA, Poueymirou WT, Panaro FJ, Na E, Dharmarajan K, Pan ZQ, Valenzuela DM, DeChiara TM, Stitt TN, Yancopoulos GD & Glass DJ (2001) Identification of ubiquitin ligases required for skeletal muscle atrophy. *Science* 294, 1704–8. Available at: http://www.ncbi.nlm.nih.gov/pubmed/11679633 [Accessed July 8, 2019].

Bonaldo P & Sandri M (2013) Cellular and molecular mechanisms of muscle atrophy. *DMM Dis. Model. Mech.* 6, 25–39.

Bonecchi R & Graham GJ (2016) Atypical chemokine receptors and their roles in the resolution of the inflammatory response. *Front. Immunol.* 7.

Bonfante H de L, Almeida C de S, Abramo C, Grunewald STF, Levy RA & Teixeira HC (2017) CCL2, CXCL8, CXCL9 and CXCL10 serum levels increase with age but are not altered by treatment with

hydroxychloroquine in patients with osteoarthritis of the knees. *Int. J. Rheum. Dis.* 20, 1958–1964.

Boraschi D, Lucchesi D, Hainzl S, Leitner M, Maier E, Mangelberger D, Oostingh GJ, Pfaller T, Pixner C, Posselt G, Italiani P, Nold MF, Nold-Petry CA, Bufler P & Dinarello CA (2011) IL-37: A new anti-inflammatory cytokine of the IL-1 family. *Eur. Cytokine Netw.* 22, 127–147.

Bowman JD & Lindert S (2019) Computational Studies of Cardiac and Skeletal Troponin. *Front. Mol. Biosci.* 6, 1–7.

Bradshaw MJ, Bhattacharyya S, Venna N & Cahill JF (2020) Neurologic Manifestations of Systemic Rheumatologic Diseases. *Curr. Clin. Neurol.*, 321–342.

Bratton D & Henson P (2011) Neutrophil clearance: when the party is over, clean-up begins. *Trends Immunol.* 32, 350–357. Available at: http://www.sciencedirect.com/science/article/pii/S1471490611000779.

Braunersreuther V, Pellieux C, Pelli G, Burger F, Steffens S, Montessuit C, Weber C, Proudfoot A, Mach F & Arnaud C (2010) Chemokine CCL5/RANTES inhibition reduces myocardial reperfusion injury in atherosclerotic mice. *J. Mol. Cell. Cardiol.* 48, 789–798. Available at: http://dx.doi.org/10.1016/j.yjmcc.2009.07.029.

Breen L, Stokes KA, Churchward-Venne TA, Moore DR, Baker SK, Smith K, Atherton PJ & Phillips SM (2013) Two Weeks of Reduced Activity Decreases Leg Lean Mass and Induces "Anabolic Resistance" of Myofibrillar Protein Synthesis in Healthy Elderly. *J. Clin. Endocrinol. Metab.* 98, 2604–2612. Available at: https://academic.oup.com/jcem/article/98/6/2604/2537326 [Accessed July 7, 2019].

Bren GD, Solan NJ, Miyoshi H, Pennington KN, Pobst LJ & Paya C V. (2001) Transcription of the RelB gene is regulated by NF-κB. *Oncogene* 20, 7722–7733.

Brigitte M, Schilte C, Plonquet A, Baba-Amer Y, Henri A, Charlier C, Tajbakhsh S, Albert M, Gherardi RK

& Chrétien F (2010) Muscle resident macrophages control the immune cell reaction in a mouse model of notexin-induced myoinjury. *Arthritis Rheum.* 62, 268–279.

Briney B, Inderbitzin A, Joyce C & Burton DR (2019) Commonality despite exceptional diversity in the baseline human antibody repertoire. *Nature* 566, 393–397.

Brooks S V. & Faulkner JA (1988) Contractile properties of skeletal muscles from young, adult and aged mice. *J. Physiol.* 404, 71–82.

Brooks S V. & Faulkner JA (1990) Contraction-induced injury: Recovery of skeletal muscles in young and old mice. *Am. J. Physiol. - Cell Physiol.* 258.

Bruusgaard JC, Liestøl K, Ekmark M, Kollstad K & Gundersen K (2003) Number and spatial distribution of nuclei in the muscle fibres of normal mice studied in vivo. *J. Physiol.* 551, 467–78. Available at: http://www.ncbi.nlm.nih.gov/pubmed/12813146 [Accessed September 9, 2019].

Brzoska E, Kowalewska M, Markowska-Zagrajek A, Kowalski K, Archacka K, Zimowska M, Grabowska I, Czerwińska AM, Czarnecka-Góra M, Stremińska W, Jańczyk-Ilach K & Ciemerych MA (2012) Sdf-1 (CXCL12) improves skeletal muscle regeneration via the mobilisation of Cxcr4 and CD34 expressing cells. *Biol. Cell* 104, 722–737.

Burd NA, Gorissen SH & Van Loon LJC (2013) Anabolic resistance of muscle protein synthesis with aging. *Exerc. Sport Sci. Rev.* 41, 169–173.

Burke RE, Levine DN, Zajac FE, Tsairis P & Engel WK (1971) Spectively, With the Lethal Products Taken As Recombinants Carrying Both. *Science (80-.).* 174, 709–712.

Burke SJ, Lu D, Sparer TE, Masi T, Goff MR, Karlstad MD & Collier JJ (2014) NF-κB and STAT1 control CXCL1 and CXCL2 gene transcription. *Am. J. Physiol. - Endocrinol. Metab.* 306, E131. Available at: /pmc/articles/PMC3920007/?report=abstract [Accessed September 7, 2020].

Burks TN & Cohn RD (2011) One size may not fit all: Anti-aging therapies and sarcopenia. *Aging*

(Albany. NY). 3, 1142–1153.

Burns JM, Summers BC, Wang Y, Melikian A, Berahovich R, Miao Z, Penfold MET, Sunshine MJ, Littman DR, Kuo CJ, Wei K, McMaster BE, Wright K, Howard MC & Schall TJ (2006) A novel chemokine receptor for SDF-1 and I-TAC involved in cell survival, cell adhesion, and tumor development. *J. Exp. Med.* 203, 2201–2213.

Busch R, Kim YK, Neese RA, Schade-Serin V, Collins M, Awada M, Gardner JL, Beysen C, Marino ME, Misell LM & Hellerstein MK (2006) Measurement of protein turnover rates by heavy water labeling of nonessential amino acids. *Biochim. Biophys. Acta - Gen. Subj.* 1760, 730–744.

Busuttil RA, Garcia AM, Cabrera C, Rodriguez A, Suh Y, Kim WH, Huang TT & Vijg J (2005) Organ-specific increase in mutation accumulation and apoptosis rate in CuZn-superoxide dismutase-deficient mice. *Cancer Res.* 65, 11271–11275. Available at: www.aacrjournals.org [Accessed October 18, 2020].

Cai D, Frantz JD, Tawa NE, Melendez PA, Oh BC, Lidov HGW, Hasselgren PO, Frontera WR, Lee J, Glass DJ & Shoelson SE (2004) IKKβ/NF-κB activation causes severe muscle wasting in mice. *Cell* 119, 285–298.

Caiozzo VJ, Baker MJ, Huang K, Chou H, Wu YZ & Baldwin KM (2003) Single-fiber myosin heavy chain polymorphism: How many patterns and what proportions? *Am. J. Physiol. - Regul. Integr. Comp. Physiol.* 285, R570–R580. Available at: https://www.physiology.org/doi/10.1152/ajpregu.00646.2002 [Accessed March 9, 2020].

Campbell MJ, McComas AJ & Petito F (1973) Physiological changes in ageing muscles. *J. Neurol. Neurosurg. Psychiatry* 36, 174–182.

Carlson BM & Faulkner JA (1989) Muscle transplantation between young and old rats: Age of host determines recovery. *Am. J. Physiol. - Cell Physiol.* 256.

Carruth LM, Demczuk S & Mizel SB (1991) Involvement of a calpain-like protease in the processing of

the murine interleukin 1α precursor. *J. Biol. Chem.* 266, 12162–12167.

Carswell EA, Old LJ, Kassel RL, Green S, Fiore N & Williamson B (1975) An endotoxin induced serum factor that cuases necrosis of tumors. *Proc. Natl. Acad. Sci. U. S. A.* 72, 3666–3670.

Catoire M, Mensink M, Kalkhoven E, Schrauwen P & Kersten S (2014) Identification of human exercise-induced myokines using secretome analysis. *Physiol. Genomics* 46, 256–267. Available at: https://www.physiology.org/doi/10.1152/physiolgenomics.00174.2013 [Accessed July 6, 2020].

Center DM, Kornfeld Cruikshank HW, Brazer W, Natke B, Zhang Y, Keane J, Nicoll J, Kim S & H Wu DM (1998) *Human and Murine IL-16 Conservation of Structure and Function Between*, Available at: http://www.jimmunol.org/content/160/12/5945 [Accessed May 20, 2020].

Chambers MC, MacLean B, Burke R, Amodei D, Ruderman DL, Neumann S, Gatto L, Fischer B, Pratt B, Egertson J, Hoff K, Kessner D, Tasman N, Shulman N, Frewen B, Baker TA, Brusniak MY, Paulse C, Creasy D, Flashner L, Kani K, Moulding C, Seymour SL, Nuwaysir LM, Lefebvre B, Kuhlmann F, Roark J, Rainer P, Detlev S, Hemenway T, Huhmer A, Langridge J, Connolly B, Chadick T, Holly K, Eckels J, Deutsch EW, Moritz RL, Katz JE, Agus DB, MacCoss M, Tabb DL & Mallick P (2012) A cross-platform toolkit for mass spectrometry and proteomics. *Nat. Biotechnol.* 30, 918–920. Available at: /pmc/articles/PMC3471674/?report=abstract [Accessed September 21, 2020].

Chan RYY, Boudreau-Larivière C, Angus LM, Mankal FA & Jasmin BJ (1999) An intronic enhancer containing an N-box motif is required for synapse- and tissue-specific expression of the acetylcholinesterase gene in skeletal muscle fibers. *Proc. Natl. Acad. Sci. U. S. A.* 96, 4627–4632.

Chanaday NL, Cousin MA, Milosevic I, Watanabe S & Morgan JR (2019) The synaptic vesicle cycle revisited: New insights into the modes and mechanisms. *J. Neurosci.* 39, 8209–8216.

Charles JP, Cappellari O, Spence AJ, Hutchinson JR & Wells DJ (2016) Musculoskeletal geometry, muscle architecture and functional specialisations of the mouse hindlimb. *PLoS One* 11.

Chaweewannakorn C, Tsuchiya M, Koide M, Hatakeyama H, Tanaka Y, Yoshida S, Sugawara S, Hagiwara

Y, Sasaki K & Kanzaki M (2018) Roles of il-1α/β in regeneration of cardiotoxin-injured muscle and satellite cell function. *Am. J. Physiol. - Regul. Integr. Comp. Physiol.* 315, R90-R103,.

Chen W, Nyasha MR, Koide M, Tsuchiya M, Suzuki N, Hagiwara Y, Aoki M & Kanzaki M (2019) In vitro exercise model using contractile human and mouse hybrid myotubes. *Sci. Rep.* 9. Available at: https://doi.org/10.1038/s41598-019-48316-9 [Accessed July 7, 2020].

Cheng H, Fan C, Zhang S-W, Wu Z-S, Cui Z-C, Melcher K, Zhang C-H, Jiang Y, Cong Y & Xu E (2015) Crystallization scale purification of α7 nicotinic acetylcholine receptor from mammalian cells using a BacMam expression system. *Nat. Publ. Gr.* 36, 1013–1023. Available at: www.chinaphar.com [Accessed March 9, 2020].

Cheng M, Nguyen MH, Fantuzzi G & Koh TJ (2008) Endogenous interferon-γ is required for efficient skeletal muscle regeneration. *Am. J. Physiol. - Cell Physiol.* 294, 1183–1191.

Ciechanover A & Kwon YT (2017) Protein quality control by molecular chaperones in neurodegeneration. *Front. Neurosci.* 11, 185.

Clark KA, McElhinny AS, Beckerle MC & Gregorio CC (2002) Striated Muscle Cytoarchitecture: An Intricate Web of Form and Function. *Annu. Rev. Cell Dev. Biol.* 18, 637–706.

Claydon AJ, Thom MD, Hurst JL & Beynon RJ (2012) Protein turnover: Measurement of proteome dynamics by whole animal metabolic labelling with stable isotope labelled amino acids. *Proteomics* 12, 1194–1206. Available at: www.proteomics-journal.com [Accessed September 14, 2020].

Clore GM & Gronenborn AM (1995) Three-dimensional structures of α and β chemokines. *FASEB J.* 9, 57–62.

Cobley JN, Moult PR, Burniston JG, Morton JP & Close GL (2015) Exercise improves mitochondrial and redox-regulated stress responses in the elderly: better late than never! *Biogerontology* 16, 249–264.

Coll JL, Ben-Ze'ev A, Ezzell RM, Rodríguez Fernández JL, Baribault H, Oshima RG & Adamson ED (1995) Targeted disruption of vinculin genes in F9 and embryonic stem cells changes cell morphology, adhesion, and locomotion. *Proc. Natl. Acad. Sci. U. S. A.* 92, 9161–9165.

Couper KN, Blount DG & Riley EM (2008) IL-10: The Master Regulator of Immunity to Infection. *J. Immunol.* 180, 5771–5777.

Cramer P (2019) Organization and regulation of gene transcription. *Nature* 573, 45–54.

Črešnar B, Črne-Finderle N, Breskvar K & Sketelj J (1994) Neural regulation of muscle acetylcholinesterase is exerted on the level of its mRNA. *J. Neurosci. Res.* 38, 294–299.

Crimi E, Chiaramondia M, Milanese M, Rossi GA & Brusasco V (1991) Increased numbers of mast cells in bronchial mucosa after the late-phase asthmatic response to allergen. *Am. Rev. Respir. Dis.* 144, 1282–1286.

Croy CH, Bergqvist S, Huxford T, Ghosh G & Komives EA (2004) Biophysical characterization of the free IκBα ankyrin repeat domain in solution. *Protein Sci.* 13, 1767–1777.

Cruz-Jentoft AJ & Sayer AA (2019) Sarcopenia. *Lancet* 393, 2636–2646. Available at: https://www.thelancet.com/journals/lancet/article/PIIS0140-6736(19)31138-9/fulltext?rss=yes [Accessed September 4, 2019].

Cui CY, Driscoll RK, Piao Y, Chia CW, Gorospe M & Ferrucci L (2019) Skewed macrophage polarization in aging skeletal muscle. *Aging Cell* 18. Available at: https://doi.org/10.1111/acel.13032 [Accessed September 21, 2020].

Cupovic J, Onder L, Gil-Cruz C & Rü T (2016) Central Nervous System Stromal Cells Control Local CD8 + T Cell Responses during Virus-Induced Neuroinflammation. *Immunity* 44, 622–633. Available at: http://dx.doi.org/10.1016/j.immuni.2015.12.022 [Accessed May 19, 2020].

Curiel-Lewandrowski C, Yamasaki H, Si CP, Jin X, Zhang Y, Richmond J, Tuzova M, Wilson K, Sullivan B,

Jones D, Ryzhenko N, Little F, Kupper TS, Center DM & Cruikshank WW (2011) Loss of nuclear pro-IL-16 facilitates cell cycle progression in human cutaneous T cell lymphoma. *J. Clin. Invest.* 121, 4838–4849.

Curtis E, Litwic A, Cooper C & Dennison E (2015) Determinants of Muscle and Bone Aging. *J. Cell. Physiol.* 230, 2618–25.

Cuthbertson D, Smith K, Babraj J, Leese G, Waddell T, Atherton P, Wackerhage H, Taylor PM & Rennie MJ (2005) Anabolic signaling deficits underlie amino acid resistance of wasting, aging muscle. *FASEB J.* 19, 1–22. Available at: https://www.researchgate.net/publication/224100006 [Accessed July 6, 2019].

Dahlman JM, Wang J, Bakkar N & Guttridge DC (2009) The RelA/p65 subunit of NF-κB specifically regulates cyclin D1 protein stability: Implications for cell cycle withdrawal and skeletal myogenesis. *J. Cell. Biochem.* 106, 42–51.

Dancey JT, Deubelbeiss KA, Harker LA & Finch CA (1976) Neutrophil kinetics in man. *J. Clin. Invest.* 58, 705–715.

Dani JA (2016) Neuronal Nicotinic Acetylcholine Receptor Structure and Function and Response to Nicotine. *Int. Rev. Neurobiol.* 124, 3–19.

Das A, Heesters BA, Bialas A, O'Flynn J, Rifkin IR, Ochando J, Mittereder N, Carlesso G, Herbst R & Carroll MC (2017) Follicular Dendritic Cell Activation by TLR Ligands Promotes Autoreactive B Cell Responses. *Immunity* 46, 106–119.

Deaton AM & Bird A (2011) CpG islands and the regulation of transcription. *Genes Dev.* 25, 1010–1022.

Debès C, Grönke S, Karalay Ö, Tain L, Nakamura S, Hahn O, Weigelt C, Zirkel A, Sofiadis K, Brant L, Wollnik B, Kubacki T, Späth M, Schermer B, Benzing T, Müller RU, Papantonis A, Antebi A, Partridge L & Beyer A (2019) Aging-associated changes in transcriptional elongation influence metazoan longevity. *bioRxiv*.

Deepa SS, Bhaskaran S, Espinoza S, Brooks S V., McArdle A, Jackson MJ, Van Remmen H & Richardson A (2017) A new mouse model of frailty: the Cu/Zn superoxide dismutase knockout mouse. *GeroScience* 39, 187–198.

Deepa SS, Van Remmen H, Brooks S V., Faulkner JA, Larkin L, McArdle A, Jackson MJ, Vasilaki A & Richardson A (2019) Accelerated sarcopenia in Cu/Zn superoxide dismutase knockout mice. *Free Radic. Biol. Med.* 132, 19–23.

Dejardin E, Droin NM, Delhase M, Haas E, Cao Y, Makris C, Li Z, Karin M, Ware CF, Green DR & Diego S (2002) The Lymphotoxin-b Receptor Induces Different Patterns of Gene Expression via Two NF-kB Pathways University of California San Diego. 17, 525–535.

Delbono O (2003) Neural control of aging skeletal muscle. *Aging Cell* 2, 21–29.

Demirel HA, Hamilton KL, Shanely RA, Tümer N, Koroly MJ & Powers SK (2003) Age and attenuation of exercise-induced myocardial HSP72 accumulation. *Am. J. Physiol. - Hear. Circ. Physiol.* 285, 1609–1615.

Demontis F, Piccirillo R, Goldberg AL & Perrimon N (2013) Mechanisms of skeletal muscle aging: Insights from Drosophila and mammalian models. *DMM Dis. Model. Mech.* 6, 1339–1352.

Deveraux Q, Van Nocker S, Mahaffey D, Vierstra R & Rechsteiner M (1995) Inhibition of ubiquitin-mediated proteolysis by the Arabidopsis 26 S protease subunit S5a. *J. Biol. Chem.* 270, 29660–29663.

Deyhle MR, Gier AM, Evans KC, Eggett DL, Nelson WB, Parcell AC & Hyldahl RD (2016) Skeletal Muscle Inflammation Following Repeated Bouts of Lengthening Contractions in Humans. *Front. Physiol.* 6, 424. Available at: http://journal.frontiersin.org/Article/10.3389/fphys.2015.00424/abstract [Accessed July 29, 2020].

Deyhle MR, Hafen PS, Parmley J, Preece CN, Robison M, Sorensen JR, Jackson B, Eggett DL, Hancock CR & Hyldahl RD (2018) CXCL10 increases in human skeletal muscle following damage but is not

necessary for muscle regeneration. *Physiol. Rep.* 6. Available at: /pmc/articles/PMC5917067/?report=abstract [Accessed July 6, 2020].

DiDonato J, Mercurio F, Rosette C, Wu-Li J, Suyang H, Ghosh S & Karin M (1996) Mapping of the inducible IkappaB phosphorylation sites that signal its ubiquitination and degradation. *Mol. Cell. Biol.* 16, 1295–1304.

Dill KA & MacCallum JL (2012) The protein-folding problem, 50 years on. *Science (80-.).* 338, 1042–1046.

Dom Inguez PM, Gonz Alez-Cintado L, Del Fresno C, Mart P, Mart Inez Del Hoyo G & Ardav C (2013) IL-4 blocks T H 1-polarizing/inflammatory cytokine gene expression during monocyte-derived dendritic cell differentiation through histone hypoacetylation. Available at: http://dx.doi.org/10.1016/j.jaci.2013.08.039 [Accessed May 20, 2020].

Dougan M, Dranoff G & Dougan SK (2019) GM-CSF, IL-3, and IL-5 Family of Cytokines: Regulators of Inflammation. *Immunity* 50, 796–811.

Draper MH & Hodge AJ (1949) Sub-microscopic localization of minerals in skeletal muscle by internal "micro-incineration" within the electron microscope. *Nature* 163, 576–577. Available at: http://www.nature.com/articles/163576a0 [Accessed March 2, 2020].

Du Y, Wang X, Xie H, Zheng S, Wu X, Zhu X, Zhang X, Xue S, Li H, Hong W, Tang W, Chen M, Cheng Q & Sun J (2019) Sex differences in the prevalence and adverse outcomes of sarcopenia and sarcopenic obesity in community dwelling elderly in East China using the AWGS criteria. *BMC Endocr. Disord.* 19, 1–11.

Durham WJ, Li YP, Gerken E, Farid M, Arbogast S, Wolfe RR & Reid MB (2004) Fatiguing exercise reduces DNA binding activity of NF-κB in skeletal muscle nuclei. *J. Appl. Physiol.* 97, 1740–1745.

Von Der Ecken J, Müller M, Lehman W, Manstein DJ, Penczek PA & Raunser S (2015) Structure of the F-actin-tropomyosin complex HHS Public Access. *Nature* 519, 114–117. Available at:

www.nature.com/reprints. [Accessed March 4, 2020].

Ehling J, Bartneck M, Wei X, Gremse F, Fech V, Möckel D, Baeck C, Hittatiya K, Eulberg D, Luedde T, Kiessling F, Trautwein C, Lammers T & Tacke F (2014) CCL2-dependent infiltrating macrophages promote angiogenesis in progressive liver fibrosis. *Gut* 63, 1960–1971.

Elchuri S, Oberley TD, Qi W, Eisenstein RS, Roberts LJ, Van Remmen H, Epstein CJ & Huang TT (2005) CuZnSOD deficiency leads to persistent and widespread oxidative damage and hepatocarcinogenesis later in life. *Oncogene* 24, 367–380. Available at: www.nature.com/onc [Accessed October 18, 2020].

Eletr ZM & Wilkinson KD (2014) Regulation of proteolysis by human deubiquitinating enzymes. *Biochim. Biophys. Acta - Mol. Cell Res.* 1843, 114–128.

Elsasser S & Finley D (2005) Delivery of ubiquitinated substrates to protein-unfolding machines. *Nat. Cell Biol.* 7, 742–749.

Evans WJ & Grimby G (1995) Muscle Performance and Structure in the Elderly as Studied Cross-sectionally and Longitudinally. *Journals Gerontol. Ser. A Biol. Sci. Med. Sci.* 50A, 17–22.

Faulkner JA, Larkin LM, Claflin DR & Brooks S V. (2007) Age-related changes in the structure and function of skeletal muscles. *Clin. Exp. Pharmacol. Physiol.* 34, 1091–1096.

Fenteany G, Gaur P, Sharma G, Pintér L, Kiss E & Haracska L (2020) Robust high-throughput assays to assess discrete steps in ubiquitination and related cascades. *BMC Mol. Cell Biol.* 21, 21. Available at: https://bmcmolcellbiol.biomedcentral.com/articles/10.1186/s12860-020-00262-5 [Accessed June 4, 2020].

Ferrington DA, Husom AD & Thompson L V (2005) Altered proteasome structure, function, and oxidation in aged muscle. *FASEB J.* 19, 644–646. Available at: www.fasebj.orgbyUniversity [Accessed April 17, 2019].

Ferrucci L & Fabbri E (2018) Inflammageing: chronic inflammation in ageing, cardiovascular disease, and frailty. *Nat. Rev. Cardiol.* 15, 505–522. Available at: /pmc/articles/PMC6146930/?report=abstract [Accessed June 29, 2020].

Ferrucci L, Penninx BWJH, Volpato S, Harris TB, Bandeen-Roche K, Balfour J, Leveille SG, Fried LP & Guralnik JM (2002) Change in muscle strength explains accelerated decline of physical function in older women with high interleukin-6 serum levels. *J. Am. Geriatr. Soc.* 50, 1947–1954.

Fillatreau S, Sweenie CH, McGeachy MJ, Gray D & Anderton SM (2002) B cells regulate autoimmunity by provision of IL-10. *Nat. Immunol.* 3, 944–950.

Folker ES & Baylies MK (2013) *Nuclear positioning in muscle development and disease*, Frontiers Media SA. Available at: http://www.ncbi.nlm.nih.gov/pubmed/24376424 [Accessed September 9, 2019].

Folz RJ, Abushamaa AM & Suliman HB (1999) Extracellular superoxide dismutase in the airways of transgenic mice reduces inflammation and attenuates lung toxicity following hyperoxia. *J. Clin. Invest.* 103, 1055–1066.

Da Fonseca PCA & Morris EP (2008) Structure of the human 26S proteasome: Subunit radial displacements open the gate into the proteolytic core. *J. Biol. Chem.* 283, 23305–23314.

Forthal DN (2014) Functions of Antibodies. *Microbiol. Spectr.* 2, 1.

Franceschi C, Bonafe M & Valensin S (2000) An evolutionary perspective on Immunosenescence. *Ann. N. Y. Acad. Sci.* 908, 244–254.

Friedrich B, Quensel C, Sommer T, Hartmann E & Kohler M (2006) Nuclear Localization Signal and Protein Context both Mediate Importin specificity of Nuclear Import Substrates. *Mol. Cell. Biol.* 26, 8697–8709.

Frontera WR, Hughes VA, Fielding RA, Fiatarone MA, Evans WJ & Roubenoff R (2000) Aging of skeletal

muscle: A 12-yr longitudinal study. *J. Appl. Physiol.* 88, 1321–1326.

Frontera WR & Ochala J (2015) Skeletal Muscle: A Brief Review of Structure and Function. *Behav. Genet.* 45, 183–195. Available at: http://link.springer.com/10.1007/s00223-014-9915-y [Accessed January 15, 2019].

Fry CS, Drummond MJ, Glynn EL, Dickinson JM, Gundermann DM, Timmerman KL, Walker DK, Volpi E & Rasmussen BB (2013) Skeletal muscle autophagy and protein breakdown following resistance exercise are similar in younger and older adults. *J. Gerontol. A. Biol. Sci. Med. Sci.* 68, 599–607. Available at: http://www.ncbi.nlm.nih.gov/pubmed/23089333 [Accessed July 7, 2019].

Fry CS, Nayeem SZ, Dillon EL, Sarkar PS, Tumurbaatar B, Urban RJ, Wright TJ, Sheffield-Moore M, Tilton RG & Choudhary S (2016) Glucocorticoids increase skeletal muscle NF-κB inducing kinase (NIK): Links to muscle atrophy. *Physiol. Rep.* 4, 1–13.

Fujita T, Nolan GP, Liou HC, Scott ML & Baltimore D (1993) The candidate proto-oncogene bcl-3 encodes a transcriptional coactivator that activates through NF-κB p50 homodimers. *Genes Dev.* 7, 1354–1363.

Furtado GC, De Curotto Lafaille MA, Kutchukhidze N & Lafaille JJ (2002) Interleukin 2 signaling is required for CD4+ regulatory T cell function. *J. Exp. Med.* 196, 851–857.

Gammeren D, Damrauer JS, Jackman RW & Kandarian SC (2009) The IκB kinases IKKα and IKKβ are necessary and sufficient for skeletal muscle atrophy. *FASEB J.* 23, 362–370.

Garcia-Faroldi G, Melo FR, Rönnberg E, Grujic M & Pejler G (2013) Active Caspase-3 Is Stored within Secretory Compartments of Viable Mast Cells. *J. Immunol.* 191, 1445–1452.

Gazzinelli-Guimarães PH, Bonne-Année S, Fujiwara RT, Santiago HC & Nutman TB (2016) Allergic Sensitization Underlies Hyperreactive Antigen-Specific CD4 + T Cell Responses in Coincident Filarial Infection . *J. Immunol.* 197, 2772–2779.

Ge X, Cho A, Ciol MA, Pettan-Brewer C, Snyder J, Rabinovitch P & Ladiges W (2016) Grip strength is potentially an early indicator of age-related decline in mice. *Pathobiol. Aging Age-related Dis.* 6, 32981.

Gearing AJH, Beckett P, Christodoulou M, Churchill M, Clements JM, Crimmin M, Davidson AH, Drummond AH, Galloway WA, Gilbert R, Gordon JL, Leber TM, Mangan M, Miller K, Nayee P, Owen K, Patel S, Thomas W & Wells G (1995) Matrix metalloproteinases and processing of pro-TNF-α. *J. Leukoc. Biol.* 57, 774–777. Available at: http://doi.wiley.com/10.1002/jlb.57.5.774 [Accessed May 1, 2020].

Gerli R, Monti D, Bistoni O, M. Mazzone A, Peri G, Cossarizza A, Di Gioacchino M, E. F. Cesarotti M, Doni A, Mantovani A, Franceschi C & Paganelli R (2001) Chemokines, sTNF-Rs and sCD30 serum levels in healthy aged people and centenarians. *Mech. Ageing Dev.* 121, 37–46.

Ghosh G, Van Duyne G, Ghosh S & Sigler PB (1995) Structure of nf-κb p50 homodimer bound to a κb site. *Nature* 373, 303–310.

Ghosh G, Wang VYF, Huang D Bin & Fusco A (2012) NF-κB regulation: Lessons from structures. *Immunol. Rev.* 246, 36–58.

Gilchrist DA, Nechaev S, Lee C, Ghosh SKB, Collins JB, Li L, Gilmour DS & Adelman K (2008) NELF-mediated stalling of Pol II can enhance gene expression by blocking promoter-proximal nucleosome assembly. *Genes Dev.* 22, 1921–1933.

Giuliano S, Guyot M, Grépin R & Pagès G (2014) The ELR+CXCL chemokines and their receptors CXCR1/CXCR2: A signaling axis and new target for the treatment of renal cell carcinoma. *Oncoimmunology* 3.

Glick D, Barth S & Macleod KF (2010) Autophagy: Cellular and molecular mechanisms. *J. Pathol.* 221, 3–12.

Gomes MD, Lecker SH, Jagoe RT, Navon A & Goldberg AL (2001) Atrogin-1, a muscle-specific F-box

protein highly expressed during muscle atrophy. *Proc. Natl. Acad. Sci. U. S. A.* 98, 14440–14445.

Gordon AM, Regnier M & Homsher E (2001) Skeletal and Cardiac Muscle Contractile Activation: Tropomyosin "Rocks and Rolls." *Physiology* 16, 49–55. Available at: https://www.physiology.org/doi/10.1152/physiologyonline.2001.16.2.49 [Accessed March 4, 2020].

Gorospe JRM, Nishikawa BK & Hoffman EP (1996) Recruitment of mast cells to muscle after mild damage. *J. Neurol. Sci.* 135, 10–17.

Greaser ML & Gergely J (1973) Purification and properties of the components from tropinin. *J. Biol. Chem.* 248, 2125–2133.

Greenfeder SA, Nunes P, Kwee L, Labow M, Chizzonite RA & Ju G (1995) Molecular cloning and characterization of a second subunit of the interleukin 1 receptor complex. *J. Biol. Chem.* 270, 13757–13765.

Greenhaff PL, Söderlund K, Ren JM & Hultman E (1993) Energy metabolism in single human muscle fibres during intermittent contraction with occluded circulation. *J. Physiol.* 460, 443–453. Available at: http://doi.wiley.com/10.1113/jphysiol.1993.sp019480 [Accessed March 9, 2020].

Gregersen N & Bross P (2010) Protein misfolding and cellular stress: An overview. *Methods Mol. Biol.* 648, 3–23.

Grimbaldeston MA, Nakae S, Kalesnikoff J, Tsai M & Galli SJ (2007) Mast cell-derived interleukin 10 limits skin pathology in contact dermatitis and chronic irradiation with ultraviolet B. *Nat. Immunol.* 8, 1095–1104.

Groisman B, Avezov E & Lederkremer GZ (2006) The E3 Ubiquitin Ligases HRD1 and SCF Fbs2 Recognize the Protein Moiety and Sugar Chains, Respectively, of an ER-Associated Degradation Substrate . *Isr. J. Chem.* 46, 189–196.

Grünberg S, Warfield L & Hahn S (2012) Architecture of the RNA polymerase II preinitiation complex and mechanism of ATP-dependent promoter opening. *Nat. Struct. Mol. Biol.* 19, 788–796.

Grune T, Catalgol B, Licht A, Ermak G, Pickering AM, Ngo JK & Davies KJA (2011) HSP70 mediates dissociation and reassociation of the 26S proteasome during adaptation to oxidative stress. *Free Radic. Biol. Med.* 51, 1355–1364. Available at: http://dx.doi.org/10.1016/j.freeradbiomed.2011.06.015.

Gschwandtner M, Derler R & Midwood KS (2019) More Than Just Attractive: How CCL2 Influences Myeloid Cell Behavior Beyond Chemotaxis. *Front. Immunol.* 10, 1–29.

Guillaume B, Chapiro J, Stroobant V, Colau D, Van Holle B, Parvizi G, Bousquet-Dubouch MP, Théate I, Parmentier N & Van Den Eynde BJ (2010) Two abundant proteasome subtypes that uniquely process some antigens presented by HLA class I molecules. *Proc. Natl. Acad. Sci. U. S. A.* 107, 18599–18604.

Gupta S (2002) Tumor necrosis factor-α-induced apoptosis in T cells from aged humans: A role of TNFR-I and downstream signaling molecules. *Exp. Gerontol.* 37, 293–299.

Ten Haaf DSMT, De Regt MF, Visser M, Witteman BJM, De Vries JHM, Eijsvogels TMH & Hopman MTE (2018) Insufficient protein intake is highly prevalent among physically active elderly. *J. Nutr. Heal. Aging* 22, 1112–1114. Available at: http://link.springer.com/10.1007/s12603-018-1075-8 [Accessed July 7, 2019].

Haak-Frendscho M, Arai N, Arai KI, Baeza ML, Finn A & Kaplan AP (1988) Human recombinant granulocyte-macrophage colony-stimulating factor and interleukin 3 cause basophil histamine release. *J. Clin. Invest.* 82, 17–20.

Haas AL, Warms JVB, Hershkog A & Rose IA (1982) Ubiquitin-activating Enzyme. *J. Biol. Chem.* 257, 2543–2548.

Haddad F, Qin AX, Bodell PW, Jiang W, Giger JM & Baldwin KM (2008) Intergenic transcription and

developmental regulation of cardiac myosin heavy chain genes. *Am. J. Physiol. - Hear. Circ. Physiol.* 294, H29–H40. Available at: https://www.physiology.org/doi/10.1152/ajpheart.01125.2007 [Accessed March 9, 2020].

Hall JL (2002) Cellular mechanisms for heavy metal detoxification and tolerance. *J. Exp. Bot.* 53, 1–11.

Hallermalm K, Seki K, Wei C, Castelli C, Rivoltini L, Kiessling R & Levitskaya J (2001) Tumor necrosis factor-α induces coordinated changes in major histocompatibility class I presentation pathway, resulting in increased stability of class I complexes at the cell surface. *Blood* 98, 1108–1115. Available at: http://www.bloodjournal.org/content/98/4/1108.long?sso-checked=true [Accessed July 8, 2019].

Ham DJ, Börsch A, Lin S, Thürkauf M, Weihrauch M, Reinhard JR, Delezie J, Battilana F, Wang X, Kaiser MS, Guridi M, Sinnreich M, Rich MM, Mittal N, Tintignac LA, Handschin C, Zavolan M & Rüegg MA (2020) The neuromuscular junction is a focal point of mTORC1 signaling in sarcopenia. *Nat. Commun.* 11. Available at: http://dx.doi.org/10.1038/s41467-020-18140-1.

Hamer M & Molloy GJ (2009) Association of C-reactive protein and muscle strength in the English Longitudinal Study of Ageing. In *Age*. Springer, pp.171–177.

Hamilton JA (2008) Colony-stimulating factors in inflammation and autoimmunity. *Nat. Rev. Immunol.* 8, 533–544.

Hansen TE & Johansen T (2011) Following autophagy step by step. *BMC Biol.* 9, 2–5.

Hanson J & Lowy J (1963) The structure of F-actin and of actin filaments isolated from muscle. *J. Mol. Biol.* 6, 46–60.

Hardin BJ, Campbell KS, Smith JD, Arbogast S, Smith J, Moylan JS & Reid MB (2008) TNF-α acts via TNFR1 and muscle-derived oxidants to depress myofibrillar force in murine skeletal muscle. *J. Appl. Physiol.* 104, 694–699.

Harding HP, Zhang Y, Bertolotti A, Zeng H & Ron D (2000) Perk is essential for translational regulation and cell survival during the unfolded protein response. *Mol. Cell* 5, 897–904.

Hardy D, Besnard A, Latil M, Jouvion G, Briand D, Thépenier C, Pascal Q, Guguin A, Gayraud-Morel B, Cavaillon J-MM, Tajbakhsh S, Rocheteau P & Chrétien F (2016) Comparative Study of Injury Models for Studying Muscle Regeneration in Mice A. Kumar, ed. *PLoS One* 11, e0147198. Available at: /pmc/articles/PMC4726569/?report=abstract [Accessed July 29, 2020].

Hardy RR, Kincade PW & Dorshkind K (2007) The Protean Nature of Cells in the B Lymphocyte Lineage. *Immunity* 26, 703–714.

Harman D (1956) Aging: a theory based on free radical and radiation chemistry. *J. Gerontol.* 11, 298–300. Available at: https://academic.oup.com/geronj/article/11/3/298/616585 [Accessed November 2, 2020].

Harvey JA, Chastin SFM & Skelton DA (2013) Prevalence of Sedentary Behavior in Older Adults: A Systematic Review. *OPEN ACCESS Int. J. Environ. Res. Public Heal.* 10, 10. Available at: www.mdpi.com/journal/ijerph [Accessed July 7, 2019].

Hashimoto D, Chow A, Noizat C, Teo P, Beasley MB, Leboeuf M, Becker CD, See P, Price J, Lucas D, Greter M, Mortha A, Boyer SW, Forsberg EC, Tanaka M, van Rooijen N, García-Sastre A, Stanley ER, Ginhoux F, Frenette PS & Merad M (2013) Tissue-resident macrophages self-maintain locally throughout adult life with minimal contribution from circulating monocytes. *Immunity* 38, 792–804.

Hassin D, Garber OG, Meiraz A, Schiffenbauer YS & Berke G (2011) Cytotoxic T lymphocyte perforin and Fas ligand working in concert even when Fas ligand lytic action is still not detectable. *Immunology* 133, 190–196.

Hayflick L (1965) The limited in vitro lifetime of human diploid cell strains. *Exp. Cell Res.* 37, 614–636.

He JQ, Zarnegar B, Oganesyan G, Saha SK, Yamazaki S, Doyle SE, Dempsey PW & Cheng G (2006) Rescue

of TRAF3-null mice by p100 NF-κB deficiency. *J. Exp. Med.* 203, 2413–2418.

Hemenway D, Solnick SJ, Koeck C & Kytir J (1994) The incidence of stairway injuries in Austria. *Accid. Anal. Prev.* 26, 675–679.

Hendricks J, Bos NA & Kroese FGM (2018) Heterogeneity of memory marginal zone B cells. *Crit. Rev. Immunol.* 38, 145–158.

Heydari AR, You S, Takahashi R, Gutsmann-Conrad A, Sarge KD & Richardson A (2000) Age-related alterations in the activation of heat shock transcription factor 1 in rat hepatocytes. *Exp. Cell Res.* 256, 83–93.

Hipp MS, Kasturi P & Hartl FU (2019) The proteostasis network and its decline in ageing. *Nat. Rev. Mol. Cell Biol.* 20, 421–435. Available at: www.nature.com/nrm [Accessed June 10, 2020].

Hiscott J, Marois J, Garoufalis J, D'Addario M, Roulston A, Kwan I, Pepin N, Lacoste J, Nguyen H & Bensi G (1993) Characterization of a functional NF-kappa B site in the human interleukin 1 beta promoter: evidence for a positive autoregulatory loop. *Mol. Cell. Biol.* 13, 6231–6240.

Hoefer J, Luger M, Dal-Pont C, Culig Z, Schennach H & Jochberger S (2017) The "aging factor" eotaxin-1 (CCL11) is detectable in transfusion blood products and increases with the donor's age. *Front. Aging Neurosci.* 9. Available at: /pmc/articles/PMC5717008/?report=abstract [Accessed September 23, 2020].

Hoffmann A, Leung TH & Baltimore D (2003) Genetic analysis of NF-kB/Rel transcription factors defines functional specificities. *Embo* 22, 5530–5539.

Hoffmann A, Levchenko A, Scott ML & Baltimore D (2002) The IκB-NF-κB signaling module: Temporal control and selective gene activation. *Science (80-.).* 298, 1241–1245.

Hollander J, Fiebig R, Gore M, Ookawara T, Ohno H & Ji L (2001) Superoxide dismutase gene expression is activated by a single bout of exercise in rat skeletal muscle. *Pflugers Arch. Eur. J. Physiol.* 442,

426–434.

Horsley V, Jansen KM, Mills ST & Pavlath GK (2003) IL-4 acts as a myoblast recruitment factor during mammalian muscle growth. *Cell* 113, 483–494.

Hsu H, Xiong J & Goeddel D V. (1995) The TNF receptor 1-associated protein TRADD signals cell death and NF-κB activation. *Cell* 81, 495–504.

Hu Z, Taylor DW, Reedy MK, Edwards RJ & Taylor KA (2016) Structure of myosin filaments from relaxed Lethocerus flight muscle by cryo-EM at 6 Å resolution. *Sci. Adv.* 2. Available at: http://advances.sciencemag.org/ [Accessed March 4, 2020].

Huang D Bin, Vu D & Ghosh G (2005) NF-κB RelB forms an intertwined homodimer. *Structure* 13, 1365–1373.

Huang TT, Yasunami M, Carlson EJ, Gillespie AM, Reaume AG, Hoffman EK, Chan PH, Scott RW & Epstein CJ (1997) Superoxide-mediated cytotoxicity in superoxide dismutase-deficient fetal fibroblasts. *Arch. Biochem. Biophys.* 344, 424–432.

Huff-Lonergan E (2009) Fresh meat water-holding capacity. In *Improving the Sensory and Nutritional Quality of Fresh Meat*. Elsevier Inc., pp.147–160.

Hughes CE & Nibbs RJB (2018) A guide to chemokines and their receptors. *FEBS J.* 285, 2944–2971. Available at: https://onlinelibrary.wiley.com/doi/abs/10.1111/febs.14466 [Accessed May 20, 2020].

Hugo M, Korovila I, Köhler M, García-García C, Cabrera-García JD, Marina A, Martínez-Ruiz A & Grune T (2018) Early cysteine-dependent inactivation of 26S proteasomes does not involve particle disassembly. *Redox Biol.* 16, 123–128. Available at: https://doi.org/10.1016/j.redox.2018.02.016.

Hunter RB, Stevenson EJ, Koncarevic A, Mitchell-Felton H, Essig DA & Kandarian SC (2002) Activation

of an alternative NF-KB pathway in skeletal muscle during disuse atrophy . *FASEB J.* 16, 529–538.

Hunter SK, Pereira XHM & Keenan KG (2016) The aging neuromuscular system and motor performance. *J. Appl. Physiol.* 121, 982–995.

Huxford T, Huang D Bin, Malek S & Ghosh G (1998) The crystal structure of the IκBα/NF-κB complex reveals mechanisms of NF-κB inactivation. *Cell* 95, 759–770.

Huxley AF & Niedergerke R (1954) Structural changes in muscle during contraction: Interference microscopy of living muscle fibres. *Nature* 173, 971–973. Available at: http://www.nature.com/articles/173971a0 [Accessed February 10, 2020].

Huxley H & Hanson J (1954) Changes in the Cross-striations of muscle during contraction and stretch and their structural interpretation. *Nature* 173, 973–976.

Hyun SJ, Komatsu S, Ikebe M & Craig R (2008) Head-head and head-tail interaction: A general mechanism for switching off myosin II activity in cells. *Mol. Biol. Cell* 19, 3234–3242.

Ikemoto N & Yamamoto T (2000) Postulated role of Inter-domain interaction within the ryanodine receptor in Ca2+ channel regulation. *Trends Cardiovasc. Med.* 10, 310–316.

Jackman RW, Cornwell EW, Wu CL & Kandarian SC (2013) Nuclear factor-κB signalling and transcriptional regulation in skeletal muscle atrophy. *Exp. Physiol.* 98, 19–24.

Jackson MJ & Mcardle A (2011) Age-related changes in skeletal muscle reactive oxygen species generation and adaptive responses to reactive oxygen species. *J. Physiol.* 589, 2139–2145.

Jackson MJ, McArdle A, Vasilaki A & Kayani A (2012) Workshop report: Can an understanding of the mechanisms underlying age-related loss of muscle mass and function guide exercise and other intervention strategies? *Longev. Heal.* 1, 5.

Jackson RJ, Hellen CUT & Pestova T V. (2010) The mechanism of eukaryotic translation initiation and principles of its regulation. *Nat. Rev. Mol. Cell Biol.* 11, 113–127.

Jacobs MD & Harrison SC (1998) Structure of an IκBα/NF-κB complex. *Cell* 95, 749–758.

Jameson SC & Masopust D (2018) Understanding Subset Diversity in T Cell Memory. *Immunity* 48, 214–226.

Jan CH, Williams CC & Weissman JS (2014) Principles of ER cotranslational translocation revealed by proximity-specific ribosome profiling. *Science (80-.).* 346, 1257521.

Jang YC, Lustgarten MS, Liu Y, Muller FL, Bhattacharya A, Liang H, Salmon AB, Brooks S V., Larkin L, Hayworth CR, Richardson A & Van Remmen H (2010) Increased superoxide in vivo accelerates age-associated muscle atrophy through mitochondrial dysfunction and neuromuscular junction degeneration. *FASEB J.* 24, 1376–1390.

Janssen I, Heymsfield SB, Wang ZM & Ross R (2000) Skeletal muscle mass and distribution in 468 men and women aged 18-88 yr. *J. Appl. Physiol.* 89, 81–88.

Jayasinghe ID & Launikonis BS (2013) Three-dimensional reconstruction and analysis of the tubular system of vertebrate skeletal muscle. *J. Cell Sci.* 126, 4048–4058.

Joanisse S, Gillen JB, Bellamy LM, McKay BR, Tarnopolsky MA, Gibala MJ & Parise G (2013) Evidence for the contribution of muscle stem cells to nonhypertrophic skeletal muscle remodeling in humans. *FASEB J.* 27, 4596–4605.

Johnson RW, White JD, Walker EC, Martin TJ & Sims NA (2014) Myokines (muscle-derived cytokines and chemokines) including ciliary neurotrophic factor (CNTF) inhibit osteoblast differentiation. *Bone* 64, 47–56.

Jongbloed SL, Kassianos AJ, McDonald KJ, Clark GJ, Ju X, Angel CE, Chen CJJ, Dunbar PR, Wadley RB, Jeet V, Vulink AJE, Hart DNJ & Radford KJ (2010) Human CD141+ (BDCA-3)+ dendritic cells (DCs) represent a unique myeloid DC subset that cross-presents necrotic cell antigens. *J. Exp. Med.* 207, 1247–1260.

Joss A, Akdis M, Faith A, Blaser K & Akdis CA (2000) IL-10 directly acts on T cells by specifically altering the CD28 co-stimulation pathway. *Eur. J. Immunol.* 30, 1683–1690.

Judge AD, Zhang X, Fujii H, Surh CD & Sprent J (2002) Interleukin 15 controls both proliferation and survival of a subset of memory-phenotype CD8+ T cells. *J. Exp. Med.* 196, 935–946.

Judge AR, Koncarevic A, Hunter RB, Liou HC, Jackman RW & Kandarian SC (2007) Role for IκBα, but not c-Rel, in skeletal muscle atrophy. *Am. J. Physiol. - Cell Physiol.* 292, 372–382.

Junttila IS (2018) Tuning the cytokine responses: An update on interleukin (IL)-4 and IL-13 receptor complexes. *Front. Immunol.* 9, 888.

Kalinauskaite-Zukauske V, Januskevicius A, Janulaityte I, Miliauskas S & Malakauskas K (2019) Expression of eosinophil β chain-signaling cytokines receptors, outer-membrane integrins, and type 2 inflammation biomarkers in severe non-allergic eosinophilic asthma. *BMC Pulm. Med.* 19.

Kanehisa M & Goto S (2000) KEGG: Kyoto Encyclopedia of Genes and Genomes. *Nucleic Acids Res.* 28, 27–30. Available at: https://linkinghub.elsevier.com/retrieve/pii/S0950352896900366.

Kang R, Zeh HJ, Lotze MT & Tang D (2011) The Beclin 1 network regulates autophagy and apoptosis. *Cell Death Differ.* 18, 571–580. Available at: http://dx.doi.org/10.1038/cdd.2010.191.

Kao AL, Lin YH, Chen RPY, Huang YY, Chen CC & Yang CC (2012) E3-independent ubiquitination of AtMAPR/MSBP1. *Phytochemistry* 78, 7–19.

Kasukawa Y, Miyakoshi N, Hongo M, Ishikawa Y, Kudo D, Suzuki M, Mizutani T, Kimura R, Ono Y & Shimada Y (2017) Age-related changes in muscle strength and spinal kyphosis angles in an elderly Japanese population. *Clin. Interv. Aging* 12, 413–420.

Katsanos CS, Kobayashi H, Sheffield-Moore M, Aarsland A & Wolfe RR (2006) A high proportion of leucine is required for optimal stimulation of the rate of muscle protein synthesis by essential amino acids in the elderly. *Am. J. Physiol. Metab.* 291, E381–E387. Available at:

http://www.physiology.org/doi/10.1152/ajpendo.00488.2005 [Accessed July 6, 2019].

Kaushik G, Spenlehauer A, Sessions AO, Trujillo AS, Fuhrmann A, Fu Z, Venkatraman V, Pohl D, Tuler J, Wang M, Lakatta EG, Ocorr K, Bodmer R, Bernstein SI, Van Eyk JE, Cammarato A & Engler AJ (2015) Vinculin network-mediated cytoskeletal remodeling regulates contractile function in the aging heart. *Sci. Transl. Med.* 7.

Kawai M & Konishi M (1994) Measurement of sarcoplasmic reticulum calcium content in skinned mammalian cardiac muscle. *Cell Calcium* 16, 123–136.

Kayani AC, Close GL, Dillmann WH, Mestril R, Jackson MJ & McArdle A (2010) Overexpression of HSP10 in skeletal muscle of transgenic mice prevents the age-related fall in maximum tetanic force generation and muscle cross-sectional area. *Am. J. Physiol. - Regul. Integr. Comp. Physiol.* 299, R268–R276. Available at: http://www.physiology.org/doi/10.1152/ajpregu.00334.2009 [Accessed September 5, 2019].

Kayani AC, Close GL, Jackson MJ & McArdle A (2008) Prolonged treadmill training increases HSP70 in skeletal muscle but does not affect age-related functional deficits. *Am. J. Physiol. - Regul. Integr. Comp. Physiol.* 294, 568–576.

Keszei AFA & Sicheri F (2017) Mechanism of catalysis, E2 recognition,& autoinhibition for the IpaH family of bacterial E3 ubiquitin ligases. *Proc. Natl. Acad. Sci. U. S. A.* 114, 1311–1316.

Khosla S, Farr JN, Tchkonia T & Kirkland JL (2020) The role of cellular senescence in ageing and endocrine disease. *Nat. Rev. Endocrinol.* 16, 263–275. Available at: www.nature.com/nrendo [Accessed November 1, 2020].

Kim HO, Kim HS, Youn JC, Shin EC & Park S (2011) Serum cytokine profiles in healthy young and elderly population assessed using multiplexed bead-based immunoassays. *J. Transl. Med.* 9, 113. Available at: http://translational-medicine.biomedcentral.com/articles/10.1186/1479-5876-9-113 [Accessed September 23, 2020].

Kim T-Y, Wang D, Kim AK, Lau E, Lin AJ, Liem DA, Zhang J, Zong NC, Lam MPY & Ping P (2012a) Metabolic Labeling Reveals Proteome Dynamics of Mouse Mitochondria. *Mol. Cell. Proteomics* 11, 1586–1594. Available at: http://www.ncbi.nlm.nih.gov/pubmed/22915825 [Accessed May 1, 2019].

Kim TY, Wangs D, Kim AK, Laus E, Lin AJ, Liem DA, Zhangs J, Zong NC, Lam MPY & Pings P (2012b) Metabolic labeling reveals proteome dynamics of mouse mitochondria. *Mol. Cell. Proteomics* 11, 1586–1594.

Kinn PM, Holdren GO, Westermeyer BA, Abuissa M, Fischer CL, Fairley JA, Brogden KA & Brogden NK (2015) Age-dependent variation in cytokines, chemokines, and biologic analytes rinsed from the surface of healthy human skin OPEN. Available at: www.nature.com/scientificreports/.

Kirkin V, McEwan DG, Novak I & Dikic I (2009) A Role for Ubiquitin in Selective Autophagy. *Mol. Cell* 34, 259–269.

Kirkland JL (2013) Inflammation and Cellular Senescence: Potential Contribution to Chronic Diseases and Disabilities With Aging. *Public Policy Aging Rep.* 23, 12–15.

Kisselev AF, Akopian TN, Castillo V & Goldberg AL (1999) Proteasome active sites allosterically regulate each other, suggesting a cyclical bite-chew mechanism for protein breakdown. *Mol. Cell* 4, 395–402.

Kleist AB, Getschman AE, Ziarek JJ, Nevins AM, Gauthier PA, Chevigné A, Szpakowska M & Volkman BF (2016) New paradigms in chemokine receptor signal transduction: Moving beyond the two-site model. *Biochem. Pharmacol.* 114, 53–68.

Kodali RB, Kim WJH, Galaria II, Miller C, Schecter AD, Lira SA & Taubman MB (2004) CCL11 (Eotaxin) induces CCR3-dependent smooth muscle cell migration. *Arterioscler. Thromb. Vasc. Biol.* 24, 1211–1216. Available at: https://pubmed.ncbi.nlm.nih.gov/15130922/ [Accessed July 14, 2020].

Kolaczkowska E & Kubes P (2013) Neutrophil recruitment and function in health and inflammation. *Nat. Rev. Immunol.* 13, 159–175.

Konarska MM, Grabowski PJ, Padgett RA & Sharp PA (1985) Characterization of the branch site in lariat RNAs produced by splicing of mRNA precursors. *Nature* 313, 552–557.

Kondo M, Weissman IL & Akashi K (1997) Identification of clonogenic common lymphoid progenitors in mouse bone marrow. *Cell* 91, 661–672.

Koper A, Schenck A & Prokop A (2012) Analysis of adhesion molecules and basement membrane contributions to synaptic adhesion at the drosophila embryonic NMJ. *PLoS One* 7.

Kostrominova TY, Hassett CA, Rader EP, Davis C, Larkin LM, Coleman S, Oleson FB & Faulkner JA (2010) Characterization of skeletal muscle effects associated with daptomycin in rats. *Muscle and Nerve* 42, 385–393.

Kotenko S V, Krause CD, Izotova LS, Pollack BP, Wu W & Pestka S (1997) *Identification and functional characterization of a second chain of the interleukin-10 receptor complex cells, blocking their ability to secrete cytokines such as interferon-γ (IFN-γ) and IL-2 (Fiorentino et al,*

Krueger BJ, Varzavand K, Cooper JJ & Price DH (2010) The mechanism of release of P-TEFb and HEXIM1 from the 7SK snRNP by viral and cellular activators includes a conformational change in 7SK. *PLoS One* 5.

Krug N, Cruikshank WW, Tschernig T, Erpenbeck VJ, Balke K, Hohlfeld JM, Center DM & Fabel H (2000) *Interleukin 16 and T-cell Chemoattractant Activity in Bronchoalveolar Lavage 24 Hours after Allergen Challenge in Asthma*, Available at: www.atsjournals.org [Accessed May 20, 2020].

Krumm A, Hickey LB & Groudine M (1995) Promoter-proximal pausing of RNA polymerase II defines a general rate-limiting step after transcription initiation. *Genes Dev.* 9, 559–572. Available at: http://www.ncbi.nlm.nih.gov/pubmed/7698646 [Accessed July 4, 2019].

Kumar SK, LaPlant BR, Reeder CB, Roy V, Halvorson AE, Buadi F, Gertz MA, Bergsagel PL, Dispenzieri A, Thompson MA, Crawley J, Kapoor P, Mikhael J, Stewart K, Hayman SR, Hwa YL, Gonsalves W, Witzig TE, Ailawadhi S, Dingli D, Go RS, Lin Y, Rivera CE, Rajkumar SV & Lacy MQ (2016)

Randomized phase 2 trial of ixazomib and dexamethasone in relapsed multiple myeloma not refractory to bortezomib. *Blood* 128, 2415–2422.

Kumar V, Selby A, Rankin D, Patel R, Atherton P, Hildebrandt W, Williams J, Smith K, Seynnes O, Hiscock N & Rennie MJ (2009) Age-related differences in the dose-response relationship of muscle protein synthesis to resistance exercise in young and old men. *J. Physiol.* 587, 211–7. Available at: http://www.ncbi.nlm.nih.gov/pubmed/19001042 [Accessed July 7, 2019].

Kunkel SL (1999) *Promiscuous Chemokine Receptors and Their Redundant Ligands Play an Enigmatic Role during HIV-1 Infection*, Available at: www.atsjournals.org [Accessed May 25, 2020].

Kunsch C, Ruben SM & Rosen CA (1992) Selection of optimal kappa B/Rel DNA-binding motifs: interaction of both subunits of NF-kappa B with DNA is required for transcriptional activation. *Mol. Cell. Biol.* 12, 4412–4421.

Kuriyan J & Thanos D (1995) Structure of the NF-κB transcription factor: a holistic interaction with DNA. *Structure* 3, 135–141.

de la Rosa M, Rutz S, Dorninger H & Scheffold A (2004) Interleukin-2 is essential for CD4+CD25+ regulatory T cell function. *Eur. J. Immunol.* 34, 2480–2488.

Lang CH, Frost RA, Jefferson LS, Kimball SR & Vary TC (2000) Endotoxin-induced decrease in muscle protein synthesis is associated with changes in eIF2B, eIF4E, and IGF-I. *Am. J. Physiol. - Endocrinol. Metab.* 278, 1133–1143.

Larkin LM, Davis CS, Sims-Robinson C, Kostrominova TY, van Remmen H, Richardson A, Feldman EL & Brooks S V. (2011) Skeletal muscle weakness due to deficiency of CuZn-superoxide dismutase is associated with loss of functional innervation. *Am. J. Physiol. - Regul. Integr. Comp. Physiol.* 301.

Larsson L & Ansved T (1995) Effects of ageing on the motor unit. *Prog. Neurobiol.* 45, 397–458. Available at: http://dx.doi.org/10.1016/0301-0082(95)98601-Z.

Larsson L, Degens H, Li M, Salviati L, Lee Y Il, Thompson W, Kirkland JL & Sandri M (2019) Sarcopenia: Aging-related loss of muscle mass and function. *Physiol. Rev.* 99, 427–511.

Larsson L, Edstrom L, Lindegren B, Gorza L & Schiaffino S (1991) MHC composition and enzyme-histochemical and physiological properties of a novel fast-twitch motor unit type. *Am. J. Physiol. - Cell Physiol.* 261.

Lavin Y, Winter D, Blecher-Gonen R, David E, Keren-Shaul H, Merad M, Jung S & Amit I (2014) Tissue-resident macrophage enhancer landscapes are shaped by the local microenvironment. *Cell* 159, 1312–1326.

Lê S, Josse J, Rennes A & Husson F (2008) *FactoMineR: An R Package for Multivariate Analysis*, Available at: http://www.jstatsoft.org/ [Accessed August 24, 2020].

Lee A-H, Iwakoshi NN & Glimcher LH (2003) XBP-1 Regulates a Subset of Endoplasmic Reticulum Resident Chaperone Genes in the Unfolded Protein Response. *Mol. Cell. Biol.* 23, 7448–7459.

Lee WT, Tai SH, Lin YW, Wu TS & Lee EJ (2018) YC-1 reduces inflammatory responses by inhibiting nuclear factor-?B translocation in mice subjected to transient focal cerebral ischemia. *Mol. Med. Rep.* 18, 2043–2051.

Leung TH, Hoffmann A & Baltimore D (2005) One Nucleotide in a κB Site Can Determine Cofactor Specificity for NF-κB Dimers. *Cell* 118, 453–464.

Lexell J & Henriksson-Larsen K (1983) Distribution of different fiber types in human skeletal muscles: effects of aging studied in whole muscle cross sections. *Muscle Nerve* 1, 588–595.

Li J, Yin Q & Wu H (2013) Structural Basis of Signal Transduction in the TNF Receptor Superfamily.

Li L & Ghosh S (1996) *A Glycine-Rich Region in NF-B p105 Functions as a Processing Signal for the Generation of the p50 Subunit*, Available at: http://mcb.asm.org/ [Accessed March 31, 2020].

Li MO & Rudensky AY (2016) T cell receptor signalling in the control of regulatory T cell differentiation

and function. *Nat. Rev. Immunol.* 16, 220–233.

Li Y-P, Chen Y, John J, Moylan J, Jin B, Mann DL & Reid MB (2005) TNF-α acts via p38 MAPK to stimulate expression of the ubiquitin ligase atrogin1/MAFbx in skeletal muscle. *FASEB J.* 19, 362–370.

Li Y, Liu M, Chen LF & Chen R (2018) P-TEFb: Finding its ways to release promoter-proximally paused RNA polymerase II. *Transcription* 9, 88–94.

Li Y, Qi X, Liu B & Huang H (2015) The STAT5–GATA2 Pathway Is Critical in Basophil and Mast Cell Differentiation and Maintenance. *J. Immunol.* 194, 4328–4338.

Li YP & Reid MB (2000) NF-κB mediates the protein loss induced by TNF-α in differentiated skeletal muscle myotubes. *Am. J. Physiol. - Regul. Integr. Comp. Physiol.* 279, 1165–1170. Available at: http://www.ajpregu.org [Accessed November 1, 2020].

Lightfoot AP, Sakellariou GK, Nye GA, McArdle F, Jackson MJ, Griffiths RD & McArdle A (2015) SS-31 attenuates TNF-α induced cytokine release from C2C12 myotubes. *Redox Biol.* 6, 253–259.

Lilienbaum A (2013) Relationship between the proteasomal system and autophagy. *Int. J. Biochem. Mol. Biol.* 4, 1–26.

Lin IH, Chang JL, Hua K, Huang WC, Hsu MT & Chen YF (2018) Skeletal muscle in aged mice reveals extensive transformation of muscle gene expression. *BMC Genet.* 19, 1–13.

Lin J, Wu H, Tarr PT, Zhang CY, Wu Z, Boss O, Michael LF, Puigserver P, Isotani E, Olson EN, Lowell BB, Bassel-Duby R & Spiegelman BM (2002) Transcriptional co-activator PGC-1α drives the formation of slow-twitch muscle fibres. *Nature* 418, 797–801.

Lin JH, Walter P & Yen TSB (2008) Endoplasmic reticulum stress in disease pathogenesis. *Annu. Rev. Pathol. Mech. Dis.* 3, 399–425.

Linehan E & Fitzgerald D (2015) Ageing and the immune system: focus on macrophages. *Eur. J. Microbiol. Immunol.* 5, 14–24.

Ling L, Cao Z & Goeddel D V. (1998) Nf-κB-inducing kinase activates IKK-α by phosphorylation of Ser-176. *Proc. Natl. Acad. Sci. U. S. A.* 95, 3792–3797.

Liou HC & Hsia CY (2003) Distinctions between c-Rel and other NF-κB proteins in immunity and disease. *BioEssays* 25, 767–780.

Liu M, Haataja L, Wright J, Wickramasinghe NP, Hua Q-X, Phillips NF, Barbetti F, Weiss MA & Arvan P (2010) Mutant INS-Gene Induced Diabetes of Youth: Proinsulin Cysteine Residues Impose Dominant-Negative Inhibition on Wild-Type Proinsulin Transport M. G. von Herrath, ed. *PLoS One* 5, e13333. Available at: https://dx.plos.org/10.1371/journal.pone.0013333 [Accessed June 10, 2020].

Liu XH, Wu G, Dan Shi D, Zhu R, Zeng HJ, Cao B, Huang MX & Liao H (2015) Effects of nitric oxide on notexin-induced muscle inflammatory responses. *Int. J. Biol. Sci.* 11, 156–167. Available at: /pmc/articles/PMC4279091/?report=abstract [Accessed July 30, 2020].

Locke M & Tanguay RM (1996) Increased HSF activation in muscles with a high constitutive Hsp70 expression. *Cell Stress Chaperones* 1, 189–196.

Loetscher H, Pan YC, Lahm HW, Gentz R, Brockhaus M, Tabuchi H & Lesslauer W (1990) Molecular cloning and expression of the human 55 kd tumor necrosis factor receptor. *Cell* 61, 351–359.

López-Otín C, Blasco MA, Partridge L, Serrano M & Kroemer G (2013) The hallmarks of aging. *Cell* 153, 1194–217. Available at: http://www.ncbi.nlm.nih.gov/pubmed/23746838 [Accessed May 3, 2019].

Luckheeram RV, Zhou R, Verma AD & Xia B (2012) CD4 + T Cells: Differentiation and Functions. *Clin. Dev. Immunol.* 2012, 12.

Lynch EA, Heijens CAW, Horst NF, Center DM & Cruikshank WW (2003) Cutting Edge: IL-16/CD4 Preferentially Induces Th1 Cell Migration: Requirement of CCR5. *J. Immunol.* 171, 4965–4968.

Mahmassani ZS, Reidy PT, Mckenzie AI, Stubben C, Howard MT & Drummond MJ (2019) Age-dependent skeletal muscle transcriptome response to bed rest-induced atrophy. *J Appl Physiol* 126, 894–902. Available at: http://www.jappl.org [Accessed September 10, 2020].

Mahmoudi S, Mancini E, Xu L, Moore A, Jahanbani F, Hebestreit K, Srinivasan R, Li X, Devarajan K, Prélot L, Ang CE, Shibuya Y, Benayoun BA, Chang ALS, Wernig M, Wysocka J, Longaker MT, Snyder MP & Brunet A (2019) *Heterogeneity in old fibroblasts is linked to variability in reprogramming and wound healing*, Springer US. Available at: http://dx.doi.org/10.1038/s41586-019-1658-5.

Malek S, Huang D Bin, Huxford T, Ghosh S & Ghosh G (2003) X-ray crystal structure of an IκBβ·NF-κB p65 homodimer complex. *J. Biol. Chem.* 278, 23094–23100.

Marcus A & Raulet DH (2013) Evidence for natural killer cell memory. *Curr. Biol.* 23.

Martínez-Lostao L, Anel A & Pardo J (2015) How Do Cytotoxic Lymphocytes Kill Cancer Cells? *Clin. Cancer Res.* 21, 5047–5056.

Martini FH, Nath JL & Bartholomew EF (2017) *Fundamentals of Anatomy & Physiology, Global Edition*, Harlow, United Kingdom, UNITED KINGDOM: Pearson Education Limited. Available at: http://ebookcentral.proquest.com/lib/liverpool/detail.action?docID=5186130.

Masiero E, Agatea L, Mammucari C, Blaauw B, Loro E, Komatsu M, Metzger D, Reggiani C, Schiaffino S & Sandri M (2009) Autophagy Is Required to Maintain Muscle Mass. *Cell Metab.* 10, 507–515. Available at: http://dx.doi.org/10.1016/j.cmet.2009.10.008.

Matthews GDK, Huang CLH, Sun L & Zaidi M (2011) Translational musculoskeletal science: Is sarcopenia the next clinical target after osteoporosis? *Ann. N. Y. Acad. Sci.* 1237, 95–105.

Mayer MP & Bukau B (2005) Hsp70 chaperones: Cellular functions and molecular mechanism. *Cell. Mol. Life Sci.* 62, 670–684.

McArdle A, Dillmann WH, Mestril R, Faulkner JA & Jackson MJ (2004) Overexpression of HSP70 in

mouse skeletal muscle protects against muscle damage and age-related muscle dysfunction. *FASEB J.* 18, 355–357. Available at: www.fasebj.org [Accessed January 9, 2020].

McArdle A, Edwards RHT & Jackson MJ (1994) Release of creatine kinase and prostaglandin E2 from regenerating skeletal muscle fibers. *J. Appl. Physiol.* 76, 1274–1278.

McArdle A & Jackson MJ (2017) The role of attenuated redox and heat shock protein responses in the age-related decline in skeletal muscle mass and function. *Essays Biochem.* 61, 339–348.

McArdle A, Pollock N, Staunton CA & Jackson MJ (2019) Aberrant redox signalling and stress response in age-related muscle decline: Role in inter- and intra-cellular signalling. *Free Radic. Biol. Med.* 132, 50–57.

McArdle A, Vasilaki A & Jackson MJ (2002) Exercise and skeletal muscle ageing: cellular and molecular mechanism. *Ageing Res. Rev.* 1, 79–93.

McCully KK & Faulkner JA (1985) Injury to skeletal muscle fibers of mice following lengthening contractions. *J. Appl. Physiol.* 59, 119–126.

McMahan CJ, Slack JL, Mosley B, Cosman D, Lupton SD, Brunton LL, Grubin CE, Wignall JM, Jenkins NA & Brannan CI (1991) A novel IL-1 receptor, cloned from B cells by mammalian expression, is expressed in many cell types. *EMBO J.* 10, 2821–2832.

Melnikov S, Ben-Shem A, Garreau De Loubresse N, Jenner L, Yusupova G & Yusupov M (2012) One core, two shells: Bacterial and eukaryotic ribosomes. *Nat. Struct. Mol. Biol.* 19, 560–567.

Meng SJ & Yu LJ (2010) Oxidative stress, molecular inflammation and sarcopenia. *Int. J. Mol. Sci.* 11, 1509–1526.

Menne J, Eulberg D, Beyer D, Baumann M, Saudek F, Valkusz Z, Rcek AW & Haller H (2017) C-C motif-ligand 2 inhibition with emapticap pegol (NOX-E36) in type 2 diabetic patients with albuminuria. *Nephrol. Dial. Transplant.* 32, 307–315.

Mercer F, Kozhaya L & Unutmaz D (2010) Expression and function of TNF and IL-1 receptors on human regulatory T cells. *PLoS One* 5.

Messa GAM, Piasecki M, Hill C, McPhee JS, Tallis J & Degens H (2019) Morphological alterations of mouse skeletal muscles during early ageing are muscle specific. *Exp. Gerontol.* 125, 110684. Available at: https://www.sciencedirect.com/science/article/pii/S0531556519303316?via%253Dihub [Accessed September 5, 2019].

Messina S, Vita GL, Aguennouz M, Sframeli M, Romeo S, Rodolico C & Vita G (2011) Activation of NF-kappaB pathway in Duchenne muscular dystrophy: relation to age. *Acta Myol. myopathies cardiomyopathies Off. J. Mediterr. Soc. Myol.* 30, 16–23. Available at: http://www.ncbi.nlm.nih.gov/pubmed/21842588 [Accessed June 29, 2020].

Mestas J & Hughes CCW (2004) Of Mice and Not Men: Differences between Mouse and Human Immunology. *J. Immunol.* 172, 2731–2738.

Meyer HJ & Rape M (2014) Enhanced protein degradation by branched ubiquitin chains. *Cell* 157, 910–921.

Michaud M, Balardy L, Moulis G, Gaudin C, Peyrot C, Vellas B, Cesari M & Nourhashemi F (2013) Proinflammatory cytokines, aging, and age-related diseases. *J. Am. Med. Dir. Assoc.* 14, 877–882.

Miller CMD, Smith NC, Ikin RJ, Boulter NR, Dalton JP & Donnelly S (2009) Immunological interactions between 2 common pathogens, Th1-inducing Protozoan Toxoplasma gondii and the Th2-inducing helminth fasciola hepatica. *PLoS One* 4.

Miller MS, Palmer BM, Toth MJ & Warshaw DM (2017) Muscle. In *Kelley and Firestein's Textbook of Rheumatology*. Elsevier, pp.66–77.

Missias AC, Chu GC, Klocke BJ, Sanes JR & Merlie JP (1996) *Maturation of the Acetylcholine Receptor in Skeletal Muscle: Regulation of the AChR Gamma-to-Epsilon Switch*,

Mitchell S, Vargas J & Hoffmann A (2016) Signaling via the NFκB system. *Wiley Interdiscip. Rev. Syst. Biol. Med.* 8, 227–241.

Mizushima N, Yoshimori T & Ohsumi Y (2011) The Role of Atg Proteins in Autophagosome Formation. *Annu. Rev. Cell Dev. Biol.* 27, 107–132.

Mobley CB, Mumford PW, Kephart WC, Haun CT, Holland AM, Beck DT, Martin JS, Young KC, Anderson RG, Patel RK, Langston GL, Lowery RP, Wilson JM & Roberts MD (2017) Aging in rats differentially affects markers of transcriptional and translational capacity in soleus and plantaris muscle. *Front. Physiol.* 8, 1–13.

Moreno-Gonzalez I & Soto C (2011) Misfolded protein aggregates: Mechanisms, structures and potential for disease transmission. *Semin. Cell Dev. Biol.* 22, 482–487.

Morton AB, Norton CE, Jacobsen NL, Fernando CA, Cornelison DDW & Segal SS (2019) Barium chloride injures myofibers through calcium-induced proteolysis with fragmentation of motor nerves and microvessels. *Skelet. Muscle* 9, 27. Available at: https://skeletalmusclejournal.biomedcentral.com/articles/10.1186/s13395-019-0213-2 [Accessed July 29, 2020].

Mosele FC, Bissi Ricci R, Abreu P & Rosa Neto JC (2020) Muscle regeneration in adiponectin knockout mice showed early activation of anti-inflammatory response with perturbations in myogenesis. *J. Cell. Physiol.* 235, 6183–6193.

Moss ML, Jin SLC, Milla ME, Bickett DM, Burkhart W, Carter HL, Chen WJ, Clay WC, Didsbury JR, Hassler D, Hoffman CR, Kost TA, Lambert MH, Leesnitzer MA, McCauley P, McGeehan G, Mitchell J, Moyer M, Pahel G, Rocque W, Overton LK, Schoenen F, Seaton T, Su JL, Warner J, Willard D & Becherer JD (1997) Cloning of a disintegrin metalloproteinase that processes precursor tumour-necrosis factor-a. *Nature* 386, 738.

Mosser DM & Edwards JP (2008) Exploring the full spectrum of macrophage activation. *Nat. Rev.*

Immunol. 8, 958–969.

Mourkioti F, Kratsios P, Luedde T, Song YH, Delafontaine P, Adami R, Parente V, Bottinelli R, Pasparakis M & Rosenthal N (2006) Targeted ablation of IKK2 improves skeletal muscle strength, maintains mass, and promotes regeneration. *J. Clin. Invest.* 116, 2945–2954.

Muller FL, Song W, Jang YC, Liu Y, Sabia M, Richardson A & Van Remmen H (2007) Denervation-induced skeletal muscle atrophy is associated with increased mitochondrial ROS production. *Am. J. Physiol. - Regul. Integr. Comp. Physiol.* 293.

Muller FL, Song W, Liu Y, Chaudhuri A, Pieke-Dahl S, Strong R, Huang T-T, Epstein CJ, Roberts LJ, Csete M, Faulkner JA & Van Remmen H (2006) Absence of CuZn superoxide dismutase leads to elevated oxidative stress and acceleration of age-dependent skeletal muscle atrophy. *Free Radic. Biol. Med.* 40, 1993–2004. Available at: https://www.sciencedirect.com/science/article/pii/S0891584906000906?via%253Dihub#bib30 [Accessed April 29, 2019].

Muramatsu T, Hatoko M, Tada H, Shirai T & Ohnishi T (1996) Age-related decrease in the inductability of heat shock protein 72 in normal human skin. *Br. J. Dermatol.* 134, 1035–1058.

Murata S, Takahama Y, Kasahara M & Tanaka K (2018) The immunoproteasome and thymoproteasome: functions, evolution and human disease. *Nat. Immunol.* 19, 923–931. Available at: http://dx.doi.org/10.1038/s41590-018-0186-z.

Nagahisa H, Okabe K, Iuchi Y, Fujii J & Miyata H (2016) Characteristics of Skeletal Muscle Fibers of SOD1 Knockout Mice. *Oxid. Med. Cell. Longev.* 2016.

Nakamura K, Kitani A & Strober W (2001) Cell contact-dependent immunosuppression by CD4+CD25+ regulatory T cells is mediated by cell surface-bound transforming growth factor β. *J. Exp. Med.* 194, 629–644.

Nakazawa H, Chang K, Shinozaki S, Yasukawa T, Ishimaru K, Yasuhara S, Yu YM, Martyn JAJ, Tompkins

RG, Shimokado K & Kaneki M (2017) iNOS as a driver of inflammation and apoptosis in mouse skeletal muscle after burn injury: Possible involvement of sirt1 S- nitrosylation-mediated acetylation of p65 NFeKB and p53. *PLoS One* 12, 1–18.

Narici M V. & Maffulli N (2010) Sarcopenia: Characteristics, mechanisms and functional significance. *Br. Med. Bull.* 95, 139–159.

Neefjes J, Jongsma MLM, Paul P & Bakke O (2011) Towards a systems understanding of MHC class i and MHC class II antigen presentation. *Nat. Rev. Immunol.* 11, 823–836.

Nelson DE, Ihekwaba AEC, Elliott M, Johnson JR, Gibney CA, Foreman BE, Nelson C, See V, Horton CA, Spiller DG, Edwards SW, McDowell HP, Unitt JF, Sullivan E, Grimley R, Benson N, Broomhead D, Kell DB & White MRH (2004) Oscillations in NF-κB signaling control the dynamics of gene expression. *Science (80-.).* 306, 704–708.

Neubauer O, Sabapathy S, Ashton KJ, Desbrow B, Peake JM, Lazarus R, Wessner B, Cameron-Smith D, Wagner KH, Haseler LJ & Bulmer AC (2014) Time course-dependent changes in the transcriptome of human skeletal muscle during recovery from endurance exercise: From inflammation to adaptive remodeling. *J. Appl. Physiol.* 116, 274–287.

Nicholas J, Voss JG, Tsuji J, Fulkerson ND, Soulakova J & Schneider BSP (2015) Time course of chemokine expression and leukocyte infiltration after acute skeletal muscle injury in mice. *Innate Immun.* 21, 266–274.

Nilsson OB, Hedman R, Marino J, Wickles S, Bischoff L, Johansson M, Müller-Lucks A, Trovato F, Puglisi JD, O'Brien EP, Beckmann R & von Heijne G (2015) Cotranslational Protein Folding inside the Ribosome Exit Tunnel. *Cell Rep.* 12, 1533–1540.

Nilwik R, Snijders T, Leenders M, Groen BBL, van Kranenburg J, Verdijk LB & Van Loon LJC (2013) The decline in skeletal muscle mass with aging is mainly attributed to a reduction in type II muscle fiber size. *Exp. Gerontol.* 48, 492–498. Available at:

https://www.sciencedirect.com/science/article/pii/S0531556513000430?via%253Dihub#f0010 [Accessed September 4, 2019].

Nishikawa SI, Fewell SW, Kato Y, Brodsky JL & Endo T (2001) Molecular chaperones in the yeast endoplasmic reticulum maintain the solubility of proteins for retrotranslocation and degradation. *J. Cell Biol.* 153, 1061–1069.

Noble EG, Milne KJ & Melling CWJ (2008) Heat shock proteins and exercise: A primer. *Appl. Physiol. Nutr. Metab.* 33, 1050–1065.

Nunes A & Annunziata C (2016) Proteasome Inhibitors: Structure and Function. *Physiol. Behav.* 176, 100–106.

O'Brien EP, Christodoulou J, Vendruscolo M & Dobson CM (2011) New scenarios of protein folding can occur on the ribosome. *J. Am. Chem. Soc.* 133, 513–526.

Ogata T & Yamasaki Y (1997) Ultra-high-resolution scanning electron microscopy of mitochondria and sarcoplasmic reticulum arrangement in human red, white, and intermediate muscle fibers. *Anat. Rec.* 248, 214–223. Available at: http://doi.wiley.com/10.1002/%28SICI%291097-0185%28199706%29248%3A2%3C214%3A%3AAID-AR8%3E3.0.CO%3B2-S [Accessed February 7, 2020].

Oh H & Ghosh S (2013) NF-κB: Roles and Regulation In Different CD4+ T cell subsets. *Immunology* 252, 41–51. Available at: https://www.ncbi.nlm.nih.gov/pmc/articles/PMC3624763/pdf/nihms412728.pdf.

Oneissi Martinez F, Sica A, Mantovani A & Locati M (2008) *Macrophage activation and polarization*,

Ordway GA & Garry DJ (2004) Myoglobin: An essential hemoprotein in striated muscle. *J. Exp. Biol.* 207, 3441–3446.

Orecchioni M, Ghosheh Y, Pramod AB & Ley K (2019) Macrophage polarization: Different gene

signatures in M1(Lps+) vs. Classically and M2(LPS-) vs. Alternatively activated macrophages. *Front. Immunol.* 10, 1084.

Orlowski M (1990) The multicatalytic proteinase complex, a major extralysosomal proteolytic system. *Biochemistry* 29, 10289–10297. Available at: https://pubs.acs.org/sharingguidelines [Accessed June 8, 2020].

Orphanides G, Lagrange T & Reinberg D (1996) The general transcription factors of RNA polymerase II. *Genes Dev.* 10, 2657–2683.

De Paepe B & De Bleecker JL (2013) Cytokines and chemokines as regulators of skeletal muscle inflammation: Presenting the case of Duchenne muscular dystrophy. *Mediators Inflamm.* 2013.

Pal M & Ponticelli AS (2005) The Role of the Transcription Bubble and TFIIB in Promoter Clearance by RNA Polymerase II The transcript from the adenovirus major late (Ad ML) promoter begins with the short repetitive sequence *Correspondence: lused@ccf.org. *Mol. Cell* 19, 101–110.

Pandorf CE, Haddad F, Roy RR, Qin AX, Edgerton VR & Baldwin KM (2006) Dynamics of myosin heavy chain gene regulation in slow skeletal muscle: Role of natural antisense RNA. *J. Biol. Chem.* 281, 38330–38342.

Parameswaran N & Patial S (2010) Tumor necrosis factor-α signaling in macrophages. *Crit. Rev. Eukaryot. Gene Expr.* 20, 87–103. Available at: https://pubmed.ncbi.nlm.nih.gov/21133840.

Park YC, Ye H, Hsia C, Segal D, Rich RL, Liou HC, Myszka DG & Wu H (2000) A novel mechanism of TRAF signaling revealed by structural and functional analyses of the TRADD-TRAF2 interaction. *Cell* 101, 777–787.

Passey SL, Bozinovski S, Vlahos R, Anderson GP & Hansen MJ (2016) Serum amyloid A induces toll-like receptor 2-dependent inflammatory cytokine expression and atrophy in C2C12 skeletal muscle myotubes. *PLoS One* 11.

Paul WE (2015) History of interleukin-4. *Cytokine* 75, 3–7.

Pavlath GK, Rich K, Webster SG & Blau HM (1989) Localization of muscle gene products in nuclear domains. *Nature* 337, 570–573. Available at: http://www.nature.com/articles/337570a0 [Accessed September 9, 2019].

Peake JM, Gatta P Della, Suzuki K & Nieman DC (2015) Cytokine expression and secretion by skeletal muscle cells: Regulatory mechanisms and exercise effects. *Exerc. Immunol. Rev.* 21, 8–25.

Pelzer C, Kassner I, Matentzoglu K, Singh RK, Wollscheid HP, Scheffner M, Schmidtke G & Groettrup M (2007) UBE1L2, a novel E1 enzyme specific for ubiquitin. *J. Biol. Chem.* 282, 23010–23014.

Persson EK, Verstraete K, Heyndrickx I, Gevaert E, Aegerter H, Percier JM, Deswarte K, Verschueren KHG, Dansercoer A, Gras D, Chanez P, Bachert C, Gonçalves A, Van Gorp H, De Haard H, Blanchetot C, Saunders M, Hammad H, Savvides SN & Lambrecht BN (2019) Protein crystallization promotes type 2 immunity and is reversible by antibody treatment. *Science* 364.

Peschon JJ, Torrance DS, Stocking KL, Glaccum MB, Otten C, Willis CR, Charrier K, Morrissey PJ, Ware CB & Mohler KM (1998) TNF receptor-deficient mice reveal divergent roles for p55 and p75 in several models of inflammation. *J. Immunol.* 160, 943–52. Available at: http://www.jimmunol.org/content/160/2/943 [Accessed May 1, 2020].

Peter JB, Barnard RJ, Edgerton VR, Gillespie CA & Stempel KE (1972) Metabolic Profiles of Three Fiber Types of Skeletal Muscle in Guinea Pigs and Rabbits. *Biochemistry* 11, 2627–2633. Available at: https://pubs.acs.org/sharingguidelines [Accessed March 9, 2020].

Peterson JM & Guttridge DC (2008) Skeletal muscle diseases, inflammation, and NF-κB signaling: Insights and opportunities for therapeutic intervention. *Int. Rev. Immunol.* 27, 375–387.

Peterson JM & Pizza FX (2009) Cytokines derived from cultured skeletal muscle cells after mechanical strain promote neutrophil chemotaxis in vitro. *J. Appl. Physiol.* 106, 130–137.

Petroski MD & Deshaies RJ (2003) Context of multiubiquitin chain attachment influences the rate of Sic1 degradation. *Mol. Cell* 11, 1435–1444.

Phelps CB, Sengchanthalangsy LL, Malek S & Ghosh G (2000) Mechanism of κB DNA binding by Rel/NF-κb dimers. *J. Biol. Chem.* 275, 24392–24399.

Pillon NJ, Bilan PJ, Fink LN & Klip A (2013) Cross-talk between skeletal muscle and immune cells: Muscle-derived mediators and metabolic implications. *Am. J. Physiol. - Endocrinol. Metab.* 304.

Pirani A, Xu C, Hatch V, Craig R, Tobacman LS & Lehman W (2005) Single particle analysis of relaxed and activated muscle thin filaments. *J. Mol. Biol.* 346, 761–772.

Pires BRB, Silva RCMC, Ferreira GM & Abdelhay E (2018) NF-kappaB: Two sides of the same coin. *Genes (Basel).* 9.

Pizza FX, Koh TJ, McGregor SJ & Brooks S V. (2002) Muscle inflammatory cells after passive stretches, isometric contractions, and lengthening contractions. *J. Appl. Physiol.* 92, 1873–1878.

Pizza FX, Peterson JM, Baas JH & Koh TJ (2005) Neutrophils contribute to muscle injury and impair its resolution after lengthening contractions in mice. *J. Physiol.* 562, 899–913. Available at: /pmc/articles/PMC1665528/?report=abstract [Accessed July 28, 2020].

Podbregar M, Lainscak M, Prelovsek O & Mars T (2013) Cytokine response of cultured skeletal muscle cells stimulated with proinflammatory factors depends on differentiation stage. *Sci. World J.* 2013. Available at: /pmc/articles/PMC3590685/?report=abstract [Accessed September 23, 2020].

Poggi M, Kara I, Brunel JM, Landrier JF, Govers R, Bonardo B, Fluhrer R, Haass C, Alessi MC & Peiretti F (2013) Palmitoylation of TNF alpha is involved in the regulation of TNF receptor 1 signalling. *Biochim. Biophys. Acta - Mol. Cell Res.* 1833, 602–612.

Pollock N, Staunton CA, Vasilaki A, McArdle A & Jackson MJ (2017) Denervated muscle fibers induce

mitochondrial peroxide generation in neighboring innervated fibers: Role in muscle aging. *Free Radic. Biol. Med.* 112, 84–92.

Porter MM, Vandervoort AA & Lexell J (1995) Aging of human muscle: structure, function and adaptability. *Scand. J. Med. Sci. Sports* 5, 129–142.

Porteu F & Nathan C (1990) Shedding of tumor necrosis factor receptors by activated human neutrophils. *J. Exp. Med.* 172, 599–607.

Prakash YS, Miller SM, Huang M & Sieck GC (1996) Morphology of diaphragm neuromuscular junctions on different fibre types. *J. Neurocytol.* 25, 88–100.

Qing G, Qu Z & Xiao G (2007) Endoproteolytic processing of C-terminally truncated NF-κB2 precursors at κB-containing promoters. *Proc. Natl. Acad. Sci. U. S. A.* 104, 5324–5329. Available at: www.pnas.org/cgi/content/full/ [Accessed March 31, 2020].

Qing G, Qu Z & Xiao G (2005) Stabilization of basally translated NF-κB-inducing kinase (NIK) protein functions as a molecular switch of processing of NF-κB2 p100. *J. Biol. Chem.* 280, 40578–40582.

Raeber ME, Zurbuchen Y, Impellizzieri D & Boyman O (2018) The role of cytokines in T-cell memory in health and disease. *Immunol. Rev.* 283, 176–193.

Ramirez GA, Yacoub M-R, Ripa M, Mannina D, Cariddi A, Saporiti N, Ciceri F, Castagna A, Colombo G & Dagna L (2018) Eosinophils from Physiology to Disease: A Comprehensive Review. *Biomed Res. Int.* 2018.

Randles L & Walters KJ (2012) Ubiquitin and its binding domains. *Front. Biosci.* 17, 2140–2157.

Rankin SM, Conroy DM & Williams TJ (2000) Eotaxin and eosinophil recruitment: Implications for human disease. *Mol. Med. Today* 6, 20–27.

Rao DV, Watson K & Jones GL (1999) Age-related attenuation in the expression of the major heat shock proteins in human peripheral lymphocytes. *Mech. Ageing Dev.* 107, 105–118.

Rayment I & Holden HM (1994) The three-dimensional structure of a molecular motor. *Trends Biochem. Sci.* 19, 129–134.

Rayment I, Rypniewski WR, Schmidt-Bäse K, Smith R, Tomchick DR, Benning MM, Winkelmann DA, Wesenberg G & Holden HM (1993) Three-dimensional structure of myosin subfragment-1: A molecular motor. *Science (80-.).* 261, 50–58.

Rea IM, Gibson DS, McGilligan V, McNerlan SE, Denis Alexander H & Ross OA (2018) Age and age-related diseases: Role of inflammation triggers and cytokines. *Front. Immunol.* 9, 586.

Reefman E, Kay JG, Wood SM, Offenhäuser C, Brown DL, Roy S, Stanley AC, Low PC, Manderson AP & Stow JL (2010) Cytokine Secretion Is Distinct from Secretion of Cytotoxic Granules in NK Cells. *J. Immunol.* 184, 4852–4862.

Reid B, Slater CR & Bewick GS (1999) Synaptic vesicle dynamics in rat fast and slow motor nerve terminals. *J. Neurosci.* 19, 2511–2521.

Van Remmen H & Jones DP (2009) Current thoughts on the role of mitochondria and free radicals in the biology of aging. *Journals Gerontol. - Ser. A Biol. Sci. Med. Sci.* 64, 171–174.

Rieu I, Magne H, Savary-Auzeloux I, Averous J, Bos C, Peyron MA, Combaret L & Dardevet D (2009) Reduction of low grade inflammation restores blunting of postprandial muscle anabolism and limits sarcopenia in old rats. *J. Physiol.* 587, 5483–5492.

Risi C, Eisner J, Belknap B, Heeley DH, White HD, Schröder GF & Galkin VE (2017) Ca2+-induced movement of tropomyosin on native cardiac thin filaments revealed by cryoelectron microscopy. *Proc. Natl. Acad. Sci. U. S. A.* 114, 6782–6787. Available at: www.pnas.org/cgi/doi/10.1073/pnas.1700868114 [Accessed March 4, 2020].

Rizzoli SO & Betz WJ (2004) The Structural Organization of the Readily Releasable Pool of Synaptic Vesicles. *Science (80-.).* 303, 2037–2039.

Rodnina M V (2016) The ribosome in action: Tuning of translational efficiency and protein folding.

Rogers S, Wells R & Rechsteiner M (1986) Amino acid sequences common to rapidly degraded proteins: The PEST hypothesis. *Science (80-.).* 234, 364–368.

Romagnani S (1999) Th 1/Th2 Cells. *Inflamm. Bowel Dis.* 5, 285–294.

Romanazzo S, Forte G, Morishima K & Taniguchi A (2015) IL-12 involvement in myogenic differentiation of C2C12 in vitro. *Biomater. Sci.* 3, 469–479.

Rooyackers OE, Adey DB, Ades PA & Nair KS (1996a) Effect of age on in vivo rates of mitochondrial protein synthesis in human skeletal muscle. *Proc. Natl. Acad. Sci. U. S. A.* 93, 15364–9. Available at: https://www.pnas.org/content/pnas/93/26/15364.full.pdf [Accessed July 6, 2019].

Rooyackers OE, Adey DB, Ades PA & Nair KS (1996b) Effect of age on in vivo rates of mitochondrial protein synthesis in human skeletal muscle. *Proc. Natl. Acad. Sci. U. S. A.* 93, 15364–15369. Available at: https://www.ncbi.nlm.nih.gov/pmc/articles/PMC26410/pdf/pq015364.pdf [Accessed July 6, 2019].

Rosenzweig R, Osmulski PA, Gaczynska M & Glickman MH (2008) The central unit within the 19S regulatory particle of the proteasome. *Nat. Struct. Mol. Biol.* 15, 573–580.

Ross SH & Cantrell DA (2018) Signaling and Function of Interleukin-2 in T Lymphocytes. *Annu. Rev. Immunol.* 36, 411–433.

Rowan SL, Rygiel K, Purves-Smith FM, Solbak NM, Turnbull DM & Hepple RT (2012) Denervation causes fiber atrophy and myosin heavy chain co-expression in senescent skeletal muscle. *PLoS One* 7.

Ryszer T (2015) Understanding the Mysterious M2 Macrophage through Activation Markers and Effector Mechanisms. *Mediators Inflamm.* 2015, 16–18.

Ryzhakov G, Teixeira A, Saliba D, Blazek K, Muta T, Ragoussis J & Udalova IA (2013) Cross-species analysis reveals evolving and conserved features of the nuclear factor κb (NF-κB) proteins. *J. Biol.*

Chem. 288, 11546–11554.

Sacheck JM, Hyatt J-PK, Raffaello A, Jagoe RT, Roy RR, Edgerton VR, Lecker SH & Goldberg AL (2007) Rapid disuse and denervation atrophy involve transcriptional changes similar to those of muscle wasting during systemic diseases. *FASEB J.* 21, 140–55. Available at: www.fasebj.org [Accessed July 8, 2019].

Sadygov RG, Avva J, Rahman M, Lee K, Ilchenko S, Kasumov T & Borzou A (2018) D2ome, Software for in Vivo Protein Turnover Analysis Using Heavy Water Labeling and LC-MS, Reveals Alterations of Hepatic Proteome Dynamics in a Mouse Model of NAFLD. *J. Proteome Res.* 17, 3740–3748. Available at: /pmc/articles/PMC6466633/?report=abstract [Accessed September 21, 2020].

Saibil H (2013) Chaperone machines for protein folding, unfolding and disaggregation. *Nat. Rev. Mol. Cell Biol.* 14, 630–642.

Sakellariou GK, Davis CS, Shi Y, Ivannikov M V., Zhang Y, Vasilaki A, Macleod GT, Richardson A, Van Remmen H, Jackson MJ, McArdle A & Brooks S V. (2014a) Neuron-specific expression of CuZnSOD prevents the loss of muscle mass and function that occurs in homozygous CuZnSOD-knockout mice. *FASEB J.* 28, 1666–1681.

Sakellariou GK, Jackson MJ & Vasilaki A (2014b) Redefining the major contributors to superoxide production in contracting skeletal muscle. The role of NAD(P)H oxidases. *Free Radic. Res.* 48, 12–29.

Sakellariou GK, Pearson T, Lightfoot AP, Nye GA, Wells N, Giakoumaki II, Vasilaki A, Griffiths RD, Jackson MJ & McArdle A (2016) Mitochondrial ROS regulate oxidative damage and mitophagy but not age-related muscle fiber atrophy. *Sci. Rep.* 6, 33944. Available at: http://www.nature.com/articles/srep33944 [Accessed September 5, 2019].

Salahuddin P, Siddiqi MK, Khan S, Abdelhameed AS & Khan RH (2016) Mechanisms of protein misfolding: Novel therapeutic approaches to protein-misfolding diseases. *J. Mol. Struct.* 1123,

311–326.

Sandri M, Coletto L, Grumati P & Bonaldo P (2013) Misregulation of autophagy and protein degradation systems in myopathies and muscular dystrophies. *Artic. J. Cell Sci.* Available at: https://www.researchgate.net/publication/259111081 [Accessed November 26, 2019].

Santulli G, Lewis DR & Marks AR (2017) Physiology and pathophysiology of excitation–contraction coupling: the functional role of ryanodine receptor. *J. Muscle Res. Cell Motil.* 38, 37–45.

Sataranatarajan K, Pharaoh G, Brown JL, Ranjit R, Piekarz KM, Street K, Wren JD, Georgescu C, Kinter C, Kinter M, Freeman WM, Richardson A & Van Remmen H (2020) Molecular changes in transcription and metabolic pathways underlying muscle atrophy in the CuZnSOD null mouse model of sarcopenia. *GeroScience* 42, 1101–1118.

Sataranatarajan K, Qaisar R, Davis C, Sakellariou GK, Vasilaki A, Zhang Y, Liu Y, Bhaskaran S, McArdle A, Jackson M, Brooks S V., Richardson A & Van Remmen H (2015) Neuron specific reduction in CuZnSOD is not sufficient to initiate a full sarcopenia phenotype. *Redox Biol.* 5, 140–148.

Savinova O V., Hoffmann A & Ghosh G (2009) The Nfkb1 and Nfkb2 Proteins p105 and p100 Function as the Core of High-Molecular-Weight Heterogeneous Complexes. *Mol. Cell* 34, 591–602.

Savli H, Szendröi A, Romics I & Nagy B (2008) Gene network and canonical pathway analysis in prostate cancer: A microarray study. *Exp. Mol. Med.* 40, 176–185.

Sayed RKA, de Leonardis EC, Guerrero-Martínez JA, Rahim I, Mokhtar DM, Saleh AM, Abdalla KEH, Pozo MJ, Escames G, López LC & Acuña-Castroviejo D (2016) Identification of morphological markers of sarcopenia at early stage of aging in skeletal muscle of mice. *Exp. Gerontol.* 83, 22–30.

Scaffidi C, Kirchhofft S, Krammert PH & Peter ME (1999) Apoptosis signaling in lymphocytes. *Immunology* 11, 277–285.

Scalabrin M, Pollock N, Staunton CA, Brooks S V., McArdle A, Jackson MJ & Vasilaki A (2019) Redox responses in skeletal muscle following denervation. *Redox Biol.* 26.

Scelsi R, Marchetti C & Poggi P (1980) Histochemical and ultrastructural aspects of M. vastus lateralis in sedentary old people (age 65-89 years). *Acta Neuropathol.* 51, 99–105.

Schaap LA, Pluijm SMF, Deeg DJH & Visser M (2006) Inflammatory Markers and Loss of Muscle Mass (Sarcopenia) and Strength. *Am. J. Med.* 119. Available at: https://pubmed.ncbi.nlm.nih.gov/16750969/ [Accessed September 23, 2020].

Schiaffino S, Dyar KA, Ciciliot S, Blaauw B & Sandri M (2013) Mechanisms regulating skeletal muscle growth and atrophy. *FEBS J.* 280, 4294–4314.

Schiaffino S, HanzlíKová V & Pierobon S (1970) Relations between structure and function in rat skeletal muscle fibers. *J. Cell Biol.* 47, 107–119.

Schiaffino S & Reggiani C (2011) Fiber types in Mammalian skeletal muscles. *Physiol. Rev.* 91, 1447–1531.

Schiraldi M, Raucci A, Muñoz LM, Livoti E, Celona B, Venereau E, Apuzzo T, De Marchis F, Pedotti M, Bachi A, Thelen M, Varani L, Mellado M, Proudfoot A, Bianchi ME & Uguccioni M (2012) HMGB1 promotes recruitment of inflammatory cells to damaged tissues by forming a complex with CXCL12 and signaling via CXCR4. *J. Exp. Med.* 209, 551–563.

Schneider M (1994) Control of Calcium Release in Functioning Skeletal Muscle Fibers. *Annu. Rev. Physiol.* 56, 463–484. Available at: www.annualreviews.org [Accessed March 5, 2020].

Schramm L & Hernandez N (2002) Recruitment of RNA polymerase III to its target promoters. *Genes Dev.* 16, 2593–2620.

Schreiner P, Chen X, Husnjak K, Randles L, Zhang N, Elsasser S, Finley D, Dikic I, Walters KJ & Groll M (2008) Ubiquitin docking at the proteasome through a novel pleckstrin-homology domain

interaction. *Nature* 453, 548–552.

Schroder K & Tschopp J (2010) The Inflammasomes. *Cell* 140, 821–832. Available at: https://www.sciencedirect.com/science/article/pii/S0092867410000759?via%253Dihub [Accessed June 21, 2019].

Schröder T, Fuchss J, Schneider I, Stoltenburg-Didinger G & Hanisch F (2013) Eosinophils in hereditary and inflammatory myopathies. *Acta Myol. myopathies cardiomyopathies Off. J. Mediterr. Soc. Myol.* 32, 148–53. Available at: http://www.ncbi.nlm.nih.gov/pubmed/24803842 [Accessed July 14, 2020].

Schubert U, Antón LC, Gibbs J, Norbury CC, Yewdell JW & Bennink JR (2000) Rapid degradation of a large fraction of newly synthesized proteins by proteasomes. *Nature* 404, 770–774.

Sedger LM & McDermott MF (2014) TNF and TNF-receptors: From mediators of cell death and inflammation to therapeutic giants - past, present and future. *Cytokine Growth Factor Rev.* 25, 453–472.

Segura E & Villadangos JA (2009) Antigen presentation by dendritic cells in vivo. *Curr. Opin. Immunol.* 21, 105–110.

Sellin LC, Molgó J, Törnquist K, Hansson B & Thesleff S (1996) On the possible origin of "giant or slow-rising" miniature end-plate potentials at the neuromuscular junction. *Pflugers Arch. Eur. J. Physiol.* 431, 325–334.

Selvin D, Hesse E & Renaud JM (2015) Properties of single FDB fibers following a collagenase digestion for studying contractility, fatigue, and pCa-sarcomere shortening relationship. *Am. J. Physiol. - Regul. Integr. Comp. Physiol.* 308, R467–R479. Available at: https://www.physiology.org/doi/10.1152/ajpregu.00144.2014 [Accessed January 23, 2020].

Sen CK, Khanna S, Reznick AZ, Roy S & Packer L (1997) Glutathione regulation of tumor necrosis factor-α-induced NF-κB activation in skeletal muscle-derived L6 cells. *Biochem. Biophys. Res. Commun.*

237, 645–649.

Shapouri-Moghaddam A, Mohammadian S, Vazini H, Taghadosi M, Esmaeili SA, Mardani F, Seifi B, Mohammadi A, Afshari JT & Sahebkar A (2018) Macrophage plasticity, polarization, and function in health and disease. *J. Cell. Physiol.* 233, 6425–6440.

Sheth KA, Iyer CC, Wier CG, Crum AE, Bratasz A, Kolb SJ, Clark BC, Burghes AHM & Arnold WD (2018) Muscle strength and size are associated with motor unit connectivity in aged mice. *Neurobiol. Aging* 67, 128–136.

Shimizu Y, Matsumoto K, Okayama Y, Sakai K, Maeno T, Suga T, Miura T, Takai S, Kurabayashi M & Saito H (2008) Interleukin-3 Does Not Affect the Differentiation of Mast Cells Derived from Human Bone Marrow Progenitors. *Immunol. Invest.* 37, 1–17. Available at: http://www.tandfonline.com/doi/full/10.1080/08820130701741742 [Accessed May 6, 2020].

Short KR, Vittone JL, Bigelow ML, Proctor DN & Nair KS (2004) Age and aerobic exercise training effects on whole body and muscle protein metabolism. *Am. J. Physiol. Metab.* 286, E92–E101. Available at: http://www.physiology.org/doi/10.1152/ajpendo.00366.2003 [Accessed June 30, 2019].

Siggers T, Chang AB, Teixeira A, Wong D, Williams KJ, Ahmed B, Ragoussis J, Udalova IA, Smale ST & Bulyk ML (2012) Principles of dimer-specific gene regulation revealed by a comprehensive characterization of NF-κB family DNA binding. *Nat. Immunol.* 13, 95–102.

da Silva PFL, Ogrodnik M, Kucheryavenko O, Glibert J, Miwa S, Cameron K, Ishaq A, Saretzki G, Nagaraja-Grellscheid S, Nelson G & von Zglinicki T (2019) The bystander effect contributes to the accumulation of senescent cells in vivo. *Aging Cell* 18.

Silverman GJ (2015) Protective natural autoantibodies to apoptotic cells: evidence of convergent selection of recurrent innate-like clones. *Ann. N. Y. Acad. Sci.* 1362, 164–175.

Silverman N & Maniatis T (2001) NF-κB signaling pathways in mammalian and insect innate immunity. *Genes Dev.* 15, 2321–2342.

Sims-Robinson C, Hur J, Hayes JM, Dauch JR, Keller PJ, Brooks S V. & Feldman EL (2013) The Role of Oxidative Stress in Nervous System Aging. *PLoS One* 8.

Singhal N & Martin PT (2011) Role of extracellular matrix proteins and their receptors in the development of the vertebrate neuromuscular junction. *Dev. Neurobiol.* 71, 982–1005.

Sketelj J, Leisner E, Gohlsch B, Škorjanc D & Pette D (1997) Specific impulse patterns regulate acetylcholinesterase activity in skeletal muscles of rats and rabbits. *J. Neurosci. Res.* 47, 49–57.

Smale ST (2012) Dimer-specific regulatory mechanisms within the NF-κB family of transcription factors. *Immunol. Rev.* 246, 193–204.

Smerdu V, Karsch-Mizrachi I, Campione M, Leinwand L & Schiaffino S (1994) Type IIx myosin heavy chain transcripts are expressed in type IIb fibers of human skeletal muscle. *Am. J. Physiol. - Cell Physiol.* 267.

Sokol CL & Luster AD (2015) The chemokine system in innate immunity. *Cold Spring Harb. Perspect. Biol.* 7, 1–20.

Solan NJ, Miyoshi H, Carmona EM, Bren GD & Paya C V (2002) RelB cellular regulation and transcriptional activity are regulated by p100. *J. Biol. Chem.* 277, 1405–1418.

Sonjak V, Jacob K, Morais JA, Rivera-Zengotita M, Spendiff S, Spake C, Taivassalo T, Chevalier S & Hepple RT (2019) Fidelity of muscle fibre reinnervation modulates ageing muscle impact in elderly women. *J. Physiol.* 597, 5009–5023.

Soukup T, Zachařová G & Smerdu V (2002) Fibre type composition of soleus and extensor digitorum longus muscles in normal female inbred Lewis rats. *Acta Histochem.* 104, 399–405.

Souza Saraiva W, Prestes J, Schwerz Funghetto S, Navalta JW, Tibana RA & da Cunha Nascimento D (2019) Relation Between Relative Handgrip Strength, Chronological Age and Physiological Age with Lower Functional Capacity in Older Women. *Open Access J. Sport. Med.* Volume 10, 185–

190.

Spiro AJ, Shy GM & Gonatas NK (1966) Myotubular Myopathy: Persistence of Fetal Muscle in an Adolescent Boy. *Arch. Neurol.* 14, 1–14. Available at: http://archneur.jamanetwork.com/article.aspx?doi=10.1001/archneur.1966.00470070005001 [Accessed September 9, 2019].

Spittler A, Schiller C, Willheim M, Tempfer C, Winkler S & Boltz-Nitulescu G (1995) IL-10 augments CD23 expression on U937 cells and down-regulates IL-4-driven CD23 expression on cultured human blood monocytes: effects of IL-10 and other cytokines on cell phenotype and phagocytosis. *Immunology* 85, 311–7. Available at: http://www.ncbi.nlm.nih.gov/pubmed/7642222 [Accessed May 20, 2020].

Spolski R, Li P & Leonard WJ (2018) Biology and regulation of IL-2: from molecular mechanisms to human therapy. *Nat. Rev. Immunol.* 18, 648–659.

Squire J (2019) Special issue: The actin-myosin interaction in muscle: Background and overview. *Int. J. Mol. Sci.* 20, 1–40.

Sriburi R, Jackowski S, Mori K & Brewer JW (2004) XBP1: A link between the unfolded protein response, lipid biosynthesis, and biogenesis of the endoplasmic reticulum. *J. Cell Biol.* 167, 35–41.

Staunton CA, Owen ED, Pollock N, Vasilaki A, Barrett-Jolley R, McArdle A & Jackson MJ (2019) HyPer2 imaging reveals temporal and heterogeneous hydrogen peroxide changes in denervated and aged skeletal muscle fibers in vivo. *Sci. Rep.* 9.

Steensberg A, Van Hall G, Osada T, Sacchetti M, Saltin B & Pedersen BK (2000) Production of interleukin-6 in contracting human skeletal muscles can account for the exercise-induced increase in plasma interleukin-6. *J. Physiol.* 529, 237–242. Available at: https://physoc-onlinelibrary-wiley-com.liverpool.idm.oclc.org/doi/full/10.1111/j.1469-7793.2000.00237.x [Accessed July 6, 2020].

Straughn AR, Hindi SM, Xiong G & Kumar A (2018) Canonical NF- kB signaling regulates satellite stem cell homeostasis and function during regenerative myogenesis. *J. Mol. Cell Biol.* 11, 53–66.

Sugamura K, Takeshita T, Kumaki S, Ohbo K & Nakamura M (1992) *The IL-2/IL-2 Receptor System : Involvement of a Novel Receptor Subunit, y Chain, in Growth Signal Transduction*,

Sung MH, Li N, Lao Q, Gottschalk RA, Hager GL & Fraser IDC (2014) Switching of the relative dominance between feedback mechanisms in lipopolysaccharide-induced NF-κB signaling. *Sci. Signal.* 7, 1–12.

Svenson M, Hansen MB, Heegaard P, Abell K & Bendtzen K (1993) Specific binding of interleukin 1 (IL-1)β and IL-1 receptor antagonist (IL-1ra) to human serum. High-affinity binding of IL-1ra to soluble IL-1 receptor type I. *Cytokine* 5, 427–435.

Swinney DC, Xu YZ, Scarafia LE, Lee I, Mak AY, Gan QF, Ramesha CS, Mulkins MA, Dunn J, So OY, Biegel T, Dinh M, Volkel P, Barnett J, Dalrymple SA, Lee S & Huber M (2002) A small molecule ubiquitination inhibitor blocks NF-κB-dependent cytokine expression in cells and rats. *J. Biol. Chem.* 277, 23573–23581. Available at: http://dx.doi.org/10.1074/jbc.M200842200.

Tanaka K (2009) The proteasome: overview of structure and functions. *Proc. Jpn. Acad. Ser. B. Phys. Biol. Sci.* 85, 12–36. Available at: http://www.ncbi.nlm.nih.gov/pubmed/19145068 [Accessed April 17, 2019].

Tang H, Inoki K, Brooks S V., Okazawa H, Lee M, Wang J, Kim M, Kennedy CL, Macpherson PCD, Ji X, Van Roekel S, Fraga DA, Wang K, Zhu J, Wang Y, Sharp ZD, Miller RA, Rando TA, Goldman D, Guan KL & Shrager JB (2019) mTORC1 underlies age-related muscle fiber damage and loss by inducing oxidative stress and catabolism. *Aging Cell* 18. Available at: https://doi.org/10.1111/acel.12943 [Accessed September 5, 2019].

Tauber AI (2003) Metchnikoff and the phagocytosis theory. *Nat. Rev. Mol. Cell Biol.* 4, 897–901.

Taylor A, Verhagen J, Akkoç T, Wenig R, Flory E, Blaser K, Akdis M & Akdis CA (2009) IL-10 suppresses

CD2-mediated T cell activation via SHP-1. *Mol. Immunol.* 46, 622–629.

Thornberry NA, Bull HG, Calaycay JR, Chapman KT, Howard AD, Kostura MJ, Miller DK, Molineaux SM, Weidner JR, Aunins J, Elliston KO, Ayala JM, Casano FJ, Chin J, Ding GJ-F, Egger LA, Gaffney EP, Limjuco G, Palyha OC, Raju SM, Rolando AM, Salley JP, Yamin TT, Lee TD, Shively JE, MacCross M, Mumford RA, Schmidt JA & Tocci MJ (1992) A novel heterodimeric cysteine protease is required for interleukin-1βprocessing in monocytes. *Nature* 356, 768–774. Available at: http://www.nature.com/articles/356768a0 [Accessed June 21, 2019].

Tomlinson BE & Irving D (1977) The numbers of limb motor neurons in the human lumbosacral cord throughout life. *J. Neurol. Sci.* 34, 213–219.

Torang A, Gupta P & Klinke DJ (2019) An elastic-net logistic regression approach to generate classifiers and gene signatures for types of immune cells and T helper cell subsets. *bioRxiv*, 1–16.

Toumi H, F'guyer S & Best TM (2006) The role of neutrophils in injury and repair following muscle stretch. *J. Anat.* 208, 459–470. Available at: /pmc/articles/PMC2100203/?report=abstract [Accessed July 14, 2020].

Trappe T, Williams R, Carrithers J, Raue U, Esmarck B, Kjaer M & Hickner R (2004) Influence of age and resistance exercise on human skeletal muscle proteolysis: A microdialysis approach. *J. Physiol.* 554, 803–813. Available at: http://doi.wiley.com/10.1113/jphysiol.2003.051755 [Accessed July 6, 2019].

Truhlar SME, Mathes E, Cervantes CF, Ghosh G & Komives EA (2008) Pre-folding IκBα Alters Control of NF-κB Signaling. *J. Mol. Biol.* 380, 67–82.

Tsui R, Kearns JD, Lynch C, Vu D, Ngo KA, Basak S, Ghosh G & Hoffmann A (2015) IκBβ enhances the generation of the low-affinity NFκB/RelA homodimer. *Nat. Commun.* 6, 7068.

Tung BT, Rodríguez-Bies E, Talero E, Gamero-Estévez E, Motilva V, Navas P & López-Lluch G (2015) Anti-inflammatory effect of resveratrol in old mice liver. Available at:

http://dx.doi.org/10.1016/j.exger.2015.02.004 [Accessed July 6, 2020].

Turner MD, Nedjai B, Hurst T & Pennington DJ (2014) Cytokines and chemokines: At the crossroads of cell signalling and inflammatory disease. *Biochim. Biophys. Acta - Mol. Cell Res.* 1843, 2563–2582. Available at: https://www.sciencedirect.com/science/article/pii/S0167488914001967 [Accessed June 14, 2019].

Unno M, Mizushima T, Morimoto Y, Tomisugi Y, Tanaka K, Yasuoka N & Tsukihara T (2002) The structure of the mammalian 20S proteasome at 2.75 Å resolution. *Structure* 10, 609–618.

Unwin N & Fujiyoshi Y (2012) Gating movement of acetylcholine receptor caught by plunge-freezing. *J. Mol. Biol.* 422, 617–634.

Uppala JK, Gani AR & Ramaiah KVA (2017) Chemical chaperone, TUDCA unlike PBA, mitigates protein aggregation efficiently and resists ER and non-ER stress induced HepG2 cell death. *Sci. Rep.* 7, 1–13.

Ushio H, Ueno T, Kojima Y, Komatsu M, Tanaka S, Yamamoto A, Ichimura Y, Ezaki J, Nishida K, Komazawa-Sakon S, Niyonsaba F, Ishii T, Yanagawa T, Kominami E, Ogawa H, Okumura K & Nakano H (2011) Crucial role for autophagy in degranulation of mast cells. *J. Allergy Clin. Immunol.* 127, 1267-1276.e6.

Valdez G, Tapia JC, Kang H, Clemenson GD, Gage FH, Lichtman JW & Sanes JR (2010) Attenuation of age-related changes in mouse neuromuscular synapses by caloric restriction and exercise. *Proc. Natl. Acad. Sci. U. S. A.* 107, 14863–14868.

Vanamee ÉS & Faustman DL (2018) Structural principles of tumor necrosis factor superfamily signaling. *Sci. Signal.* 11.

Varambally S, Bar-Dayan Y, Bayry J, Lacroix-Desmazes S, Horn M, Sorel M, Bar-Dayan Y, Ruberti G, Kazatchkine MD & Kaveri S V (2004) Natural human polyreactive IgM induce apoptosis of lymphoid cell lines and human peripheral blood mononuclear cells. *Int. Immunol.* 16, 517–524.

Available at: https://academic.oup.com/intimm/article-abstract/16/3/517/656740 [Accessed May 18, 2020].

Vasilaki A, Jackson MJ & McArdle A (2002) Attenuated HSP70 response in skeletal muscle of aged rats following contractile activity. *Muscle and Nerve* 25, 902–905.

Vasilaki A, Mansouri A, Van Remmen H, van der Meulen JH, Larkin L, Richardson AG, McArdle A, Faulkner JA & Jackson MJ (2006a) Free radical generation by skeletal muscle of adult and old mice: Effect of contractile activity. *Aging Cell* 5, 109–117. Available at: https://onlinelibrary.wiley.com/doi/full/10.1111/j.1474-9726.2006.00198.x [Accessed November 2, 2020].

Vasilaki A, McArdle F, Iwanejko LM & McArdle A (2006b) Adaptive responses of mouse skeletal muscle to contractile activity: The effect of age. *Mech. Ageing Dev.*

Vasilaki A, Van Der Meulen JH, Larkin L, Harrison DC, Pearson T, Van Remmen H, Richardson A, Brooks S V., Jackson MJ & McArdle A (2010) The age-related failure of adaptive responses to contractile activity in skeletal muscle is mimicked in young mice by deletion of Cu,Zn superoxide dismutase. *Aging Cell* 9, 979–990.

Vasilaki A, Pollock N, Giakoumaki I, Goljanek-Whysall K, Sakellariou GK, Pearson T, Kayani A, Jackson MJ & McArdle A (2016) The effect of lengthening contractions on neuromuscular junction structure in adult and old mice. *Age (Omaha).* 38, 259–272. Available at: http://dx.doi.org/10.1007/s11357-016-9937-7.

Vella L, Caldow MK, Larsen AE, Tassoni D, Della Gatta PA, Gran P, Russell AP & Cameron-Smith D (2012) Resistance exercise increases NF-κB activity in human skeletal muscle. *Am. J. Physiol. Integr. Comp. Physiol.* 302, R667–R673. Available at: https://www.physiology.org/doi/10.1152/ajpregu.00336.2011 [Accessed July 7, 2019].

Vella L, Markworth JF, Peake JM, Snow RJ, Cameron-Smith D & Russell AP (2014) Ibuprofen

supplementation and its effects on NF-κB activation in skeletal muscle following resistance exercise. *Physiol. Rep.* 2, 1–11.

Verdijk LB, Koopman R, Schaart G, Meijer K, Savelberg HHCM & Van Loon LJC (2007) Satellite cell content is specifically reduced in type II skeletal muscle fibers in the elderly. *Am. J. Physiol. - Endocrinol. Metab.* 292.

Vignali DAA, Collison LW & Workman CJ (2008) How regulatory T cells work. *Nat. Rev. Immunol.* 8, 523–532.

Voehringer D (2013) Protective and pathological roles of mast cells and basophils. *Nat. Rev. Immunol.* 13, 362–375.

Voehringer D (2017) Recent advances in understanding basophil functions in vivo. *F1000Research* 6.

Volpi E, Ferrando AA, Yeckel CW, Tipton KD & Wolfe RR (1998) Exogenous amino acids stimulate net muscle protein synthesis in the elderly. *J. Clin. Invest.* 101, 2000–2007.

Volpi E, Mittendorfer B, Rasmussen BB & Wolfe RR (2000) The response of muscle protein anabolism to combined hyperaminoacidemia and glucose-induced hyperinsulinemia is impaired in the elderly. *J. Clin. Endocrinol. Metab.* 85, 4481–90. Available at: http://www.ncbi.nlm.nih.gov/pubmed/11134097 [Accessed July 6, 2019].

Volpi E, Mittendorfer B, Wolf SE & Wolfe RR (1999) Oral amino acids stimulate muscle protein anabolism in the elderly despite higher first-pass splanchnic extraction. *Am. J. Physiol. Metab.* 277, E513–E520. Available at: http://www.physiology.org/doi/10.1152/ajpendo.1999.277.3.E513 [Accessed July 6, 2019].

Volpi E, Sheffield-Moore M, Rasmussen BB & Wolfe RR (2001) Basal muscle amino acid kinetics and protein synthesis in healthy young and older men. *JAMA* 286, 1206–1212. Available at: http://jama.jamanetwork.com/article.aspx?doi=10.1001/jama.286.10.1206 [Accessed July 6, 2019].

Vosshenrich CAJ, Samson-Villéger SI & Di Santo JP (2005) Distinguishing features of developing natural killer cells. *Curr. Opin. Immunol.* 17, 151–158.

Waldmann TA (1989) The Multi-Subunit Interleukin-2 Receptor. *Annu. Rev. Biochem.* 58, 875–905. Available at: http://www.annualreviews.org/doi/10.1146/annurev.bi.58.070189.004303 [Accessed May 19, 2020].

Walker JA & McKenzie ANJ (2018) TH2 cell development and function. *Nat. Rev. Immunol.* 18, 121–133.

Wall BT, Gorissen SH, Pennings B, Koopman R, Groen BBL, Verdijk LB & van Loon LJC (2015) Aging Is Accompanied by a Blunted Muscle Protein Synthetic Response to Protein Ingestion A. Philp, ed. *PLoS One* 10, e0140903. Available at: http://dx.plos.org/10.1371/journal.pone.0140903 [Accessed July 6, 2019].

Walsh ME, Bhattacharya A, Sataranatarajan K, Qaisar R, Sloane L, Rahman MM, Kinter M & Van Remmen H (2015) The histone deacetylase inhibitor butyrate improves metabolism and reduces muscle atrophy during aging. *Aging Cell* 14, 957–970.

Walston J, Fedarko N, Yang H, Leng S, Beamer B, Espinoza S, Lipton A, Zheng H & Becker K (2008) The physical and biological characterization of a frail mouse model. *Journals Gerontol. - Ser. A Biol. Sci. Med. Sci.* 63, 391–398.

Wang B, Li J & Xiao X (2000) Adeno-associated virus vector carrying human minidystrophin genes effectively ameliorates muscular dystrophy in mdx mouse model. *Proc. Natl. Acad. Sci. U. S. A.* 97, 13714–13719. Available at: http://www.ncbi.nlm.nih.gov/pubmed/11095710 [Accessed September 9, 2019].

Wang C, Deng L, Hong M, Akkaraju GR, Inoue JI & Chen ZJ (2001) TAK1 is a ubiquitin-dependent kinase of MKK and IKK. *Nature* 412, 346–351.

Wang J, Yang G, Wang D, Liu K, Ma Y, Liu H, Wu J & Fang M (2017) Changes of peripheral lymphocyte

subsets and cytokine environment during aging and deteriorating gastrointestinal tract health status. *Oncotarget* 8, 60764–60777. Available at: www.impactjournals.com/oncotarget [Accessed September 23, 2020].

Wang T, Hu Y, Wangkahart E, Liu F, Wang A, Zahran E, Maisey KR, Liu M, Xu Q, Imarai M & Secombes CJ (2018) Interleukin (IL)-2 is a key regulator of T helper 1 and T helper 2 cytokine expression in fish: Functional characterization of two divergent IL2 paralogs in salmonids. *Front. Immunol.* 9, 1–22.

Wang VYF, Huang W, Asagiri M, Spann N, Hoffmann A, Glass C & Ghosh G (2012) The Transcriptional Specificity of NF-κB Dimers Is Coded within the κB DNA Response Elements. *Cell Rep.* 2, 824–839.

Wang X, Sathe AA, Smith GR, Ruf-Zamojski F, Nair V, Lavine KJ, Xing C, Sealfon SC & Zhou L (2020) Heterogeneous origins and functions of mouse skeletal muscle-resident macrophages. *Proc. Natl. Acad. Sci. U. S. A.* 117, 20729–20740.

Wang X, Watson C, Sharp JS, Handel TM & Prestegard JH (2011) Oligomeric structure of the chemokine CCL5/RANTES from NMR, MS, and SAXS data. *Structure* 19, 1138–1148.

Welle S, Thornton C, Jozefowicz R & Statt M (1993) Myofibrillar protein synthesis in young and old men. *Am. J. Physiol. Metab.* 264, E693–E698. Available at: http://www.ncbi.nlm.nih.gov/pubmed/8498491 [Accessed July 6, 2019].

Wen Y, Murach KA, Vechetti IJ, Fry CS, Vickery C, Peterson CA, McCarthy JJ & Campbell KS (2018) Myo Vision: Software for automated high-content analysis of skeletal muscle immunohistochemistry. *J. Appl. Physiol.* 124, 40–51.

Westbury LD, Fuggle NR, Syddall HE, Duggal NA, Shaw SC, Maslin K, Dennison EM, Lord JM & Cooper C (2018) Relationships Between Markers of Inflammation and Muscle Mass, Strength and Function: Findings from the Hertfordshire Cohort Study. *Calcif. Tissue Int.* 102, 287–295. Available at: /pmc/articles/PMC5818589/?report=abstract [Accessed September 23, 2020].

Will CL & Lührmann R (2001) Spliceosomal UsnRNP biogenesis, structure and function. *Curr. Opin. Cell Biol.* 13, 290–301.

Winston JT, Strack P, Beer-Romero P, Chu CY, Elledge SJ & Harper JW (1999) The SCF(β-TRCP)-ubiquitin ligase complex associates specifically with phosphorylated destruction motifs in IκBα and β-catenin and stimulates IκBα ubiquitination in vitro. *Genes Dev.* 13, 270–283.

Wittinghofer A & Geeves MA (2016) Review: The ATPase mechanism of myosin and actomyosin. *Biopolymers* 105, 483–491.

Wood SJ & Slater CR (1997) The contribution of postsynaptic folds to the safety factor for neuromuscular transmission in rat fast- and slow-switch muscles. *J. Physiol.* 500, 165–176. Available at: http://doi.wiley.com/10.1113/jphysiol.1997.sp022007 [Accessed March 9, 2020].

Worden EJ, Padovani C & Martin A (2014) Structure of the Rpn11-Rpn8 dimer reveals mechanisms of substrate deubiquitination during proteasomal degradation. *Nat. Struct. Mol. Biol.* 21, 220–227.

Wu CH, Yamaguchi Y, Benjamin LR, Horvat-Gordon M, Washinsky J, Enerly E, Larsson J, Lambertsson A, Handa H & Gilmour D (2003) NELF and DSIF cause promoter proximal pausing on the hsp70 promoter in Drosophila. *Genes Dev.* 17, 1402–1414.

Wu CL, Cornwell EW, Jackman RW & Kandarian SC (2014) NF-κB but not FoxO sites in the MuRF1 promoter are required for transcriptional activation in disuse muscle atrophy. *Am. J. Physiol. - Cell Physiol.* 306.

Xie P (2013) TRAF molecules in cell signaling and in human diseases. *J. Mol. Signal.* 8, 7.

Xu M, Pirtskhalava T, Farr JN, Weigand BM, Palmer AK, Weivoda MM, Inman CL, Ogrodnik MB, Hachfeld CM, Fraser DG, Onken JL, Johnson KO, Verzosa GC, Langhi LGP, Weigl M, Giorgadze N, LeBrasseur NK, Miller JD, Jurk D, Singh RJ, Allison DB, Ejima K, Hubbard GB, Ikeno Y, Cubro H, Garovic VD, Hou X, Weroha SJ, Robbins PD, Niedernhofer LJ, Khosla S, Tchkonia T & Kirkland JL (2018) Senolytics improve physical function and increase lifespan in old age. *Nat. Med.* 24, 1246–

1256. Available at: http://dx.doi.org/10.1038/s41591-018-0092-9.

Xu M, Tchkonia T, Ding H, Ogrodnik M, Lubbers ER, Pirtskhalava T, White TA, Johnson KO, Stout MB, Mezera V, Giorgadze N, Jensen MD, LeBrasseur NK & Kirkland JL (2015) JAK inhibition alleviates the cellular senescence-associated secretory phenotype and frailty in old age. *Proc. Natl. Acad. Sci. U. S. A.* 112, E6301–E6310.

Yadava RS, Foff EP, Yu Q, Gladman JT, Kim YK, Bhatt KS, Thornton CA, Zheng TS & Mahadevan MS (2014) TWEAK/Fn14, a pathway and novel therapeutic target in myotonic dystrophy. *Hum. Mol. Genet.* 24, 2035–2048.

Yamaguchi Y (2013) Transcription Elongation, Mechanisms. In *Encyclopedia of Systems Biology*. Springer New York, pp.2221–2224.

Yamaki T, Wu CL, Gustin M, Lim J, Jackman RW & Kandarian SC (2012) Rel A/p65 is required for cytokine-induced myotube atrophy. *Am. J. Physiol. - Cell Physiol.* 303.

Yamamoto M & Takeda K (2008) Role of nuclear IκB proteins in the regulation of host immune responses. *J. Infect. Chemother.* 14, 265–269. Available at: http://dx.doi.org/10.1007/s10156-008-0619-Y [Accessed April 7, 2020].

Yamamoto M, Yamazaki S, Uematsu S, Sato S, Hemmi H, Hoshino K, Kaisho T, Kuwata H, Takeuchi O, Takeshige K, Saitoh T, Yamaoka S, Yamamoto N, Yamamoto S, Muta T, Takeda K & Akira S (2004) Regulation of Toll/IL-1-receptor- mediated gene expression by the inducible nuclear protein I. *Nature* 430, 218–222.

Yang T, Wang S, Zheng Q, Wang L, Li Q, Wei M, Du Z & Fan Y (2016) Increased plasma levels of epithelial neutrophil-activating peptide 78/CXCL5 during the remission of Neuromyelitis optica. *BMC Neurol.* 16, 96. Available at: http://bmcneurol.biomedcentral.com/articles/10.1186/s12883-016-0622-3 [Accessed July 14, 2020].

Yarasheski KE (2003) Aging, exercise, and muscle protein metabolism. *J. Appl. Physiol.* 58A, 918–922.

Yarasheski KE, Welle S & Nair KS (2002) Muscle Protein Synthesis in Younger and Older Men—Reply. *JAMA* 287, 317. Available at: http://jama.jamanetwork.com/article.aspx?doi=10.1001/jama.287.3.313 [Accessed July 6, 2019].

Yarasheski KE, Zachwieja JJ & Bier DM (2017) Acute effects of resistance exercise on muscle protein synthesis rate in young and elderly men and women. *Am. J. Physiol. Metab.* 265, E210–E214. Available at: http://www.ncbi.nlm.nih.gov/pubmed/8368290 [Accessed July 6, 2019].

Yarasheski KE, Zachwieja JJ & Bier DM (1993) Acute effects of resistance exercise on muscle protein synthesis rate in young and elderly men and women (American Journal of Physiology) (August 1993) 265 (E210-E214)). *Am. J. Physiol. - Endocrinol. Metab.* 265, 2–6.

Yoshimoto T (2018) The hunt for the source of primary interleukin-4: How we discovered that natural killer T cells and basophils determine T helper type 2 cell differentiation in vivo. *Front. Immunol.* 9, 1–8.

Yu G, Wang LG, Han Y & He QY (2012) ClusterProfiler: An R package for comparing biological themes among gene clusters. *Omi. A J. Integr. Biol.* 16, 284–287. Available at: /pmc/articles/PMC3339379/?report=abstract [Accessed August 24, 2020].

Zambrano S, de Toma I, Piffer A, Bianchi ME & Agresti A (2016) NF-κB oscillations translate into functionally related patterns of gene expression. *Elife* 5, 1–38.

Zandi E, Rothwarf DM, Delhase M, Hayakawa M & Karin M (1997) The IκB kinase complex (IKK) contains two kinase subunits, IKKα and IKKβ, necessary for Iκb phosphorylation and NF-κB activation. *Cell* 91, 243–252.

Zerba E, Komorowski TE & Faulkner JA (1990) Free radical injury to skeletal muscles of young, adult, and old mice. *Am. J. Physiol. - Cell Physiol.* 258.

Zhang Q, Lenardo MJ & Baltimore D (2017) 30 Years of NF-κB: A Blossoming of Relevance to Human

Pathobiology. *Cell* 168, 37–57.

Zhang Y, Center DM, Wu DMH, Cruikshank WW, Yuan J, Andrews DW & Kornfeld H (1998) Processing and activation of pro-interleukin-16 by caspase-3. *J. Biol. Chem.* 273, 1144–1149.

Zhang Y, Davis C, Sakellariou GK, Shi Y, Kayani AC, Pulliam D, Bhattacharya A, Richardson A, Jackson MJ, McArdle A, Brooks S V. & Van Remmen H (2013) CuZnSOD gene deletion targeted to skeletal muscle leads to loss of contractile force but does not cause muscle atrophy in adult mice. *FASEB J.* 27, 3536–3548.

Zhao B, Barrera LA, Ersing I, Willox B, Schmidt SCSS, Greenfeld H, Zhou H, Mollo SB, Shi TT, Takasaki K, Jiang S, Cahir-McFarland E, Kellis M, Bulyk ML, Kieff E & Gewurz BE (2014) The NF-κB Genomic Landscape in Lymphoblastoid B Cells. *Cell Rep.* 8, 1595–1606. Available at: http://www.ncbi.nlm.nih.gov/pubmed/25159142 [Accessed January 17, 2019].

Zhou H, Wertz I, O'Rourke K, Ultsch M, Seshagir S, Eby M, Xiao W & Dixit VM (2004) Bcl10 activates the NF-κB pathway through ubiquitination of NEMO. *Nature* 427, 167–171.

Zhou LZHH, Johnson AP & Rando TA (2001) NFκB and AP-1 mediate transcriptional responses to oxidative stress in skeletal muscle cells. *Free Radic. Biol. Med.* 31, 1405–1416.

Zhu S, Tian Z, Torigoe D, Zhao J, Xie P, Sugizaki T, Sato M, Horiguchi H, Terada K, Kadomatsu T, Miyata K & Oike Y (2019) Aging- and obesity-related peri-muscular adipose tissue accelerates muscle atrophy A. Kumar, ed. *PLoS One* 14, e0221366. Available at: http://dx.plos.org/10.1371/journal.pone.0221366 [Accessed January 13, 2020].

Zlotnik A & Yoshie O (2012) The Chemokine Superfamily Revisited. *Immunity* 36, 705–716.

Zlotnik A, Yoshie O & Nomiyama H (2006) The chemokine and chemokine receptor superfamilies and their molecular evolution. *Genome Biol.* 7, 243.

Zouridakis M, Zisimopoulou P, Poulas K & Tzartos SJ (2009) Recent advances in understanding the

structure of nicotinic acetylcholine receptors. *IUBMB Life* 61, 407–423. Available at: http://doi.wiley.com/10.1002/iub.170 [Accessed March 9, 2020].